

POLITECNICO DI MILANO  
*Department of Architecture,  
Built Environment and Construction Engineering*



**Dottorato di ricerca in Ingegneria dei Sistemi Edilizi**

*Ph. D. Post-graduate School of Engineering of Building Systems*

- XXV ciclo -

SOLAR POTENTIAL  
AND  
MICROSCALE CLIMATE INTERACTIONS IN URBAN AREAS  
*DESIGN STRATEGIES AND USE OF DYNAMIC SIMULATION TOOLS  
FOR SOLAR PLANNING*

Dissertazione finale di

***Ing. Gabriele Lobaccaro***

Matr. 753300

Relatori  
Prof. Tiziana Poli

Correlatore  
Prof. Deo Prasad

Prof. Gabriele Masera

Dr. Francesco Fiorito

Coordinatore di Dottorato  
Prof. Manuela Grecchi



## **Abstract**

How will be the city of tomorrow?

This is the biggest question that everybody does when thinks about the future destiny of the built environment and more in general of the wonderful planet where we are living. A question that today is became a priority seen the situation of the world's climate with the global warming and energy comes from non-renewable sources increasing. These signals oblige to search one's soul in order to understand what everybody can do for improving the global condition.

In this scenario is collocated this research that wants to give a new holistic design approach starting from the European Performance Building Directives that go towards Zero Energy Buildings, communities and cities.

The major part of the solar radiation available for producing the solar energy exploiting the building envelope today remains unutilized. For increasing the solar potential could be enough optimize the volume and guarantee the solar access in order to improve the solar harvest from the façades. The use of the energy comes from the sun it's one of the ways to reduce our environmental impact on climate and secure future supply of energy. The built environment accounts for over 40% of the world's total primary energy use and 24% of greenhouse gas emissions. While three quarters of CO<sub>2</sub> emissions are produced in towns, 75% of the world's energy is consumed in towns. It is easier to understand that there refurbishing interventions and new developments must have more energy-efficient and increasing the use of renewable energy, reducing the non-renewable energy use and greenhouse gas emissions.

This research is focused on solar potential in urban areas and on microscale microclimate interactions using the available simulation tools for designers in order to develop a new design approach for a conscious solar and sustainable design process.

The research starts from the analyses of simple model in order to find the analytic relationships for a sustainable solar design studying the solar radiation, solar access, overshadowing and solar reflections (first section), and the effect on a global warming and wind flows in a district (second section).

Then the approach was tested onto two case studies for verifying if the analytic design relations studied work well in a real urban context. The analyses are conducted on an intervention of demolition and rebuilding of a residential building in a medium density district of the city of Milan (Italy) in order to minimize the overshadowing effect of the neighbourhood buildings and maximize the solar radiation on the facades optimizing the volume of the building, over qualitative analyses on the temperatures and wind flows on the façades as well as the benefit of the green system on a district's microclimate.

---

On the case study of a high density as the downtown of the city of Surfers Paradise (Gold Coast - Australia) was conducted a solar access and solar radiation analysis using a new solar design tool to exploit the solar potential in existing urban areas.

The purpose of this research is to give a new design approach for urban planners, architects and engineers for a sustainable design considering multidisciplinary aspects which influence the urban environment, as solar radiation, wind flows, air temperature and green system. The study compares the current urban morphology scenario with designed scenario elaborated by urban planner and architects and solar optimized design created after solar and microclimate dynamic simulation, in order to develop a conscious and sustainable solar design. Furthermore among other aspects the work explores the different effects of solar access and solar potential in existing urban areas of low, medium and high density. The effects of overshadowing by the built environment surrounding and the benefit in term of solar access from the solar reflection coming from the nearby buildings are investigated. Analyses on thermal comfort, district's global warming, temperature and wind speed on the façades permitted to analyse how the solar systems installation on a building envelope influence the district's microclimate comfort and the thermal stress at the ground level as well as the benefit given from the presence of the green systems in terms of average global temperature and reducing the temperature at the ground level to guarantee a thermal comfort of the inhabitants and of the pedestrians.

Solar irradiation values and solar access evaluation obtained through dynamic simulations tools (*Autodesk Ecotect Analysis, Daysim and DIVA*) constitute the core part of the method as well as the use of generative modeling tools (*Grasshopper*) for optimizing the building shape's volume to harvest as much solar radiation as possible and the surface's panelling (*Rhinoceros-PanelingTools*). The method adopted for the set of simulations consisted in modelling, using *AutoCAD, Autodesk Ecotect Analysis* and *Rhinoceros/Grasshopper*, the digital model of each building or group of buildings to exporting them to urban performance analysis software (*Radiance software package*). Spatial distributions of solar irradiation overall building façades were calculated using ray-tracing simulation techniques to determine the annual solar radiation.

The microclimate analysis on the lower part of the atmosphere is directly influenced by local exchange processes. Especially in urban areas the great variety of different surfaces and sheltering obstacles produces a pattern of distinct microclimate systems. To simulate the interactions between the environment and the atmosphere on local scale, microscale three-dimensional non-hydrostatic model *ENVI-met* was used.

The results demonstrated the new design approach permits to optimize the building volume to capture solar radiation maintaining the same volume and guaranteeing the urban microclimate comfort.

---

## **Index**

1. Introduction.....	9
1.1. Topic of the research.....	9
1.2. State of the art.....	11
1.3. Objectives.....	17

## **Section 1 - Solar Potential in Urban Areas**

2. Overshadowing and Solar Access.....	20
2.1. Introduction.....	21
2.2. Material and method.....	23
2.2.1. First part: simple models analysis and case study of Milan .....	23
2.2.2. Second part: SolarPW tool and case of Surfers Paradise .....	25
2.3. Theory and calculation.....	26
2.3.1. Description of the solar analysis tool: Ecotect.....	26
2.3.2. Description of the solar analysis tool: Daysim .....	28
2.3.3. Comparison of solar irradiation tools .....	35
2.3.4. Overshadowing effect: example of shadow's percentage calculation on a façade.....	40
2.3.5. Matlab algorithm .....	43
2.3.6. Validation of matlab algorithm .....	44
2.4. Results and discussion.....	47
2.4.1. Analysis on simplified models of urban areas .....	47
2.4.2. Analysis on a case study of Milan (Italy) .....	50
2.4.3. Analysis of shadow effect on the façades of neighbouring buildings.....	52
2.4.4. Analysis of energy production with solar building envelope .....	53
2.4.5. Analysis on a case study of Surfers Paradise - Gold Coast (Australia).....	54
2.5. Conclusion and outcomes .....	61
3. Solar geometric optimisation: simple volume transformation and solar reflection and ground reflection contributes.....	62
3.1. Introduction.....	63
3.2. Material and method.....	64
3.2.1. Solar reflection in urban canyon and effect on a buildings .....	64
3.2.2. Radiance materials.....	65
3.3. Theory and calculation.....	70
3.3.1. Analyses and main objectives .....	70

---

3.3.2. Sensitivity analysis .....	73
3.4. Results and discussion.....	75
3.4.1. Simulation of a single building - solar exposure.....	75
3.4.2. Simulation of the building in a district – solar access.....	76
3.5. Conclusion .....	80
4. Solar geometric optimization: parametric generative modeling and dynamic solar analysis... 81	
4.1. Introduction.....	82
4.2. Material and method.....	84
4.2.1. Generative modeling tools: Grasshopper for Rhinoceros and some its plug-ins.....	85
4.2.2. Solar dynamic analysis tool: DIVA for Rhino toolbar .....	87
4.3. Theory and calculation .....	88
4.3.1. Description of Grasshopper’s script.....	89
4.4. Results and discussion.....	100
4.4.1. Solar geometric optimisation of isolated buildings.....	100
4.4.2. Analyses of the isolated optimized building inserted a district (solar access).....	104
4.5. Conclusion .....	107
5. Paneling surfaces and energy production.....	108
5.1. Introduction.....	109
5.2. Material and method.....	110
5.2.1. Overview of the paneling tools.....	110
5.3. Theory and calculation.....	111
5.3.1. Paneling surface using PanelingTools in Rhinoceros .....	111
5.3.2. Paneling surface using Grasshopper .....	114
5.4. Results and discussion.....	119
5.4.1. Paneling façade surfaces for installing a solar systems .....	119
5.4.2. Estimation of the energy production .....	124
5.5. Conclusion .....	128
6. Conclusion Section 1 .....	129
6.1. A New Solar Design Approach .....	130
6.2. Future developments and outcomes.....	133

---

## **Section 2 - Microscale Climate Interactions**

7. Micro-climate environmental analysis: surface temperatures.....	136
7.1. Introduction.....	137
7.2. Material and method.....	139
7.2.1. Clear-sky simulations and simulation parameters .....	139
7.2.2. Urban climate.....	142
7.3. Theory and calculation.....	146
7.3.1. Description of the micro-climate tool ENVI-met.....	146
7.3.2. The physical model .....	148
7.3.3. The atmosphere.....	149
7.3.4. The soil system .....	152
7.3.5. The vegetation .....	153
7.3.6. Ground surface and building surface.....	155
7.3.7. Radiative fluxes.....	156
7.3.8. Turbulent fluxes of sensible heat and vapour.....	157
7.3.9. Soil heat flux and heat flux through building walls.....	157
7.3.10. Numerical aspect: solution techniques .....	158
7.3.11. Computational domain and grid structure .....	159
7.3.12. Limits of the Tool.....	161
7.3.13. Method of data extraction .....	162
7.3.14. Leonardo .....	163
7.3.15. Xtract .....	163
7.3.16. Type of analysis and aim.....	164
7.3.17. Methodology.....	167
7.3.18. Parametric microclimate analysis on simple models .....	169
7.3.19. Case study of the city of Milan: current scenario.....	175
7.3.20. Case study of the city of Milan: actual design scenario.....	176
7.3.21. Case study of the city of Milan: solar optimized scenario .....	177
7.4. Results and discussion.....	181
7.4.1. Parametric Microclimate analysis on simple model: results .....	181
7.4.2. Case study of the city of Milan: actual design scenario .....	191
7.4.3. Case study of the city of Milan: solar optimized design scenario.....	198
7.5. Conclusion and outcomes .....	205

---

8. Qualitative microclimate analysis: air temperature, leaf temperature and wind speed on the facades.....	208
8.1. Introduction.....	209
8.2. Material and method.....	210
8.3. Results and discussion.....	212
8.3.1. Distribution of surface temperatures .....	212
8.3.2. Distribution of mean radiant temperatures.....	213
8.3.3. Distribution of potential temperatures .....	215
8.3.4. Calculation of operative temperatures .....	218
8.3.5. Distribution of leaf temperatures .....	220
8.3.6. Distribution of wind speed in the urban canyons.....	222
8.3.7. Profile of the wind speed on the façade.....	227
8.4. Conclusion and outcomes .....	231
9. Conclusion Section 2 .....	232
9.1. The Climate interaction in a new design approach .....	232
9.2. Future developments and outcomes.....	235
<b>References</b> .....	<b>236</b>

---

*È delle città come dei sogni:  
tutto l'immaginabile può essere sognato ma anche il sogno più inatteso è un rebus che nasconde un desiderio  
oppure il suo rovescio, una paura.  
Le città come i sogni sono costruite di desideri e di paure.*

[Italo Calvino, "Le città invisibili"]

## 1. Introduction

### *Questions of the research*

1. The surfaces of the roofs are sufficient for installing the solar panels in order to produce the energy and reduce the non-renewable energy demand?
2. Why not using the most exposed surfaces: the façade?

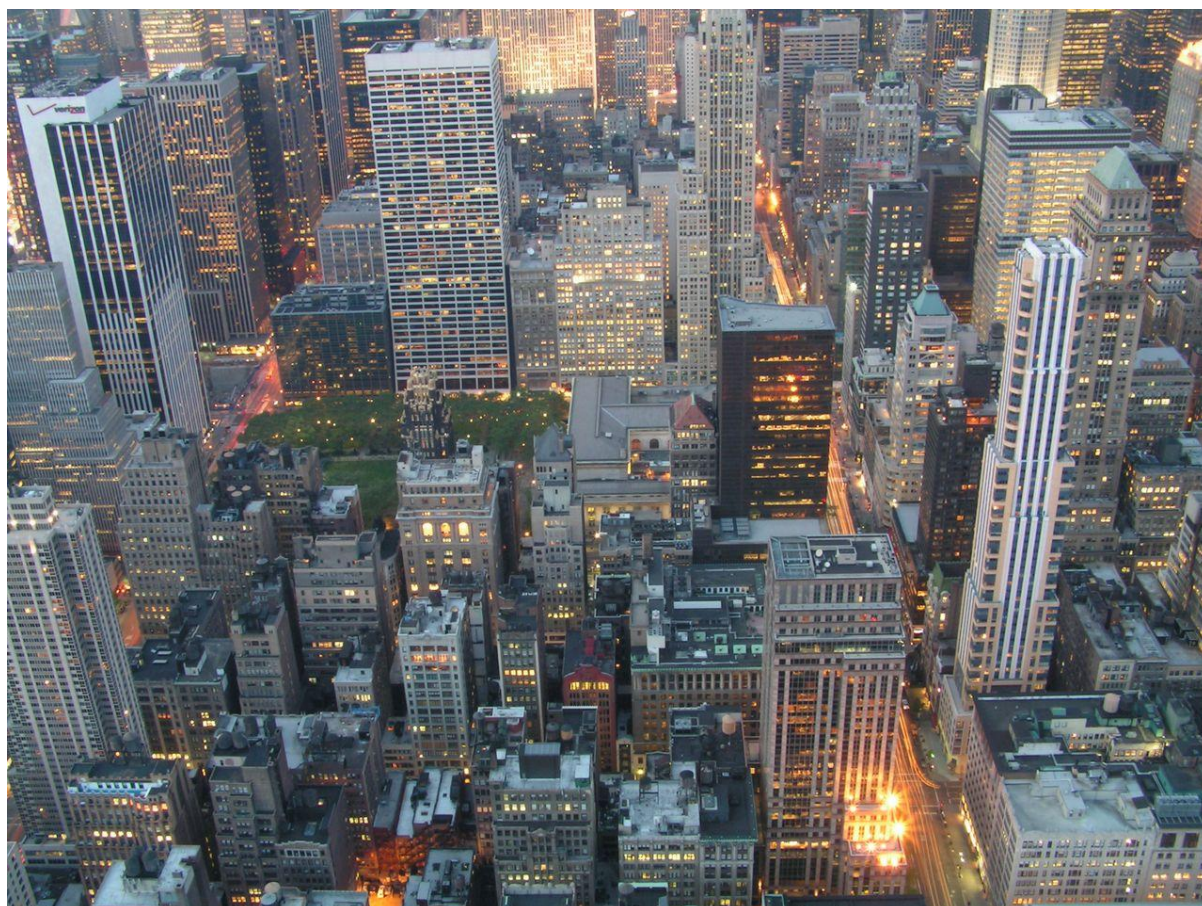


Figure 1. Manhattan - New York (USA)

### 1.1. Topic of the research

Nowadays in urban areas are contained around half of the world's population and the forecasts indicate that on the next forty-three years its increment will be about to 70% as shown in Table 1. Furthermore, some 75% of global resource consumption takes place within urban settlements, which cover only 2% of the earth's surface [1]. Therefore it is imperative to think how to minimise resource consumption in the urban environment. This is could be achieved on one hand with better energy

conservation and on the other hand with the increment of renewable energy use that will substitute the fossil fuels widely used today.

Table 1. Urban and rural areas in 2007 and a perspective for 2025 and 2050 [2].

Country or area	Population in billion					
	2007		2025		2050	
	Urban	Rural	Urban	Rural	Urban	Rural
World	3294 (49%)	3377	4584 (57%)	3426	6398 (70%)	2793
More developed regions <sup>a</sup>	0.910	0.313	0.995	0.264	1.071	0.174
Less developed region <sup>b</sup>	2.384	3.064	3.590	3.162	5.327	2.619
Least developed countries <sup>c</sup>	0.225	0.580	0.452	0.734	0.967	0.775
Other less developed countries <sup>d</sup>	2.159	2.485	3.137	2.428	4.360	1.844
Less developed regions, excluding China	1.815	2.297	2.758	2.538	4.290	2.238
Sub-Saharan Africa <sup>e</sup>	0.290	0.517	0.539	0.654	1.065	0.696

<sup>a</sup> More developed regions comprise Europe, Northern America, Australia/New Zealand and Japan

<sup>b</sup> Less developed regions comprise all regions of Africa, Asia (excluding Japan), Latin America and the Caribbean plus Melanesia, Micronesia and Polynesia

<sup>c</sup> The least developed countries are 50 countries, 34 in Africa, 10 in Asia, 5 in Oceania plus one in Latin America and the Caribbean

<sup>d</sup> Other less developed countries comprise the less developed regions excluding the least developed countries

<sup>e</sup> Sub-Saharan Africa refers to all of Africa except Northern Africa, with the Sudan included in sub-Saharan Africa

In this scenario, the aim of the research is to develop a new multidisciplinary design approach for optimizing a building volume in existing urban areas in order to harvest as much solar radiation as possible to maximize its solar access and solar potential.

The study wants to provide urban design approach also to guarantee the thermal comfort reducing the global warming caused by the installation of solar systems on the façades. Furthermore, the development of this new sustainable design approach is conducted from the analyses using a dynamic tools enable to calculate some of the most important urban aspects that influence the urban environment, as air temperature, wind speed and solar radiation. In this the consequent objective is to minimize the urban energy consumption.

The final aim is to collect the data required to estimate the energy productions and energy saving by district's models analysed for the case study of the city of Milan (Italy) and Surfers Paradise (Gold Coast - Queensland - Australia).

## 1.2. State of the art

### Energy and regulations

Nowadays urban planning and architectural design are more and more complex due to the new policies regulations which go towards the minimization of the use of the land and reduction of energy consumptions and from a technical and conceptual point of view. Considering these latter aspect is easily to notice that today, the only possible development is towards a vertical direction. The tall buildings contribute to increase the urban density and technical questions to solve thus they are involved numerous and different specialists in the urban and architectural process [3]. All figures which today are involved in urban and architectural process are conscious that have as main goal to develop a sustainable design in a compact city model.

Furthermore in the area where the climate changes, the cities represent the solution and not the problem: in fact in a cities characterized by individual housing and a long distance among the buildings, covered with the use of cars are more polluting than concentrated cities in which good public service transportation's connect the energy efficient buildings with combination of housing and activities.

In this scenario, the development of renewable energy sources, further motivated by the climate change and the CO<sub>2</sub> emissions' reduction, is necessary. Among renewable energy sources, solar energy represents the source that has the largest potential: it could cover 2850 times the annual global energy need [4] (Figure 2).

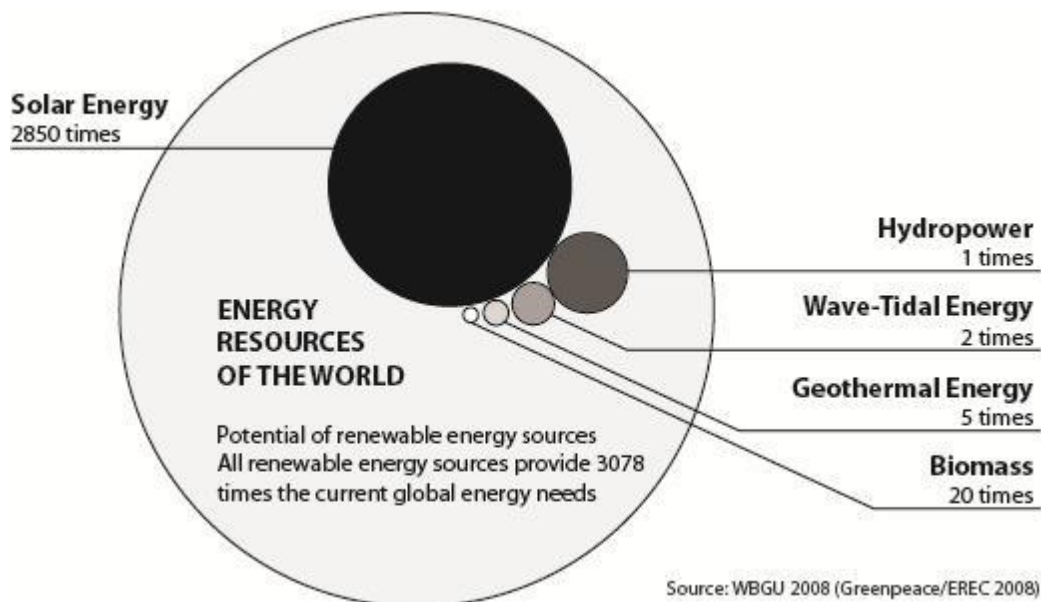


Figure 2. Theoretical Potential of Renewable energy sources compared to the global energy needs (Source: European Renewable Energy Council, 2010)

Therefore the energy policies are going toward a reduction of energy consumptions and fix the limits of primary energy demand for new buildings. In Europe, the European Directive on Energy Performance of Buildings (EPBD), lay down minimum requirements of the energy performance of buildings. While considering the national and local energy regulations (DGR 22 December 2008 - N° 8/8745) fix the limits of thermal transmittance (U-Values – W/m<sup>2</sup>K) of building envelope (façades, roof and windows) for every new construction or refurbishment in order to achieve the energy standard consumption limits in terms of primary energy consumption of a building (EP<sub>H</sub> - kWh/m<sup>2</sup>yr).

However, the major part of its potential still remains unutilized today. According to the International Energy Agency [5], among others, some important causes are about that are:

- Economic factors;
- Lack of technical knowledge;
- Reluctance to use “new” technologies;
- Architectural (aesthetic) factors.

While for the first factor, the cost of solar energy had a significant decrement, it is fundamental to give attention to the last three factors.

As just written before, not only the European Union Parliament with the EPBD has established a goal to achieve Net-Zero Energy building standards in 2019, but also the California Public Utility Commission has set this requirement to apply to all new residential buildings by 2020 and all new commercial buildings by 2030 (Zero Net Energy, Action Plan: Commercial Building Sector, 2010-2012).

In this legislation and initiatives scenarios, urban planners, architects and engineers have a relevant role in the future, for contributing the success of net-zero energy strategies as design and retrofit buildings, or as very low energy use and implementation of solar energy systems and technologies for new and existing buildings. Their competence will become fundamental to achieve this goal especially during the early design phase because:

1. Are taken important decisions of buildings projects, such as orientation, shape, size of the openings which represent the first responsibility of the designers;
2. These decisions taken in this phase have the greatest impact on the durability and performance of any project [6].

As many design approaches for a high efficient buildings design presented in the literature, underline that the greatest advantages in terms of energy use depended upon decisions taken and verified in the first

phase of design [7]. In fact, the most important decisions are taken during the first few weeks of design, and they have a dramatic impact on the energy consumption of the building and its lifecycle cost [8].

#### *Internationalization of the research*

The research is framed in a wider international discussion on the topic of solar energy in urban areas. In fact as a member of the International Energy Agency Solar Heating and Cooling Programme (IEA SHC) Task 41, it had the possibility to develop the study starting from the suggestions and the topics provided from the meetings' discussions on solar energy in urban areas. Solar Energy and Architecture, gathered researchers and practicing architects from 14 countries (Australia, Austria, Belgium, Canada, Denmark, Germany, Italy, Norway, Portugal, Singapore, South Korea, Spain, Sweden and Switzerland) in the three year project whose aim was to identify the obstacles architects are facing when incorporating solar design in their projects, to provide resources for overcoming these barriers and to help improving architects' communication with other stakeholders in the design of solar buildings.

In details the objectives of Task 41 were:

- To support the development of high quality architecture for buildings integrating solar energy systems and technologies;
- To improve the competence of the architects and the communication skills and interactions between engineers, manufacturers, clients and architects.

The purpose is to increase the use of passive and active solar energy in buildings, in order to reduce the non-renewable energy consumption and greenhouse gas emissions.

To reach these goals, the work plan of Task 41 was organized onto three main subtasks:

- Subtask A: architectural quality criteria; guidelines for architects and product developers by technology and application for new product development.
- Subtask B: methods and tools for solar design, focusing on tools for early design phase and tools for the evaluation of integration quality of various solar technologies;
- Subtask C: Integration concepts and examples, and derived guidelines for architects [9].

#### *Urban-Scale energy models*

Nowadays for refining the prediction of the energy potential to utilise solar radiation in the urban context, good progress has been done. During these years were developed a computer method for producing irradiation histograms to identify the proportion of the urban surface (building façades and

roofs) for which photovoltaic solar systems may be viable [10]. This approach was applied to calculate both passive and active systems as well as daylighting technologies for specific urban surfaces [11] [12]. In literature is possible to find some other examples that permit to calculate the solar irradiation using similar techniques [13] [14] [15] (Figure 3).

The urban structures can have a significant influence on a building's energy consumption: the geometry of both the building and its urban context can influence the availability of passive solar gains and the daylight and furthermore can offset buildings' demands for heating and artificial lighting.

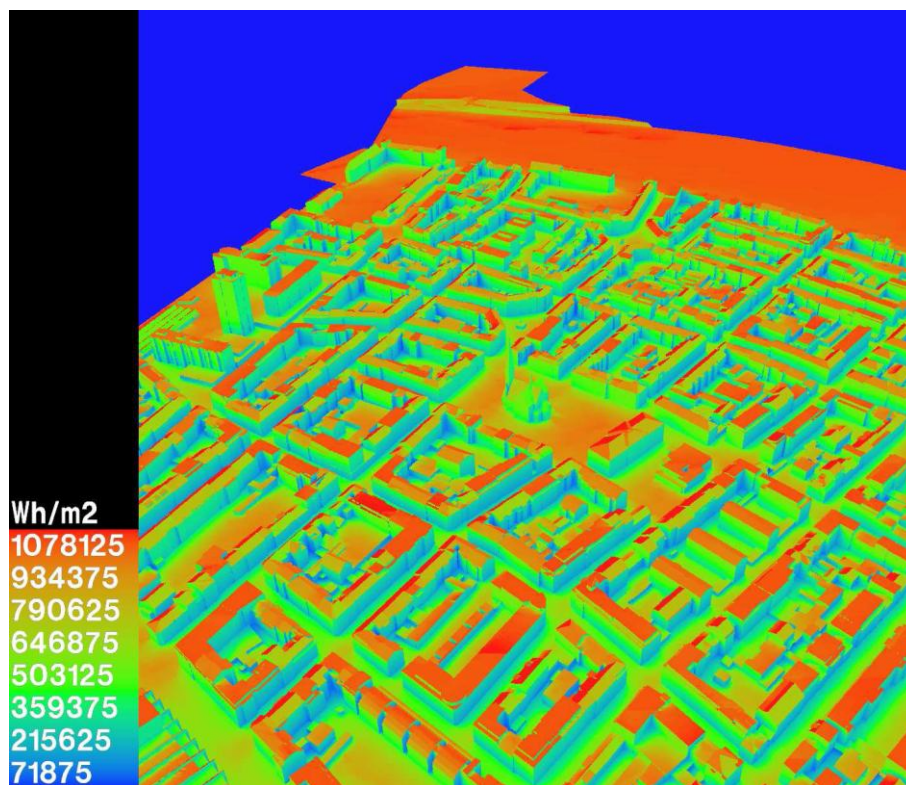


Figure 3. An annual irradiation image for the Matthäus district in Basel, Switzerland.

As known the solar radiation, utilizing appropriate technologies, can provide the hot water and electricity, but the issue in urban planning is the placement of the solar energy conversion technology. For analysing these aspects in complex urban environments, the irradiation images have been created, using the popular ray tracing software *Radiance* [16]. *Radiance* is the well-known ray-tracing program used to predict as precisely as possible the irradiation on buildings [16]. Set a scene of arbitrary geometric complexity, considering obstructions both to the sun and the sky due to the urban surrounding landscape, as well as reflected energy from this landscape, the *Radiance* backward ray-tracing tool can simulate radiant energy exchanges. *Radiance* is based on a virtual geometric model, characterized with grid-points and normal vectors on each surface in which a program called *rtrace* can calculate the incident irradiance

( $\text{W}/\text{m}^2$ ) given a sky radiance distribution and sun position and radiance. In *Radiance* specific text files [17] format are contained the virtual geometrical model and materials of the surfaces of the elements in the scene and one or more light sources. Was defined a cumulative sky [14], in order to compute the irradiation ( $\text{Wh}/\text{m}^2$ ). The sky is defined by 145 patches, Tregenza model, with corresponding cumulative radiance ( $\text{Wh}\cdot\text{m}^{-2}\cdot\text{sr}^{-1}$ ) in three channels (red, green and blue) for the corresponding shortwave part of the electro-magnetic spectrum. Thus with a single *Radiance* simulation is possible to simulate the irradiation during a chosen period for the analysis. This method to produce this irradiation ( $\text{Wh}/\text{m}^2$ ) allows to calculate the total irradiation ( $\text{Wh}$ ) harvested by each grid points ( $\text{m}^2$ ) of the building's surfaces. This procedure of irradiation's calculation is explained in Figure 4.

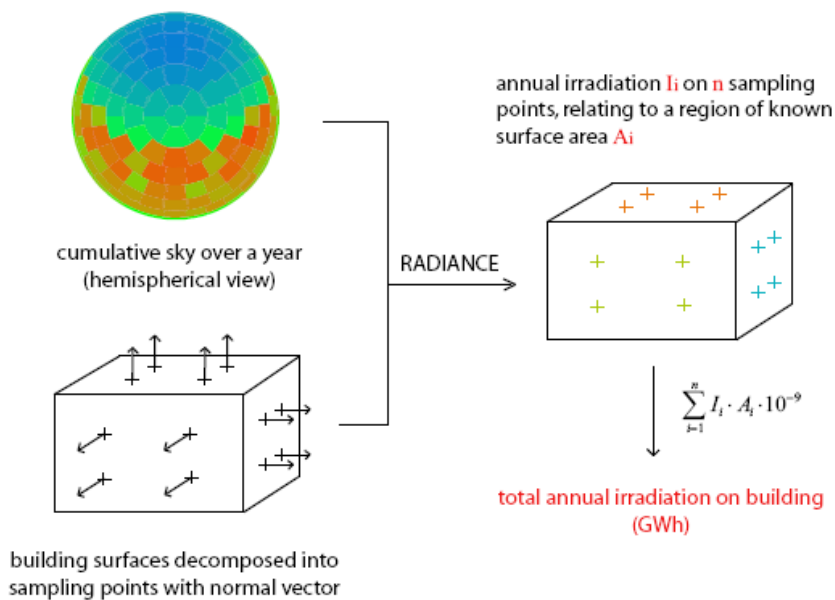


Figure 4. Principle of irradiation calculation using *Radiance*

The irradiation is supposed to be uniform in each measuring point corresponds to a sub-surface. The grid-points' distribution on the building surfaces should be uniform as possible for calculating the total irradiation with precision. Each patch's barycentre is an irradiance sensor: the precision of surface's subdivision in patches depends on the criteria of the subdivision, from the original surface's shape and from the grade of precision desired. In the Chapter 2 is presented a sensitivity analysis to find a compromise between accuracy and simulation computing time.

The sets of simulations run in this dissertation were conducted using *Daysim*: validated dynamic daylighting analysis software that calculates the annual daylight availability in arbitrary buildings based on the *Radiance* backward raytracer [18]. *Daysim* will widely describe in the Chapter 2.

Using this tool is possible to localize which are the most irradiative surfaces where is better to install the energy conversion systems [11] [19], as solar thermal collectors or photovoltaic panels, considering also the overshadowing effect created from the surrounding.

#### *Microscale climate models*

The forecasts of population growth and ongoing population movements indicate that the urbanization can only grow.

In this period characterized by global warming it is necessary to make attention on urban microclimate environment and on the thermal conditions outside. Furthermore the distribution of land-use and land-cover characteristics influences closely the receipt and loss of radiation of urban surfaces.

In order to reduce the global warming effect it should be better to increase the presence of vegetation, as trees, parks, green façades and roofs, in the urban environment. In fact their contribution allows to decrease the air temperature with three specific effects: shade, evapotranspiration and the effect of natural ventilation. Therefore the green spaces permit to store the heating and to humidify the atmosphere through evaporation: in this way is possible a significant air temperature's reduction. Furthermore in terms of protection from nuisance, the interests of vegetation are various: reducing air pollution and improving air quality by attaching some dust, decrease the effect of runoff by intercepting rainfall, protection against erosion due to wind and water.

The image and morphology of the neighbourhood and town is significantly influenced by the urban development projects and the microclimatic component can unite several actors as architect, urban planners, landscapes, political, developers, engineering firms in order to achieve the energy savings for improving thermal conditions of the urban spaces. The presence of vegetation act as a porous barrier for sun and wind and as a source of control the air temperature and the temperature of surrounding surfaces [20]. The benefits of green spaces depend on their density, shape, size and position. Furthermore the mitigation of air temperature in the presence of vegetation can be explained by the decrement of surface temperature that induces a lower air temperature [21].

All these climatic conditions have consequences on the behaviour of its inhabitants. The increment of surface temperature is caused by the absence of evaporative cooling created by the presence of paved surfaces such as asphalt. Consequently the high temperatures induce high radiative exchanges wavelength greater than in the case of surface plant.

Asphalt, concrete and granite, for these inert coatings nature, store heat during the day and return it during the night. These dark materials contribute to increase the effect of urban heat island. The presence of a park is an excellent factor able to mitigate the urban heat island and refresh the air and the choice of species is important because the quality of the shade of a tree depends on its density. In fact the foliage of a tree can filter from 60% to 90% of solar radiation and also reduce the solar radiation reflected by the

ground.. It should be better integrated the vegetation during the building's construction in order to improve the immediate environment of each constriction. The two important effects of vegetation are the shading effect of solar radiation and the maintenance of canopy temperatures between 20°C -35°C, below the temperatures of the surfaces of common urban materials such as asphalt, concrete blocks, etc. [22]. Furthermore the leafs can absorb 90% of UV.

To reduce the global warming of the air in an urban environment, the huge presence of green space and trees must be a priority. The reduction of urban heat island is based on the plans for green system, creation of parks and squares.

For studying the real impact of vegetation on air temperature, surface temperature and mitigation of urban heat island, microclimate simulations are necessary. To conduct these kind of analyses was chosen a three dimensional numerical tool: *ENVI-met*, of which there is a detailed description in Chapter 6.

Therefore in the second part of the research are discussed the thermal effects of urban green spaces and the use of vegetation for covering the buildings' roofs on the microclimate in the built environment, for various design scenarios and urban canyon geometries.

### **1.3. Objectives**

After the overview of the energy, the regulations and the urban models available, in this section are presented the main aims of the study.

The research is divided in two sections: the first section is focused on the solar potential in urban areas, the second on urban microclimate analyses.

The aims of the first section are:

- Maximize the solar access of a new building in existing urban areas minimizing the overshadowing on the nearby buildings;
- Optimize the building volume to exploit the solar radiation for producing energy from the building envelope;
- Develop a new approach for urban planners, architects and engineers for a conscious and sustainable solar urban design utilizing the available modeling and solar simulations tools;

While the aims of the second section are:

- Calculate the surface temperature of solar façades in various design scenarios in order to estimate the benefit of the green system in the urban environment;
- Calculate the average temperatures of an analyzed district in various design scenarios;

- Assess the improvements of microclimatic characteristics of cities in warm climate conditions by introduction of vegetation;
- Estimate the impact of vegetation in the urban environment by using a numerical modeling technique.

**SECTION 1**  
**SOLAR POTENTIAL IN URBAN AREAS**

## 2. Overshadowing and Solar Access

### Questions of the chapter

1. How is possible to reduce the overshadowing among the buildings?
2. How is possible to increase the solar access for a new building designed in the existing urban area?
3. Which are the effects of solar reflections coming from the surrounding, from existing buildings, from ground reflection and sky component, on a building? How can calculate their contributions?

### Abstract

The new Energy Performance Building Directive (2010/31/EU) requires that new buildings comply with the “nearly zero energy” standard by 2020: this means first of all a very high energy efficiency of fabric and services, and then the production of most of the remaining energy from renewable sources.

The sun is obviously the main renewable energy source for buildings, considering the large surfaces these typically expose towards the sky; prototype buildings exist, generating all the energy they need through photovoltaic or solar thermal panels. These examples are generally isolated buildings, but it should not be underestimated that the European trend in urban policies goes towards a reduction in the use of new land and the redevelopment of areas through demolition and rebuilding.

In the first part of the chapter is investigated what sort of influence energy issues can have on the design of new districts or buildings in urban areas, where the overshadowing by existing constructions can reduce the potential for solar energy production.

This is the beginning of a wider study aiming to provide a new design approach for the assessment of solar potential in urban areas: as a first step, simple models were analysed in order to understand energy needs versus potential energy production under different design conditions (height and size of buildings, distance between blocks, cladding materials, etc.) and then a real case study was assessed.

In the second part of the chapter is presented a new solar design tool that can be used to optimize the building’s shape and solar access in existing urban areas. The presented methodology was used in order to analysis a case study of the city of Surfers Paradise in Queensland, where in the past the urban and buildings development changed completely the morphology of the city. Since in the medium term the Zero Energy building will be the standard for new constructions, urban development should follow the Integrated Sustainable Design approach and the principles of solar design in order to exploit solar radiation using PV modules and solar thermal collectors in the building envelopes. The tool is based on Matlab algorithm and on *Radiance-Daysim*, a dynamic daylighting simulation tool.

The main aim of this chapter is the development of a new design approach for urban planners, architects and engineers in order to maximize the solar access and minimize the overshadowing on a new building in existing urban area.

## **2.1. Introduction**

Our cities have been undergoing continuous transformation and adaptation processes to adapt to demands from their inhabitants. Population growth on one side and environmental problems on the other, have created new demands, to which the city has to answer. In addition, the economic crisis has given another dimension to these complex problems. The built environment accounts for over 40% of the world's total primary energy use and for 24% of greenhouse gas emissions [23]. A combination of making buildings (new and refurbished) more energy-efficient and using a larger fraction of renewable energy is therefore a key issue to reduce non-renewable energy use and greenhouse gas emissions. At a global scale, political statements and directives are already aiming towards zero-energy buildings, communities and whole cities. In Europe, the recast of the Directive on the energy performance of buildings (2010/31/EU) requires that new buildings comply with the “nearly zero energy” standard by 2020 [23]: this means first of all a very high energy efficiency of fabric and services, and then the production of most of the remaining energy need from renewable sources [24] [25]. Although the standard definition of a nearly zero energy building is still under discussion, it is clear that the aim of the Directive is about reconciling the energy need of the building with the amount of energy that can be sourced on (or near) the site. Some existing buildings prove the feasibility of scenarios where the energy used for heating and cooling is offset by the yearly production of renewable solar energy [26]. Nonetheless, these buildings are generally isolated prototypes, and low-rise buildings with optimal solar exposure. On the other hand, most of the world's population is living in dense urban areas [27], where the orientation, availability of surfaces exposed to the sun and the overshadowing conditions can be far from optimal. The question of a correct urban design, that takes into account the growing problem of energy self-sufficiency of buildings, then arises.

Nowadays more than three-fourths of the world's population lives and works within cities, where up to 80% of all available energy is consumed and over half of greenhouse gas emissions are produced [28], so the improvement of the energy efficiency of cities is central to the de-carbonisation of economy. A new approach is then required to design new buildings with particular attention to volume, shape, orientation and with larger use of the renewable sources integrated in the envelope, paying attention to the relationship between the building and its urban context.

Of course, cities are complex organisms, whose growth and regeneration depend on a large number of factors: the places we know today derive from a continuous transformation process since their foundation. Their survival relies upon continuous adaptation and transformation to fulfil the demands of their citizens. Urban design and strategic choices about the regeneration of cities and districts require subtle approaches, taking into account multiple, independent factors that can hardly be simplified.

Nonetheless, the problems of energy efficiency cannot be underestimated: on the one hand, to maximise the solar potential of buildings or whole districts in view of 2020 requirements; on the other, to

consider the effect that new constructions or changes to the existing urban fabric can have on the energy performance of existing buildings. Tall buildings, or the modification of building masses, can lead to overshadowing and thus to a reduction of potential energy production or a worse energy rating if the buildings rely largely upon passive solar gains.

This chapter investigates some basic aspects of the relationship between urban design and solar potential of buildings. The analyses of simple models allow the energy needs' assessment and the calculation of potential energy production under different design conditions (height and size of buildings, distance between blocks, cladding materials, etc.).

Some studies have already been developed about the influences of urban design on the availability of renewable energy. Most of the available examples analyse the solar potential of current situations performing energy calculations of buildings with solar thermal collectors and/or photovoltaic panels installed on the roof of the buildings [29] [30]. A few studies use simulation software to optimize building designs in terms of cost [31]. Some examples, like *ENVI-met*, simulate the surface-plant-air interactions in urban environment; others analyse the energy efficiency of solar roofs or solar façades with software like *Trnsys* [32] and *Energyplus* [33]; others map the solar potential of roofs with *GIS* tools [34]. No studies appear to be available about solar optimized design balancing the energy demand of a new inner-city district and its effects on the nearby existing buildings. Moreover it is not easy to find studies about the optimization of energy request and energy production in existing districts and related new developments, evaluating also the effects inside and outside the area. However there are a few studies about urban form, density and use of solar energy [35].

Different researches [36] [37] demonstrate that the zero energy annual balance can be reached, with a combination of a conscious design strategy, good performance of the building envelope, and exploitation of energy from renewable sources, such as photovoltaic systems, to reduce the environmental impact and secure future supply of energy [25] [24].

However, if the feasibility of energy autonomy and optimized use of renewable sources has already been demonstrated for isolated buildings, the implications of energy efficiency and of mutual relationships among buildings in neighbourhoods are still to be fully understood.

This research work investigates the relationship between urban morphology and energy consumption, knowing that the energy efficiency of cluster of buildings is completely different than the performances of isolated ones.

This chapter sketches out some new basic design principles suggesting the use of a tool to support the use of solar energy as one of the measures that can improve the energy efficiency of districts.

## **2.2. Material and method**

As was said at the beginning, this chapter is divided onto two parts.

The first part treats the analysis on simple models conducted with Autodesk *Ecotect Analysis* [38] in order to study an analytic relationship between the solar radiation and heights or distance among the buildings. At the end of the first part is presented a case study of the city of Milan (Italy) where was applied the regulations studied in the simple models in order to improve the solar radiation on the new building designed guaranteeing the solar access of the neighbourhood buildings.

In the second part of the chapter is presented a new solar design tool development with Matlab [39] in order to optimize the exposure of two isolated buildings to harvest as much solar radiation as possible from the building façades and to study the influence of overshadowing created by one building on the opposite façade of the other. This tool was used to optimize the new volumes of the buildings of Surfers Paradise's downtown in Gold Coast (Australia) for maximizing the direct solar radiation on the façades.

### **2.2.1. First part: simple models analysis and case study of Milan**

Regarding the first part of the study presented in this chapter the specific objectives are:

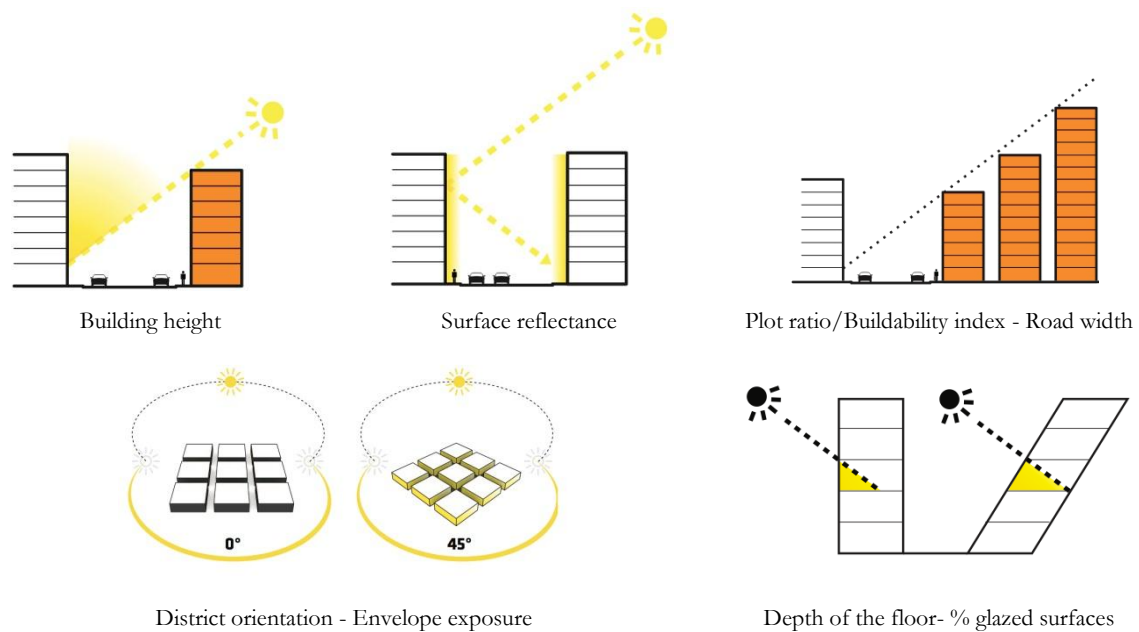
1. Optimization of the shape of the building with respect to solar access and the existing urban context;
2. Organization of the building volume to maximise solar exposure and minimize thermal losses;
3. Evaluation of the solar potential of the building, applying the concept to a case study: comparison of current situation, actual design situation and solar optimized design situation.

The analysis focuses on the availability of solar radiation on the building façades, while the roof is considered separately. The reasons for this choice are manifold. First of all, in relatively tall buildings, the amount of roof space per apartment floor area is relatively limited and can then produce just a limited portion of the energy need of the building. Second, the roof surface has often to be shared among different concurrent functions (services, shafts, terraces, etc.) thus limiting the potential for the installation of solar panels. In dense urban conditions, then, it may be sensible to explore the potential of other exposed surfaces, such as façades, although their orientation and tilt are not optimal for solar energy production over the year.

As a first step, the study will show that through analyses related to different technical aspects it is possible to maximise solar access, solar exposure and energy production using the building envelope. These analyses are carried out on simple models with the aim of finding analytic relationships among the design inputs. The analysis criteria are:

- a) Solar radiation: analysis of solar radiation and shadows on the building envelope during the year;
- b) Building orientation: analysis of solar exposure and adequate distance between buildings and streets;
- c) Envelope exposure: study of the adequate façade orientation to maximise solar gains and energy production;
- d) Shadows: analysis of overshadowing of the neighbouring buildings due to new constructions;
- e) Urban density: analysis in different existing situations – low, medium and high density.

The analysis parameters are presented in the figures below.



All analyses were conducted using cumulative insolation in the solar access analysis: were always done annual simulations in order to calculate the solar direct radiation on the building envelope. It is possible to display the distribution and availability of solar radiation over an entire building or even a city blocks. This can be particularly useful when considering shading requirements or assessing the best areas to install photovoltaic panels in order to maximize the solar radiation.

The analysis calculates the variation of incident solar radiation on a surface divided into smaller subdivision, choosing the size x, y and z of the cells and defining the time of simulation. *Autodesk Ecotect Analysis* calculates the incident solar radiation using the settings specified.

The analysis on the case study was conducted in the same way regarding the calculation of incident solar radiation, but the optimization of the designed building was done with the shading design tool using

the solar profiling to generate the maximum solar envelope for designed building. Once upon a time that was chosen the heights of the nearby buildings which don't want to overshadow, the tool draws a line of cut's projection in the volume of designed building along a solar angle that permit to guarantee the solar access of the buildings behind the designed one as shown in Figure 5.

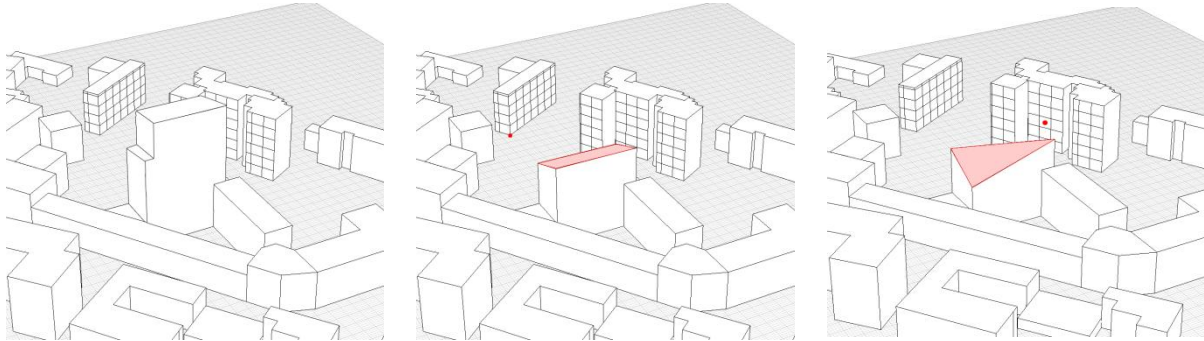


Figure 5. Process of shading solar on designed building using the solar profiling and solar angle.

After this operation the volume of designed building was organized in a different way that the actual design situation. The Figure 6 shows the comparison among, current scenario, the actual design scenario and the solar optimized one.

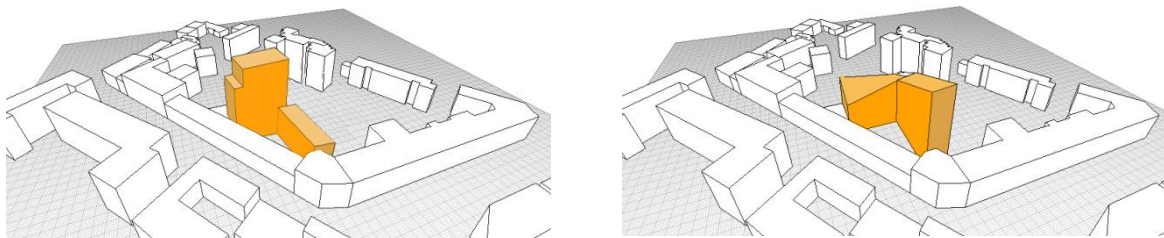


Figure 6. Actual design scenario (on the left) and Solar optimized design (on the right) with designed building in orange

### **2.2.2. Second part: SolarPW tool and case of Surfers Paradise**

Starting from the world scenario described previously, the study in the second part of the chapter gives indications about the influence by building and façade on the total amount of solar radiation (direct, diffuse, reflected) incident on the external building envelope.

Optimizing the shape of buildings in the district morphology may in fact lead to increased energy production from integrated solar systems. The influence of the distribution of volumes on the overshadowing among buildings and on solar access has been assessed and validated through different tools. In the preliminary analysis, *Autodesk Ecotect Analysis* [38] was used to study the overshadowing

effect. In the second part of the study, *Daysim* [40], a dynamic daylighting simulation tool, was used to evaluate global solar radiation incident on the building envelope and its increment or decrement with respect to the optimized shadowing conditions.

The process of optimization is the result of the use of new solar design tool, The Solar Potential poWer tool, called Solar PW.

The tool is a Matlab algorithm developed, in order to evaluate the distribution of shadows on the façades of the building and the organization of the building volumes for maximizing the direct solar radiation.

The program uses an existing sun position algorithm available in the literature [41], based on numerical approximations of the exact equations for sun position. The input entries were represented by the location data (latitude, longitude, altitude, year, UTC time) and the geometrical characteristic of the reference buildings (width, height of buildings, distance between buildings). The program outputs are the shadows' graph on the façade of the analysed buildings.

These analyses, done with Solar PW, were performed on an area of the coastal city of Gold Coast, Surfers Paradise, located in the South East of the Queensland state, Australia. Surfers Paradise is the second most populated city of the state [42], with a growing amount of population. The conspicuous morphological feature of Gold Coast, as well as other cities in South Eastern Queensland, is a dispersed and diffused pattern, with high-rise buildings in the strip close to the sea.

## **2.3. Theory and calculation**

In this section are described the tools used for the solar radiation analyses, their limits and the comparison between them in order to justify the use of the software used and give an overview about their characteristics.

### **2.3.1. Description of the solar analysis tool: Ecotect**

All analyses of the first part of the chapter were done using *Autodesk Ecotect Analysis*.

In the Subtask B of the IEA Task 41 was done a state of art of the existing solar tools available and used by architect, urban planners and engineers. The description reported below summarized the characteristics of *Autodesk Ecotect Analysis* reported in the deliverable of the Subtask B [43].

*Autodesk Ecotect Analysis* was developed by Dr. Andrew Marsh and Square One Research Limited. In June 2008, the rights of the program were acquired by Autodesk.

### Functions

*Autodesk Ecotect Analysis* is a graphical building and environmental analysis tool. The program utilizes 3D models imported from CAAD-BIM predecessor software, but also allows for the direct creation of models with *Autodesk Ecotect Analysis*'s integrated drafting tools. *Autodesk Ecotect Analysis* can perform a large number of different analyses within a 3D model, including shadows and reflection analysis, shading design, solar analysis, lighting design, analysis of views and light and more others.

### 3d Modeling

*Autodesk Ecotect Analysis* can perform analyses of varying complexity based on simple or detailed CAAD-BIM models, and is therefore suitable for most design stages. The tool particularly focuses on supporting decision making in early design phase.

### Import/export

Export is supported to *Radiance* (ray-traced rendering), POV-Ray and .wrl, .dxf (compatible with most CAAD software), EnergyPlus, DOE-2/eQUEST and SBEM for detailed energy simulations as well as AIOLOS and HTB2.

*Autodesk Ecotect Analysis* also supports the export and import of data to several computational fluid dynamics (CFD) tools such as NIST-FDS, Fluent and WinAir4. Coupled with climate data files containing average wind data, this allows the program to analyse airflow both through and around buildings or complex urban environments.

*Autodesk Ecotect Analysis* is intended as a conceptual design tool. The program therefore only requires a minimum of input data in order to perform initial sun shading studies and preliminary assessments. As the design process continues, the amount of data input into the model can be increased, allowing acoustic and thermal simulations and resource modeling.

### Actual solar calculation

*Autodesk Ecotect Analysis* uses the integrated climate data files to correctly calculate solar positions and incident radiation.

The program uses this data to generate daily and yearly sun path diagrams and shading tables, shadows and shadow range diagrams for indoor and outdoor locations, reflection analysis and interactive visualization/shadow generation. Shading design tools can generate the exact shading shape to perfectly shade a window for any specified period as well as modeling light redirection systems. Solar analysis

diagrams can be generated to visualize incident solar radiation on all surfaces of the model, assisting in identifying optimum positions for solar collectors and other solar energy components. Solar availability can also be calculated at an urban level.

Using solar access analysis, the amount of solar radiation incident on any object can be calculated. Combined with total annual radiation, this can assist in determining the best position and orientation for active solar components. The tools also allow the calculation of the solar radiation incident on any solar collector, making it possible to estimate likely energy production through the year.

### **2.3.2. Description of the solar analysis tool: Daysim**

From the same deliverable presented above [43], written in the Subtask B of the IEA Task 41, about the state of art of the existing solar tools available and used by architect, below is reported an overview of *Daysim advanced daylighting simulation software*.

*Daysim* is a *Radiance*-based backward raytracer daylighting analysis tool that has been developed at the National Research Council of Canada in collaboration with the Fraunhofer Institute for Solar Energy Systems in Germany. The actual version of *Daysim* is called version number 3.1 b.

#### Functions

While *Radiance* has been initially developed to simulate luminances and illuminances under selected sky conditions or under artificial lighting systems, *Daysim* uses the *Radiance* simulation algorithms and the daylight coefficient method to efficiently calculate illuminance distributions under all appearing sky conditions in a year (dynamic simulation) [44].

The task of a daylight simulation algorithm is to predict indoor illuminances and luminances at a particular point (or at a particular sensor) in time step, based on a 3D building model and the sky condition at this point in time.

#### Design

*Daysim* is available software for architects, engineers and researchers that permits to assess the daylight contribution in a building during the design phase. The combination of flexibility (due to the *Radiance* engine) and accuracy makes it a good tool for assessing the daylight autonomy, daylight level or annual irradiation on a defined sensor. For this reason, *Daysim* can also be used to predict the incident radiation on a photovoltaic panel or a thermal collector but the program is not suited for sizing these components taking into account the mechanical or electrical systems.

### 3D modeling

The input required for a simulation in *Daysim* is a description of the 3D surface geometry, materials (optical properties), and light sources in a scene. For carrying out a time-series simulation within *Daysim*, additional specifications for the sensors grid (x,y,z coordinates and x,y,z directions) are required.

### Coordinates

*Daysim* 3D model, as in *Radiance*, is performed according to x, y and z axes. The right hand system of coordinates is used for the surface orientation. The coordinates can be given in any unit of length.

### Import/export

To perform a simulation with *Daysim Radiance*, two input files are required: the building geometrical model and the weather data file. The description of a building for a daylight simulation requires a 3D model of the building which contains information on the geometry of the building and its surroundings as well as optical properties of all material surfaces (e.g. RGB, red green blue, reflectance, specular reflectance, roughness, etc.). CAD modelers are used to create two or three dimensional virtual models of a building. Several tools exist to convert .dxf or .dwg files together with .3ds files into .rad description files [[www.schorsch.com/download/radiance.html](http://www.schorsch.com/download/radiance.html)]. It is also possible to easily export *Radiance* or *Daysim* files using *Autodesk Ecotect Analysis*.

### Actual solar calculation

As mentioned above, *Daysim* is based on the *Radiance* engine. *Daysim* results tend to be very similar to *Radiance* classic results especially under overcast sky conditions. *Daysim* is a program specifically dedicated to daylight utilization studies i.e. estimate daylight autonomy and replacement potential of electric lighting by daylighting. It does not specifically calculate solar gains through windows or allow sizing photovoltaic and thermal installations although part of the results might be used with some creativity in the process of planning other solar aspects.

### Radiance simulation parameters

*Radiance* is a backward raytracer, i.e. light paths are traced backward from the spectator's eye to the light sources. In principle, forward raytracing could be employed just the same, but for a great number of scenes the former approach is more economical considering the required calculation times. The *Radiance* simulation parameters are a set of parameters that can be individually set for each simulation. The parameters guide *Radiance* how to carry out a simulation. The most intuitive parameter is the number of "ambient bounce" (ab). The parameter instructs *Radiance* how many surfaces a ray can bounce of or

transmit through before it is discarded by *Radiance*. A detailed description of all simulation parameters for the *Radiance* program “rtrace” are described under [45].

- Ambient bounces (ab): This parameter describes the number of diffuse inter reflections which will be calculated before a ray path is discarded. An ab-value of 5 is already sufficient for a standard room without any complicated façade elements.
- Ambient division (ad) and ambient sampling (as): The ad-parameter determines the number of sample rays that are sent out from a surface point during an ambient calculation. This parameter needs to be high if the luminance distribution in a scene with a high brightness variation. An ambient sampling parameter greater than zero determines the number of extra rays, that are sent in sample areas with a high brightness gradient.
- Ambient accuracy (aa) and ambient resolution (ar): The combination of these two parameters with the maximum scene dimension provides a measure of how fine the luminance distribution in a scene is calculated. According to page 385 in *Rendering with Radiance*, the combination of aa=0.1, ar=300 and a maximum scene dimension of 100m yields a minimum spatial resolution for cached irradiances of:

$$\text{ambient resolution} = \text{maximum scene dimension} \times \text{ambient accuracy}$$

- Direct threshold (dt): This option switches off the selective source testing, i.e. each light source is equally considered during each shadow testing. This option is automatically set to zero when direct daylight coefficients are calculated using *Daysim*.
- Direct sub sampling (ds): This option switches off the direct sub sampling threshold, i.e. only one ray is always send into the centre of each light source. As during the calculation of the direct daylight coefficients only solar discs with an angular size of 0.5 are present, disabling direct sub sampling speeds up the calculation without impeding its accuracy.

#### Weather data sources

To describe the annual amount of daylight available inside a building, it is usually need to know the amount of solar radiation at the building site over the course of the year. This kind of information is usually provided in the form of test reference years (TRY). TRYs provide typical annual profiles of exterior climate data such as ambient temperature, wind direction and velocity, precipitation and direct and diffuse irradiances. The time step is usually one hour. An excellent free source of TRYs is the US Department of Energy’s website [46]. The site provides hourly climate data for over 660 locations

worldwide (.epw format). *Daysim* directly imports .epw files and extracts the information required for an annual daylight simulation (global horizontal radiation and diffuse radiation or direct and diffuse radiation). The other information in the header file that are automatically extracted by *Daysim* for an annual daylight simulation are the name of site, time and date, latitude, longitude, altitude, time zone, direct, and diffuse irradiances [45].

Using the Perez sky model these irradiances are first converted into illuminances and then into a series of sky luminous distributions of the celestial hemisphere for all sky conditions of the year. All of these calculations are carried out in the background without requiring any further user input.

The climate data files used for the simulations conducted with *Daysim* are:

- Brisbane’s weather data for Surfers Paradise’s case study (AUS\_QLD.Brisbane.945780\_IWEC.epw);
- Milan Malpensa’s weather data for Milan’s case study (ITA\_Milano-Malpensa.160660\_IGDG.epw).

The Australian’s weather data sources are RMY Australia Representative Meteorological Year Climate Files. They are developed for the Australia Greenhouse Office for use in complying with Building Code of Australia. These data are licensed through ACADS BSG Ltd for use by EnergyPlus users [46].

The Italian’s weather data sources are the Italian Climatic data collection “Gianni De Giorgio” (IGDG). They are developed for use in simulating renewable energy technologies, this set of 66 weather files is based on a 1951-1970 period of record. The data were created by Professor Livio Mazzarella, Politecnico di Milano, and is named in honor of Gianni de Giorgio [46].

### *Sky models*

As written before *Daysim* is a dynamic daylighting simulation: dynamic in this context means that is variable with the time due to changing sky conditions and shading device settings, in contrast to static modeling [47].

Dynamic daylight simulations yield annual time series of illuminances under changing sky conditions. Such annual illuminance profiles can be used to calculate daylight performance indicators such as the energy saving potential of different lighting and shading control strategies, annual light exposure, and the daylight autonomy. *Daysim* is a simulation tool that efficiently calculates annual illuminance/luminance profiles [45].

The choice of the sky model is usually done among the “old” CIE overcast and clear skies. For daylight factor calculations, the CIE overcast sky is particularly used. This CIE overcast sky model has a limitation that its input is limited to a single scaling factor on a fixed distribution. This limit has been analysed in a study conducted before [48] that compares different dynamic *Radiance*-based daylight

simulation methods, the ones based on the CIE sky model performed consistently worse than methods based on the all weather conditions Perez sky model [49].

In Perez sky model all inputs including hourly time series of direct and diffuse irradiances for all sky conditions. This latter aspect is important for conducting an annual analysis on a building performance.

The Perez all weather sky luminance model has been developed in the early nineties by Richard Perez et al. and requires date, time, site and direct and diffuse irradiance values to calculate the sky luminous distribution for a given sky condition. The model consists of two independent models [45]:

- The Perez luminous efficacy model calculates the mean luminous efficacy of the diffuse and the direct sunlight for a considered sky condition. Input parameters are the solar zenith angle, solar altitude, direct and diffuse illuminances as well as the atmospheric precipitable water content.
- The Perez sky luminous distribution model yields the sky luminous distribution based on date, time, direct and diffuse illuminances. The model comprises five parameters which influence the darkening or brightening of the horizon, the luminance gradient near the horizon, the relative intensity of the circumsolar region, the width of the circumsolar region and the relative intensity of light back-scattered from the earth's surface.



Figure 7. Bright overcast sky conditioned for Freiburg, Germany on January 1st at 10:00 am simulated with Perez (on the left) and CIE overcast (on the right).

The comparison of two sky model reveals the superiority of the Perez sky model compared to the CIE model. Figure 7 in fact shows that while in the Perez sky model are well distinguished the dark and bright overcast part of the sky and provides some details in the sky luminous distribution, instead the CIE overcast sky is rotationally invariant.

The correct modeling of overcast skies is a fundamental quality aspect of a sky model, as in many densely populated areas worldwide more than half of all appearing sky conditions are overcast. For very dark or bright sky conditions the Perez sky model reduces to the CIE overcast or clear sky.

#### *Definition of sky and solar division scheme*

The sky and solar division scheme for a dynamic daylight simulation tools are distinguished between contributions from various luminous sources, as follows [47]:

- 145 diffuse sky segments
- 1 diffuse ground segment
- 145 indirect solar positions
- 2305 direct solar positions

Daylight coefficients corresponding to each segment or position can be coupled with a sky model, e.g. the All Weather Perez model (1993), as described in eq. 1:

$$E = \sum_{\alpha=1}^{145} DC_{\alpha}^{sky} L_{\alpha}^{sky} S_{\alpha}^{sky} + DC_{\alpha}^{gr} L_{\alpha}^{gr} S_{\alpha}^{gr} + \sum_{\alpha}^{145} w_{\alpha}^{isun} DC_{\alpha}^{isun} L_{\alpha}^{isun} S_{\alpha}^{isun} + \sum_{\alpha=1}^{2305} w_{\alpha}^{dsun} DC_{\alpha}^{dsun} L_{\alpha}^{dsun} S_{\alpha}^{dsun} \quad \text{eq. 1}$$

Diffuse sky contributions

The first part of eq. 1 represents the diffuse contribution from the sky, necessitating a one-to-one mapping of 145 diffuse sky daylight coefficients to 145 diffuse sky segments. While the original division scheme [50] divided the hemispheres into circular sky segments with a cone opening angle of 10.15°, as shown in Figure 8 (on the left), the *Daysim* approach, illustrated in Figure 8 (on the right), of rectangular sky segments that completely cover the celestial hemisphere without any overlap, i.e. no rays hitting the hemisphere are ever discarded or double counted. The centres of the rectangular segments correspond to the centres of the original Tregenza circular segments [47].



Figure 8. Sky division schemes: (on the left) according to Tregenza: 145 sky segments with a cone opening angle of 10.15°, with 68% of the celestial hemisphere covered by sky segments; (on the right) continuous division, as used by *Daysim*

Diffuse ground contributions

The second daylight coefficient in eq. 1 represents the total diffuse contribution from the ground, simulated as a single daylight coefficient matching the entire ground hemisphere surrounding a building scene. If no surrounding landscape is simulated, the actual diffuse ground contribution is calculated as a function of average ground albedo. While it is highly recommended to explicitly model the surrounding landscape as part of the building scene [51] [52], the ground daylight coefficient has been added to avoid bookkeeping errors caused by downward rays that may miss the simulated ground plane, notably near the horizon. Such rays can lead to substantial simulation errors especially for ceiling mounted photocell controls [48].

#### *Solar contribution*

In the past, daylight coefficient methods mostly differed in how they treated contributions from direct sunlight. *Daysim* defines a set of around 65 representative, latitude-dependent solar positions that form a grid amongst all possible solar positions throughout the year. The positions nearest to the horizon are set by default at a minimum altitude of 2°; below which sky conditions cannot be adequately captured [53], given the significance of local effects of the atmosphere and surrounding landscape.

#### *Indirect solar contributions*

Similarly to daylight coefficient methods [54] [55], dynamic daylighting simulation considers indirect and direct solar contributions separately, as presented in eq. 1. The indirect contribution comprises only solar rays that are reflected off surfaces, while the direct contribution consists only of the direct beam of sunlight that hits a sensor, excluding all reflected contributions. *Daysim* distributes 145 indirect solar positions across the hemisphere; more precisely at the centre of each of the 145 diffuse sky segments.

#### *Direct solar contributions*

For direct solar contributions, i.e. excluding all reflected rays, set solar positions are also evenly distributed across the hemisphere, yet with greater spatial resolution than for indirect contributions. This higher resolution stems from a desire to increase the accuracy of direct solar daylight coefficient methods, notably for sensors often subjected to sudden changes in solar exposure, e.g. in an urban canyon or if located far from a window, as a result of the ever-changing shadow patterns cast from the sun.

As with indirect contributions, the resulting direct solar daylight coefficients are latitude and orientation independent. The 2305 positions are obtained by quadrupling the original number of Tregenza horizontal rows of sky segments, then quadrupling the original number of Tregenza segments per row, while keeping a single zenith position<sup>4</sup>. Altogether, the proposed standard defines 2596 daylight coefficients per sensor for a given setting, 89% of which describe direct solar contributions. Details on the distribution and on how to increase the default resolution are provided in Appendix A.

### 2.3.3. Comparison of solar irradiation tools

In literature is possible to find several approaches that have been developed to date to model monthly or annual solar irradiances with different results in terms of time cost and numeric accuracy and they have been compared each other. In particular the study conducted by Diego Ibarra and Christoph F. Reinhart [56] compares six solar distribution calculation methods (*Daysim* Daylighting Simulation and Dynamic Daylighting Simulation, GenCumulativeSky, *Ecotect* Points and Tiles, Manual Method in Excel) of increasing complexity in two comparison cases: unobstructed and obstructed. Furthermore in the study are compared the different calculation approaches accounting for solar angles, time series and sensor-grid orientations.

Methods are analysed in terms of their numeric accuracy, reliability and appropriateness for application in architectural practice. The simulation have been done on two set of simulations on The Bank of America Tower in New York City (One Bryant Park, New York, NY): the first considering unobstructed building and the second on a complex urban environment with south facing sensors.

Considering the unobstructed case the Table 2 shows a comparison of total annual irradiances by sensor orientation for all six methods studied in contrast with measured data. Table 3 shows the Mean Bias Errors (MBE) and Root Mean Square Errors (RMSE) for all monthly irradiances. Table 4 describes passive heating seasonal performance.

In general terms the comparison shows reasonable correlations between the measured data and all the methods tested for all orientations. However, *Ecotect* Points also reported a strong error on the South orientation. *Daysim* DS method reports the lowest absolute error.

*Daysim* DS method reports the lowest absolute error, MBE and RMSE for South and West orientations.

Error values are somewhat higher on the North orientation as a result of a small under-estimation on low-rising direct beam contributions during early morning for the summer months. The same difficulties of accurately accounting for very low sun altitudes explains most of the discrepancies found during summer months on East and West. This can be attributed to limitations of the Perez All-Weather sky model used by DS and DDS -s to accurately simulate sky conditions at solar altitudes bellow 2°.

For total annual irradiances on the South façade *Daysim* methods are most accurate, reporting a 0.2% and a 0.7% MBE, and a 21% and 28% RMSE for DS and DDS -s respectively. In contrast, *Ecotect* Points results in an important 8.5% over-prediction and *Ecotect* Tiles in a -10.4% under-prediction.

However, what is most relevant is the low MBE 0.8% but extremely high RMSE 518%. *Ecotect* Points completely missed the monthly irradiance profiles, reporting a -55.5% under-prediction in January and an 85.9% over-prediction in July [56].

Table 2. Relative error for annual irradiation for all simulation methods by orientation.

Distribution Method	North		East		South		West		Horizontal	
	Absolute Error [kWh/m <sup>2</sup> ]	Relative Error [%]	Absolute Error [kWh/m <sup>2</sup> ]	Relative Error [%]	Absolute Error [kWh/m <sup>2</sup> ]	Relative Error [%]	Absolute Error [kWh/m <sup>2</sup> ]	Relative Error [%]	Absolute Error [kWh/m <sup>2</sup> ]	Relative Error [%]
Measured Data	234	reference	584	reference	798	reference	562	reference	1162	reference
Excel	98	41.9	-76	-13.1	-37	-4.6	107	19.0	-144	-12.4
Ecotect Points	112	47.7	42	7.2	68	8.5	23	4.2	-52	-4.5
Ecotect Tiles	44	18.9	6	1.0	-83	-10.4	-70	-12.4	-62	-5.3
GenCumulativeSky	-2	-0.8	10	1.8	30	3.7	34	6.1	-9	-0.8
Daysim-DS	-12	-5.0	-22	-3.8	-6	-0.8	-11	-1.9	-61	-5.3
Daysim DDS -s	-18	-7.8	-31	-5.4	-12	-1.6	-11	-1.9	-58	-5.0

Table 3. MBE and Relative RMSE for monthly irradiations for all simulation methods by orientation

Distribution Method	North		East		South		West		Horizontal	
	RMSE [%]	MBE [%]	RMSE [%]	MBE [%]						
Measured Data	reference	reference								
Excel	564	47.0	169	-14.1	82	-5.3	297	24.7	6	-0.5
Ecotect Points	589	49.1	111	6.9	518	0.8	47	3.3	48	-4.0
Ecotect Tiles	258	21.5	196	-16.3	130	-10.8	112	8.0	49	-4.1
GenCumulativeSky	24	-0.5	32	1.2	73	4.0	101	8.4	16	-0.9
Daysim-DS	45	-3.4	57	-3.9	21	-0.7	47	0.2	59	-4.9
Daysim DDS -s	73	-6.0	70	-5.8	28	-1.3	50	0.7	54	-4.5

Table 4. Relative error for passive heating season irradiation for all simulation methods by orientation

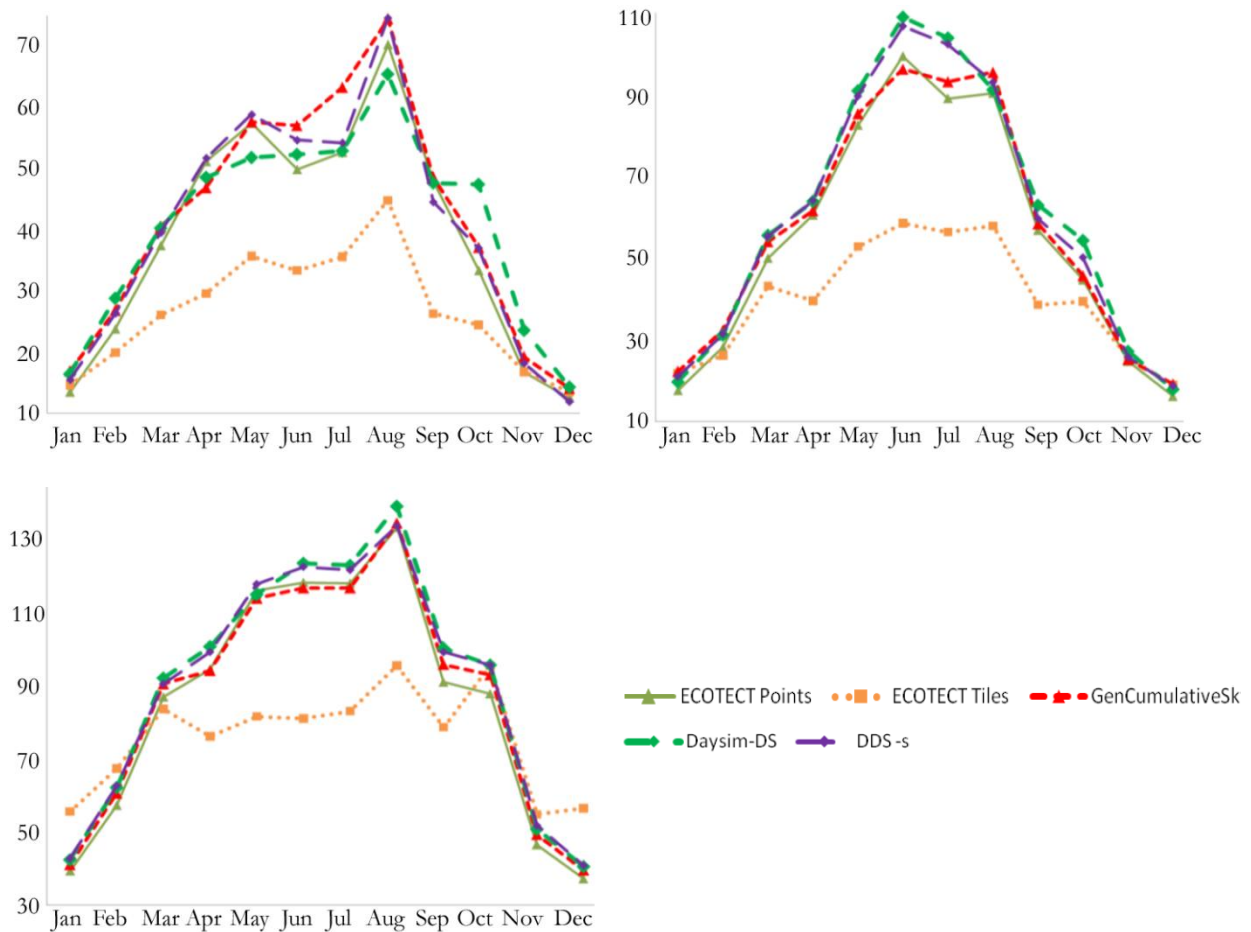
Distribution Method	North		East		South		West		Horizontal	
	Absolute Error [kWh/m <sup>2</sup> ]	Relative Error [%]	Absolute Error [kWh/m <sup>2</sup> ]	Relative Error [%]	Absolute Error [kWh/m <sup>2</sup> ]	Relative Error [%]	Absolute Error [kWh/m <sup>2</sup> ]	Relative Error [%]	Absolute Error [kWh/m <sup>2</sup> ]	Relative Error [%]
Measured Data	reference	reference								
Excel	56	46.9	-36	-12.3	-26	-5.5	63	23.6	-2	-0.4
Ecotect Points	57	48.0	16	5.4	-68	-14.4	10	3.6	32	-5.7
Ecotect Tiles	26	21.8	-52	-17.9	-52	-11.0	29	10.9	-25	-4.5
GenCumulativeSky	-2	-1.7	3	1.2	32	-6.9	22	8.3	-6	-1.2
Daysim-DS	-5	-4.6	-10	-3.6	2	-0.4	22	8.3	-27	-4.9
Daysim DDS -s	-9	-7.3	-16	-5.7	1	0.2	0	0.0	-26	-4.7

Regarding the a simulation on a complex urban environment Table 5 shows the absolute error (kWh/m<sup>2</sup>) and relative errors (%) for annual irradiancies for South facing sensors located on the building's facade at heights of 2.0m, 100m and 220m from the ground plane.

Table 6 shows MBE and RMSE for all methods and Table 3 and Table 7 show errors for cooling and heating season respectively.

All methods, except for *Ecotect* Tiles, result in reasonable predictions for the "unobstructed" sensor at 220m high (relative error < 6% and MBE < 6%). *Ecotect* Points somewhat underpredicts irradiancies for the 2.0m and 100m sensor, but still remains bellow a 10% MBE. All *Radiance* based methods maintain the accuracy even at the lower sensor points (MBE < 4%). However at 2.0m the RMSE for all methods rises above 100%. This can be somewhat expected in such a complex scene. At such a low elevation and with tall surrounding buildings small discrepancies in direct beam and diffuse contributions due to specific solar positions make an important difference.

Graph 1. Comparison of monthly vertical irradiancies at 2.0m (on the left) at 100m (on the right) and at 220m (on the bottom) of elevation (kWh/m<sup>2</sup>/annum).



The 100m elevation is the one most affected by surrounding buildings with a high variability of direct beam and shaded areas. As a result the different approaches used to account for direct beam within the *Radiance*-based methods produce different irradiation predictions. The cumulative sky patch approach of GenCumulativeSky reports a 3% MBE and 93% RMSE in contrast with the more accurate DDS -s which reports a 1% MBE and a 37% RMSE.

*Ecotect* Tiles consistently under-predicts irradiations for all elevations with MBE of -31% (2.0m), -25% (100m) and -8% (220m). Most importantly, it strongly under-predicts cooling season solar radiation (May-August in NYC), reflected by RMSE's of 376% (2.0m), 336% (100m) and 269% (220m).

Table 5. Relative error for **South annual** irradiation for all simulation methods by elevation

Distribution method	2.0m		100m		220m	
	Absolute Error	Relative Error	Absolute Error	Relative Error	Absolute Error	Relative Error
	[kWh/m <sup>2</sup> ]	[%]	[kWh/m <sup>2</sup> ]	[%]	[kWh/m <sup>2</sup> ]	[%]
Daysim-DS	489	reference	727	reference	1086	reference
Ecotect Points full res	-23	-4.7	-68	-9.3	-59	-5.5
Ecotect Tiles full res	-169	-34.5	-249	-34.3	-176	-16.2
GenCumulativeSky	17	3.4	-35	-4.8	-41	-3.8
Daysim DDS -s	-3	-0.5	-10	-1.4	-7	-0.7

Table 6. MBE and RMSE for South monthly irradiation calculation by elevation.

Distribution Method	2.0m		100m		220m	
	RMSE [%]	MBE [%]	RMSE [%]	MBE [%]	RMSE [%]	MBE [%]
Daysim-DS	reference	reference	reference	reference	reference	reference
Ecotect Points full res	144	-8	116	-10	75	-6
Ecotect Tiles full res	376	-31	336	-25	269	-8
GenCumulativeSky	112	1	93	-3	42	-4
Daysim DDS -s	127	-4	37	-1	17	0

Table 7. Relative error for total **cooling season** irradiation by elevation.

Distribution method	2.0m		100m		220m	
	Absolute Error	Relative Error	Absolute Error	Relative Error	Absolute Error	Relative Error
	[kWh/m <sup>2</sup> ]	[%]	[kWh/m <sup>2</sup> ]	[%]	[kWh/m <sup>2</sup> ]	[%]
Daysim-DS	317	reference	512	reference	697	reference
Ecotect Points full res	6	1.9	50	-9.7	32	4.6
Ecotect Tiles full res	117	37	209	-40.8	181	26.0
GenCumulativeSky	-21	-6.5	38	-7.4	26	3.7
Daysim DDS -s	-6	-2.0	11	-2.1	6	0.9

Six solar radiation distribution methods were compared in two simulation cases (six in an unobstructed case and five in a complex). On the first unobstructed case all *Radiance*-based methods reported reasonable accuracy with MBE < 10% and RMSE < 75% for all cardinal directions. Excel, *Ecotect* Points and *Ecotect* Tiles reported a somewhat higher error with MBE of up to 50% and RMSE up to 580%. All methods had difficulties accurately accounting for North irradiations (South on the southern hemisphere) due to the difficulties of accounting for early mornings low-solar angles during summer months. However, one can conclude that all methods, except for *Ecotect* Points, were able to track the irradiation yearly profile for an unobstructed sensor with reasonable accuracy. Especially when considering the variability that inherently exists with the source weather data.

On the second test case, a complex urban environment with South facing sensors, almost all methods reported annual MBE < 10%, but high RMSE (up to 140% RMSE for the 2.0m height sensor). *Ecotect* Tiles was the exception with a consistently high RMSE > 269%. The method's limitation to reasonably trace monthly irradiances should be a concern for practitioners who rely on it for seasonal performance analysis. However, the accuracy reported by GenCumulativeSky gives practitioners a valuable option for reporting irradiances on false color images with a reliable and resource-efficient method.

Finally, the design practice applications explored demonstrate that in some cases these variations may crucially influence the design recommendations of different energy conservation measures. Furthermore, practitioners should pay special attention to which solar radiation distribution method to use when carrying out season specific analyses.

This study demonstrated that the tools available for running the simulations on solar irradiation on buildings have more or less accuracy respect to the measured data in an unobstructed case and to the *Daysim DS* in a complex urban environment. Below of the dissertation was decided to conduct some tests of simulations in order to compare the different tools for calculating the solar radiation on the most irradiative façade and the effect of overshadowing between two buildings. However for all sets of simulations, especially for a simple or complex urban district, *Daysim DS* is the tool that has been chosen for all further simulations.

### 2.3.4. Overshadowing effect: example of shadow's percentage calculation on a façade

The Solar Potential poWer tool (Solar PW) aims at improving solar access in dense urban districts and optimizing the shape of buildings to harvest solar radiation. In this way, it may contribute to increasing the potential of using PV panels or solar thermal collectors integrated in the building envelope to produce clean energy.

The study started from the analysis of simple models of two adjacent residential buildings in which different parameters are considered: height and size of the buildings and distance between blocks.

In this section of the work was analysed the influence of the overshadowing created by one building on the opposite façade of the other. All simulations have been performed in *Autodesk Ecotect Analysis* using the weather data file of Brisbane (lat.  $-27^{\circ}38'E$ , long.  $153^{\circ}17'N$ ). The analyses included different ratios of building heights ( $h_1/h_2$ ) and of distance and height ( $d/h_2$ ), for an azimuth varying in steps of 22.5 degrees from  $-135$  to  $135$  degrees from the North. Analyses considered direct solar radiation only.

Graph 2 summarizes the results: once the ratios  $h_2/h_1$  and  $d/h_2$  are known, following the corresponding line it is possible to know the percentage of shading created by the building with  $h_1$  on the façade of building with height  $h_2$ .

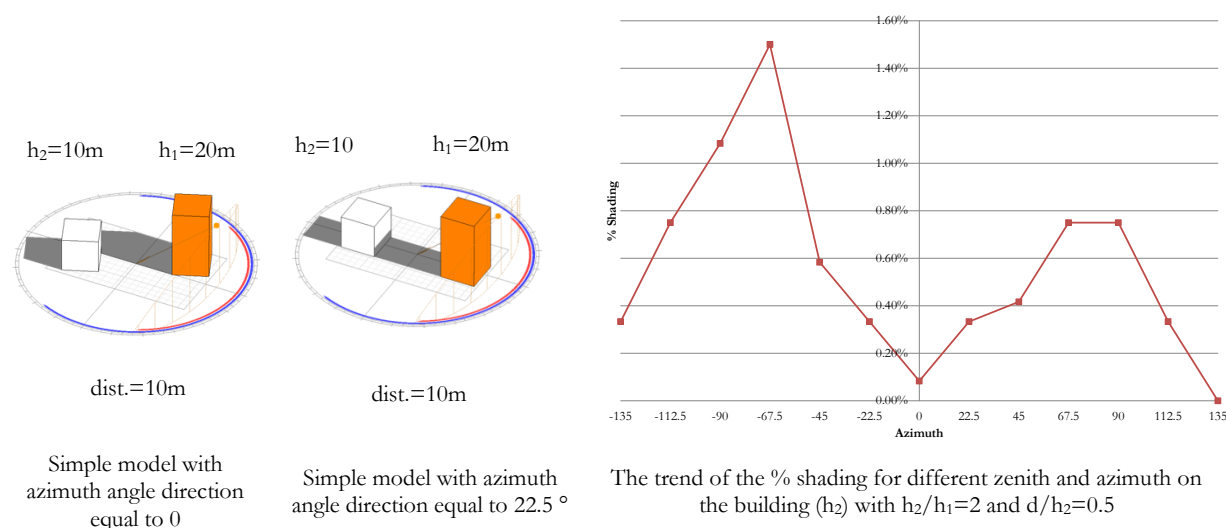


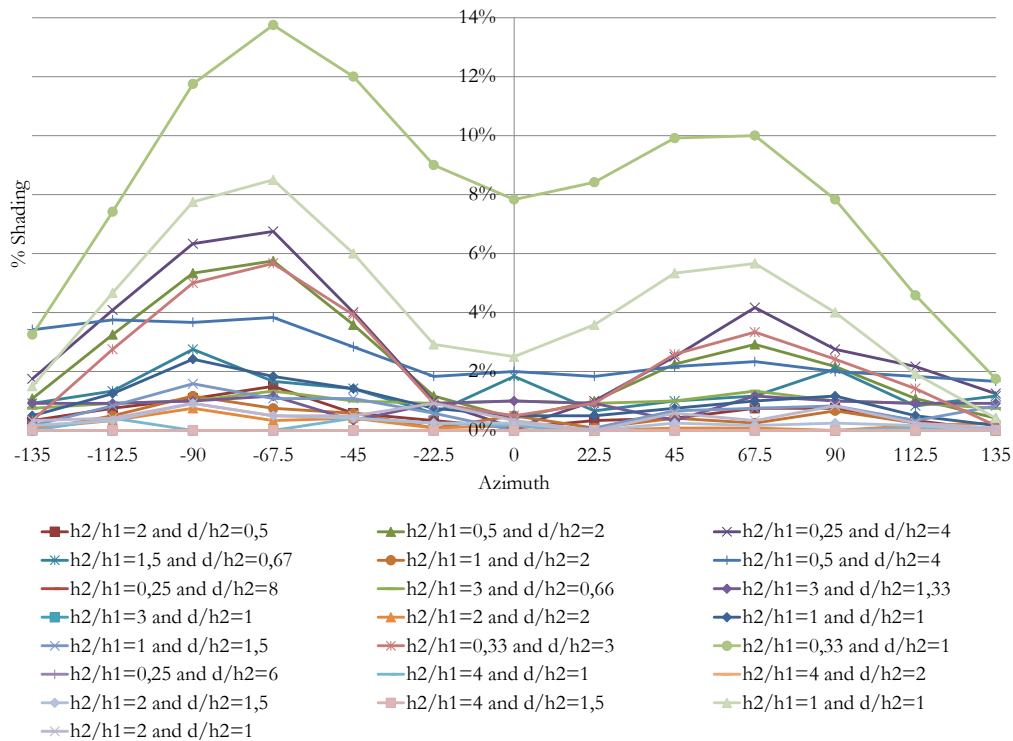
Figure 9. Example of simple model analysis: annual solar direct radiation simulations for different azimuth angle direction with ratio  $h_2/h_1=2$  and  $d/h_2=0.5$ :  $h_1$  represented the height of the building volume projecting its shadow on building volume with height equal to  $h_2$

The building volumes of a case study in Surfers Paradise were analysed in two different scenarios: the designed scenario – the outcome of a workshop organized in Gold Coast from 10<sup>th</sup> to 23<sup>rd</sup> of July, 2011 by Politecnico di Milano, University of Queensland, University of New South Wales and Griffith

University – and the solar optimized scenario, created through the tool elaborated from simple models analyses and systematized with a Matlab algorithm [39]. The optimization of volumes starts considering the closest value ratio ( $d/h_2$ ) of the examined couple of buildings with respect to the simple models (two rectangular boxes with different heights). From the corresponding shadow graph it is possible to optimize the relative heights of the buildings in order to increase the annual direct solar radiation for the highest façade, at different zenith and azimuth values and different  $h_1/h_2$  and  $d/h_2$  ratios.

Figure 9 shows an example of optimization using this method: the graph relative to the simple case with  $d/h_2$  ratio equal to 0.5 and azimuth angle direction from buildings equal to  $0^\circ$  was used. The corresponding simple model minimizing the influence of shadows on the buildings is the case study with  $h_1/h_2$  ratio equal to 2 and  $d/h_2$  equal to 0.5. The design situation presents an  $h_1/h_2$  ratio of 0.6,  $d/h_2$  equal to 0.83 and an azimuth angle direction of  $0^\circ$ . Using the graph of the closest available ratio for the corresponding simple model (in this case  $d/h_2$  equal to 0.5, as shown in the rectangle on the right in Figure 9) it is possible to derive the  $h_1/h_2$  ratio minimizing the overshadowing effects.

Graph 2. Trends of the % of the façades in shade vs azimuth, for different height and distances' ratios.



Results of the optimization by using the simple model tool are presented in the Figure 10.

The accuracy of the tool was validated with dynamic yearly solar simulations using *Daysim* (Daynamic Daylighting Simulation). *Daysim* is a validated *Radiance*-based program [51], developed and validated for

daylight calculations of complex transparent systems [57], that combines a backward-ray-tracing algorithm, a daylight coefficient approach and the Perez Sky Model to simulate time series of solar irradiances.

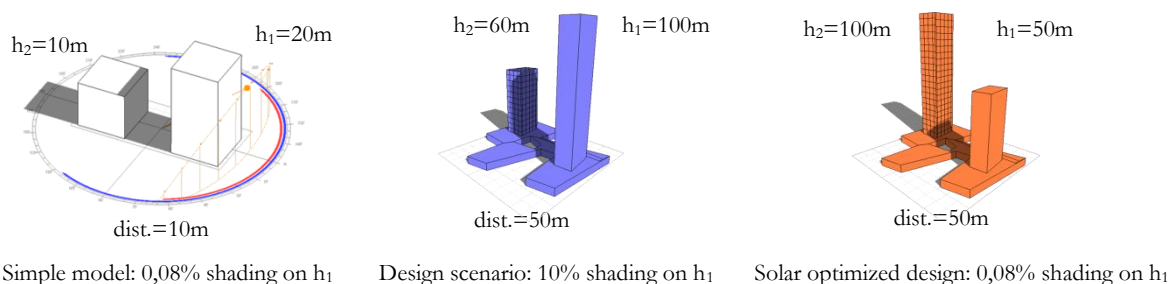


Figure 10. Results of one example of the optimization of buildings volumes using the simple model tool.

Table 8. Results simulation conducted by using *Daysim* in design scenario.

Façade	Conditions	Design scenario isolated		Design scenario (two buildings)		
	Ambient bounces (ab) and ground reflectance (Gr. refl. [%])	Global solar radiation (kWh/year)	(kWh/m <sup>2</sup> year)	Global solar radiation (kWh/year)	(kWh/m <sup>2</sup> year)	Decrease of global solar radiation [%]
North	ab=0, Gr. Refl.=15	191,065	139	168,590	123	12%

Table 9. Results simulation conducted by using *Daysim* in solar optimized scenario.

Façade	Conditions	Solar optimized scenario isolated		Solar optimized scenario (two buildings)		
	Ambient bounces (ab) and ground reflectance (Gr. refl. [%])	Global solar radiation (kWh/year)	(kWh/m <sup>2</sup> year)	Global solar radiation (kWh/year)	(kWh/m <sup>2</sup> year)	Decrease of global solar radiation [%]
North	ab=0, Gr. Refl.=15	1,284,743	520	1,271,827	515	1%

It was developed by the National Research Council of Canada and the Fraunhofer Institute for Solar Energy Systems in Germany. *Radiance* files, generated with the graphical interface of *Autodesk Ecotect Analysis* and including the model scenes, have been imported in *Daysim* software and dynamic analyses have been run, in order to collect hourly data during the simulated year. The validation of the case study previously analysed with Ecotect is presented in Table 8 and Table 9. First the isolated building with height  $h_2$  has been analysed, and then the couple of buildings together.

Results demonstrated that the percentages in term of solar radiation lost due to the overshadowing are close (differences of about 1-2%) to those extracted with the previous analysis.

A relationship between all analyzed parameters is translated in an analytic formula through a “Matlab matrix”. This relationship was elaborated with solar radiation data, to optimize the exposure of the

volume to the sun. The final aim is to create a tool that, based on geographic coordinates, allows to optimally the collocation of the buildings in a dense district with respect to heights and distances.

### 2.3.5. Matlab algorithm

A Matlab algorithm was firstly developed, in order to evaluate in a simplified way the shadows distribution on two reference buildings, finding key information regarding the optimization of building heights and reaching the goal of maximization of direct solar radiation.

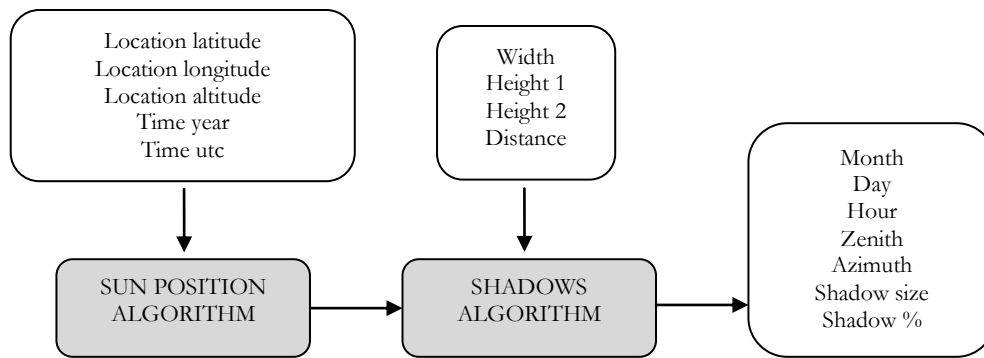


Figure 11. Block diagram of the Matlab algorithm procedure.

The program made use of a sun position algorithm originally developed and presented in literature [41], based on numerical approximations of the exact equations for sun position. The input entries were represented by the location data (latitude, longitude, altitude, year, UTC time) and the geometrical characteristic of the reference buildings (width, height of building 1, height of building 2, distance between buildings). Building 1 represented the building projecting his shadow on building 2

By applying the algorithm, a 8760 rows matrix was created, listing results as zenith angle (measured clockwise from the horizontal plane), azimuth angle (measured east-wise from geographical North), size of the projected shadow and percentage of shade on building 2, for every hour of the year. The procedure is shown in the block diagram.

The size of the projected shadow was determined by means of simple geometrical considerations, by splitting into horizontal length governed by the azimuth angle and a vertical one, depending on the zenith. The negative zenith angles were firstly set equal to zero, in order to avoid taking into account even the shadows projected during night.

The hourly percentage of shadows on the façade of building 2 was then estimated by dividing the area in shade by the total area.

This algorithm was developed as a fast and easy tool for the optimization of building heights, or building distances. Starting from this code, parametric analyses can be carried out, finding useful information for the preparation of new solar design approach.

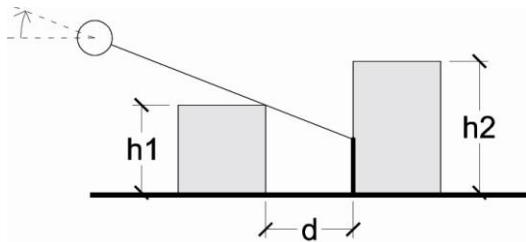


Figure 12. View of the shadow's process calculation

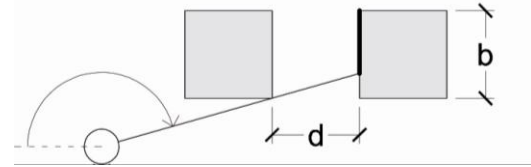


Figure 13. View in plan of the shadow's process calculation

### 2.3.6. Validation of matlab algorithm

The MATLAB algorithm was validated by selecting a reference day (June 18th) and comparing the results with numerical data coming from *Autodesk Ecotect Analysis* and *Daysim* tools. Before that, the sun position algorithm was checked by comparing the azimuth and zenith angles with the ones coming from a sun position tool free available [58].

In general, the sun angles estimated by means of the sun position algorithm are coincident with the ones coming from the solar tool. Bigger differences are highlighted for zenith angles close to zero, since the solar tool provides simplified calculation techniques, if compared to the *Matlab* procedure that takes into account several distinct phenomena [56].

The second step of the validation process took into account the percentage in shade of the building 2 façade facing the sun. At this purpose, data coming from *Daysim*, *Autodesk Ecotect Analysis* and *Matlab* were collected and compared. In particular, the percentage of shadows was estimated in *Daysim* by calculating the difference between the solar radiation insisting on the façade analysing the isolated building (just building 2) and the solar radiation level in a model including building 1 (at this purpose, just the direct solar radiation was considered, setting the ambient bounces equal to 0 in both the analyses).

Finally, all the values unequal to zero were averaged, to obtain a single number referred to the selected day of the year. In *Autodesk Ecotect Analysis*, the shadows percentage was estimated by averaging the unequal to zero solar shade data collected in the results file. Similarly, the unequal to zero hourly percentages calculated by the *Matlab* algorithm were selected and averaged. It's worthy of notice that *Matlab* and *Daysim* perform an hourly calculation centred in the middle of the reference hour (for example, 8:30); *Autodesk Ecotect Analysis*, on the contrary, gives as output an hourly value centred at the

beginning of the reference hour (for instance 8:00), therefore implying computational differences related to the non-coincident Sun positions.

The following Table 10 show the final results.

Table 10. Comparison of sun position's values calculated using Solar Tool [58] and Solar position Matlab algorithm [41].

Time	SOLAR TOOL		MATLAB		Error %	
	Zenith	Azimuth	Zenith	Azimuth	Zenith	Azimuth
00:30	-84.09	227.46	-84.10	227.38	0.01%	0.03%
01:30	-79.88	111.45	-79.88	111.44	0.00%	0.01%
02:30	-66.87	94.46	-66.86	94.45	0.01%	0.01%
03:30	-53.58	87.17	-53.57	87.17	0.02%	0.00%
04:30	-40.34	81.62	-40.33	81.62	0.02%	0.00%
05:30	-27.28	76.38	-27.28	76.37	0.02%	0.01%
06:30	-14.52	70.86	-14.51	70.86	0.06%	0.00%
07:30	-2.2	64.66	-1.47	64.65	33.30%	0.01%
08:30	9.44	57.3	9.54	57.29	1.06%	0.01%
09:30	20.04	48.22	20.10	48.21	0.28%	0.01%
10:30	29.06	36.77	29.09	36.76	0.10%	0.03%
11:30	35.66	22.45	35.69	22.44	0.08%	0.03%
12:30	38.91	5.62	38.93	5.61	0.06%	0.14%
13:30	38.17	348.03	38.19	348.02	0.05%	0.00%
14:30	33.59	331.99	33.61	331.98	0.06%	0.00%
15:30	26	318.75	26.03	318.74	0.10%	0.00%
16:30	16.32	308.24	16.37	308.23	0.33%	0.00%
17:30	5.29	299.86	5.44	299.86	2.75%	0.00%
18:30	-6.63	292.98	-6.64	292.98	0.15%	0.00%
19:30	-19.13	287.08	-19.14	287.07	0.06%	0.00%
20:30	-32.02	281.72	-32.03	281.72	0.02%	0.00%
21:30	-45.15	276.46	-45.16	276.45	0.03%	0.00%
22:30	-58.43	270.54	-58.44	270.54	0.01%	0.00%
23:30	-71.7	261.64	-71.71	261.62	0.01%	0.01%

The results shown a good accordance of the MATLAB solar shade with the data coming from numerical analyses and was therefore proved that the geometrical considerations implemented in the algorithm could provide useful information for the optimization of building heights and distances.

The Table 11 presented below summarized the all results carried out from the simulations started above and the shading's percentages for every hour of simulation's day.

Table 11. Comparison of shadows' percentages on building 2 calculated with different Solar tools.

Time	Isolated	Two buildings	Shading %	Time	Shade %
	Wh	Wh		Time	Shade %
00:30	0	0	-	07:00	0%
01:30	0	0	-	08:00	0%
02:30	0	0	-	09:00	5%
03:30	0	0	-	10:00	44%
04:30	0	0	-	11:00	73%
05:30	0	0	-	12:00	95%
06:30	0	0	-	13:00	63%
07:30	7600	7600	0.00%	14:00	29%
08:30	25900	25900	0.00%	15:00	0%
09:30	43500	31292	28.06%	<b>Average</b>	<b>51.50%</b>
10:30	54600	21404	60.80%	Shadings' percentages calculated using <i>Ecotect</i>	
11:30	58600	5538	90.55%	Time	Shade %
12:30	58400	11952	79.53%	00:30	0%
13:30	51500	25854	49.80%	01:30	0%
14:30	39100	33820	13.50%	02:30	0%
15:30	20600	20600	0.00%	03:30	0%
16:30	400	400	0.00%	04:30	0%
17:30	0	0	-	05:30	0%
18:30	0	0	-	06:30	0%
19:30	0	0	-	07:30	0%
20:30	0	0	-	08:30	0%
21:30	0	0	-	09:30	25%
22:30	0	0	-	10:30	59%
23:30	0	0	-	11:30	90%
				12:30	79%
				13:30	47%
				14:30	12%
				15:30	0%
				16:30	0%
				17:30	0%
				18:30	0%
				19:30	0%
				20:30	0%
				21:30	0%
				22:30	0%
				23:30	0%
		<b>Average</b>	<b>53.71%</b>	<b>Average</b>	<b>52.00%</b>
Shadings' percentages calculated using <i>Daysim</i>				Shadings' percentages calculated using Matlab (Solar PW tool)	

The results demonstrated that the *Solar PW tool* developed works with a good accuracy: in fact the difference of the average value of shading's percentage calculated using *Daysim* is equal to 1.73%, while using *Autodesk Ecotect Analysis* the different lowers until 0.50%.

## 2.4. Results and discussion

### 2.4.1. Analysis on simplified models of urban areas

The first studies on simplified models of urban areas were instrumental to understand basic mathematical relationships between the height of buildings, their reciprocal distance and the availability of solar radiation on façades. Two of the simplified case studies are described below; the pattern of buildings is shown in Figure 14.

The analyses were carried out with *Autodesk Ecotect Analysis*.

- a) The first case study investigates the relationship between the height of buildings and solar radiation availability.

Were analysed three case studies of a simple district composed by 9 buildings and located in Milan. The climate data file used was the Milan weather data file (Italy-Milano.wea) available in directly in *Ecotect* weather database.

For all case studies are setting the same district's data reported in the Table 12 below:

Table 12. District set parameters (Case 1).

Building footprint [m <sup>2</sup> ]	Entire district's footprint [m <sup>2</sup> ]	Orientation	Rectangular size of surface subdivision [m <sup>2</sup> ]	Plot ratio of entire district
100	2500	North - South	2.5	0.36

The characteristics of every single district are summarized in Table 13.

Table 13. District construction's parameters of the case studies.

Case study	Height of the buildings [m]	Volume of the buildings [m <sup>3</sup> ]	Surface/Volume	District's buildability index [m <sup>3</sup> /m <sup>2</sup> ]
Case 1.A	10	9000	0.5	3.6
Case 1.B	15	13500	0.47	5.4
Case 1.C	20	18000	0.45	7.2

Table 14. Results of the analysis (case 1)

Results	Case 1.A (h = 10 m)	Case 1.B (h = 15 m)	Case 1.C (h = 20 m)
Annual direct radiation on the façades of the central building [kWh]	181,352	229,002	282,405
Annual direct radiation per square metre of façade [kWh/m <sup>2</sup> ]	362.7	327.1	313.8

The results of set of simulations are summarized in Table 14.

The relationship between building height and normalised incident solar radiation is not linear. Further analyses are required to define a more precise mathematical relationship, but it can be inferred that it is a quadratic function. The shows that, for the most overshadowed building (the central one), available solar radiation obviously decreases as the height of buildings increases. The potential energy production with solar collectors and PV panels placed on the building envelope consequently decreases.

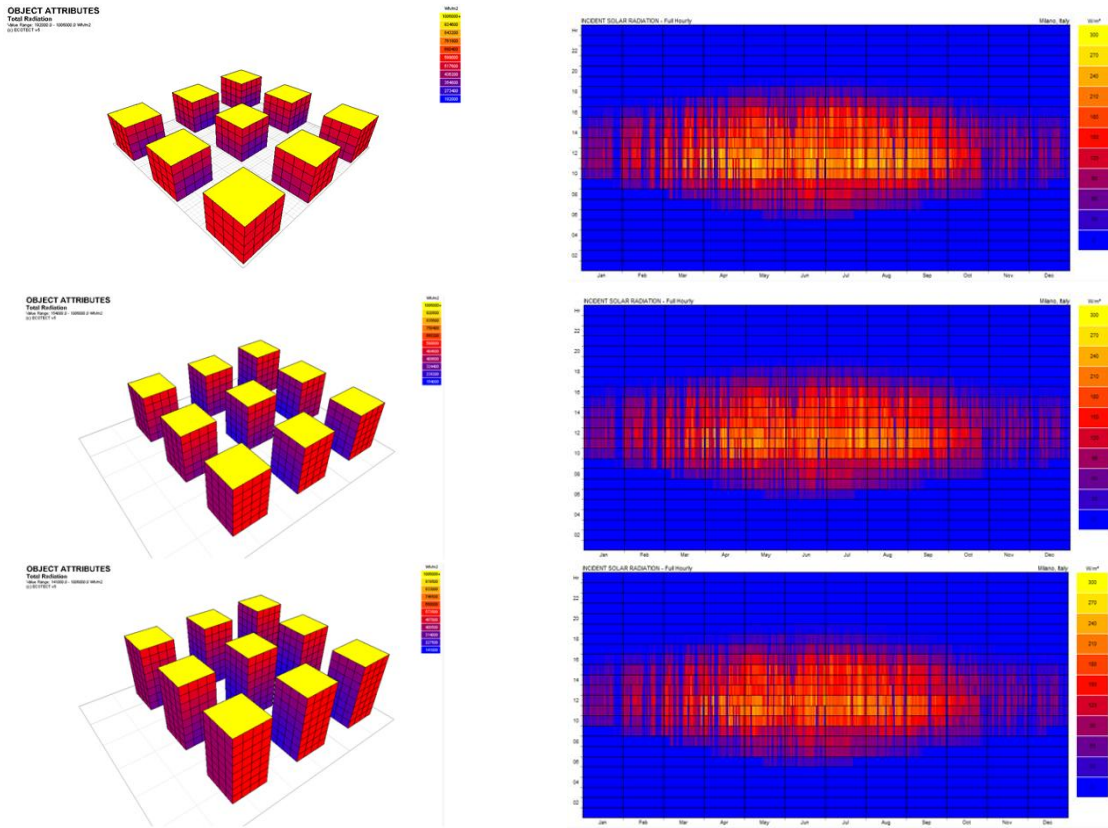
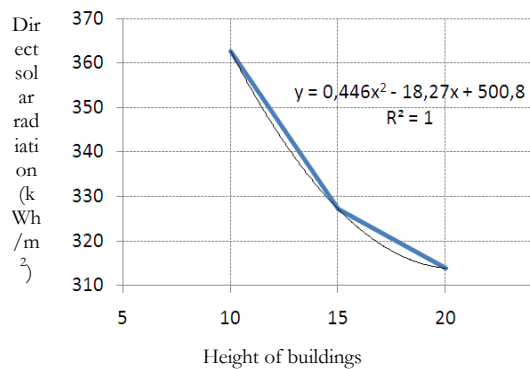


Figure 14. Results of case studies 1.A, 1.B and 1.C and solar radiation map full hourly on the central building.

Graph 3. Trend of direct solar radiation available on the façades of the central building according to the height of buildings.



- b) The second case study investigates the relationship between the distance among buildings and the available solar radiation.

Were analysed three case studies of a simple district composed by 9 buildings always located in Milan characterized by following parameters:

Table 15. District set parameters (Case 2).

Building footprint [m <sup>2</sup> ]	Entire district's footprint [m <sup>2</sup> ]	Orientation	Rectangular size of surface subdivision [m <sup>2</sup> ]	Plot ratio of entire district
100	2500	North/South	2.5	0.36 (2.A) - 0.25 (2.B) - 0.18 (2.C)

The distance among the building varies from 10 m (case 2.A) to 15m (case 2.B) until 20m (case 3.B). Results are summarized in Table 16.

Table 16. Results of the analysis (case 2)

Results	Case 2.A (h = 10 m)	Case 2.B (h = 15 m)	Case 2.C (h = 20 m)
Annual direct radiation per square metre of façade [kWh/m <sup>2</sup> ]	309.7	365.1	393.3

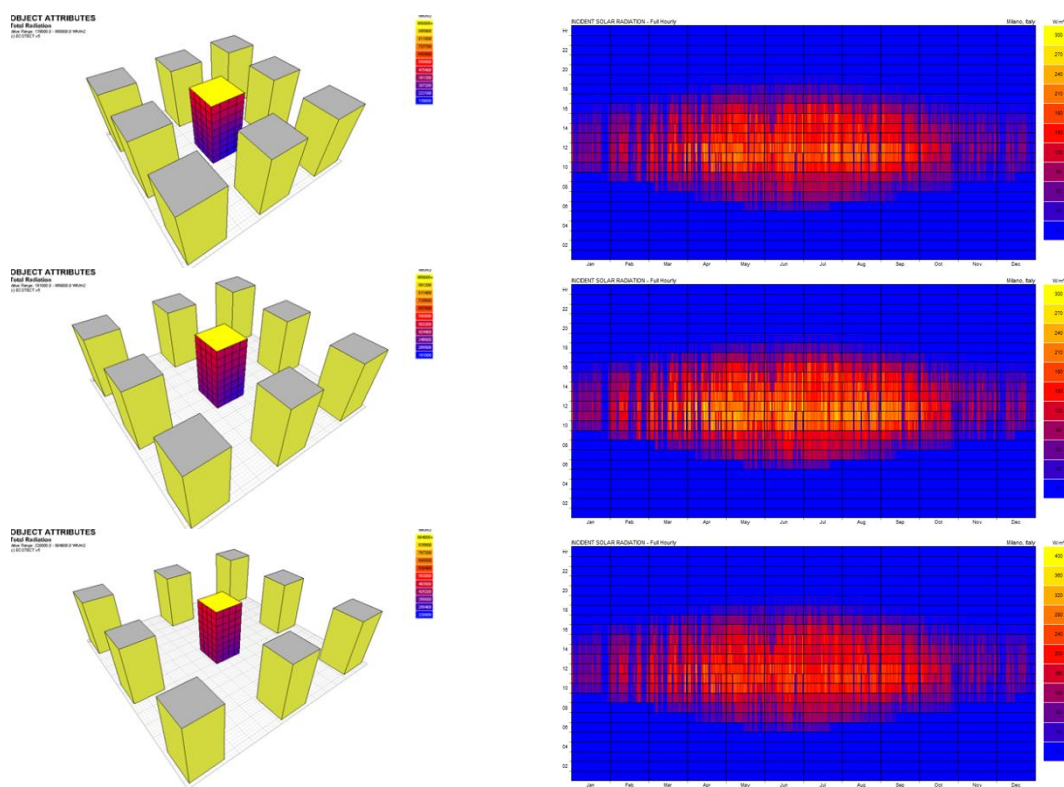
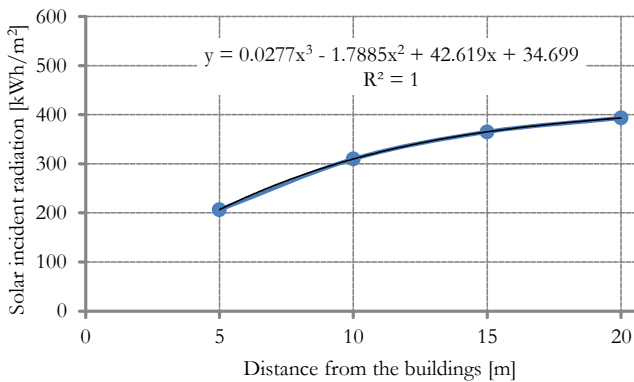
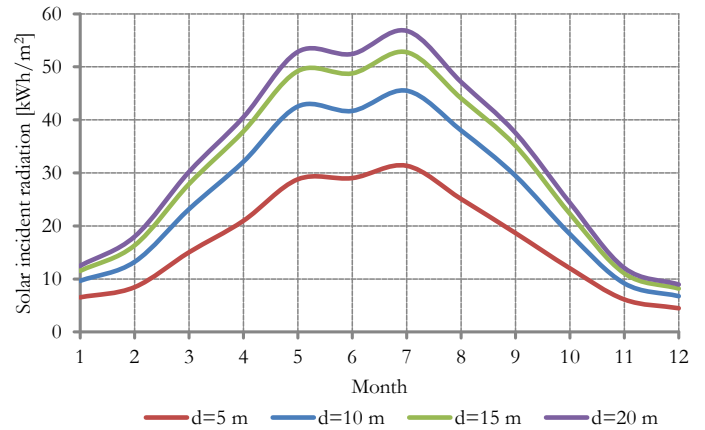


Figure 15. Results of case studies 2.A, 2.B and 2.C and solar radiation map full hourly on the central building.

The Graph 4 shows the total incident solar radiation on the vertical building envelope (the roof is not considered because its incident solar radiation is constant). Results are approximated by a cubic function. When the distance is roughly equal to the building height (15 m), setting the buildings further apart only leads to small increases in the incident solar radiation.



Graph 4. Trend of the incident solar radiation on vertical building surfaces according to distance between buildings



Graph 5. Annual direct radiation on the vertical envelope of the central building according to the distance among buildings

The general results of these analyses were subsequently tested in the real case study described below.

### 2.4.2. Analysis on a case study of Milan (Italy)

The case study presented is representative of a typical operation in Milan: demolition of the existing building and reconstruction of the same volume, but with a different shape, in a medium density area of the city.



Figure 16. Google Earth view of the selected site (highlighted in red) in the northwest of the city of Milan.

The actual design scenario elaborated by a developer and the solar optimized design scenario (which maintains the same building volume) were compared. In both scenarios the potential energy production obtained by covering the building envelope with solar thermal panels or with photovoltaic panels was calculated. Moreover, overshadowing of nearby buildings was compared in the two different scenarios.

The first analysis is about the shadow range in the current scenario and in the scenario of the company's project. This study helps to compare the situation before and after the construction of the new building, assessing whether the proposed design guarantees the existing solar access to the neighbouring buildings to the North. In order to assess the worst insolation conditions, the analyses were conducted on December 21<sup>st</sup>.

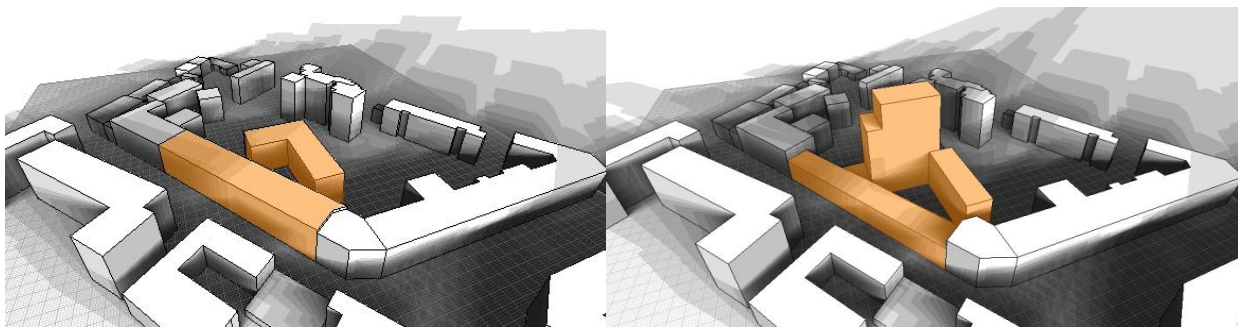


Figure 17. Shadow range in the current scenario (on the left) and in the actual design scenario (on the right) on 21<sup>st</sup> December.

Subsequently, the shape of the building was optimised keeping the additional volume constant. The aim is to minimize overshadowing of the neighbouring buildings and to find an adequate shape to maximize potential energy production from the envelope with solar collectors or photovoltaic panels. The final goal is an optimized design with respect to building orientation and projected shadows.

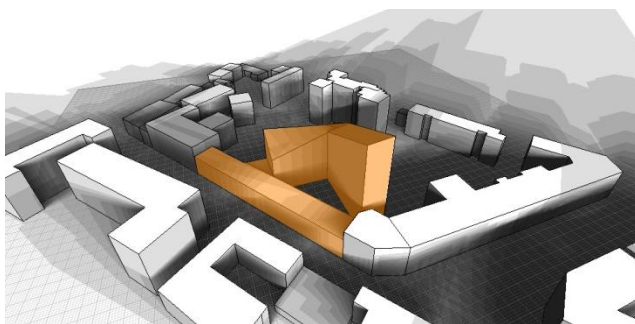


Figure 18. Shadow range in the solar optimized design scenario on 21<sup>st</sup> December.

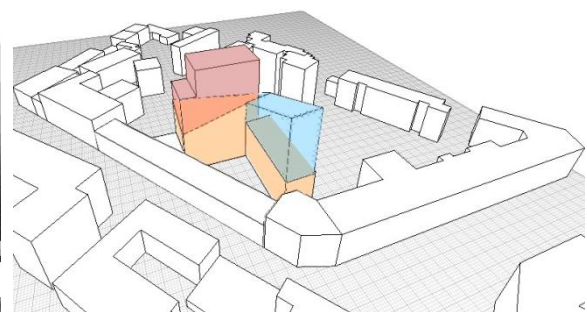


Figure 19. The blue volume in the solar optimized design is the same of the red one in the actual design scenario

### 2.4.3. Analysis of shadow effect on the façades of neighbouring buildings

The results of the analyses conducted in different scenarios are summarized in Figure 20, showing the different shading conditions. It is important to underline that in this case study the all surfaces have been considered: in fact the surface of the roof is very relevant for the energy production in both scenario because the buildings are not very tall.

These are the main results for the analyses on the 21st December:

- c) The solar optimized design maintains the existing amount of solar radiation on the buildings to the North, as shown by the red dots;
- d) The façade of the analysed building to the North is completely irradiated from 1 p.m. onwards;
- e) In the actual design scenario, the new building casts a significant shadow behind it;
- f) The façade of the building to the North is never completely irradiated in the actual design scenario;
- g) The shadow graph shows the highest solar radiation is in the solar optimized design scenario;
- h) The shadow graph shows the smallest solar radiation is in the actual design scenario.

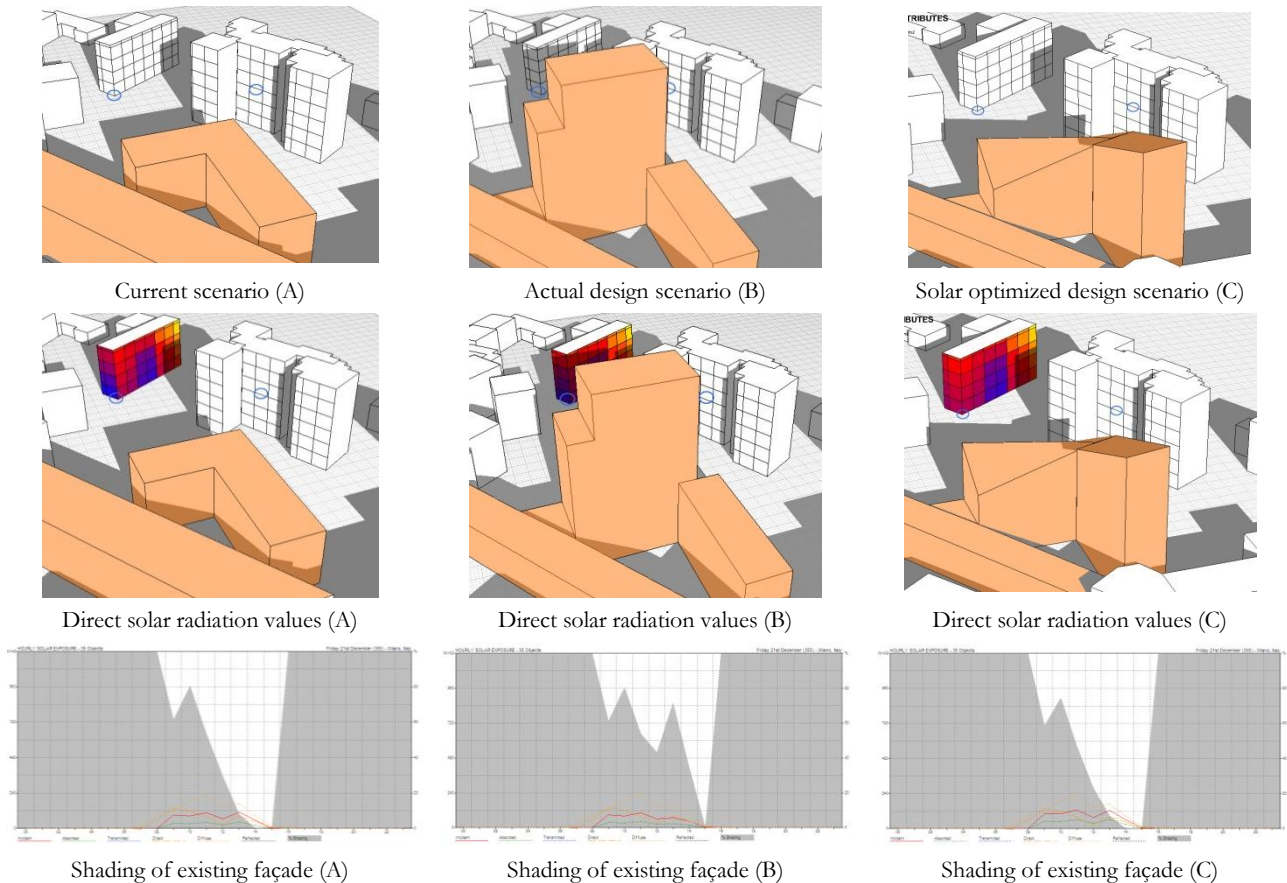


Figure 20. Analysis of shading effects in the different scenarios.

### 2.4.4. Analysis of energy production with solar building envelope

The final analysis shows the difference in the potential energy production from the building envelope in the two different scenarios: actual design scenario and solar optimized design scenario. The results of the analysis show that the energy production in the solar optimized design scenario is actually greater than the one in the design scenario. The comparison of the two different scenarios is shown in Figure 21 and Figure 22. In this case study, the roof is considered completely available for energy production.

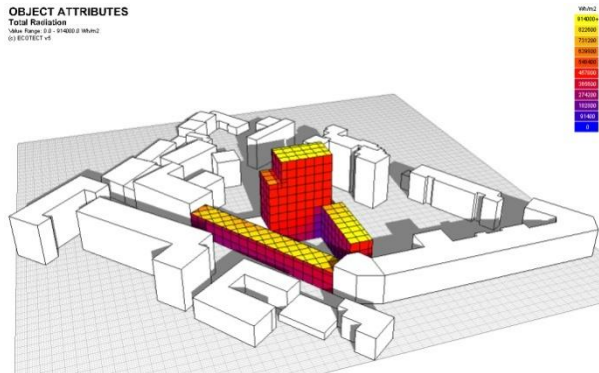


Figure 21. Radiation on actual design scenario.

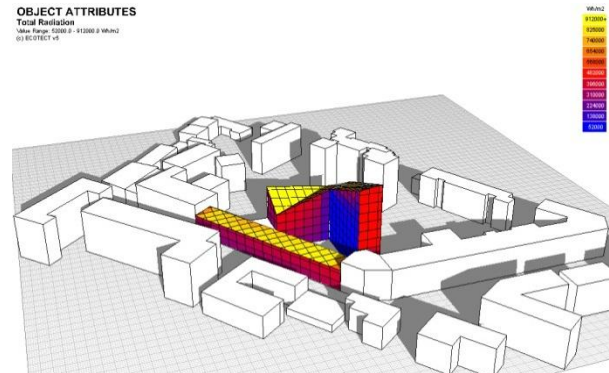


Figure 22. Radiation on solar optimized design scenario.

The results are summarized in the Table 17: it is better to specify that for the efficiency of photovoltaic panels was assigned a value equal to 16%, while for the solar thermal collectors is equal to 20%.

Table 17. Potential for energy production in the two scenarios ( $EP_H$  = primary energy index for heating = 49,6 kWh/m<sup>2</sup>yr).

	Actual design scenario		Solar optimized design scenario		
Energy Production	Façade (1,654 m <sup>2</sup> )	Roof (476 m <sup>2</sup> )	Energy production	Façade (1,681 m <sup>2</sup> )	Roof (1,202 m <sup>2</sup> )
Photovoltaic panels	8.3 kWh/m <sup>2</sup> yr (16% of $EP_H$ )	4.4 kWh/m <sup>2</sup> yr (8% of $EP_H$ )	Photovoltaic panels	4.6 kWh/m <sup>2</sup> yr (9% of $EP_H$ )	9.1 kWh/m <sup>2</sup> yr (18% of $EP_H$ )
Solar collectors	79.8 kWh/m <sup>2</sup> yr (160% of $EP_H$ )	42 kWh/m <sup>2</sup> yr (85% of $EP_H$ )	Solar collectors	43.8 kWh/m <sup>2</sup> yr (88% of $EP_H$ )	87 kWh/m <sup>2</sup> yr (170% of $EP_H$ )

This case study shows that even in densely built areas it is possible to manipulate the allowable building volume in order to maximize solar exposure and minimize negative effects on existing neighbouring buildings. It has to be pointed out that the analysis was carried out prioritising energy production aspects, but other factors (such as the increased sale prices of high-rise apartments) may influence the overall massing strategy as well [59].

### 2.4.5. Analysis on a case study of Surfers Paradise - Gold Coast (Australia)

The preliminary tool was applied to different urban contexts, in order to test the analytic relationships found in the simple models. To this purpose, dynamic annual simulations with the *Radiance* software [16] were carried out to assess the solar energy harvested by the buildings. All the solar radiation components (diffuse and direct radiation, sky component and reflections from external surfaces) were considered in this case.

The study investigates the difference in the solar potential of the façades of each single building in the design scenario and in a solar optimized design scenario. In the following analyses only the solar radiation on the façades was considered, excluding the roofs as these have limited surface areas.

The analysis has been conducted in both scenarios: the actual design scenario and the solar optimized design, defined using *Daysim*. The constant number of façades (capturing surfaces) exposed to solar radiation and the constant total volume of the buildings (new buildings volume) added with respect to the current scenario, has been considered as parameters of the analysis. Table 18 summarizes the parameters in both scenarios. In the first analysis, the raytrace values of ambient bounces was set equal to 0 and the ground reflectance equal to 0%, in order to consider only the effect of overshadowing on the façades of other buildings.

The main aim of this analysis was to evaluate if the optimization of the volume improves the solar access, increasing the available solar radiation on the façade of every building. The results in Graph 6 show that the solar radiation on the building envelope increases in every building of the compound.

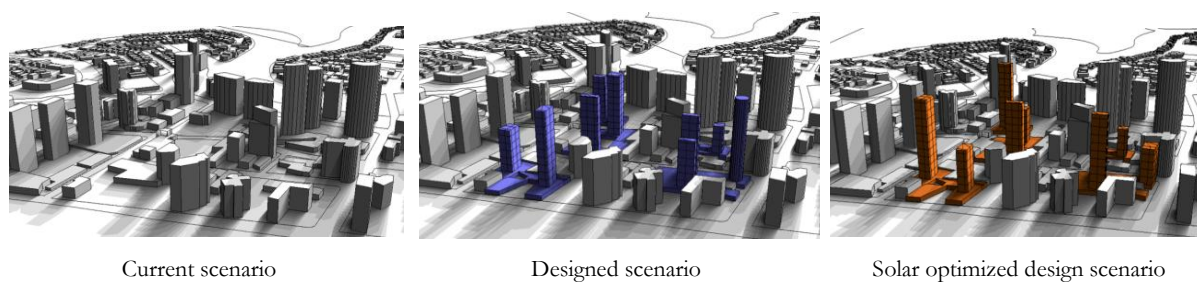


Figure 23. Two different scenarios are investigated: design scenario and solar optimized design starting from current scenario.

Table 18. Parameters of analysis in designed scenario and solar optimized design scenario.

Parameters of the analysis	Actual design scenario	Solar optimized design scenario
Capturing surfaces	47,938 m <sup>2</sup>	46,739 m <sup>2</sup>
New buildings volume	180,724 m <sup>3</sup>	179,263 m <sup>3</sup>

In particular the optimization has been done for couples of buildings at a time, in order to reduce the effect of reciprocal shading.

In the Figure 24 were presented the new designed building in the actual design scenario, isolated respect to the urban context, while in Figure 25 are shown the new buildings in the solar optimized scenario.

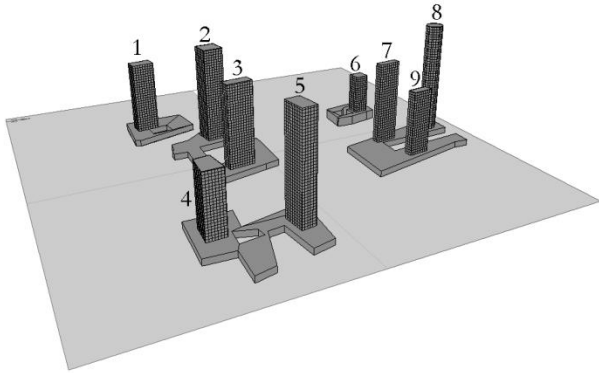


Figure 24. Actual design scenario: new designed buildings

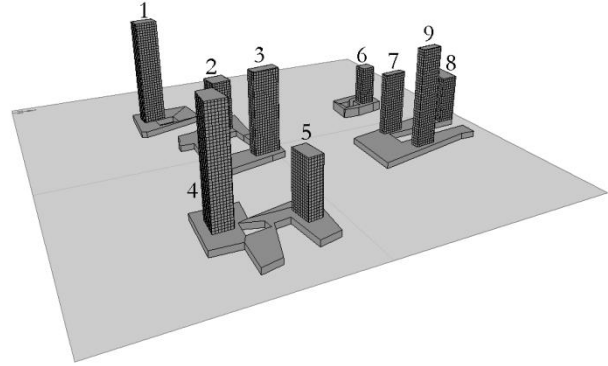
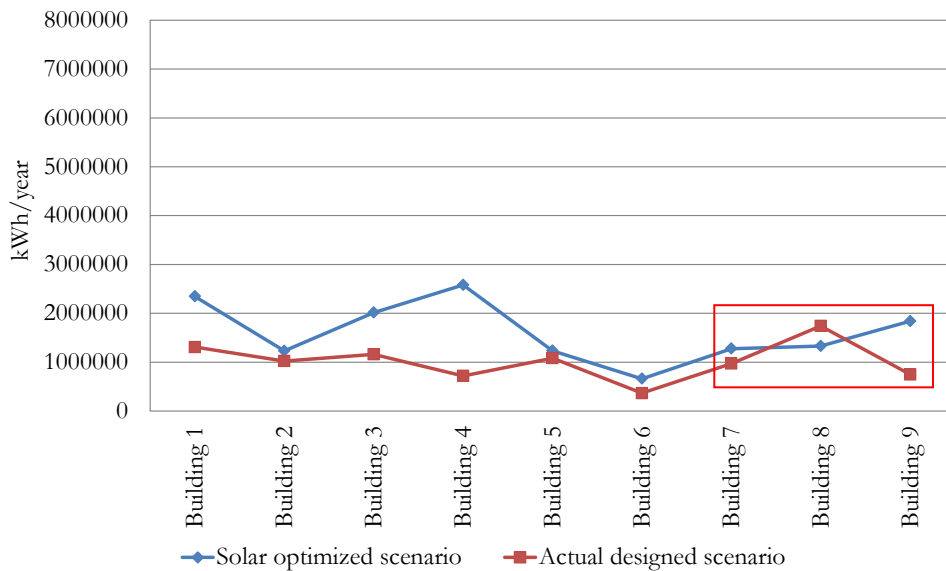


Figure 25. Solar optimized scenario: new designed buildings

Graph 6. Results of the direct solar radiation for designed scenario and solar optimized scenario with ambient bounces equal to 0 and ground reflectance equal to 0.0%.



All simulation were conducted setting the *Radiance* parameters reported in Table 19.

Table 19. Set of “rtrace” parameters used for all *Radiance*-based simulations.

ambient bounces	ambient division	ambient super-sample	ambient resolution	ambient accuracy	specular threshold	direct sampling	direct relays
0 – 3	1000	20	300	0.1	0.15	0.20	2

It is necessary to underline that the analyses were performed considering all the new buildings as isolated volumes. This aspect guarantees the lack of the overshadowing due to the context, but not the mutual influence among the different buildings of the district.

Table 20. Results, considering only the direct solar radiation in designed scenario and solar optimized design scenario.

Building	Conditions Ambient bounces (ab) and ground reflectance (Gr. refl. [%])	Designed scenario		Solar optimized design scenario		Results Increment or decrement [%]
		Direct solar rad. (kWh/year)	(kWh/m <sup>2</sup> year)	Direct solar rad. (kWh/year)	(kWh/m <sup>2</sup> year)	
Building 1	ab=0, Gr=0,0	1,310,364	213	2,345,411	334	44%
Building 2	ab=0, Gr=0,0	1,023,747	143	1,231,154	311	17%
Building 3	ab=0, Gr=0,0	1,160,552	199	2,013,512	345	42%
Building 4	ab=0, Gr=0,0	719,987	160	2,579,154	319	72%
Building 5	ab=0, Gr=0,0	1,082,529	149	1,232,091	311	12%
Building 6	ab=0, Gr=0,0	366,701	172	659,899	323	44%
Building 7	ab=0, Gr=0,0	972,523	208	1,276,659	357	24%
Building 8	ab=0, Gr=0,0	1,741,104	310	1,329,160	315	-31%
Building 9	ab=0, Gr=0,0	748,828	206	1,838,254	334	59%
Total	ab=0, Gr=0,0	9,126,335	1,760	14,505,296	2949	37%

The values within the red rectangle in Graph 6 and Table 20 underline the specific configuration for buildings 7, 8 and 9, which have been optimized considering two buildings at a time. However, results demonstrate that in this case the optimization is not as efficient as in others, because three buildings were considered simultaneously. The relationship among three or more buildings is obviously more complex than between a couple of buildings and should be calculated with more sophisticated analyses. Results are presented in Table 20.

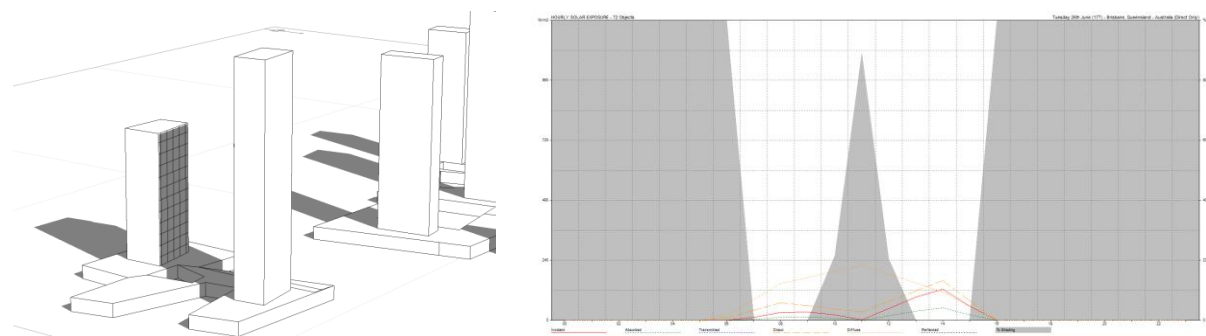


Figure 26. Actual design scenario - Overshadowing effect on the building on the 26<sup>th</sup> of June at 11:00 a.m.

As example is reported a couple of buildings in the actual design scenario (Figure 26) and in the solar optimized scenario (Figure 27) with the shading map of the analysed façade.

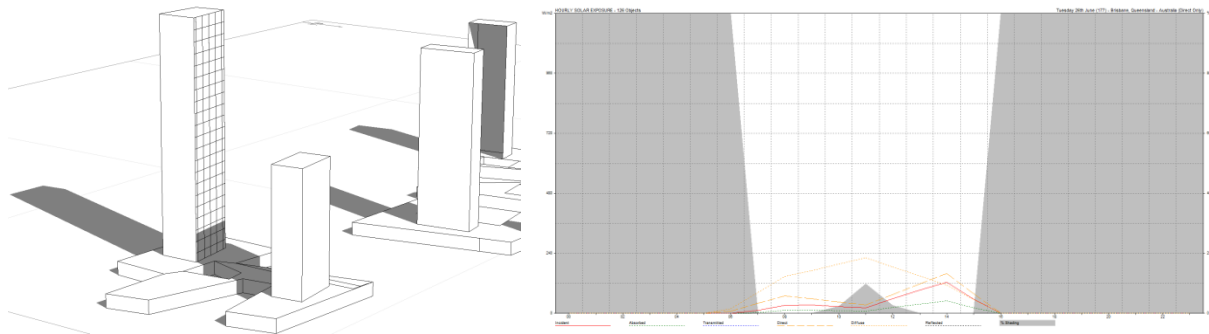
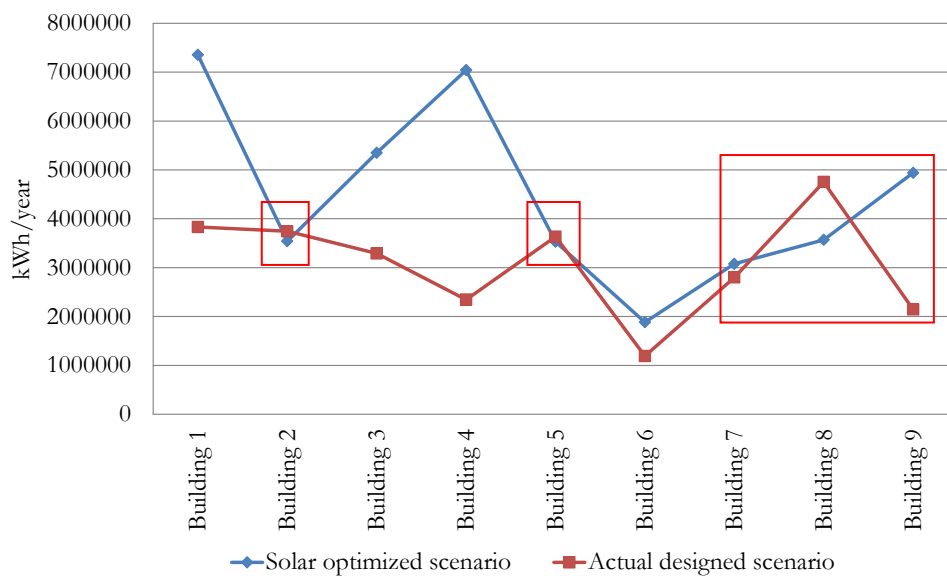


Figure 27. Solar optimized scenario- Overshadowing effect on the building on the 26<sup>th</sup> of June at 11:00 a.m.

The second analysis is conducted on all buildings in both scenarios, setting the raytrace conditions to values of 3 for ambient bounces and 15% for the ground reflectance.

The aim of this analysis was to confirm the results of the first simulation with different raytrace parameters, considering the mutual interaction among buildings and the solar reflections on each other.

Graph 7. Results of all contribution of solar radiation for the designed scenario and solar optimized design scenario with ambient bounces equal to 3 and ground reflectance equal to 15%.



All buildings, except number 1, lost part of the solar radiation increment due to the effects of overshadowing by the neighbouring buildings. Only the building 1 achieved an increment of solar radiation due to reflections. Furthermore, it is fair to underline three situations where the increments of

the first analysis decreased until they assumed negative values (building number 2 and 5). Solar radiation available on the group of three buildings (7, 8 and 9) is worse than the one in the first analysis. Finally, considering the global solar radiation the increment is about 31%. Results are summarized in Table 21.

Table 21. Results considering all contribution of solar radiation in designed scenario and solar optimized design scenario.

Building	Conditions Ambient bounces (ab) and ground reflectance (Gr. refl. [%])	Designed scenario		Solar optimized design scenario		Results Increment or decrement [%]
		Direct solar rad. (kWh/year)	(kWh/m <sup>2</sup> year)	Direct solar rad. (kWh/year)	(kWh/m <sup>2</sup> year)	
Building_1	ab=3, Gr=0,15	3,830,655	616	7,353,787	926	48%
Building_2	ab=3, Gr=0,15	3,744,028	523	3,541,690	894	-6%
Building_3	ab=3, Gr=0,15	3,290,385	564	5,348,066	917	38%
Building_4	ab=3, Gr=0,15	2,344,903	520	7,040,202	871	67%
Building_5	ab=3, Gr=0,15	3,633,246	501	3,529,665	892	-3%
Building_6	ab=3, Gr=0,15	1,190,870	558	1,884,143	884	37%
Building_7	ab=3, Gr=0,15	2,798,506	597	3,077,191	862	9%
Building_8	ab=3, Gr=0,15	4,752,258	846	3,567,626	864	-33%
Building_9	ab=3, Gr=0,15	2,144,541	591	4,938,909	898	57%
Total	ab=3, Gr=0,15	27,729,391	5,317	40,281,278	8,008	31%

The last analysis is conducted with the same raytrace parameters than the previous simulation, but considering the volumes of the new buildings within the existing context.

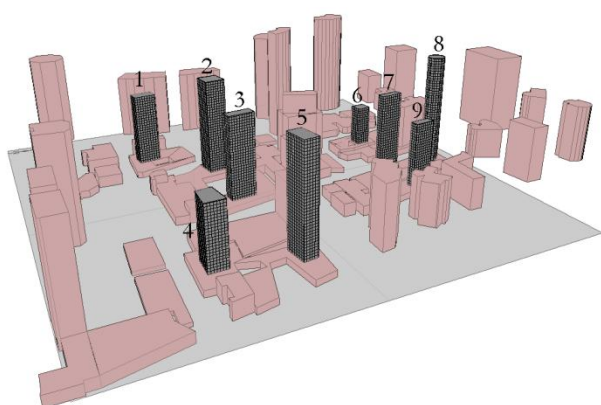


Figure 28. Actual design scenario: the new designed buildings inserted in the district

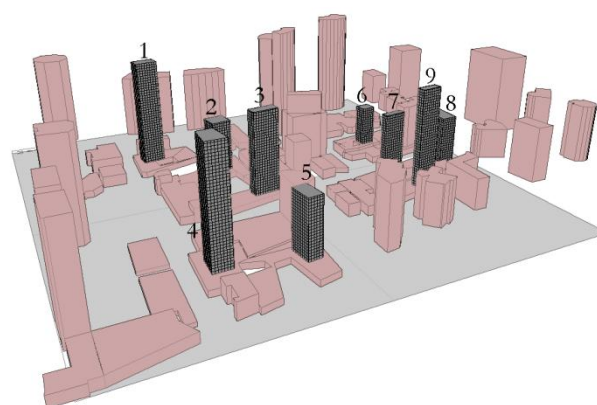


Figure 29. Solar optimized scenario: the new designed buildings inserted in the district

The aim of this simulation is to calculate the overshadowing and solar reflection effects on the façades of the buildings, in terms of increment or decrement of the available solar radiation, caused by the neighbouring existing buildings.

Graph 8. Results of all contribution solar radiation for the designed scenario and solar optimized design scenario in existing context with ambient bounces equal to 3 and ground reflectance equal to 15%.

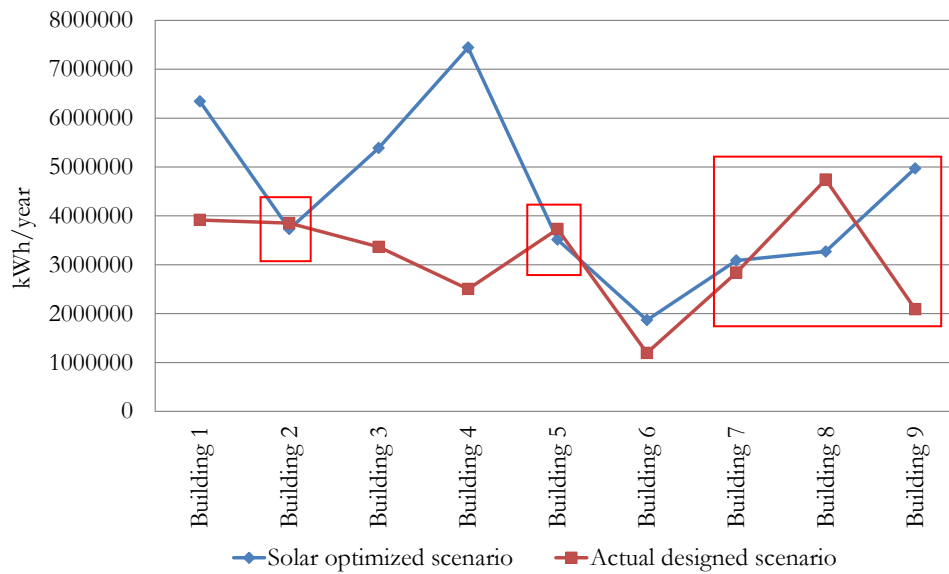


Table 22. Results considering all contribution of solar radiation in designed scenario and solar optimized design scenario within context.

Building	Conditions Ambient bounces (ab) and ground reflectance (Gr. refl. [%])	Designed scenario		Solar optimized design scenario		Results Increment or decrement [%]
		Direct solar rad. (kWh/year)	(kWh/m <sup>2</sup> year)	Direct solar rad. (kWh/year)	(kWh/m <sup>2</sup> year)	
Building_1	ab=3, Gr=0,15	3,915,044	630	6,343,403	902	38%
Building_2	ab=3, Gr=0,15	3,851,539	538	3,730,433	942	-3%
Building_3	ab=3, Gr=0,15	3,365,208	577	5,388,376	924	38%
Building_4	ab=3, Gr=0,15	2,503,552	555	7,442,971	921	66%
Building_5	ab=3, Gr=0,15	3,731,127	515	3,514,016	888	-6%
Building_6	ab=3, Gr=0,15	1,194,520	560	1,866,805	876	36%
Building_7	ab=3, Gr=0,15	2,839,061	606	3,086,986	864	8%
Building_8	ab=3, Gr=0,15	4,741,891	844	3,270,032	792	-45%
Building_9	ab=3, Gr=0,15	2,091,513	577	4,971,688	904	58%
Total	ab=3, Gr=0,15	28,233,456	5,401	39,614,710	8,013	29%

Results are very close to the previous ones, although the overshadowing effect, caused by the neighbouring existing buildings, has some influence on the solar availability. In fact only for three buildings (buildings 2, 7 and 9) the value of global solar radiation on the façades is increased, although the increments are not very high. On the contrary, the decrements due to the overshadowing effect are

substantial, especially for building number 1, which loses 10% of the global solar radiation. Results are collected in Table 22 [60].

The contents of this chapter were presented in the publication entitled “SolarPW: A New Solar Design Tool to Exploit Solar Potential in Existing Urban Areas” [60] at SHC 2012 – International conference “Solar Heating and Cooling for Buildings and Industry” in San Fransco on the 9-11<sup>th</sup> July, 2012.

## **2.5. Conclusion and outcomes**

### *Conclusion of the first part*

Although the presented analyses are only preliminary, this paper showed the influence that a “solar conscious design” may have on the massing and orientation of buildings in urban areas. The next steps of this study will include dynamic annual simulations of the energy performance of buildings, considering the other components of solar radiation (diffuse, sky component and reflections from external surfaces).

With the help of simulation tools, it is possible to control the potential energy production from the envelope of new buildings and their effect on neighbouring buildings in terms of overshadowing.

The reduction of performances in existing buildings due to a new neighbouring building (in terms of passive solar gain and renewable energy production) is a very critical issue that at the moment is hardly regulated by the law. It is very likely that in the near future the attention to this issue will grow, as current energy certificates will expire and may have to be re-issued in different conditions of solar exposure, leading to worse rating and loss of value for the owner of the building.

### *Conclusion of the second part*

The simulation conducted with *Daysim*, considering all of the new building volumes in both scenarios, demonstrated that the increments of direct solar radiation (Table 20) are positive when comparing the solar optimized scenario to the original one, for every building except for building 8, as a result of a partial optimization of three buildings (buildings 7, 8 and 9). This explains that the tool works well if two buildings are considered, while the optimization of three or more buildings required more refined analyses. The differences among values increase when considering the effects of overshadowing and solar reflections from other buildings (Table 21), with increments or decrements of global solar radiation values. These effects increase if the analysis is done in the context (Table 22).

It is important to underline that the analyses have been conducted assigning only concrete plaster as finishing material for all façades, with its specific solar reflection. It is reasonable to guess that using other materials with different reflection values, the increments or decrements of global solar radiation available on the façade would increase or decrease. Further studies to analyse the effects of other materials or by using the same material with different RGB reflection values will be a part of the future work.

The development of this study will include the evaluation of the façade areas where solar radiation is higher thanks to direct radiation and to reflection from nearby buildings. This will identify areas with more potential for solar exploitation using photovoltaic or solar thermal panels installed on the façades. The amount of energy that could be produced under different boundary conditions will be evaluated as well, together with payback periods of investments.

### **3. Solar geometric optimisation: simple volume transformation and solar reflection and ground reflection contributes**

#### *Questions of the chapter*

1. How is possible to maximize the solar radiation of the building in existing urban area?
2. How is possible to localize the best area for installing the solar systems on the façade?
3. How is possible to panelling a complex surfaces of the façade for installing the solar systems on it?

#### *Abstract*

This chapter shows the results of a research aimed at assessing the amount of energy that can be produced by solar envelopes (facades and roofs) in urban contexts.

This section of the study presents the first part of the optimization process of the building volume starting with simple parametric transformations of reference construction volume equal to 1000m<sup>3</sup>: were tested different combinations of heights and ground level geometric shapes for percentages of footprint.

In fact a preliminary set of simulations was carried out, through dynamic yearly analyses on a sample building, to identify the main parameters influencing the availability of solar radiation and to optimize the building's shape. The purpose of this part of the study is focused on calculation the best solar exposure of the building in order to improve the solar radiation on the bulding envelope and in particular to estimate the solar radiation harvest on the façades.

The general target is to maximise solar radiation available on the external building envelope, in order to exploit it through building integrated solar systems and calculate the energy production that is possible to reach from their installation especially on the façades which are the most exposed building's surfaces.

Furthermore the second part of this section is focused on the effect of reflected solar radiation that has been analysed by simulating different finishing materials (green façades, glazed façades, concrete façades and aluminium façades) on the neighbouring buildings, considering the orientation north-south and north-south/east-west.

### **3.1. Introduction**

The built environment accounts for over 40% of the world's total primary energy use and for 24% of greenhouse gas emissions [1]. With the aim of reducing the energy consumption of buildings and the related environmental impact, several regulations and demonstration activities are pushing for the adoption of the “net zero energy” standard. Among these regulations, the European Directive on the energy performance of buildings (2010/31/EU), requiring that new buildings comply with the “nearly zero energy” standard by 2020, is probably the one with the largest potential impact, as it regards all of the 27 Member States of the European Union.

Although the standard definition of a nearly zero energy building is still under discussion [2], the spirit of the Directive is about matching a very limited energy need of the building with the amount of energy that can be sourced on (or near) the site. Some existing buildings prove the feasibility of scenarios where the energy used for heating and cooling is offset by the yearly production of renewable solar energy [3]. However, these prototypes are generally isolated, low-rise buildings with optimal solar exposure, while most of the world's population live in dense urban areas [4], and in Europe, policies promote increasing density in existing urban areas to reduce sprawl [5]. This means that most of the buildings will have to aim for the nearly zero energy standard in a context where the orientation, availability of surfaces exposed to the sun and the overshadowing conditions can be far from optimal.

In view of the European 2020 requirements, it is then interesting to assess the solar potential of buildings located in urban areas, where the availability of solar radiation on the building envelope depends also on the shading conditions and on the reflections from nearby surfaces. On the other hand, it should not be underestimated that a higher amount of solar radiation on facades and roofs means higher cooling loads in summer and increased surface temperatures. The latter can have an impact on the air circulation and the temperature distribution within urban canyons, leading to high summertime outdoor air temperatures (Urban Heat Island effect – UHI) that increase cooling-energy use and accelerate the formation of urban smog [6].

### **3.2. Material and method**

Within this scenario, the general aims of the work are to demonstrate the influence that building and façade design have on the total amount of solar radiation incident on the external building envelope and to increase the energy production of integrated solar systems by optimizing the shape of the buildings in the district morphology. Distribution of volumes, road pattern and building orientation, finishing materials, street width and relative buildings height are all parameters that could potentially affect solar rays' access on buildings. These aspects could also have a strong influence on general and local climatic variations (mitigation of urban heat island effect), as well as on users comfort, both indoors and outdoors.

In particular, this chapter presents a parametric study on the optimization of the building's volume and the numerical evaluation of the solar radiation insisting on the building envelope, in order to assess if facades can be exploited, in parallel with the roof, for energy production in dense urban areas, where there may be significant overshadowing caused by existing constructions. The analysis of basic models allows assessing energy need and calculating potential energy production under different design conditions (height and size of buildings, distance between blocks, cladding materials, etc.).

As just extensively written above in chapter 2 about the different tools available for calculating the solar irradiation on the buildings, *Daysim* daylighting dynamic simulation tool has been chosen for conducting the sets of simulations.

#### **3.2.1. Solar reflection in urban canyon and effect on a buildings**

Reflected light from another buildings or from the ground can be used to illuminate interiors, influencing not only the quantity of light, but the quality as well. Under specific conditions, the main problem that the sunlight can cause is the glare. Under clear-sky conditions, the impact of ground-reflected light on the interior illuminance is minor. Under overcast-sky conditions the light from the ground plane may increase the illuminance on a vertical surface by as much as 50%.

Conversely, on clear days vertical surfaces can significantly increase light levels on facing vertical surfaces, while their impact is minimal under overcast conditions. For these reasons, ground-reflected light is more useful under overcast conditions, while reflected light from vertical surfaces is more useful in clear-sky climates.

The light that is reflected from vertical surfaces (such as fscing building walls) is affected by:

- their dimensions;
- their reflectivity;
- their orientation.

One advantage of these surfaces is that they can be most effective during winter months, when it may be difficult to maintain the design interior illuminance in the building.

Walls opposite north-facing windows have the best opportunity to reflect sunlight, while east or west oriented walls can be useful only in the morning or in the evening.

The use of reflected light to increase the light penetration into a space can be accomplished by placing reflective surfaces in the field of view of the window. Since the lower parts of the window reflect light more deeply into the space, a good design target is to maintain a view of the sky from the upper part of the window, leaving the lower part for reflected light. The heights of different vertical surfaces that are to be used as reflectors for north-facing apertures.

With the increasing interest in passive solar design, many architects have come to realize that the design of the building façade is critical if radiant energy from the sky is to be used. During recent years coated glazings have found widespread application in order to, among other reasons, reflect heat or reduce glare. This may be desirable for the occupants of the building in question, but people opposite or on the road may have problems due to glare. Vertical glazed surfaces may only cause problems when the sun is low in the sky (during the sunrise or sunset). If the façade is inclined with respect to the vertical, problems may occur even when the sun is high in the sky [61].

### **3.2.2. Radiance materials**

#### *From radiance materials to Daysim materials' definition*

Regarding the simulation programmed in this section was important to manage the materials given that sets of simulations expected to test different materials and colors. The process of colors' application in *Daysim* is articulated: in fact is possible to modify the material definition changing .rad file presented in the folder of case study analysed.

Below is reported the part on the process to set the material definition from *Radiance* to *Daysim* described in *Daysim* tutorial [45].

However for the most part, is easier to use a *Radiance* scene and import it straight into *Daysim*. But, since *Daysim* does not support all material modifiers available within *Radiance*, it might edit an otherwise valid *Radiance* files to make it accessible to *Daysim*. This process can be automated using the *Radiance* to

*Daysim* converter radfiles2daysim. Table 23 summarizes the difference between the *Radiance* and *Daysim* file format.

Table 23. Difference between the *Radiance* and *Daysim* file format.

Item to check	
Daysim only supports a fraction of all Radiance materials. Should your Radiance scene contain an unsupported material, your simulation will generate an error. The following Radiance material modifiers are currently supported in Daysim:	
RADIANCE	DAYSIM
light	Light sources in the Radiance files are replaced by a black plastic in Daysim. The reason is that during the daylight coefficient calculation Daysim automatically adds a sky to the scene. If other light sources were activated in the scene, the contribution of these light sources to the daylight coefficients would lead to wrong results.
glow	same as light
plastic	fully supported in Daysim; the materials with this type are turned monochrome in the Daysim file. The reason for this is that Daysim uses only one color channel to calculate a set of daylight coefficients for all sensors provided in your sensor file.
metal	same as plastic
mirror	same as plastic
trans	same as plastic
glass	same as plastic
If your Radiance scene file(s) contain links to secondary files, e.g. <code>!xform -t 0 0 0 other_file.rad</code> the file you import into Daysim needs to contain the absolute path for the secondary file so that Daysim can find it: <code>!xform -t 0 0 0 ABSOLUTE_PATH\other_file.rad\</code> Note that radfiles2daysim won't explicitly pass through secondary files. Your secondary files therefore have to be already in a valid Daysim format. Otherwise, the simulation will generate an error.	
If a color has been modified in the Radiance input file, a message in the Daysim GUI will inform you of the change	
PC files are sometimes not properly read into Daysim. In case you run into any difficulties, save your Radiance model files in UNIX format instead.	

### Defining material properties

Defining physically correct material properties for all surfaces in the scene is crucial for the overall simulation. *Radiance/Daysim* allows you to correctly model a wide number of diffuse and specular, opaque and transparent material properties. Even though *Daysim* aims to simplify the job of assigning for you,

you should acquire at least a basic understanding of the *Radiance* file format. The *Radiance* file format is described in detail in *Rendering with Radiance* book as well as the online *Radiance* manual pages.

The remaining of this section describes how and where to modify material properties in *Daysim*.

Once you have successfully implemented a building model into *Daysim*, your “Building” menu within the *Daysim* GUI resemble as shown in Figure 30.

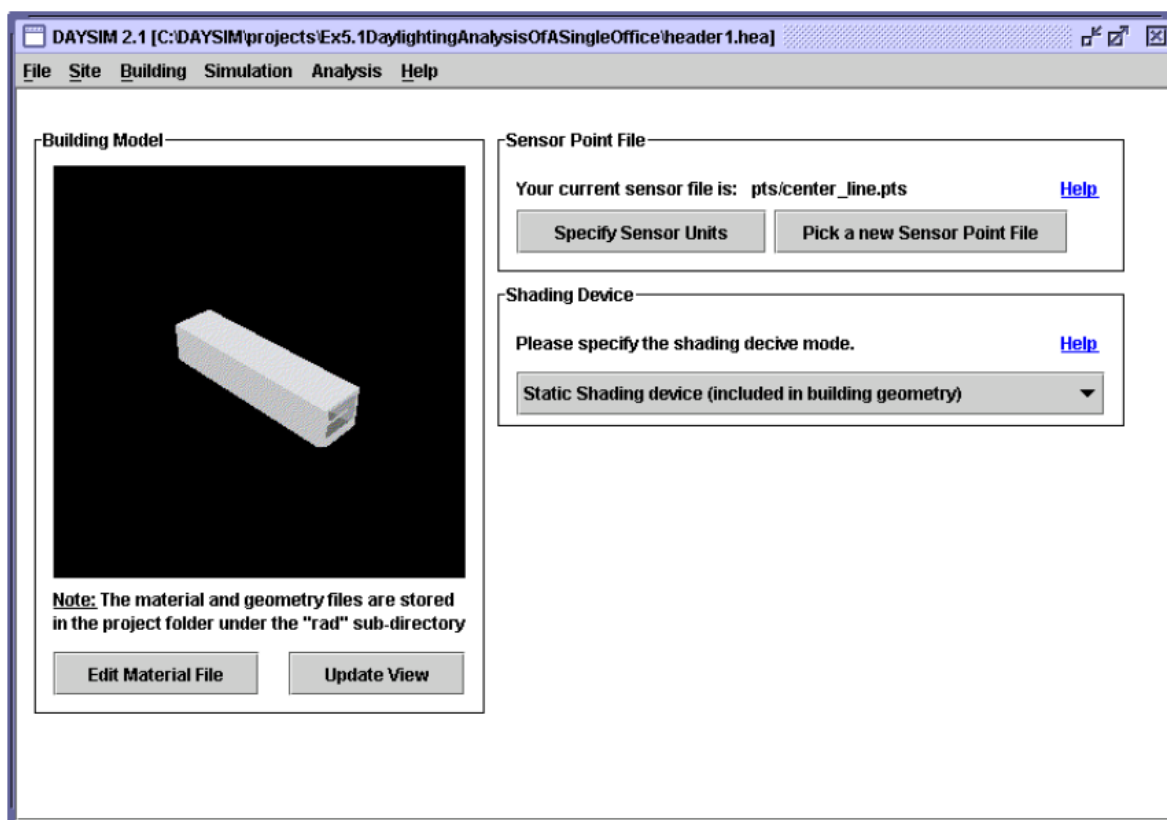


Figure 30. Building menu in *Daysim*

After importing a building model, it should always review the *Daysim* material file of the project.

The *Daysim* material file contains material properties for all materials used in the building model. You can access the *Daysim* material file by the “Edit Material File” option within the “Building Model” section. This will open the material file in the text editor you specified during the *Daysim* installation. Figure 31 shows the *Daysim* material file as an example.

It is possible to edit the *Daysim* material at will. The note that in Figure 31, all materials in the file have been taken from the *Daysim* material database which suggests that they all represent “physically meaningful” materials. The user should decide to edit the *Daysim* material file, should always verify whether, that the file format is still valid by selecting the “Update View” button in the “Building Model” section. *Daysim* will try to rebuild the building model using the *Radiance* program “oconv”. If successful,

an updated version of the building model will appear. Otherwise, the error generated by *Radiance* will be shown in an error box.

```
#####
# Daysim Material File
#####
# All comments start with an '#'
#####

# SOURCE FILE: C:/DAYSIM/projects/Ex5.1DaylightingAnalysisOfASingleOffice/tmp/ImportFrom3ds.mat.rad

#<-----
# The material description for GenericInteriorFloor is taken from the Daysim database
# material GenericFloor30
# material_type opaque
# comment: This is a purely diffuse reflector with a reflectivity of 30% which
# according to the Lighting Handbook of the International Engineering
# Society of North America (IESNA) is a typical floor reflectivity.
#
void plastic GenericFloor30
0
0
5 0.3 0.3 0.3 0 0
#<-----

#<-----
# The material description for GenericInteriorWall is taken from the Daysim database
# material GenericWall60
# material_type ...
void plastic GenericWall60
0
0
5 0.6 0.6 0.6 0 0
#<-----

#<-----
# The material description for GenericInteriorCeiling is taken from the Daysim database
# material GenericCeiling80
# material_type ...
void plastic GenericCeiling80
0
0
5 0.8 0.8 0.8 0 0
#<-----

#<-----
# The material description for DblGlazSpecSel72 is taken from the Daysim database
# material DblGlazSpecSel72
# material_type transparent
# comment: This is a generic, spectrally selective double glazing with a
# visual transmittance of 72%.
void glass DblGlazSpecSel72
0
0
3 0.784590 0.784590 0.784590
#<-----

#<-----
# The material description for SingGlazClear90 is taken from the Daysim database
# material SingGlazClear90
# material_type ...
void glass SingGlazClear90
0
0
```

Daysim header information

material properties for "GenericInteriorFloor"

Radiance material "plastic".

5 values: ref<sub>red</sub> ref<sub>green</sub> ref<sub>blue</sub> specularity roughness

This line indicates that "GenericInteriorWall" has been automatically substituted with the entry from the Daysim material database

Radiance material "glass".

Figure 31. Example *Daysim* Material File.

Adding materials to the Daysim material database

The *Daysim* material database is in fact simply a directory (set in the *Daysim* GUI under File>> Preferences) that contains a number of *Radiance* files. Each file contains the material description for one material entry. The name of the file corresponds to the name of the material modifier followed by “.rad”. E.g., the material description for a GenIntWall (generic interior wall) is:

```
# material GenIntWall (Generic Interior Wall)
# material_type opaque
# comment: This is a purely diffuse reflector with a reflectivity of 60% which
# according to the Lighting Handbook of the International Engineering
# Society of North America (IESNA) is a typical floor reflectivity.
# author: C Reinhart
void plastic GenIntWall
0
0
5 0.6 0.6 0.6 0 0
```

Figure 32. the material description for a generic interior wall - File name:GenItWall.rad

To add a new entry to the database, it simply need to enter the *Radiance* material description into a file and have the file in the *Daysim* material database directory under <material name>.rad.

Some *Radiance* material description database are available on *Radiance* website [62] or on the U.S. Department of Energy of Lawrence Berkeley National Laboratory website [63].

### **3.3. Theory and calculation**

The analyses of this chapter are divided onto two parts: in the first part were simulated the isolated buildings in order to conduct an initial parametric process for studying the optimisation of building volume's shape, while in the second set of simulations were analysed the same buildings previously analysed without context in order to study the contribution of solar radiation coming from the surrounding testing different configuration of materials and colour on the façades.

#### **3.3.1. Analyses and main objectives**

The specific aims of this study are:

- optimization of the building shape with respect to solar access, keeping the volume constant;
- organization of the building volume in order to maximize solar exposure;
- evaluation of the solar potential of the building, considering the influence of solar reflection of the external surfaces of the neighbouring buildings, in different scenarios of painting colours and finishing materials;
- qualitative analysis of the impact of radiative properties of surfaces on urban heat island effect (mean radiant temperature increase).

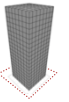
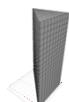
In particular, the availability of solar radiation on the building façades has been mainly considered, while the roof has been calculated separately. The reasons for this choice are that for tall buildings, the amount of roof space per apartment floor area is relatively limited and the roof surface has often to be shared among different concurrent functions (services, shafts, terraces, etc.) that limit the potential for the installation of solar panels; because of this, is thus possible to cover just a limited portion of the energy demand of the building. In dense urban conditions, then, it may be sensible to explore the potential of other exposed surfaces, such as façades, although their orientation and tilt are not optimal for solar energy production over the year.

Simulations have been carried out in two different steps: in the first part, the global annual radiation on the building envelopes of simple volumes has been estimated; in the second part the analysed volume has been included into a hypothetical district consisting of nine blocks about 1000 m<sup>3</sup> each. All the simulations have been carried out for the city of Milan – Italy (latitude 45.27° N, longitude 9.11° E) using statistical data recorded at the Milan Malpensa airport (source: EnergyPlus weather data website).

The first analyses (irradiance variation due to shadowing) have been conducted on a constant volume of 1000 m<sup>3</sup>, varying the covering ratio of the development ( $S_c$ , i.e. the ratio between the building's footprint and the area of the lot) between 100% and 25%. Different footprints (square, rectangular, trapezoidal and triangular shapes) and different heights (in the range between 10 and 40 m) have been

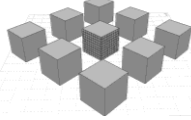
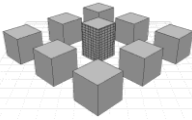
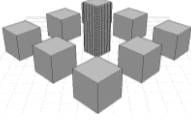
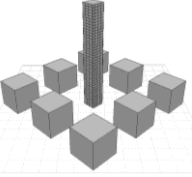
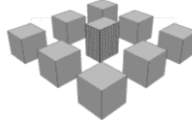
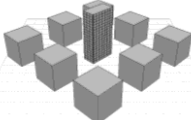
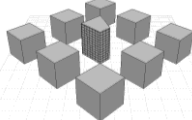
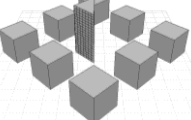
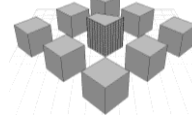
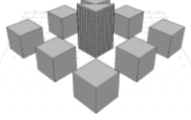
simulated. Orientation and shapes of the building plan have been selected in order to minimize the north façade surface and to guarantee a minimum ratio between two adjacent sides of at least 1:2, as shown in Table 24.

Table 24. Buildings simulated in analysis 1: different footprints, covering ratios ( $S_c$ ) and building height (H), keeping the building's volume constant.

Shape \ Sc&H	100% - H=10 m	75% - H=13.3 m	50% - H=20 m	25% - H=40m
Square	100_NS_sq 100_NWSE_sq	75_NS_sq 75_NWSE_sq	50_NS_sq 50_NWSE_sq	25_NS_sq 25_NWSE_sq
				
Rectangle		75_NS_rect 75_NWSE_rect	50_NS_rect 50_NWSE_rect	
				
Trapezium Triangle		75_NS_trap_NE 75_NWSE_trap_NE	50_NS_tr_NE 50_NWSE_tr_NE	
				
		75_NS_trap_NW 75_NWSE_trap_NW	50_NS_tr_NW 50_NWSE_tr_NW	
				

Afterwards, the reference building has been included into a simple district composed of nine blocks, 1000 m<sup>3</sup> (10x10x10 m) each (Table 25). As in the previous set of simulations, the variations of covering ratio, as well as the changing of shape and height of the reference building have been simulated, maintaining constant the building's total volume. Reflection of energy from nearby surfaces has been taken into account under different hypotheses: the reflectance properties of surrounding envelope surfaces have been modified according to several assumed claddings (plaster with different colours from black to white, aluminium facade, concrete facade, glass facade and green facade).

Table 25. Analysis 2: simulated buildings into hypothetical districts consisting of nine blocks of about 1000 m<sup>3</sup> each.

Shape \ S <sub>c</sub> &H	100% - H=10m	75% - H=13.3 m	50% - H=20m	25% - H=40m
Square	100_NS_sq 100_NWSE_sq	75_NS_sq 75_NWSE_sq	50_NS_sq 50_NWSE_sq	25_NS_sq 25_NWSE_sq
				
Rectangle		75_NS_rect 75_NWSE_rect	50_NS_rect 50_NWSE_rect	
				
Trapezium Triangle		75_NS_trap_NE 75_NWSE_trap_NE	50_NS_tr_NE 50_NWSE_tr_NE	
				
		75_NS_trap_NW 75_NWSE_trap_NW	50_NS_tr_NW 50_NWSE_tr_NW	
				

All the simulations have been performed with the program *Daysim* (version 3.1 b), developed by the National Research Council of Canada and the Fraunhofer Institute for Solar Energy Systems in Germany. *Radiance* files, generated with the graphical interface of *Autodesk Ecotect Analysis* and including the model scenes have been imported in *Daysim* software and dynamic analyses have been run, in order to collect hourly data during the simulated year. At the end of the solving procedure, the rather large resulting files have been managed with Matlab algorithm.

*Daysim* is a validated *Radiance*-based program [7], developed and validated for daylight calculations of complex transparent systems [8], that combines a backward-ray-tracing algorithm, a daylight coefficient approach and the Perez Sky Model to simulate time series of solar irradiances. Two simulation methods are allowed: the “DS” method and a revised method added in 2008, denominated “DDS –s” standard daylight coefficient model with overshadowing [9]. Both daylight coefficient methods differ in how direct

and diffuse irradiances are treated. DDS allows for a more detailed analysis of direct solar contributions while sacrificing time and computing resources [10].

Table 26. Set of “rtrace” parameters used for all *Radiance*-based simulations.

ambient bounces	ambient division	ambient super-sample	ambient resolution	ambient accuracy	specular threshold	direct sampling	direct relays
1 – 3	1000	20	300	0.1	0.15	0.20	2

Table 26 details the final parameters for all *Radiance*-based simulations developed in the first and second part of the study. The set of “rtrace” parameters has been simplified with respect to the parameters used in previous works concerning the simulations of solar availability [10]: this choice has been taken after demonstrating that this simplification does not affect the final results.

“Ambient bounces (ab)” is the variable parameter in the simulations: it represents the maximum number of diffuse bounces computed by indirect calculations. While in the first part of the analyses an ab equal to 1 and a ground reflectance of 0 have been used in order to consider only the effect of global sky solar radiation, in the second part of the analyses a ground reflectance of 0.15 (corresponding to a weathered asphalt) and an ab equal to 3 have been used for computing multiple solar reflections between the main and the neighbouring buildings.

Each set of simulation has been run with different orientation, so as to consider the solar exposure of the buildings façades, with respect to the directions of the roads: the solar radiation values have been calculated in North – South (NS), and North - West, South - East (NWSE) orientations.

### 3.3.2. Sensitivity analysis

A sensitivity analysis has been carried out in order to define the sensors’ distribution on the building envelope: it is thus possible to assess how the increase of resolution settings affects the accuracy of simulation results. This analysis has been done on the base case (100\_NS\_Sq) with different sensors distribution and hence different areas of influence.

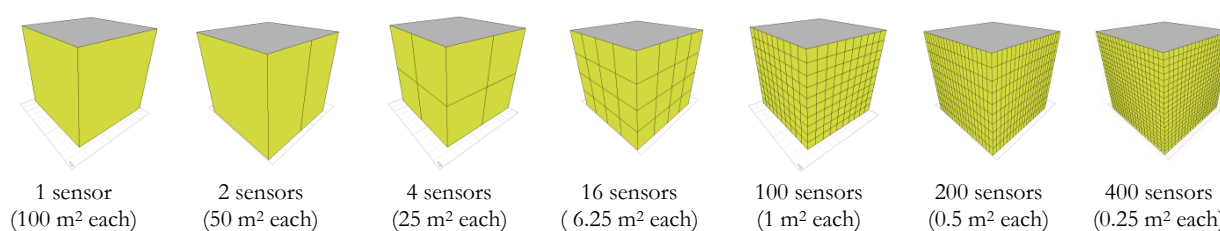
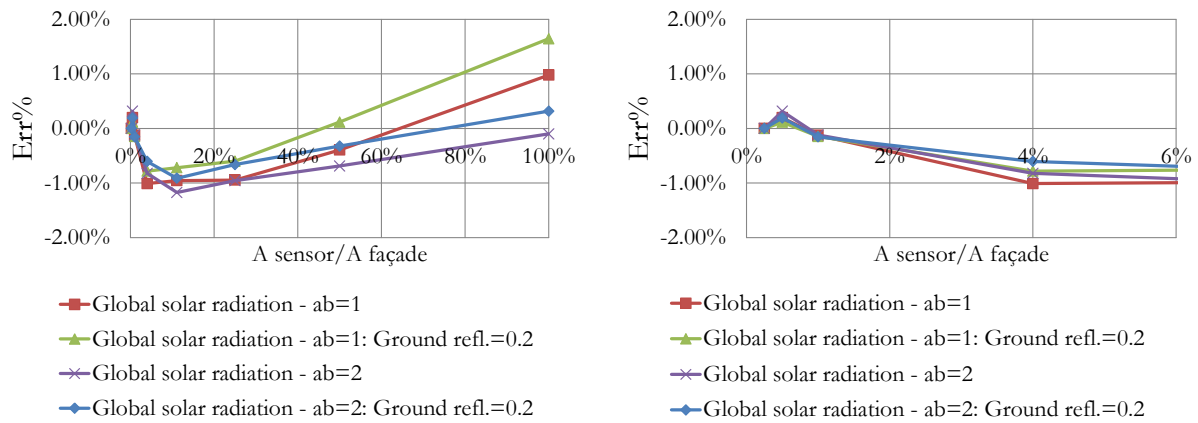


Figure 33. Subdivision on façades’ surfaces: indication of influence area of each sensor.

Graph 9 shows the results of the sensitivity analysis: the error (Err%), calculated as the deviation between the solar radiation calculated on each grid and the one obtained on a reference grid of 400 sensors, is displayed as a function of grid size ( $A_{\text{sensor}} / A_{\text{façade}}$ ). As evident from Graph 9 (b), a grid composed of 100 sensors ( $A_{\text{sensor}}/A_{\text{façade}} = 1.0\%$ ) has an acceptable error of 0.15% and a convergence speed higher than the one related to finer grids. (i.e. 200 and 400 sensors) and thus has been chosen for the further analyses.

Graph 9.(a) Results of the sensitivity analysis with different simulation conditions and accuracy of the sensors distribution; (b) Enlargement of the sensitivity analysis ( $A_{\text{sensor}}/A_{\text{façade}} < 6\%$ ).

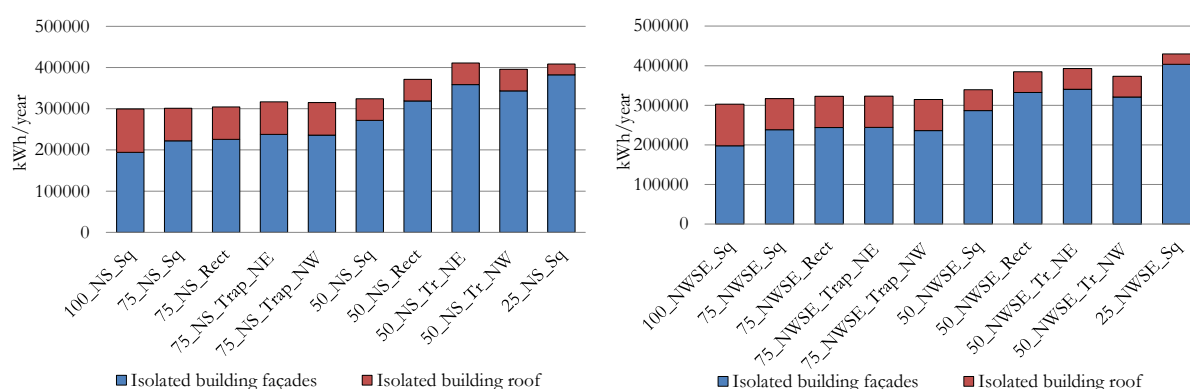


### 3.4. Results and discussion

#### 3.4.1. Simulation of a single building - solar exposure

The first set of simulations has been carried out on a single building with four different values of covering ratio  $Sc$ : 100%, 75%, 50% and 25% and keeping constant the building's volume to 1000 m<sup>3</sup>. The results of the simulations, expressed in term of global radiation (kWh/year), are summarized in the column graphs of Fig. 2. In order to split the global amount of solar radiation on building envelope, contributions of vertical surfaces and of roofs are shown in the graphs. In this way different footprints are easily comparable. On the NS orientation, the 50\_NS\_Tr\_NE (triangular footprint with 50% of covering ratio and NS orientation) has the highest global radiation, equal to 410,937 kWh/year (561 kWh/m<sup>2</sup>year), sum of 358,427 kWh/year on the facades and of 52,510 kWh/year on the roof. If only the facade's contribution is considered, the highest value of annual solar radiation (382,196 kWh/year) is obtained for the building 25\_NS\_Sq (square footprint with 25% of covering ratio).

Graph 10.(a) solar radiation analyses for different configurations of the volumes for NS orientation: (b) and NWSE orientation.



On the NWSE orientation the building 25\_NWSE\_Sq (square footprint with 25% of covering ratio) has the highest global solar radiation incidence (429,902 kWh/year or 521 kWh/m<sup>2</sup>year), and also the highest incidence of solar radiation on vertical surfaces (403,647 kWh/year).

It is furthermore noticeable how, on an isolated building, the decrease of  $Sc$  is highly beneficial for the increase of global incident solar radiation (for both the two exposures NS and NWSE): an increase of about 40% of global solar radiation incident on the building's envelope is obtained, mainly due to the increase of total exposed surface. Finally, it can be noticed how, keeping  $Sc$  constant, the most beneficial solutions are the ones for which the total surface exposed to SE/SW is maximized (triangular and trapezoidal versus rectangular and square).

### 3.4.2. Simulation of the building in a district – solar access

In the second part of the study, a parametric analysis on the reference building included in a simple district composed of nine buildings (1000 m<sup>3</sup> each) has been performed.

All simulations have been carried out in two different scenarios, in order to calculate the different contributions of solar shadings and of indirect solar radiation reflected by neighbouring buildings. Four external cladding materials (green, glazing, concrete plaster and aluminium) have been simulated (Table 27). For the concrete plaster material, six different colours have been simulated, with reflectance values variable within the range 0.0% to 100%. The extreme values 0% and 100%, respectively for an ideally totally black and ideally totally white facade, have been considered only as maximum and minimum reference values.

Table 27. List of *Radiance* materials properties.

Material	Radiance material description	Number of values	R reflectance	G reflectance	B reflectance	Specularity	Roughness
Conc plaster 0% R	void plastic	0 0 5	0.000	0.000	0.000	0.00	0.00
Conc plaster 30% R	void plastic	0 0 5	0.296	0.296	0.296	0.00	0.00
Conc plaster 55% R	void plastic	0 0 5	0.549	0.549	0.549	0.00	0.00
Conc plaster 60% R	void plastic	0 0 5	0.596	0.596	0.596	0.00	0.00
Conc plaster 90% R	void plastic	0 0 5	0.890	0.890	0.890	0.00	0.00
Conc plaster100%R	void plastic	0 0 5	1.000	1.000	1.000	0.00	0.00
Green facade	void plastic	0 0 5	0.150	0.600	0.200	0.00	0.00
Concrete facade	void plastic	0 0 5	0.549	0.549	0.549	0.00	0.00
Aluminum facade	void plastic	0 0 5	0.900	0.880	0.880	0.80	0.20
Glazed façade	void glass	0 0 3	0.750	0.820	0.820	/	/

The results of the analyses have been compared to reference case (NS\_100\_Sq for the NS orientation and NWSE\_100\_Sq for the NWSE orientation): the percentages of variation of global solar radiation on vertical surfaces are collected in Table 28 and Table 29.

The results show that the effect of the shadowing by neighbouring buildings produces a decrease of the global solar radiation reaching the reference building facade of about 17% (100\_NS\_Sq 0.0% on Table 28 and Table 29). Furthermore the shadowing effect reduces the yearly global radiation on the most exposed facade of about 27%.

The shadowing effect is generally balanced by the diffuse solar radiation reflected by neighbouring buildings: for the base case (square footprint with 100% of covering ratio), neighbouring cladding materials with more than 60% of reflectance are able to totally compensate the solar energy losses due to the shadows.

Table 28. Parametric analysis of solar access on buildings in a district NS oriented.

Analysis Shape	0.0% Refl.	30% Refl.	55% Refl.	60% Refl.	80% Refl.	100% Refl.	Green façades	Glazed façades	Concrete plaster façades	Alum. façades
100_NS_Sq	-17%	-9%	-1%	0%	7%	14%	-13%	-9%	-1%	9%
75_NS_Sq	5%	14%	21%	23%	32%	36%	9%	15%	21%	28%
75_NS_Rect	7%	15%	23%	24%	34%	38%	11%	14%	23%	30%
75_NS_Trap_NE	10%	18%	26%	27%	37%	41%	14%	17%	26%	34%
75_NS_Trap_NW	9%	17%	25%	27%	37%	41%	13%	16%	25%	33%
50_NS_Sq	40%	48%	55%	57%	66%	70%	44%	47%	55%	61%
50_NS_Rect	50%	57%	66%	67%	77%	81%	54%	57%	66%	72%
50_NS_Tr_NE	69%	78%	87%	89%	100%	104%	74%	78%	87%	94%
50_NS_Tr_NW	68%	77%	85%	87%	98%	102%	72%	76%	85%	92%
25_NS_Sq	116%	122%	128%	129%	137%	140%	119%	121%	128%	131%

Table 29. Parametric analysis of solar access on buildings in a district NWSE oriented.

Analysis Shape	0.0% Refl.	30% Refl.	55% Refl.	60% Refl.	80% Refl.	100% Refl.	Green façades	Glazed façades	Concrete plaster façades	Alum. façades
100_NS_Sq	-18%	-10%	-2%	0%	9%	13%	-14%	-7%	-2%	9%
75_NS_Sq	5%	13%	20%	22%	31%	35%	9%	14%	20%	28%
75_NS_Rect	5%	13%	21%	23%	32%	36%	9%	15%	21%	29%
75_NS_Trap_NE	9%	18%	26%	27%	37%	41%	14%	17%	26%	33%
75_NS_Trap_NW	8%	16%	24%	27%	35%	40%	12%	15%	24%	32%
50_NS_Sq	39%	47%	54%	55%	65%	69%	43%	47%	54%	60%
50_NS_Rect	61%	69%	77%	78%	88%	92%	65%	69%	77%	83%
50_NS_Tr_NE	68%	77%	86%	88%	99%	103%	73%	77%	86%	92%
50_NS_Tr_NW	64%	73%	82%	84%	95%	99%	68%	72%	82%	89%
25_NS_Sq	114%	120%	126%	127%	134%	137%	117%	119%	126%	129%

Also the building shape is greatly affecting the total amount of solar radiation incident on facades. As for the isolated building, the increase of building height tends to increase the global amount of solar radiation on vertical envelope, but the effects of reflections from neighbouring buildings are reduced with a reduction of covering ratio. Extracting, for example, from Table 5 the results for the square footprint

(100\_NS\_Sq, 75\_NS\_Sq, 50\_NS\_Sq and 25\_NS\_Sq), is evident that the increase of global solar radiation on vertical envelopes due to reflections is reduced from a global 26% for Sc = 100% to a global 15.2% for Sc = 25%.

Furthermore also the footprint shape has an impact on global solar access on buildings: generally for both covering ratios of 75% and 50%, trapezoidal/triangular footprints are more beneficial than the square/rectangular ones, due to the increase of the facade area most exposed to solar radiation (SE and SW orientations).

Comparing, instead, Table 28 and Table 29, it can be recognized that the orientation is only minimally affecting the global annual amount of solar radiation on vertical surfaces (less than 2% of decrease for a 45° rotation of the district orientation).

In Figure 34 the distribution of global annual solar radiation on the most exposed facade is shown. In these simulations, concrete facades have been used, as well as different footprints (square, rectangular, trapezoidal and triangular) and covering ratios (100%, 75%, 50% and 25%) have been compared for a district perfectly north-south oriented. It is noticeable how the increase of facade's height is highly beneficial, increasing the maximum value of global specific solar radiation. Due to the effect of reflected component, the facade strip between 15 m and 30 m has the maximum amount of global solar radiation: this is evident looking at the elevation of 25\_sq south façade.

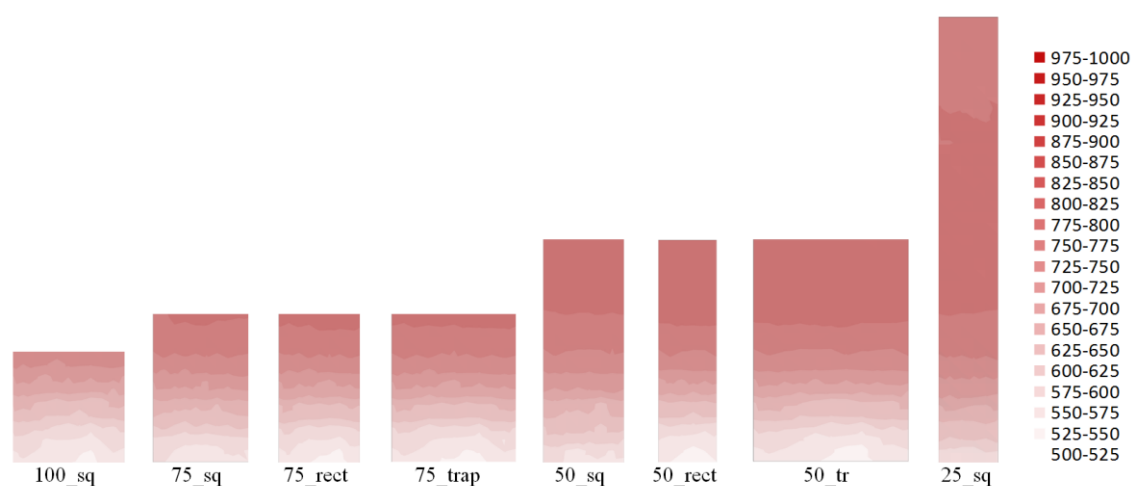
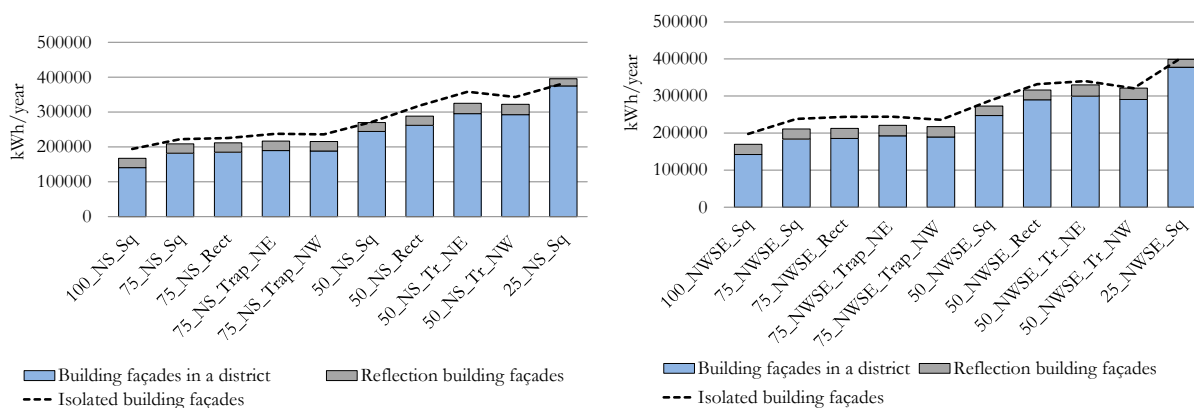


Figure 34. Concrete facades: distribution of global annual solar radiation on the South-exposed facade (values expressed in kWh/m<sup>2</sup>y).

In Graph 11, global solar radiation on vertical surfaces of each building's shape within the ideal district is compared with the equivalent value on the isolated building's envelope. Due to the lower percentage of facade's surface that is directly shaded, only the 25% covered square footprint is not considerably affected

by surrounding buildings: in this case the reflected solar components totally compensate the energy losses due to solar shading .

Graph 11. Concrete facades global and reflected solar radiation components as a function of building’s footprint. (a) NS oriented district; (b) NWSE oriented district.



The contents of this chapter were presented in the publication entitled “District Geometry Simulation: A Study for the Optimization of Solar Façades in Urban Canopy Layers” [64] at SHC 2012 – International conference on Solar Heating and Cooling for Buildings and Industry in San Fransco on the 9-11<sup>th</sup> July, 2012.

### **3.5. Conclusion**

The study has shown for different covering ratios and building footprints, how the distribution of the volume is able to maximize the solar radiation on building envelope, pointing out the importance of building façades, in terms of solar potential and energy production.

Different cladding materials have been simulated in order to consider the beneficial effects on total solar energy due to reflections. Some general considerations can be drawn.

- If the building's volume is kept constant, the solar exposure, as well as the solar access to building's façade is greatly affected by building shape: the relative increase of total annual solar radiation on vertical surfaces, changing building's covering ratio from 100% to 25%, is up to 95% for isolated buildings and up to 138% for surrounded buildings.
- The component of solar radiation reflected by surrounding buildings, globally on all the exposed facades, is able to compensate the losses due to shadowing if light colours are provided (with solar reflectance higher than 60%).
- Highly reflective materials beneficially increase reflected solar radiation, but visual and thermal comfort assessment has to be carried out: local increases of solar radiation on building's envelopes (as the ones obtained in the strip between 15 m and 30 m in the 25% covered square footprint building) could cause overheating and glare effects, especially if the building has wide and unshaded windows.
- Dark surfaces of surrounding buildings are not only reducing the solar access on reference building (due to the minimal amount of reflected solar component) but are also potentially increasing the UHI effect due to the increase of air and superficial temperatures. A good solution able to mitigate the UHI effects is the green facade, even if for the general aim of this study its contribution is limited.

Still open issues are referred to the reduction of solar access of surrounding buildings due to the shape modification of the reference building and to the relationship of solar access requisite with other urban environmental issues (increase of cross ventilation due to the Urban Canyon effect caused by the modification of the ratio between building's heights and distances, reduction of facade's superficial temperatures, solar access of surrounding buildings).

Next steps of this study will answer to these issues as well as will consider the complex transformation of volume and building's footprint with the aid of parametric softwares manipulating geometrical transformations (*Grasshopper for Rhinoceros*, *Galapagos* and *Geco* plug-in).

## **4. Solar geometric optimization: parametric generative modeling and dynamic solar analysis**

### *Questions of the chapter*

1. How is possible to maximize the solar radiation of the building in existing urban area?
2. How is possible to localize the best area for installing the solar systems on the façade?
3. How is possible to panelling a complex surfaces of the façade for installing the solar systems on it?

### *Abstract*

This chapter treats a part of research focused to study the parametric geometric transformation of the building volume and modeling of façade surfaces in order to reach the best solar geometric optimization for maximizing the solar access of buildings in an existing urban district. Photovoltaic systems are generally installed on roof tops of buildings located in low density areas due to the availability of horizontal surfaces, but the developments of cities with tall buildings and the lack of available horizontal surfaces have encouraged photovoltaic integration on façades.

The new policies of regulations to contain the horizontal city's development and to increase the use of renewable resources suggest a conscious and responsible design process.

Within this scenario the main aim of this study is to find the way to improve solar energy capture in the urban existing context. The study wants to localize the best areas on the façade surfaces to install the solar systems and optimize the solar energy production in order to cover a part of energy demands.

The optimization process starts from a simple three-dimensional volumetric modelling, with fixed parameters (height, floor area and volume of the building). Then façade surfaces are manipulated in an iterative parametric design process to evaluate the solar radiation of different geometric transformations using generative digital modeling software (*Rhinoceros + Grasshopper*) and solar dynamic simulation tool (*Radiance/Daysim and DIVA*).

The proposed method is restricted to the relationship between solar access and solar applications, but the further development of the research aims investigate the mutual effects among neighbouring buildings in term of solar reflections and increase of superficial temperatures.

The global process has been validated through a case study, analysing a typical development in Milan, involving the demolition of an existing building and the reconstruction of the same volume, with a solar optimized shape.

## 4.1. Introduction

Nowadays European directives are focused on solar access analysis in order to increase the potential production of energy from renewable sources, and to reduce buildings' energy demands as well as impact on climate and secure future supply of energy [65] [31]. Re-developments, characterized by the demolition of existing buildings and the construction of new ones with a higher volume and different shape, have encouraged the integration of photovoltaic systems not only in horizontal envelopes, but also in facades.

In this scenario, to increase the use of solar energy strategies (active and passive), the process of solar technologies integration into buildings should start from the beginning of the design phase. Many tools are currently available to run a preliminary analysis of solar radiation and solar access. Creating a map of solar irradiances onto building façades, designers are able to identify the most suitable area for solar systems' installation as well as calculate solar energy potentials [30] [23] [25].

Furthermore the value of annual solar radiation (along with its direct, diffuse and reflected beam components) allows designers to identify solar energy surplus and to optimize shading devices, in order to respond more precisely to seasonal performances [66] [29].

The most of the tools already available are working in a design environment integrated with the most used CAD programs, but the issue of their accuracy should be arisen. For example, a comparative study of several tools has been developed, in order to assess their numeric accuracy, reliability and appropriateness for application in architectural practice [56]. The study considered a wide range of calculation approaches, from a simplified method widely-used in practice (*Autodesk Ecotect Analysis*), to a detailed validated hourly simulation (Manual Method in Excel), to highly-resource efficient algorithm (GenCumulativeSky, *Daysim* DS (Daylighting Simulation), *Daysim* DDS (Dynamic Daylighting Simulation)). The results confirmed how the most integrated tools reported high accuracy errors (with a Mean Bias Error up to 50%), while the *Radiance*-based ones showed lower accuracy errors (MBS < 10%). Moreover, the results clearly demonstrated that, being these variations crucial for the calculation accuracy, the right tool should be selected early in the design phase.

Hence, these results open the issue of how to manage accuracy problems of the existing approaches adopted by integrated tools with the high demand from profession of complex geometric transformations of external envelope.

Within this scenario, the general aim of this work is to provide a new solar design approach creating a new tool composed of a combination of generative modelling (*Grasshopper* [67]), evolutionary solver (*Galapagos* [68]) and high accurate *Radiance*-based solar calculator tool (*Daysim* and *DIVA* [18]). Starting from urban fixed data, as footprint, floor area, height of storeys and building, and volume, the tool optimizes the shape of the building using digital tools for a better and more sustainable design. The innovation is in the possibility to formulate complex parametric transformations on 3D initial shape using a generative modelling, maintaining all urban data fixed at the beginning for every geographic location.

The integration with a *Radiance* type model will give to the designers the possibility to calculate, on complex geometrical shapes, highly accurate values of solar radiation to be used for planning the integration of active solar systems.

In particular this paper provides a first feedback of the tool, in the case of assessing the influence of solar access on the design of a new re-development in an existing urban area.

## **4.2. Material and method**

The work here presented is part of a wider study aiming to provide a new design approach for the assessment of solar potential in urban existing areas. In particular it is the prosecution of previous parametric modellings on the relationships between simple buildings and districts. While in the first study [59] a first optimization of the volume organization within an intervention of demolition and reconstruction has been analysed for searching the shape with the highest solar access, in a second study [64], a sensitivity analysis of the levels of total solar radiation on external envelope has been carried out for several building's geometrical transformations. These were involving changes of the total height, of the footprint shape and orientation of a reference building, considered either isolated or included in a simple regular district of nine buildings. After the first simulations, a more complex transformation strategy, involving also complex transformations, was needed. The work here summarized aims to describe the procedures adopted for integrating more flexible transformation strategies in the parametric analysis of solar access on buildings, through the use of advanced modelling techniques. Furthermore a validation of the procedure is here described, introducing the boundary conditions of a real intervention of demolition and reconstruction, where some restrictions to the general procedure may be produced.

A case study in the city of Milan (Italy) is here presented, and a parametric solar design approach is described, in order to maximize the solar access and solar potential of a new development in an existing urban area. The aspect investigated is the influence that building and façade design has on the total amount of solar radiation incident on the external envelope and on the related increase of efficiency of building integrated photovoltaic systems (BIPV).

The parametric optimization process, that allows to guarantee the most solar radiation and to localize the best areas of the façade for integration, starts from the initial design scenario imposed by the developer, with fixed parameters: number of buildings' storeys, volume, footprint area and height of each building. The parametric transformation examined in this case study, are the floor twist and the global building's slope from the vertical. In particular the floors twist varies from 45° west (Twist\_W45) to 45° east (Twist\_E45) with steps of 15° (Twist\_W45, Twist\_W30, Twist\_W15, Twist\_S0, Twist\_E15, Twist\_E30, Twist\_E45), instead slope from the vertical direction on south (Slope\_S), east (Slope\_E) and west (Slope\_W) orientations varies from 0° to 20° considering steps of 5° (Slope\_S5/E5/W5, Slope\_S10/E10/W10, Slope\_S15/E15/W15, Slope\_S20/E20/W20). These parametric transformations follow linear equation values of twist and movement deviation of the storeys, and permit new developments of the study begun previously where the analyses have been conducted on a constant volume, varying the covering ratio of the development [64].

More specifically the identification and parameterization of the building shapes is composed by consequent and logical stages. Initially, three-dimensional simple modelling is performed, as to create

restrictions and allow variations in building shape. In the second stage, the model is considered isolated and geometric transformations (twist, slope, and twist + slope) are correlated to the solar incidence. Finally the solar optimized shape is inserted in an existing district in order to calculate the solar radiation incident on external envelope and the mutual effects among neighbouring buildings.

The advantage of using the parametric geometric transformations is that permits a set of optimal solutions, integrating generative design methods with energy performance evaluation [69]. The introduction of generative systems, coupled with computational tools in the design process, allows a quick exploration of a large number of alternatives, thereby increasing the chance of choosing the best solution. Genetic algorithms and parametric systems constitute generative approaches capable of generating an almost infinite set of variations, from which the best solutions can be selected [70]. The script can work automatically fixing the data input (urban fixed data) and solving with a *Galapagos Evolutionary Solver*. The solver combines all shapes until when it finds the best volume's transformation that optimizes the data input. Alternatively the optimization could also be carried out manually, fixing the data input and imposing the transformations. In this study the second approach has been selected, as a sensitivity analysis of the variation's parameters was required.

The approach allow to reach the optimization of the building's volume and the numerical evaluation of the solar radiation insisting on the building envelope, in order to assess if façades can be exploited for energy production in dense urban areas. The analysis of basic models allows assessing energy need and calculating potential energy production under different design conditions (height and size of buildings, distance between blocks, cladding materials, etc.).

#### **4.2.1. Generative modeling tools: Grasshopper for Rhinoceros and some its plug-ins**

For developing the parametric transformations of the volume have been used the combination of modeling and calculation tools. A complete script has been done in order to joined the modeling tools to calculation tools directly. About *Daysim* has been extensively described in Chapter 2, below are presented a shortly overview on the modeling and calculation tools used for developing the new design solar tool.

##### *Grasshopper*

For designers who are exploring new shapes using generative algorithms, *Grasshopper* is a graphical algorithm editor tightly integrated with *Rhinoceros's* 3-D modeling tools. Unlike *Rhinoceros* script, *Grasshopper* requires no knowledge of programming or scripting, but still allows designers to build form generators from the simple to the awe-inspiring [71]. For a thorough overview on all potentialities of *Grasshopper* it easily to download the tutorial entitled "*The Grasshopper Premier*" on its specific website [72].

One of the interesting aspect of *Grasshopper* is that works with many plug-in developed by users and they are free downloadable. In the script for a new solar design tool some of these plug-in have been used and below are presented shortly.

### *Galapagos*

The term "Evolutionary Computing" may very well be widely known at this point in time, but they are still very much a programmers tool. 'By programmers for programmers' if you will. The applications out there that apply evolutionary logic are either aimed at solving specific problems, or they are generic libraries that allow other programmers to piggyback along. It is my hope that *Galapagos* will provide a generic platform for the application of Evolutionary Algorithms to be used on a wide variety of problems by non-programmers [67].

Any in-depth analyses about *Galapagos* and the theory behind are reported on the dedicated web page on "Evolutionary Principle applied to Problem Solving" [68].

### *Geco*

The other plug-in, called *Geco*, was very important in order to join the modeling tools, as *Grasshopper*, with solar simulation tool as *Autodesk Ecotect Analysis*.

*Ecotect* is a highly visual software for architects to work with environmental performance issues. It is designed for early stages of conceptual design, and encourages play to understand environmental factors and interactions.

So making use of *Grasshopper* has been developed a new interface named *Geco*, which offers a direct link between *Rhinoceros/Grasshopper* models and *Autodesk Ecotect Analysis*.

The plug-in allows you to export complex geometries very quickly, evaluate your design in *Autodesk Ecotect Analysis* and access the performances data, to import the results as feedback to *Grasshopper*.

This could be done as single process or loop to improve performance and the design of a building in the context of its environment.

The single results of the process could be saved inside *Rhinoceros* in the vertices of the analysis mesh to store data for later use inside different design approaches [73].

### *WeaverBird*

*Weaverbird* is a specific plug-in for subdividing any complex surface: *Weaverbird* is a topological modeler that contains many of the known subdivision and transformation operators, readily usable by designers. Instead of doing the work repeatedly, or sometimes using complicated scripts, this plug-in reconstructs the shape, subdivides any mesh, even made by polylines, and helps preparing for fabrication [74].

#### **4.2.2. Solar dynamic analysis tool: DIVA for Rhino toolbar**

*DIVA for Rhino* consists of a series of compiled *Rhino* and native *Grasshopper* scripts that are accessible within the *Rhinoceros* nurbs for Windows modeler via a dedicated toolbar. *DIVA for Rhino* has been developed by Harvard University's research group [75].

*DIVA for Rhino* uses the following third party software:

- *Radiance* [76];
- Evalglare [77];
- GenCumulativeSky [78];
- *Daysim* [79].

The toolbar was developed in order to bring *Radiance*, *Daysim* and other daylighting analysis tools to the *Rhinoceros* environment, avoiding the necessity of exporting the *Rhino* model to *Autodesk Ecotect Analysis*, and thereby making validated daylighting analysis more accessible, easier to use, and less likely to be compromised by user error.

The toolbar works as follows: the user creates a model using standard *Rhino* modeling methods. The user then selects a surface or series of surfaces from which a grid of sensor nodes will be generated. The toolbar, which is displayed like other *Rhino* toolbars, can be used to setup and perform the analyses. The final results are either images generated in *Radiance* and displayed a separate image viewer, or consist of a grid of false-colored panels with accompanying legends.

For any other details of *DIVA for Rhino* is available the “Quick Start Guide for the *DIVA for Rhino* Toolbar” directly downloadable on the specific website [80].

### 4.3. Theory and calculation

The façade optimization model considers three orientations (south, east and west) and consists in consequential and iterative steps, using a combination of design and analysis tools, as shown in Figure 35.

After selecting the best shape, the three-dimensional model is put in the district, in order to calculate the total solar radiation incident on its building envelope, taking in account also the mutual effects among neighbouring buildings in term of solar reflections, overshadowing effect and albedo.

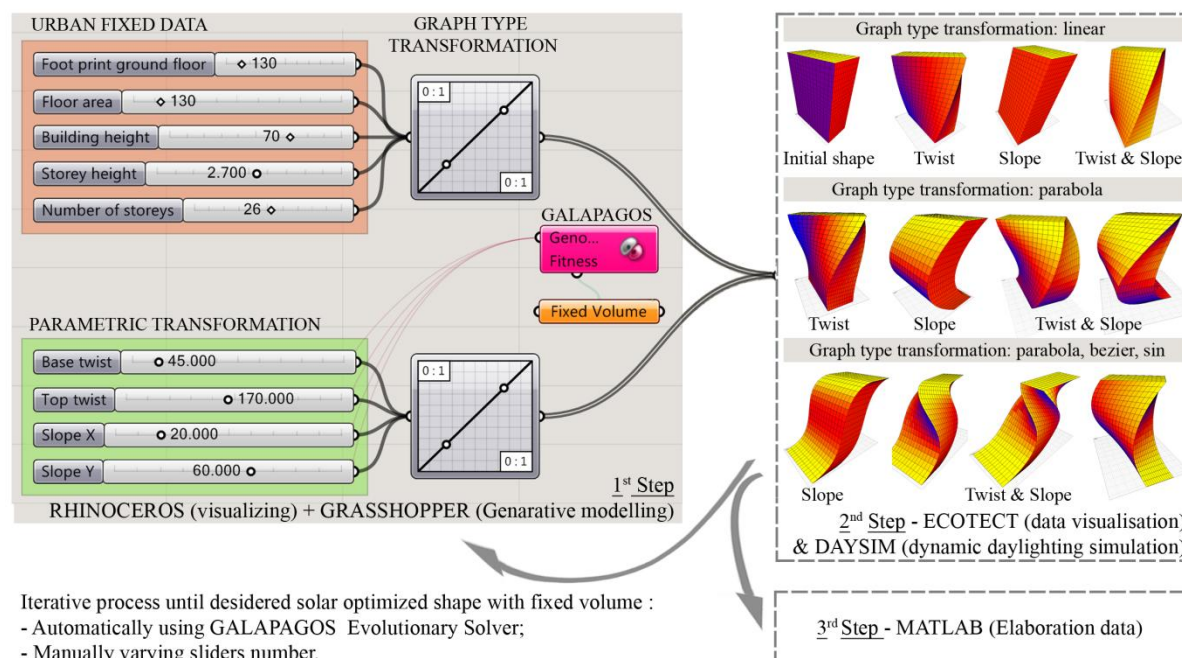


Figure 35. Flow chart of the optimization process using a combination of modelling and solar simulation tools.

As mentioned before, the calculation of the values of solar radiation incident on external envelope have been performed with the program *Daysim* (version 3.1 b), developed by the National Research Council of Canada and the Fraunhofer Institute for Solar Energy Systems in Germany. *Daysim* is a validated *Radiance*-based program [51], validated for complex daylight calculations [49]. In a previous work [8], *Daysim* program has been adopted and validated for a similar case of calculating solar radiation values on external envelope. Among the two simulation methods allowed, calculations have been performed with the DDS model, allowing for a more detailed analysis of direct solar radiation [47] [56].

Simulations have been carried out in two different steps: in a first part, the global annual radiation on the building envelopes has been estimated, in the hypothesis of simple isolated volumes, in order to optimized solar design; in the second part the analysed volumes have been included into an existing district of medium density area located in the north-west of the city of Milan.

Table 30. Set of “rtrace” parameters used for all *Radiance*-based simulations.

ambient bounces	ambient division	ambient super-sample	ambient resolution	ambient accuracy	specular threshold	direct sampling	direct relays
1 – 3	1000	20	300	0.1	0.15	0.20	2

Table 30 details the final parameters for all *Radiance*-based simulations developed in the first and second part of the study. The selection of these parameters has been validated in a previous work [64].

Table 31. list of *Radiance* materials for simulation phase 2.

Material	Radiance material description	Number of values	R reflectance	G reflectance	B reflectance	Specularity	Roughness
Conc plaster 70% R	void plastic	0 0 5	0.760	0.760	0.760	0.00	0.00

In Table 31, a list of radiance materials adopted for surrounding buildings is included. In particular all the external surfaces of neighbouring buildings have been treated with an average colour (grey) of existing districts.

All the simulations have been carried out using statistical data recorded for the city of Milan-Malpensa Airport (latitude 45.27° N, longitude 9.11° E) using *EnergyPlus* weather data climate file.

### 4.3.1. Description of Grasshopper’s script

In this paragraph is shortly described the *Grasshopper*’s definition used for developing a tool in order to modify the volume by generative parametric modeling transformations.

A *Grasshopper* definition can consist of many different kinds of objects, but in order to get started it is necessary only to familiarize with two of them:

- Parameters;
- Components.

Parameters contain data, meaning that they store stuff. Components contain actions, meaning that they do stuff. Each *Grasshopper*’s object have some input and output parameters in base to its function.

The all specific details about *Grasshopper*’s objects are explained in detail, as written before, by the tutorial entitled “*The Grasshopper Premier*” on its specific website [72].

The Figure 36 shows the complete *Grasshopper*’s definition of the entire district.

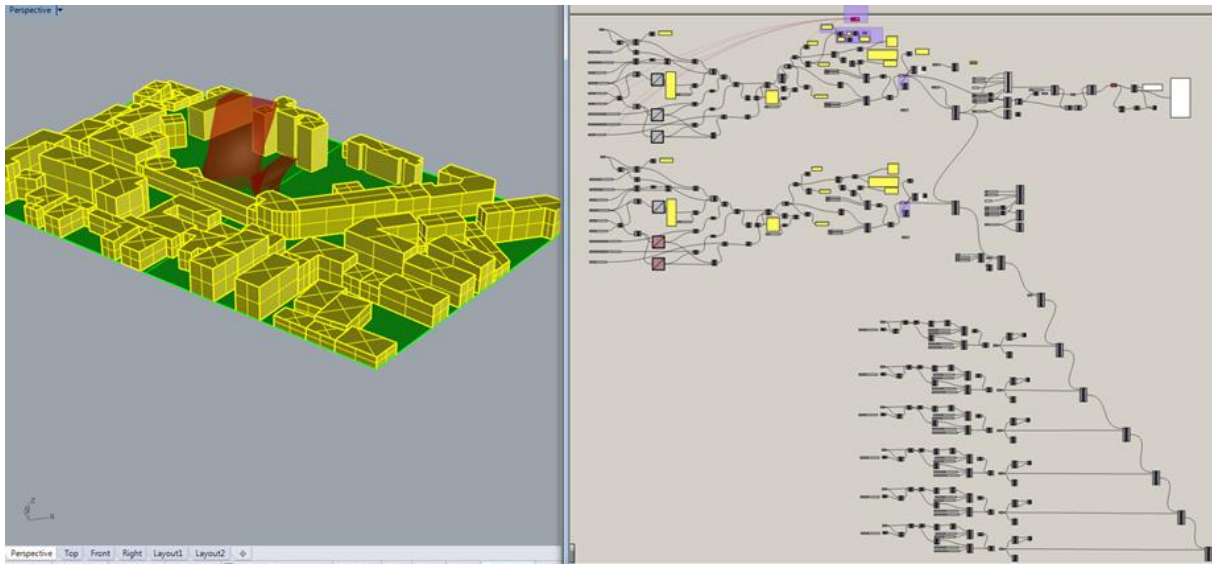


Figure 36. The complete *Grasshopper's* definition of the entire district (on the right) and its visualization in *Rhinceros* environment (on the left)

In particular, analyzing each part of this definition, is possible to isolate the main important sections in order to simplify the total process.

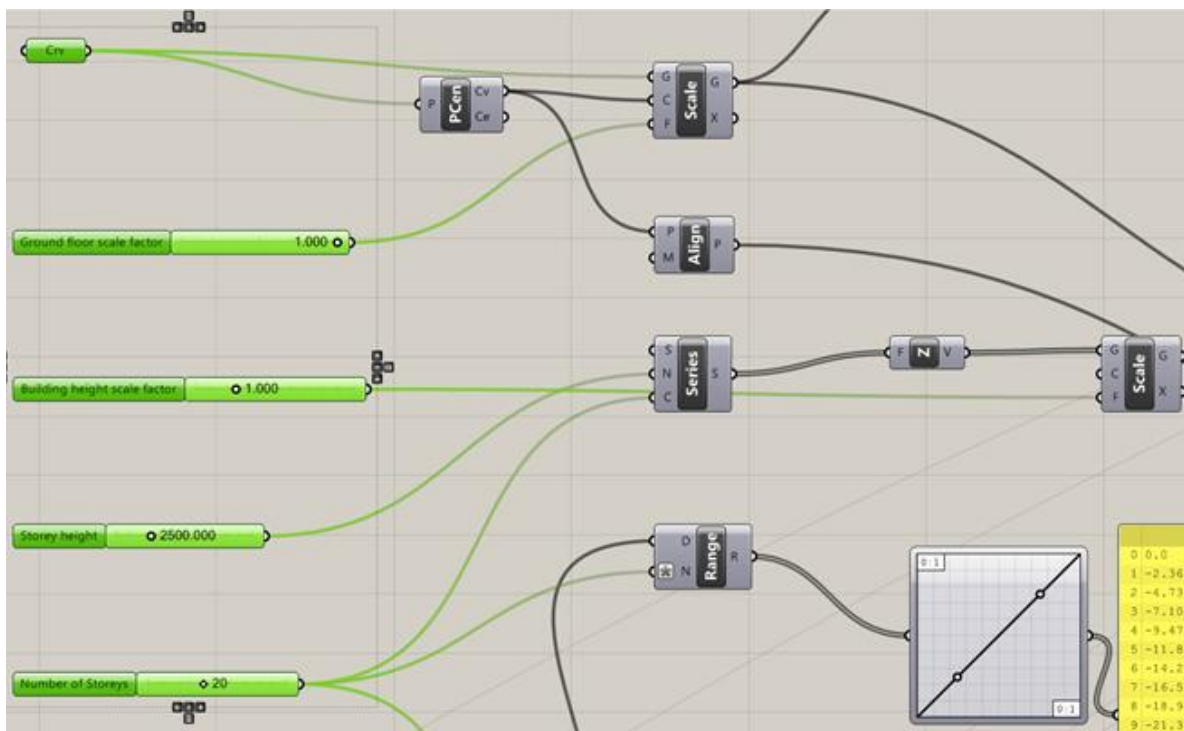


Figure 37. On the left are underlined in green the list of the urban fixed data in following order: Curve, Ground floor scale factor, Building height scale factor, Storey height, Number of storeys.

In the first definition's part, on the left, there is the list of the urban fixed data (Figure 37) and the parameters of transformations (Figure 38). The parameters' list is composed by "slide number" that permit to changes the values of each parameters from the lower to upper limit fixed by the user. The domain of the values can be choose among three options: in fact the slider's default value type is initially set to Floating Point (which results in a decimal numeric value) that is possible to change in an Integer, or in any whole number.

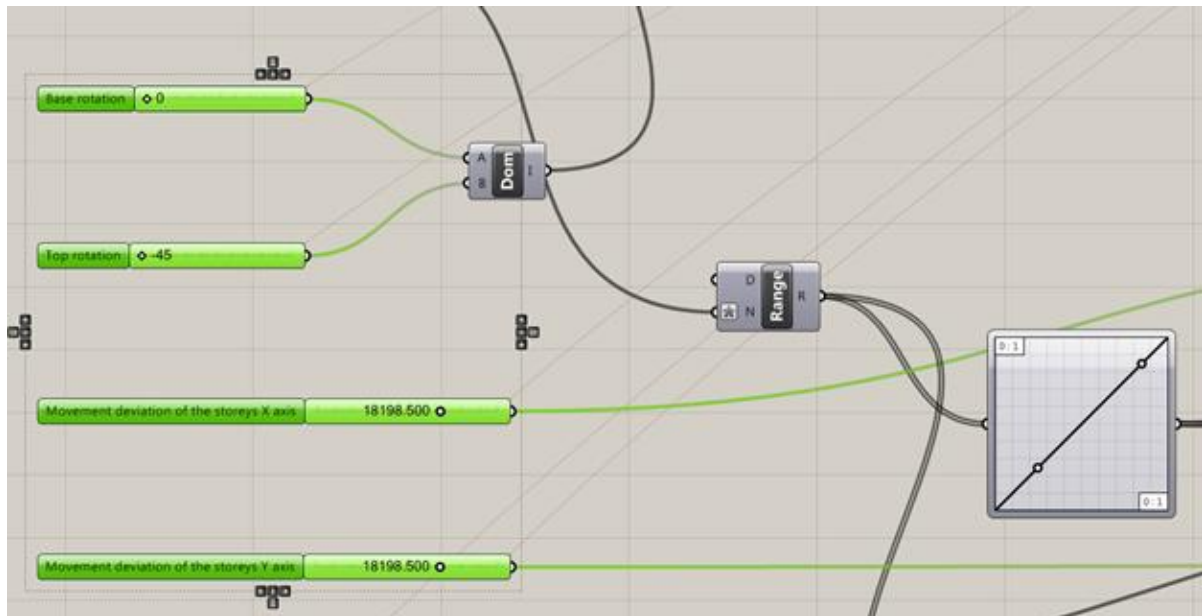


Figure 38. On the left are underlined in green the list of the parameters of transformations: Base rotation, Top rotation, Movement deviation of the storeys X axis, Top rotation, Movement deviation of the storeys Y axis.

All of these parameters are linked to other different *Grasshopper* definition objects which allow the parametric transformation: for example the "scale" object permit to scale the dimension in all direction of the geometry object associated to the "scale" *Grasshopper* object. Its input parameters are the "Base geometry" (G), the "Center of scaling" (C) and the "Scaling factor" (F), while as output parameters it has the "Scaled geometry" (G) and the "Transformation data" (X). In this the case, the "Scale" object, was used in order to scale the geometry of the floor area, selected by "Curve" object: this is the "Base geometry" (G) input parameters. While for a "Center of scaling" were fixed the "Average of polyline vertices" (Cv), of the "Polygon Center" object that is usually used in order to find the center point (average) for a polyline, of the starting floor area ("Curve" object). As last input parameter, "Scaling factor", was linked the input of urban fixed data called "Ground floor scale factor". This latter object is a "Slide number", that allows to choose the appropriate scale of the floor area and it is very useful when the

size of the floor area is an offset from the site construction. The Figure 39 shows the process just described.

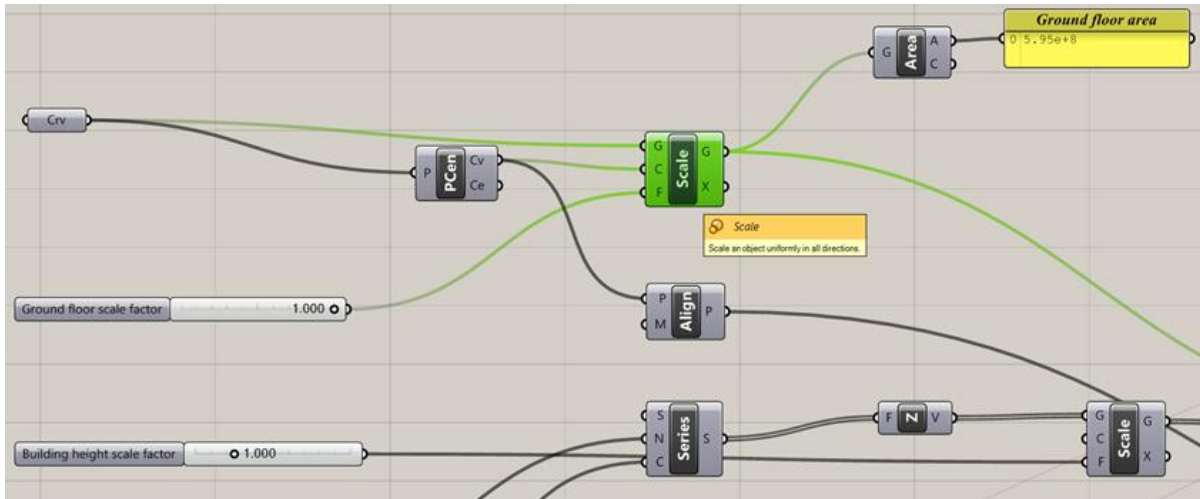


Figure 39. In green is underlined the “Scale” component described above.

As other example, the “range” object, that it is a mathematical function, allows to create a range of numbers: the numbers are spaced equally inside a numeric domain, and the use of this component is useful if it is necessary to create numbers between extremes, or for controlling over the interval between successive numbers, it should be using the “series” component. The “range” input parameters are the “Domain of numeric range” (D) and the “Number of steps” (N), while the unique output is “Range of numbers” (R). In this case, in Figure 40, is reported the process to create the twist of the storeys.

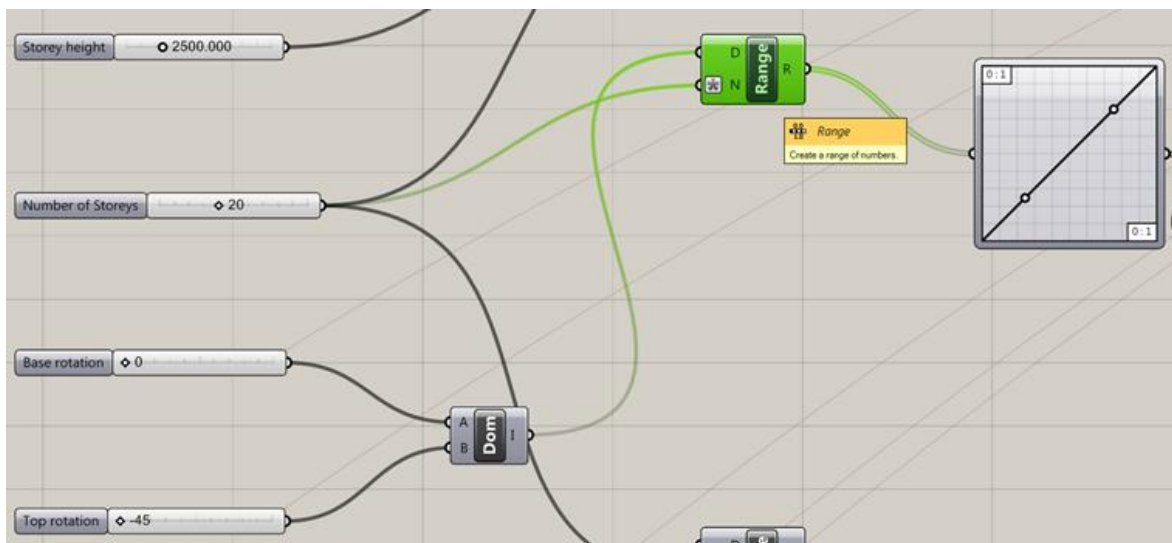


Figure 40. In green is underlined the “Range” component described above.

The input transformation data are the “Base rotation” and “Top rotation” which are linked in a “Domain” object, as “start” (A) and “end” (B) numeric extremes of the domain, that has as output the “Numeric domain between (A) and (B)” (I), that in this case are the building’s storeys. At the same time the output of the “Domain” is one of the “Range”’s object input, in this case is represented by “Domain of numeric range” (D), while the “Slide number” object, named “Number of storeys” is the “Number of steps” (N) of the “Range” object. For this input was fixed a mathematical expression,  $n-1$ , and here indicated with a star, in order to exclude the ground floor from the rotation. The “Range of numbers” output of the “Range”, are the angles of rotation of each storey (Figure 41): in this case the total angle of rotation from  $0^\circ$  of the ground floor to  $45^\circ$  of the top, is divided into 20 steps thanks to the “Range” object. The other *Grasshopper*’s objects are the same logic constitution.

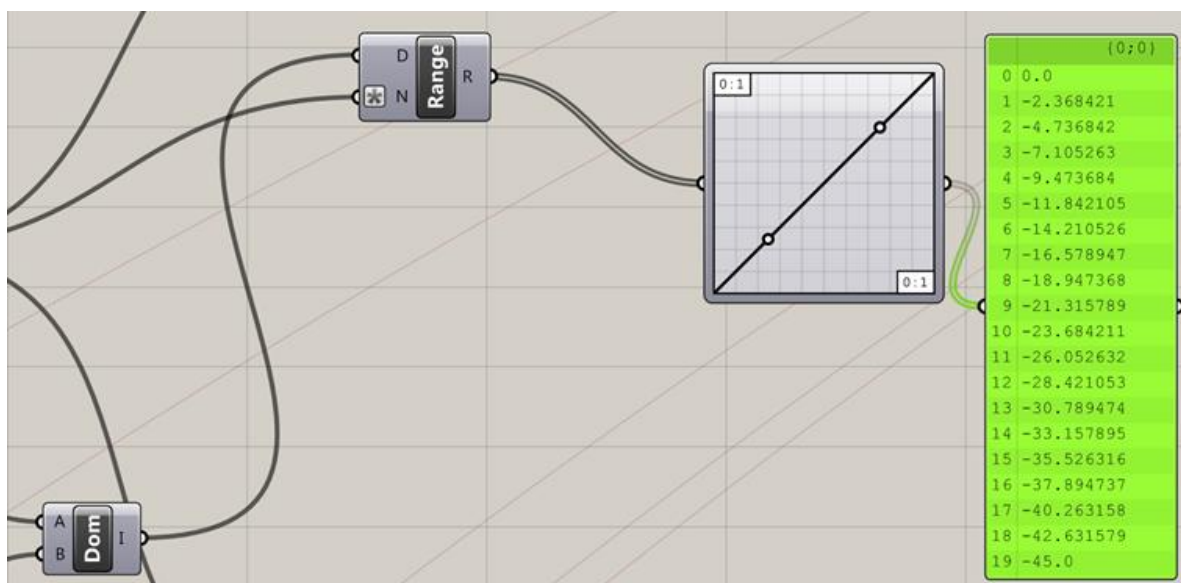


Figure 41. In green is underlined the all angles of storeys’ rotation.

Then the parameters are linked with an important specific *Grasshopper*’s object: the “Graph mapper”.

In Figure 42 there is one example of this object.

“Grasph mapper” object allows to remap a set of numbers. By default the [x] and [y] domains of a graph function are unit domains [0.0 ~1.0], but these can be adjusted via the “Graph editor”. Graph mapper can contains a sigle mapping function which can be picked through the context menu. Graphs typically have grips (little circles) which can be used to modify the variables that define the graph equation. Is possible to activate the “Graph Editor” in order to alter the range and domain of the mapping function as well as one important setting: the “Graph Types” that can varies in these following

options: “None, Bezier, Conic, Gaussian, Linear, Parabola, Perlin, Power, Sinc, Sine, Sine Summation, Square Root”.

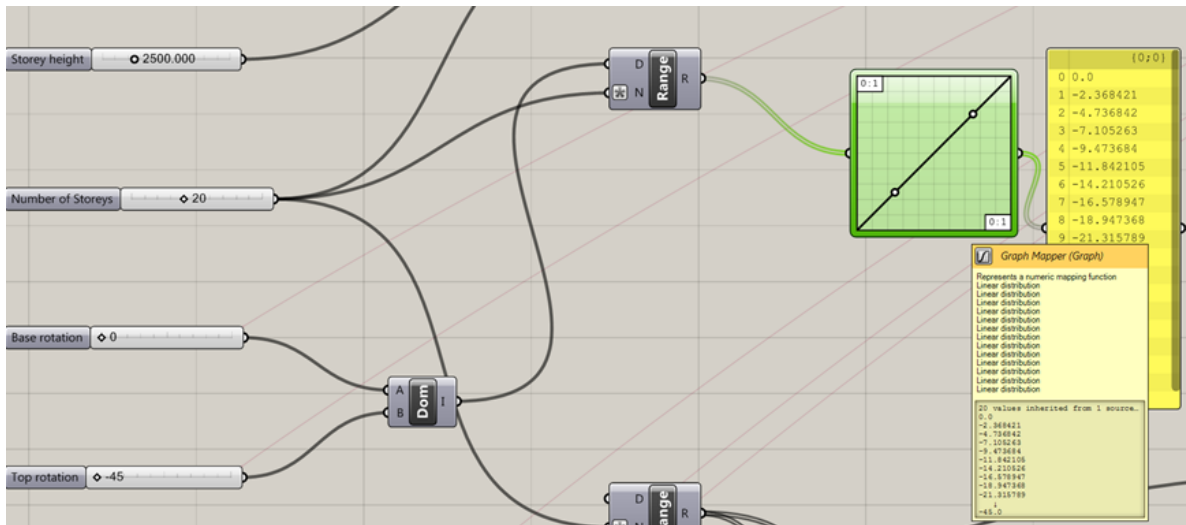


Figure 42. In green is underlined the “Graph Mapper” component described above.

That, in the situation reported on the Figure 43, allows to change the steps of the angle’s division from the bottom to the top following the function set on the “Graph Types” of the “Graph Mapper” object. In this case the graph type chosen was linear.

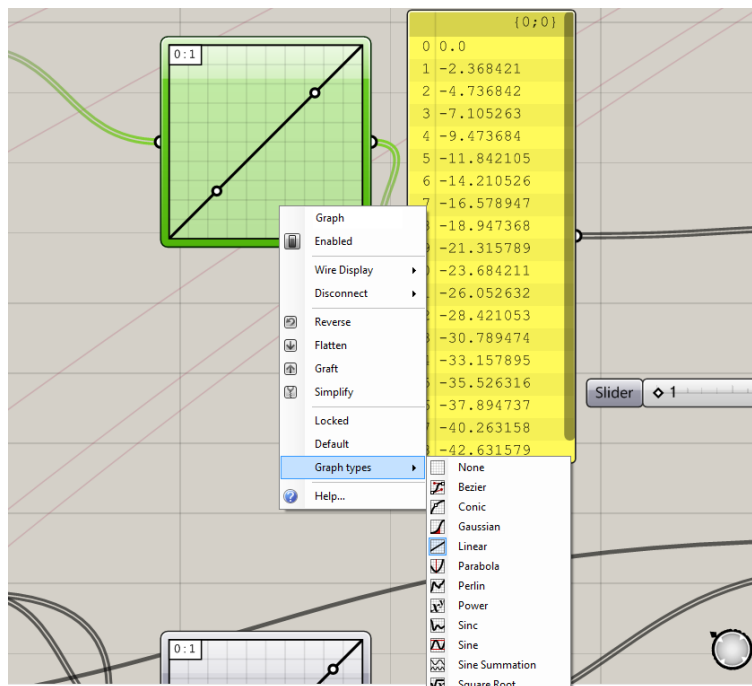


Figure 43. In green is underlined the “Graph Mapper” component with the “Graph Types” options.

Connected the all parameters and component and created the all links from them in order to permit the shape transformations, the *Galapagos* plug-in has been introduced. *Galapagos* asks to fix two different parameters: define the numbers that represent the “Fitness”, and define the all sliders that are part of the “Genome”. In order to define the “Fitness”, *Galapagos* requires a single parameter which provides a fitness value: in this script the fitness value is the volume of the building, given that the definition’s goal is to modify the shape of the building always maintaining the same volume. As *Galapagos* runs, it will attempt to maximize or minimize the fitness.

For setting the “Genome” input, *Galapagos* can operate on any number of “Sliders” objects. It is possible to assign certain sliders to the *Galapagos* object for them to become part of the “Genome”. It is better to limit the slider range as much as possible, as this reduces the size of the search space. In this definition, as sliders of “Genome”, the sliders of number which compose the parameters of transformations have been chosen. In this way the shape of the building changes varying the values of slide numbers, but its volumes remains always the same because was fixed as the fitness of *Galapagos*’ function. The all process that has just been described is summarized in the Figure 44.

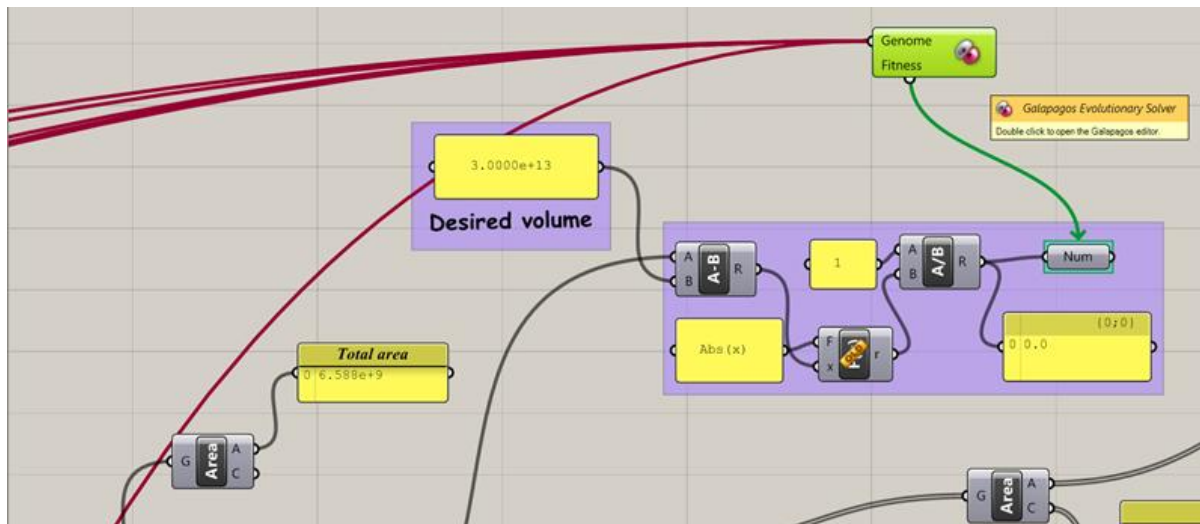


Figure 44. In green is underlined the “*Galapagos*” component described above.

The last two most important parts that are necessary to described in order to provide a shortly overview of the entire process are the way to export the complex model created with generative modeling tools: the way to create the mesh in order to run the insolation calculation and the way to link and export the model from the modeling tools to the solar simulation tools.

After defining the surfaces of the buildings using the “Loft” object, that creates a lofted surface through a set of section curves, with “Cap Holes” are built the all surfaces componed the building (in this case Building A in Figure 45) .

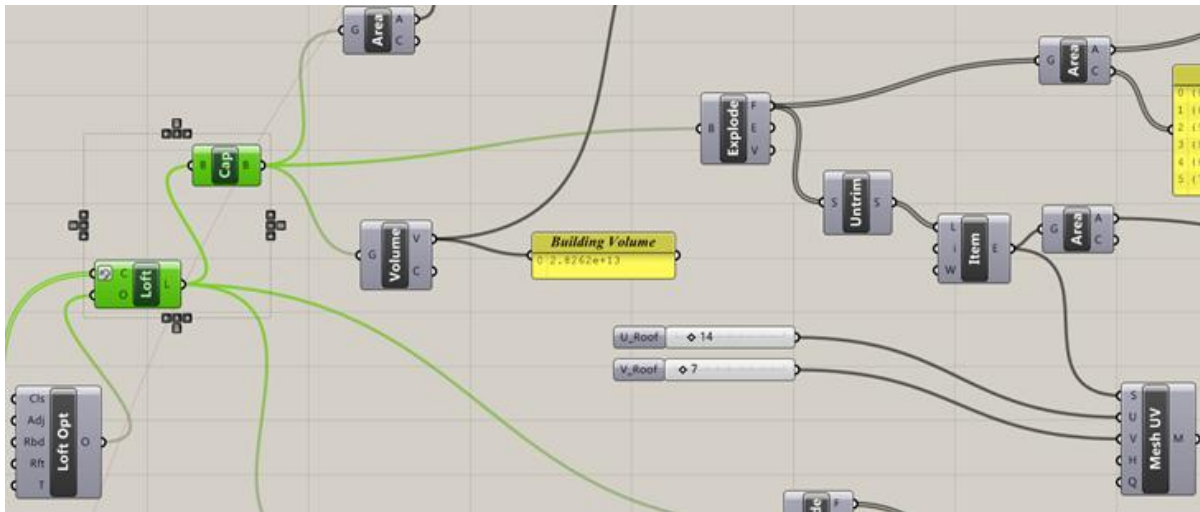


Figure 45. In green is underlined the “Loft” and “Cap Holes” components described above.

Thank to the *WeaverBird*'s “Edges Component” is possible to visualize the wireframe representation of a mesh linking the mesh created on the input parameter “Mesh” (M).

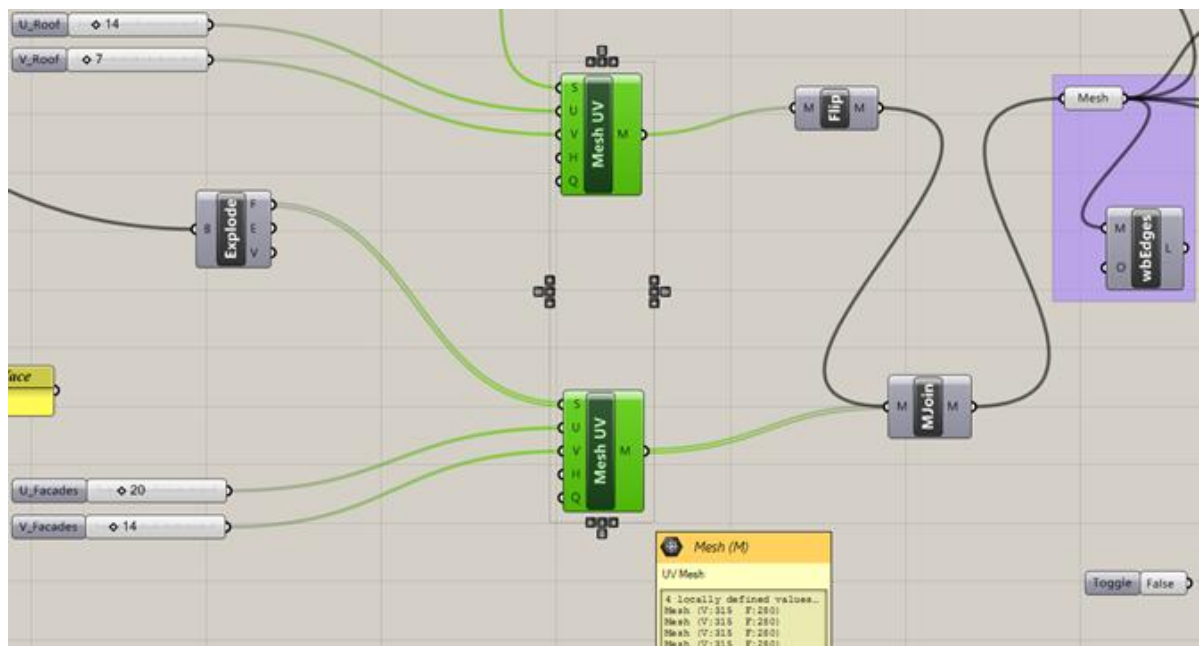


Figure 46. In green is underlined the “Mesh UV” components described below.

Regarding to the mesh's creation is useful to underline that were linked four "Slide number", two for managing the roof mesh ("U\_Roof" and "V\_Roof") and other two for managing the facades' mesh (U\_Facades" and "V\_Facades") with two "Mesh UV" objects, that permit to create a surface UV mesh, linking respectively the U "slide number" with the U input of parameter that allows to subdivide the U direction in number of quads indicated on the slide number linked, and the same process is valid for the V direction. The Figure 47 shows the process that has just been described.

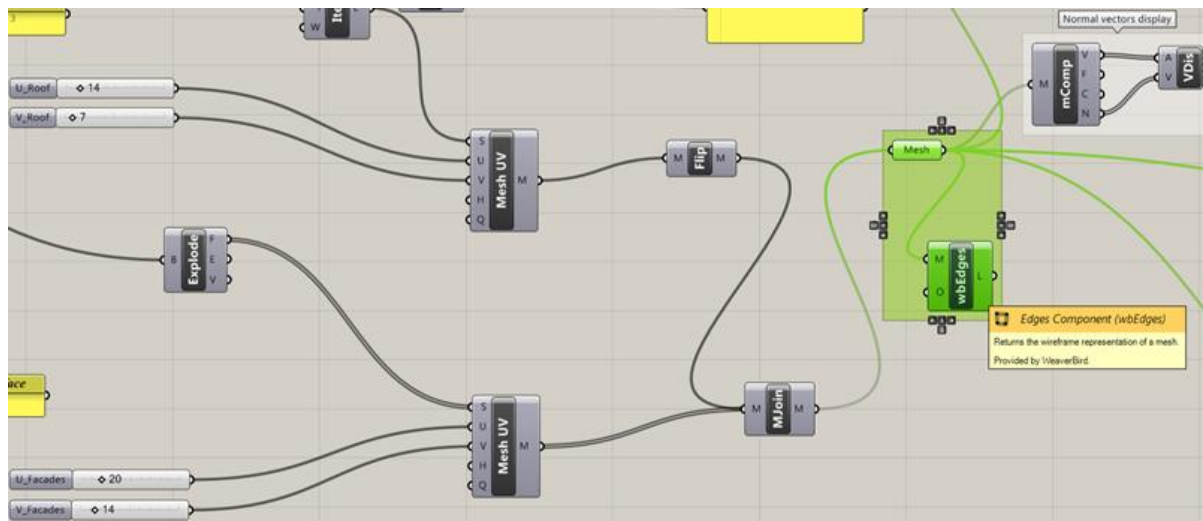


Figure 47. In green is underlined the "Mesh" and "Edges component" components.

In this situation the mesh of the building's roof is composed by 14 quads in U direction and 7 quads in V direction, while each façade's surface of the building is composed by 20 quads in U direction and 14 quads in V direction, as indicated in "Slides numbers" in the Figure 46 .

Finally was written the part for exporting the geometry models from *Grasshopper* to *Autodesk Ecotect Analysis 2011* through *Geco*. In particular was used the "EcoMeshExport" object in order to export the attached mesh data to *Autodesk Ecotect Analysis 2011* and the "EcoSolCal" object for calculating the incident solar radiation levels (insolation) over either the current analysis grid of objects within the model. After setting the all parameters and linking all objects each other, the "EcoLink" object allows to start the *Autodesk Ecotect Analysis 2011*.

Furthermore in this way is possible to run the insolation calculation directly from *Grasshopper* uploading the weather data climate (the yellow rectangular in the Figure 48) typical of the region that the site construction is located.

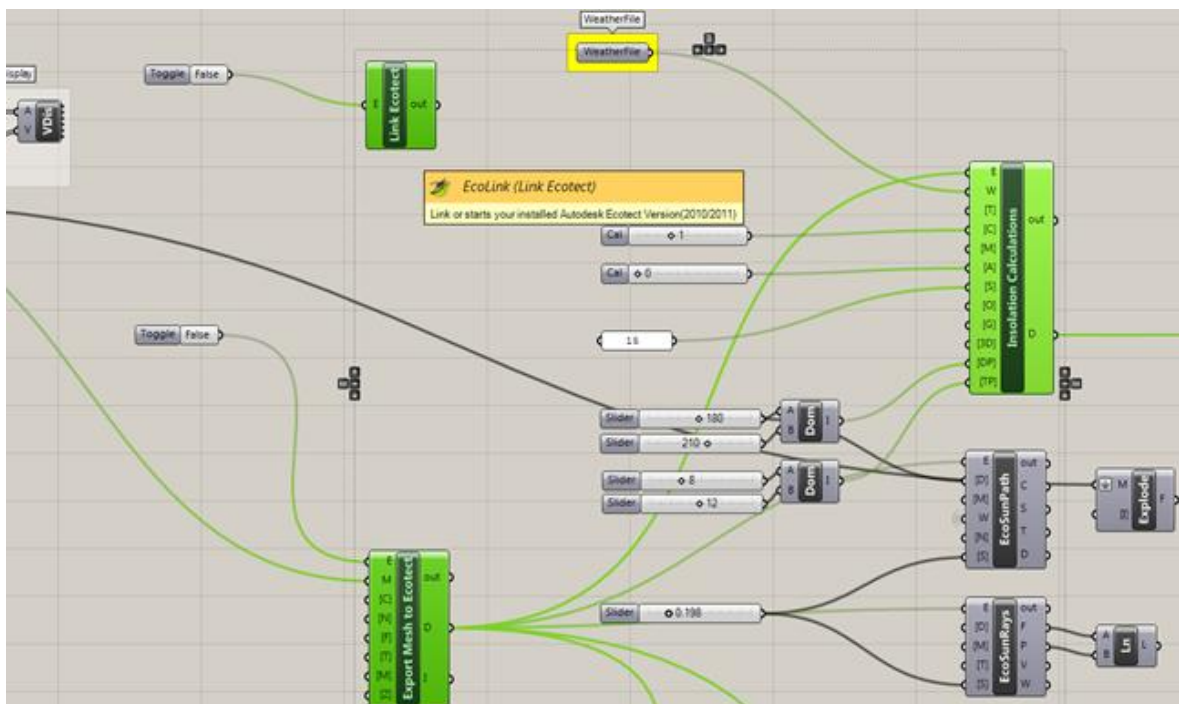


Figure 48. In green is underlined the *Grasshopper's* objects for linking the model to *Autodesk Ecotect Analysis 2011* and starting the insolation calculation .

At this time the model is exported into *Autodesk Ecotect Analysis 2011* environment, as shows in Figure 49, and the scene of the entire district modeled is constituted by surfaces and the solar optimized buildings are composed by mesh: the solar simulation was run directly from *Grasshopper* using the object of “EcoSolCal” that was presented above.

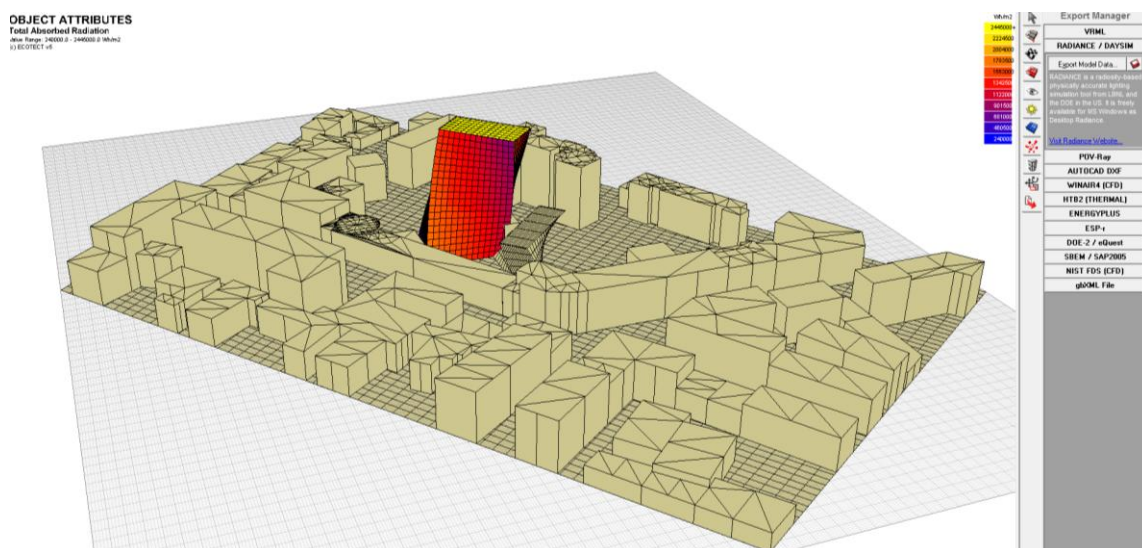


Figure 49. The result of the model’s export from *Grasshopper* to *Autodesk Ecotect Analysis 2011* with the insolation calculation for the Building A run directly from *Grasshopper*.

Now the model is ready for more detailed analyses using *Autodesk Ecotect Analysis* or for exporting the geometry in *Daysim* in order to run the solar dynamic simulation.

In this section was given a brief overview about the *Grasshopper's* definition and its logic. The most important aspect was to demonstrate that was possible to build a sort of a tool permits the complex parametric transformations in order to improve the solar exposure of the building façades that was the goal to achieve after the first part of the study described in chapter 3.

However this script can improve much more especially considering the different goal of the building's optimization it wants to achieve: in fact is possible to set different "Slide numbers", in order to vary the parameters' values that the users fixed, or maintaining constant one or more parameters using *Galapagos*, changing the others linked with.

Therefore this script represents an example of a good way to use the tools available for architects, urban planners and engineers in order to develop a conscious and sustainable urban and building design.

#### 4.4. Results and discussion

The case study analysed is representative of a typical development in the city of Milan, consisting in the demolition of an existing building and on the reconstruction of the same volume, but with a different shape.

A first design scenario, not already optimized for solar purposes is compared with several scenarios in which each volume has been transformed for searching the most efficient solution. The actual design scenario is composed of two buildings: one 20 storeys residential building (building A) of about 570 m<sup>2</sup> each floor for a total volume of about 28500m<sup>3</sup> and one 8 storeys residential building (building B) of about 450m<sup>2</sup> each floor, for a total volume of about 9000m<sup>3</sup>. In Figure 2 a 3D view of the area of intervention within the city of Milan is shown.

##### 4.4.1. Solar geometric optimisation of isolated buildings

The first analyses have been conducted on constant volumes for buildings A and B. Starting from the initial shape, different combinations of parametric transformations have been tested: Twist (T), Slope (S) and combined Twist and Slope (T & S). A scheme of single parametric transformations types are summarized in the Figure 50.

Constant data of the building	Initial Shape	Twist West	Twist East	Slope South	Slope West – East	Twist and Slope
	Without any transformation	Rotation of the roof from 15° to 45° west	Rotation of the roof from 15° to 45° east	Slope of the façades from on south direction 5° to 20° from the vertical	Slope of the façades on east or west direction 5° to 20° from the vertical	Combination of twist and slope on south and east/west direction
Building A Footprint: 570 m <sup>2</sup> Floor area: 570 m <sup>2</sup> Height: 50 m Volume: 28500 m <sup>3</sup>						
Total surfaces area	5535 m <sup>2</sup>	5586 m <sup>2</sup>	5586 m <sup>2</sup>	5765 m <sup>2</sup>	5647 m <sup>2</sup>	5993 m <sup>2</sup>
Building B Footprint: 450 m <sup>2</sup> Floor area: 450 m <sup>2</sup> Height: 20 m Volume: 9000 m <sup>3</sup>						
Total surfaces area	2300 m <sup>2</sup>	2476.5 m <sup>2</sup>	2476.5 m <sup>2</sup>	2336 m <sup>2</sup>	2417.5 m <sup>2</sup>	2630 m <sup>2</sup>
Transformation's IDs	0	T_W15 T_W30 T_W45	T_E15 T_E30 T_E45	S_S5 S_S10 S_S15 S_S20	S_W5 – S_E5 S_W10 – S_E10 S_W15 – S_E15 S_W20 – S_E20	T_W/E15/45 – S_S5/20 – S_W/E5/20

Figure 50. Summary of building's constant data and parametric transformation considered for analyses. Simple transformations of twist and slope.

Afterwards, the buildings (both the ones of the initial design scenario and the solar optimized ones) have been included into a district (Figure 51 and Figure 52) in order to compare the different scenarios and estimate the overshadowing and reflections effect from the neighbouring buildings and ground reflection contribution in term of solar radiation increment.

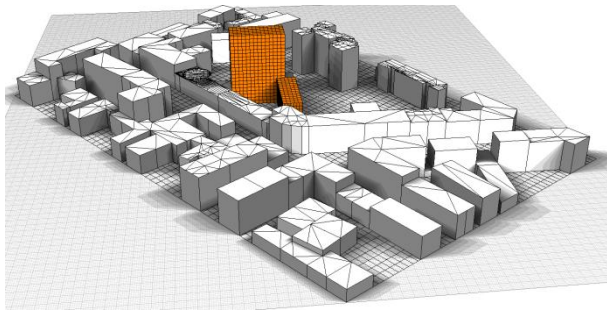


Figure 51. Shadow range of actual design scenario.

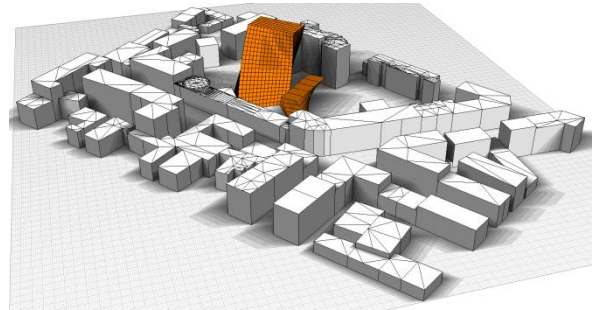


Figure 52. Shadow range of solar optimized design scenario.

#### *Analyses of an isolated building*

The first set of simulations has been carried out on the isolated buildings A and B. The results of the simulation expressed in term of annual global radiation (kWh/year and kWh/m<sup>2</sup>year), are summarized for the building A in the Table 32 and for the building B in the Table 33.

The data included in the tables, collecting the most significant results of the simulation performed, show the highest annual solar radiation values for different types of parametric transformation. The codes created specify the parametric transformation have been done: on every code is indicated the first type of transformation (T for Twist or S for Slope), its direction (S for South, W for west and E for east) and the amount of transformation (from 45° west to 45° east for the twist transformation and from 0° to 20° from the vertical direction for the slope transformation). All percentages of radiation increment have been compared to the value of the initial building shape considered as reference case (0).

Some limits of the parametric transformations have been adopted, in order to generate real, buildable and stable configurations: the maximum slope (20°) has been calculated considering the building's barycentre always projected inside the building footprint, while the maximum rotation has been limited to 45°, in order to limit the relative rotation between each floor.

From the analysis of the following Table 3 for the building A, is evident how simple transformations of twist and slope are not able to provide relevant increases of the levels of incident solar radiation, while the highest increase is due to the combined slope and twist transformations. The maximum values of incident solar radiation is reached for the configuration that have both a twist of 45° on west orientation and a double slope of 20° on south and east. This is not only depending on the increase of the average superficial solar radiation (9.2%), but also to the increment of the total exposed surface.

Furthermore, it is crucial to note that very complex transformations have a high impact on the losses of usable floor area, with up to 970 m<sup>2</sup> lost over 11400 m<sup>2</sup> (a percentage of about 8.5%).

Table 32. Building A. Results of solar radiation analysis. ES: total exposed area (external envelope). L: loss of usable floor area. R: total solar radiation impacting on external envelope. RA: average solar radiation on external envelope. Δ: percentage of variation of solar radiation.

Parametric transf.	E <sub>S</sub> [m <sup>2</sup> ]	L [m <sup>2</sup> ]	R [kWh/yr]	R <sub>A</sub> [kW h/m <sup>2</sup> y]	Δ [%]	Parametric transf.	E <sub>S</sub> [m <sup>2</sup> ]	L [m <sup>2</sup> ]	R [kWh/yr]	R <sub>A</sub> [kW h/m <sup>2</sup> y]	Δ [%]
0	5535	0	2881181	521	0.0%						
T_W45	5586.4	287.3	2951721	528	2.4%	S_S5	5549.1	74.3	2953795	532	2.5%
T_W30	5558.0	194.2	2926737	527	1.6%	S_S10	5591.8	151.8	3039105	543	5.5%
T_W15	5540.8	95.0	2903536	524	0.8%	S_S15	5664.7	232.6	3134549	553	8.8%
T_E15	5540.8	95.0	2876193	519	-0.2%	S_S20	5770.7	316.5	3262099	565	13.2%
T_E30	5558.0	194.2	2873811	517	-0.3%						
T_E45	5586.4	287.3	2875658	515	-0.2%						
S_W20	5649.5	651.7	2918788	517	1.3%	T_W45 & S_S20	5794.3	686.2	3287390	567	14.1%
S_W15	5598.0	478.8	2896639	517	0.5%	T_W30 & S_S20	5780.5	685.6	3274406	566	13.6%
S_W10	5562.6	312.6	2888659	519	0.3%	T_W15 & S_S20	5773.0	668.4	3262099	565	13.2%
S_W5	5541.8	153.0	2882033	520	0.0%	0 & S_S20	5770.7	316.5	3262099	565	13.2%
S_E5	5541.8	153.0	2898394	523	0.6%	T_E15 & S_S20	5773.0	668.4	3241009	561	12.5%
S_E10	5562.6	312.6	2919482	525	1.3%	T_E30 & S_S20	5780.5	685.6	3232408	559	12.2%
S_E15	5598.0	478.8	2943726	526	2.2%	T_E45 & S_S20	5794.3	686.2	3225093	557	11.9%
S_E20	5649.5	651.7	2979663	527	3.4%						
T_W45 & S_S20 & S_W20	5851.4	763.3	3286125	562	14.1%	T_W45 & S_S20 & S_E20	5993.0	963.5	3407463	569	18.3%
T_W30 & S_S20 & S_W20	5846.1	803.8	3285195	562	14.0%	T_W30 & S_S20 & S_E20	5955.5	971.1	3391399	569	17.7%
T_W15 & S_S20 & S_W20	5859.1	875.7	3287481	561	14.1%	T_W15 & S_S20 & S_E20	5918.7	961.0	3373501	570	17.1%
0 & S_S20 & S_W20	5885.2	928.7	3285926	558	14.0%	0 & S_S20 & S_E20	5885.2	928.7	3349341	569	16.2%
0 & S_S20 & S_E20	5885.2	928.7	3349341	569	16.2%	0 & S_S20 & S_W20	5885.2	928.7	3285926	558	14.0%
T_E15 & S_S20 & S_E20	5859.1	875.7	3324558	567	15.4%	T_E15 & S_S20 & S_W20	5918.7	961.0	3287093	555	14.1%
T_E30 & S_S20 & S_E20	5846.1	803.8	3296062	564	14.4%	T_E30 & S_S20 & S_W20	5955.5	971.1	3287206	552	14.1%
T_E45 & S_S20 & S_E20	5851.4	763.3	3273265	559	13.6%	T_E45 & S_S20 & S_W20	5993.0	963.5	3288017	549	14.1%

From the analysis of the Table 4, the highest value of the solar radiation for building B has been obtained for the building with a twist of 45° on west, and a combined slope of 20° both on south and on west. From the calculations it turns out an increase of about 24.1% of the solar incident radiation if compared with the undeformed building.

Table 33. Building B. Results of solar radiation analysis. ES: total exposed area (external envelope). L: loss of usable floor area. R: total solar radiation impacting on external envelope. RA: average solar radiation on external envelope. Δ: percentage of variation of solar radiation.

Parametric transf.	Es [m <sup>2</sup> ]	L [m <sup>2</sup> ]	R [kWh/yr]	RA[kWh/m <sup>2</sup> y]	Δ [%]	Parametric transf.	Es [m <sup>2</sup> ]	L [m <sup>2</sup> ]	R [kWh/yr]	RA[kWh/m <sup>2</sup> y]	Δ [%]
0	2301.3	0	1270337	552	0.0%						
T_W45	2476.4	304.92	1414415	571	11.3%	S_S5	2303.4	19.32	1299153	565	2.3%
T_W30	2383.3	205.1	1350343	567	6.3%	S_S10	2309.8	39.48	1328188	575	4.6%
T_W15	2322.6	103.6	1300252	560	2.4%	S_S15	2320.6	60.48	1357591	585	6.9%
T_E15	2322.6	103.6	1272701	548	0.2%	S_S20	2336.2	82.32	1387265	594	9.2%
T_E30	2383.3	205.1	1303590	547	2.6%						
T_E45	2476.4	304.92	1354602	547	6.6%						
S_W20	2417.6	274.4	1326154	549	4.4%	T_W45 & S_S20	2520.3	381.59	1520395	603	19.7%
S_W15	2365.5	201.6	1298260	549	2.2%	T_W30 & S_S20	2423.6	286.89	1460750	603	15.0%
S_W10	2329.4	131.6	1282550	551	1.0%	T_W15 & S_S20	2359.1	189.25	1414664	600	11.4%
S_W5	2308.3	64.4	1273108	552	0.2%	0 & S_S20	2336.2	82.32	1387265	594	9.2%
S_E5	2308.3	64.4	1280012	555	0.8%	T_E15 & S_S20	2359.1	189.25	1390759	590	9.5%
S_E10	2329.4	131.6	1295818	556	2.0%	T_E30 & S_S20	2423.6	286.89	1419492	586	11.7%
S_E15	2365.5	201.6	1318233	557	3.8%	T_E45 & S_S20	2520.3	381.59	1464384	581	15.3%
S_E20	2417.6	274.4	1352230	559	6.4%						
T_W45 & S_S20 & S_W20	2632.9	456.57	1577114	599	24.1%	T_W45 & S_S20 & S_E20	2562.5	420.81	1550679	605	22.1%
T_W30 & S_S20 & S_W20	2549.6	458.05	1526048	599	20.1%	T_W30 & S_S20 & S_E20	2486.4	351.19	1506494	606	18.6%
T_W15 & S_S20 & S_W20	2488.1	392.64	1481806	596	16.6%	T_W15 & S_S20 & S_E20	2449.8	339.59	1480435	604	16.5%
0 & S_S20 & S_W20	2452.5	371.07	1447823	590	14.0%	0 & S_S20 & S_E20	2452.5	371.07	1474275	601	16.1%
0 & S_S20 & S_E20	2452.5	371.07	1474274	601	16.1%	0 & S_S20 & S_W20	2452.5	371.07	1447823	590	14.0%
T_E15 & S_S20 & S_E20	2488.1	392.64	1483963	596	16.8%	T_E15 & S_S20 & S_W20	2449.8	339.59	1431768	584	12.7%
T_E30 & S_S20 & S_E20	2549.6	458.05	1507674	591	18.7%	T_E30 & S_S20 & S_W20	2486.4	351.19	1444080	581	13.7%
T_E45 & S_S20 & S_E20	2632.9	456.57	1539507	585	21.2%	T_E45 & S_S20 & S_W20	2562.5	420.81	1477949	577	16.3%

However, as shown in Figure 6 and Figure 7, due to construction problems (due to the intersection of the proposed new building with the existing neighbouring buildings), this solution has been discarded and a final transformation with a twist of 45° on west and a slope of 20° on both south and east orientations has been chosen as the most efficient solution. Also in this case, the increasing of value of total solar radiation incident annually on external surfaces is due not only to the increase of the average superficial solar radiation (9.6%), but also to the increase of the total exposed envelope's surface.

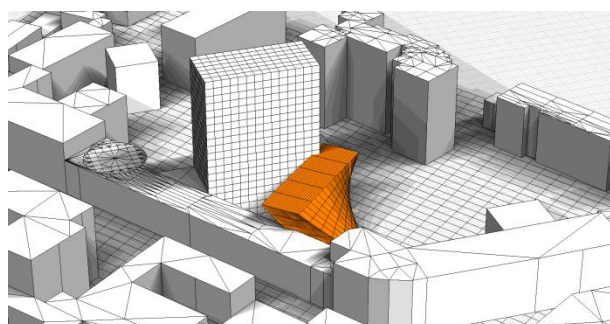


Figure 53. Point of interpenetration among three-dimensional models of new (in orange) and existing buildings (in white).

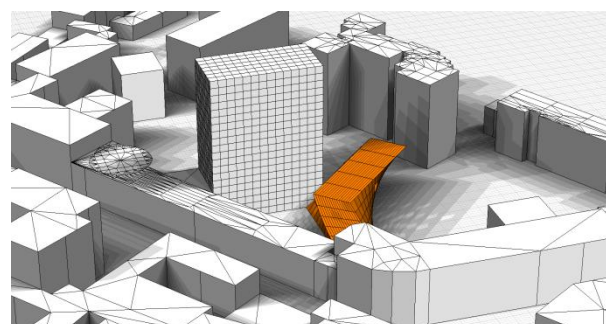


Figure 54. Scenario without any interpenetration among new and existing buildings three-dimensional models.

Also the transformed building B is affected by the same problems found in building A of reduction of the total usable floor area. In this case, the amount of indoor usable surface lost is up to 460 m<sup>2</sup>, over 3600 m<sup>2</sup> (12.78 %). The higher impact suggests managing carefully complex transformations in low-rise building.

Another potential critical aspect of this approach is revealed in Table 3 and Table 4: all the transformations produce an increase of the total surfaces area. This is affecting not only the capacity of the building to capture solar radiation, but also the potential heat losses and gains through the envelope. This issue could be solved with a more integrated simulation approach in which the solar optimization is only one component of the overall energy use optimization of the building. This is the general aim of the study, but limitations in computer processor's speed have been the cause of choosing a mono-parametric optimization.

#### **4.4.2. Analyses of the isolated optimized building inserted a district (solar access)**

In the second set of simulations, the initial buildings shape and the solar optimized buildings' shape obtained from the first set of simulations have been modelled as included in the district, in order to calculate the effects of overshadowing and of the indirect solar radiation reflected by the neighbouring buildings.

Several different configurations of the district have been analysed:

- A first configuration (scenario 1) in which the variation of global solar radiation on building A has been calculated in the hypothesis of a non optimized shape.
- A second configuration (scenario 2) in which the variation of global solar radiation on building B has been calculated in the hypothesis of a non optimized shape.
- A third configuration (scenario 3) in which the variation of global solar radiation on building A has been calculated in the hypothesis of an optimized shape.
- A fourth configuration (scenario 4) in which the variation of global radiation on building B has been calculated in the hypothesis of an optimized shape.

All the scenarios have been compared with the reference cases (0) of either isolated building A or isolated building B and the percentage of variation has been calculated.

Table 34. Parametric analysis of solar access on building A and building B included in the district.

Scenario	ab	gr. refl.	kWh/ year	kWh/m <sup>2</sup> year	Radiation variation [%]
Scenario 1	3	0	3012945	544	4.6%
Scenario 1	3	0.15	3229624	583	12.1%
Scenario 3	3	0	3656858	610.	26.9%
Scenario 3	3	0.15	3911416	653	35.8%
Scenario 2	3	0	1068820	464	-15.9%
Scenario 2	3	0.15	1173885	510	-7.6%
Scenario 4	3	0	1472276	559	15.9%
Scenario 4	3	0.15	1607978	611	26.6%

Every scenario has been analysed with different parameters of analysis: the first with ab equal to 3 and ground reflection of 0, to calculate only the solar reflection effect by the neighbouring buildings, and the second with ab equal to 3 and ground reflection of 0.15, to calculate also the ground reflection contribution. The results of the analyses are summarized in Table 5.

Focusing on the building A, while the solar optimized isolated shape (T\_W45 & S\_S20 & S\_E20) gains a 18.3% if compared with the unmodified shape (0), the effects of surrounding buildings' reflections contribute for a further increase of 8.6% (total gain of 26.9%). The combined effect of buildings' and ground reflections contribute for an increase of 17.5% (total gain of 35.8%). Focusing on building B the percentages of increase are 22.1%, 15.9% and 26.6% in the same conditions (isolated, included in the

district with only the contribution of neighbouring buildings, included in the district with both the contribution of surrounding buildings and ground).

The results show that for the building A the overshadowing effect is not such negative as for the building B, but both for building A and B the ground reflection contributions allows to completely compensate the losses due to the district's shadows.

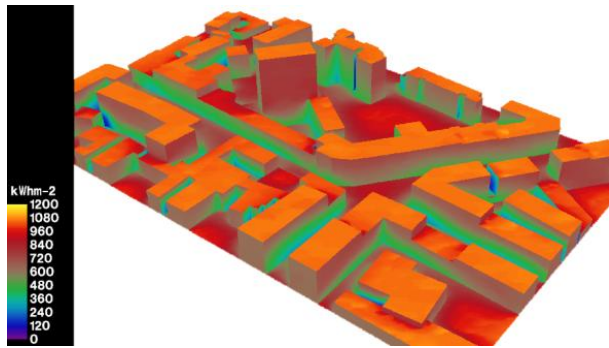


Figure 55. Irradiances' values of the entire district in actual design scenario (*DIVA* simulation)

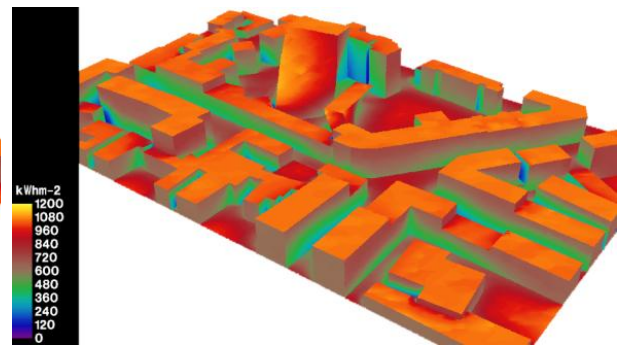


Figure 56. Irradiances' values of the entire district in solar optimized scenario (*DIVA* simulation)

The contents of this chapter were presented in the publication entitled “Urban solar district: a case study of geometric optimization of solar façades for a residential building in Milan.” [81] at Solar 2012 Conference in Melbourne on the 6-7<sup>th</sup> December, 2012.

#### **4.5. Conclusion**

The study has shown that the optimization of building shape can have dramatic effects on the improvement of the solar radiation on the façades. Moreover, the boundary conditions for the building designed have to be carefully evaluated: the indirect ground reflected solar radiation increase has to be compared with the losses due to overshadowings created by the neighbouring buildings. Regarding the issue of building integration of solar system and their related energy production efficiency, an appropriate type of solar or photovoltaic panels has to be chosen, depending on the highest amount of the different solar radiation contributions (direct, diffuse, indirect). Furthermore this study permits to localise the best areas for installing the solar systems: with *Daysim* simulation and Matlab function is possible to extract the amount of annual solar radiation of the most irradiative sensors on the façades.

Next steps of the research will analyse more complex transformations, using non-linear equations (parabolic, bezel, conic transformations). Furthermore the analysis of the panels' efficiency will be carried out, as well as the related assessment of surfaces temperatures increase effects on the façades, due to the integration of solar systems.

## 5. Paneling surfaces and energy production

### Questions of the chapter

1. How is possible to panelling a complex surfaces of the façade for installing the solar systems on it?
2. How much energy is possible to produce installing the solar systems on the façades?

### Abstract

Nowadays the architecture is going more always toward freeform surfaces. The tendency to apply the freeform shape in a large scale in architecture creates big challenges to the industrialization of such structures. The most important aspect is study the way to approximate the design surfaces by a union of all patches, or better known as panels. The process of freeform surfaces' paneling is more complex and implies sophisticates studies from the beginning of their design to the phase of their production and application. The manufacture technologies currently existing can permit to produce the panels with a selected technology at reasonable cost and to achieve the aesthetic quality of panel layout and surface smoothness [82]. The creation of moulds is the most industrialization's practice for producing the curved panels. Given that the cost of mould fabrication is often dominates in the panel cost, it should be better to use the same mould for multiple panels.

This chapter discuss the problem of covering a freeform surface. In particular are shown possible ways which is possible to subdivided the surface of the *Building A*'s façade optimized for capturing as much as solar radiation possible in the case study of the city of Milan in order to install the solar system panels on it.

## **5.1. Introduction**

Modern architecture is moving towards different kinds of geometric primitives until the freeform shape into simpler parts for the purpose of building construction. For the major kinds of finishing materials, as glass panels, wooden panels, metal sheets etc., used for covering the façades, it is very expensive to produce general double-curved shapes. A most common way is to use approximation by flat panels, which most of the time are triangular [83].

Freeform shapes have more and more increasingly importance in contemporary architecture. In the current scenario, where the generative parametric architecture is developing more and more every day, contemporaneously to the aesthetic taste towards female's shapes, the essential question that arises is on how proceed from a geometrically complex design towards a feasible and affordable way of production.. The paneling problem can arise both for the exterior and interior skin of a building, and plays a central role in the design specification phase of any architectural project involving freeform geometry [82].

This problematic becomes more relevant when it wants to install the solar systems on the façades. In spite of freeform surfaces could permit to maximize the solar radiation harvest from the façades, it remains complicated to exploit the maximum efficiency of the solar system, but first of all to solve the problem of their installation following the complex pattern of a freeform surface.

However nowadays many innovative technologies are going towards the creation of a flexible solar systems the permits to apply the solar cell on any surfaces.

In fact in the market today exist organic, inorganic and organic-inorganic solar cells that can be deposited over flexible substrates by high-throughput (often roll-to-roll printing) technologies to afford lightweight, economic solar modules that can be integrated into, not installed on, various surfaces.

Current conversion efficiencies under standard conditions are in the 3–15% range, but in real applications the overall productivity is high.

The new photovoltaic technologies are ready to provide cheap and clean energy reducing the use of fossil fuel resources for producing the electricity as well as reducing the costs and energy consumptions.

The most important achievements in the area of flexible solar cells, highlights the principles behind the main technologies, and discusses future challenges in this area and further developments in the field of BIPV in order to adopt on any surfaces'.

In this chapter are presented some considerations and the generative computers tools that allow to design a surface paneling, subdividing in a limited range of panel's sizes, thus to reduce the number of different types of panels that is necessary to produce for cover the façade.

## 5.2. Material and method

Nowadays the digital technologies allow to modeling any kind of surfaces and subdivide them in many different ways.

For studying the subdivision of surfaces were used *Rhinoceros*, using *PanelingTools*, and *Grasshopper*.

Below are presented an overview of these tools.

### 5.2.1. Overview of the paneling tools

#### *Paneling tools for Rhinoceros*

*PanelingTools* helps designers create paneling solution from concept to fabrication: it is a plugin of *Rhinoceros* that allows generating 2D and 3D cellular patterns and populates them over rectangular grids [84].

Forms that can be paneled with *PanelingTools* can be represented with a 2-dimensional point grid. *PanelingTools* provides many functions to turn base geometry of points, curves, surfaces, and polysurfaces into an ordered 2-dimensional grid. The grid is then used as basis to apply 2D and 3D patterns.

In the chapter are reported only the most important concepts for using this tools that explain the way that is possible to use for paneling the surfaces.

For the all details about the *PanelingTools* make reference to a specific manual free downloadable as well as the tool, from the McNeel's website [85]. Furthermore for any other commands and functions' description regarding *Grasshopper* and its plugin it suggests looking the relative website [71]and manual [86].

#### *Paneling surfaces using Grasshopper*

*Grasshopper*, as a generative modeling tool, other than permit to create complex surfaces and parametric design, can also be used for subdividing the surfaces. Also in this case is possible to panel the surfaces in different ways, but in this chapter is illustrated only one of these in order to give an overview of the tool's capabilities.

For any other research material about the use of *Grasshopper* for paneling the surfaces and other topics it suggests to watch and study many tutorials video, documentation and discussions on *Grasshopper's* website, where it is also possible to download the plugin for free.

#### *Main difference between PanelingTools for Rhinoceros and Grasshopper*

*Rhinoceros* works different from *Grasshopper* and in Annex B is described a funny example carried out from the literature that explains in a simple and synthetic way how is the main difference on the process of modeling in general between the two tools [87].

The great difference between the two tools is the logic of the process: while *Rhinoceros* start from the physical geometry and permits to modify and works on it, *Grasshopper* doesn't work with the real geometries, but it works on the logic behind the geometries.

### 5.3. Theory and calculation

As just written above are possible two different approaches for paneling the surfaces: starting from the geometry using *PanelingTools* in *Rhinoceros* work environment and working behind the geometry using *Grasshopper*.

#### 5.3.1. Paneling surface using PanelingTools in Rhinoceros

The paneling process is done in two steps: first, create a paneling grid, and then generate the paneling geometry of curves, surfaces and polysurfaces.

Generating the paneling creates patterns and applies the patterns to a valid paneling grid of points. The resulting paneling is standard *Rhinoceros* geometry in the form of curves, surfaces, or a mesh. To further processes panels (with the Unroll, Offset, Pipe, or Fin commands, for instance) use paneling utility functions and other *Rhinoceros* commands.

The two-step process gives more flexibility and better control over the result. Normally, the initial grid is generated interactively and is a good indicator of scale. The grid can be generated using the many grid-generating commands or with scripting. The grid can be directly edited and refined before any paneling is applied. Panels can be created using built-in patterns or user-defined free-form patterns [84].

The following parts describe the process used for paneling the surface of the *Building A* of the case study of the city of Milan treated before.

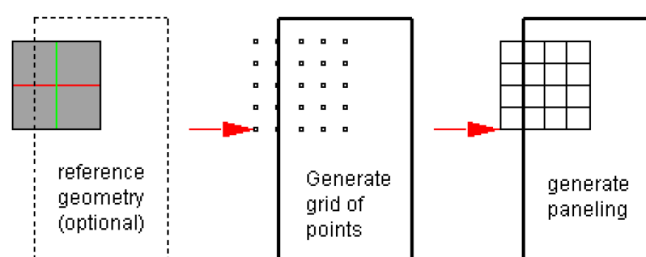


Figure 57. Flow chart of the paneling tools process in *Rhinoceros*.

From *Grasshopper* definition was extracted the surface of most irradiative facade that it wants to panel using the “baked” the surface that wants to panel (Figure 58).

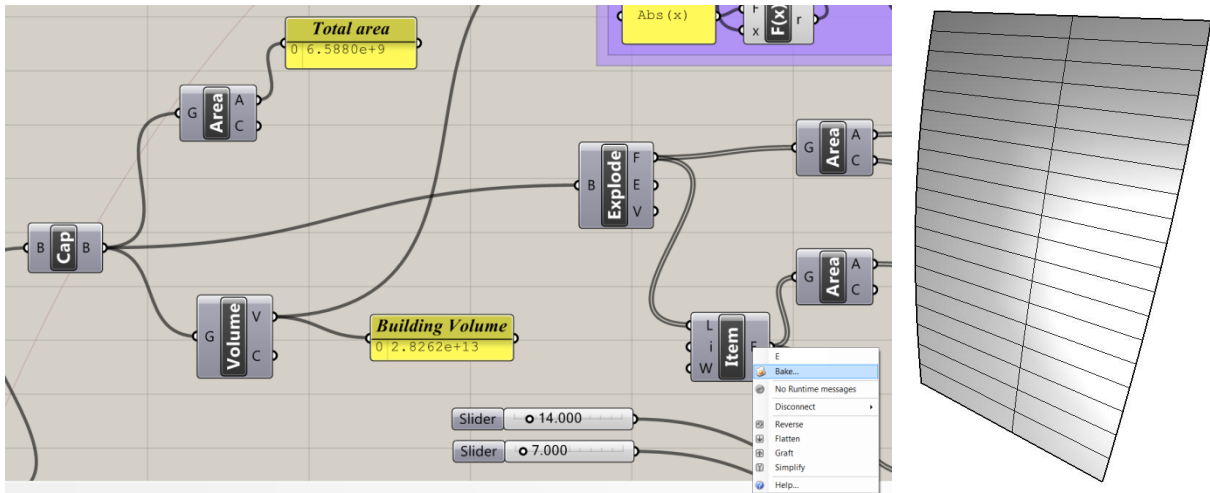


Figure 58. *Grasshopper* definition (on the left) where was extracted the façade's surface (on the right) to panel.

In *Rhinoceros* work environment it creates the grid starting from the surface: using the *Paneling Tools*, choosing among the possible options, it makes the UV grid on the surface as shown in the Figure 59. The grid permits to divide a surface following its u and v directions. Division can be by number, distance, or chord length using any combination in u and v directions.

In Figure 59 are presented two different kinds of paneling surface setting number of spaces between points: before were set values equal to 20 for number of space in u direction and 10 in v (on the left) and then were set values 10 and 5 for u and v direction respectively.

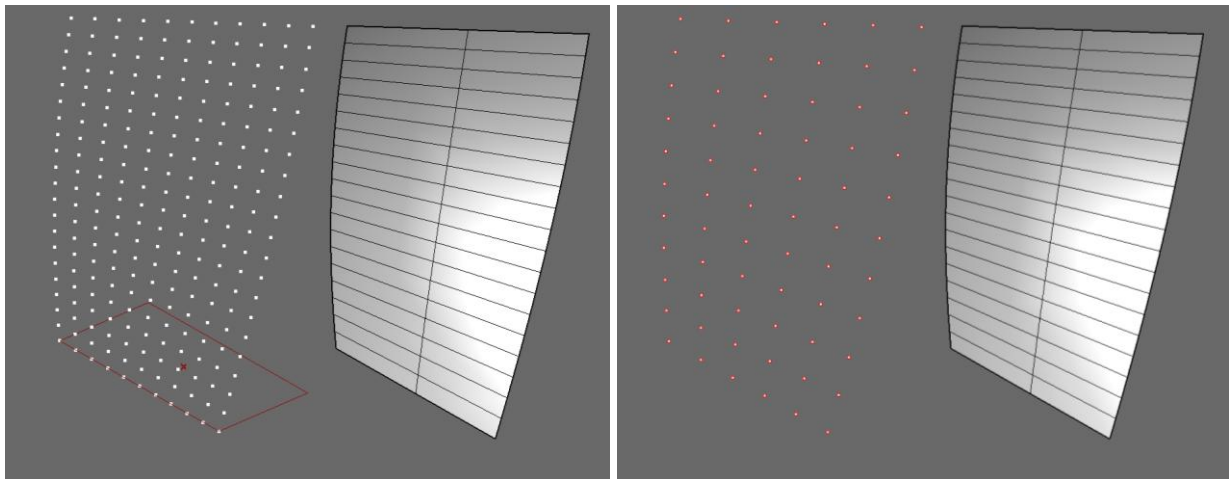


Figure 59. Two example of grid point one setting different number of spaces between point in u and v direction

Now created the grid is possible to apply different kind of pattern 2D or also 3D.

From the “paneling tools’ panel selecting the command “paneling from grid” is possible to decide which type of paneling surface applying from “Panel 2D grid, panel custom 2D, panel custom 2D

variable, panel 3D grid, panel custom 3D, panel 3D variable, oriented 2D/3D module to grid, panel planar quads”.

For paneling the surface of the Building A, in order to subdivide the surface to install the solar systems, is possible using one of the options indicated above: some examples of 2D paneling patterns in order to explore the capacities of the tool to create the surface paneling.

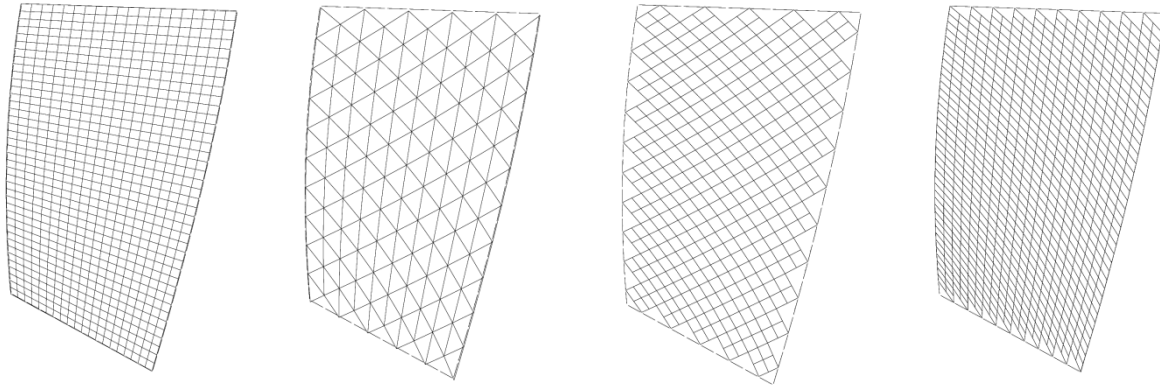


Figure 60. Four of all patterns of paneling using the Panel 2D grid (in order from left to right: box, triangular, diamond and angle box)

The Figure 60 shows four of the all options for panel 2D grid: in fact is possible to choose among box, boxX, triangular, tribasic, dense, diamond, angleBox, wave or brick pattern. However the *PanelingTools* allows also applying pattern invented from the custom as shown in Figure 61.

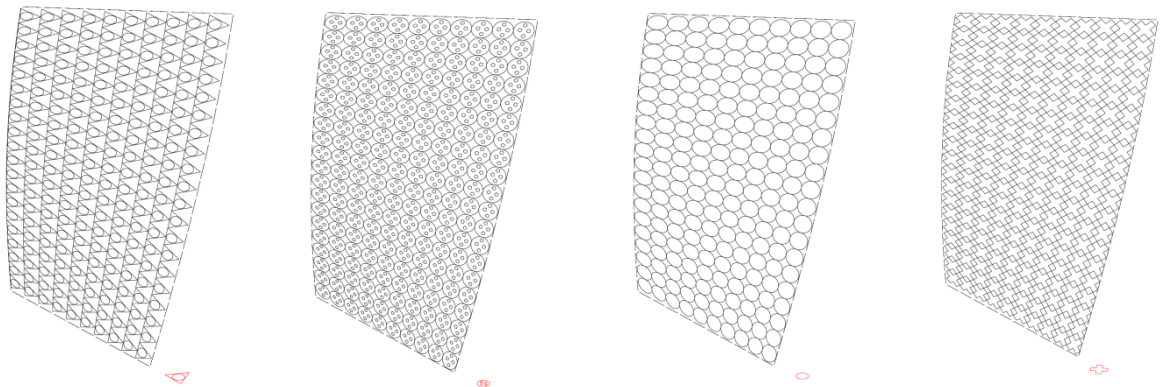


Figure 61. Examples of patterns of paneling using the custom panel 2D grid

It better to underline that for the examples presented was used the same grid, but are possible many grid sizes and patterns, also 3D, but they aren't object of this research. By the way, on the web it is possible to find many videos tutorial and documentation free available on the website [85] and on the manual [84].

### 5.3.2. Paneling surface using Grasshopper

Using *Grasshopper* is possible to proceed directly on the *Grasshopper* definition, described synthetically in the chapter 4.

Starting from the same point where it is started with *PanelingTools* as reported in the Figure 58, the surface is divided along u and v direction using the a ‘number slider’ (in the *Grasshopper*’s definition reported in Figure 62 are indicated with “subdivision along u/v direction). In Figure 62 the value used for subdividing the surface is equal to 25 along u direction and equal to 10 along the v direction. However sliders permit to divide the surface in different number of subdivisions as desired from the custom in a quick way.

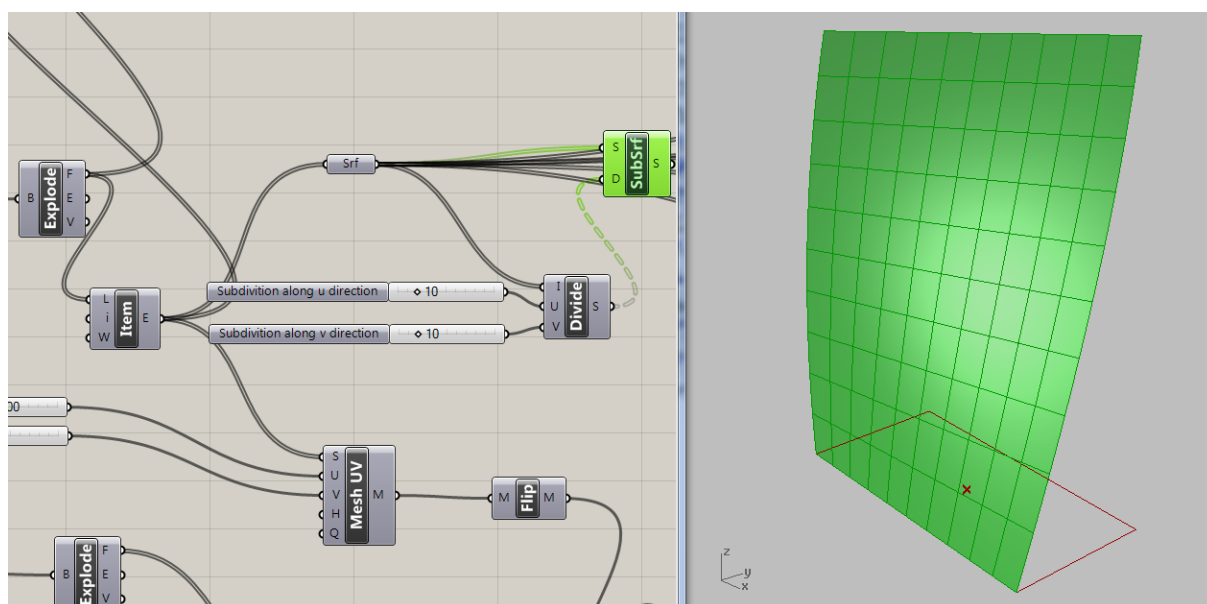


Figure 62. *Grasshopper* definition (on the left) for subdividing the surface visualizing in *Rhinoceros* work environment (on the right)

As written above, and how is possible to look in Figure 62, the geometry of the surface doesn't exist: it works behind of geometry's logic. Usually the all definition is “baked” when the logic's writing is concluded, however is possible exporting the definition in *Rhinoceros* every time is necessary.

At this point there is different ways to proceed for drawing the panels: below are presented two of them regarding the surface's paneling and one for the entire building.

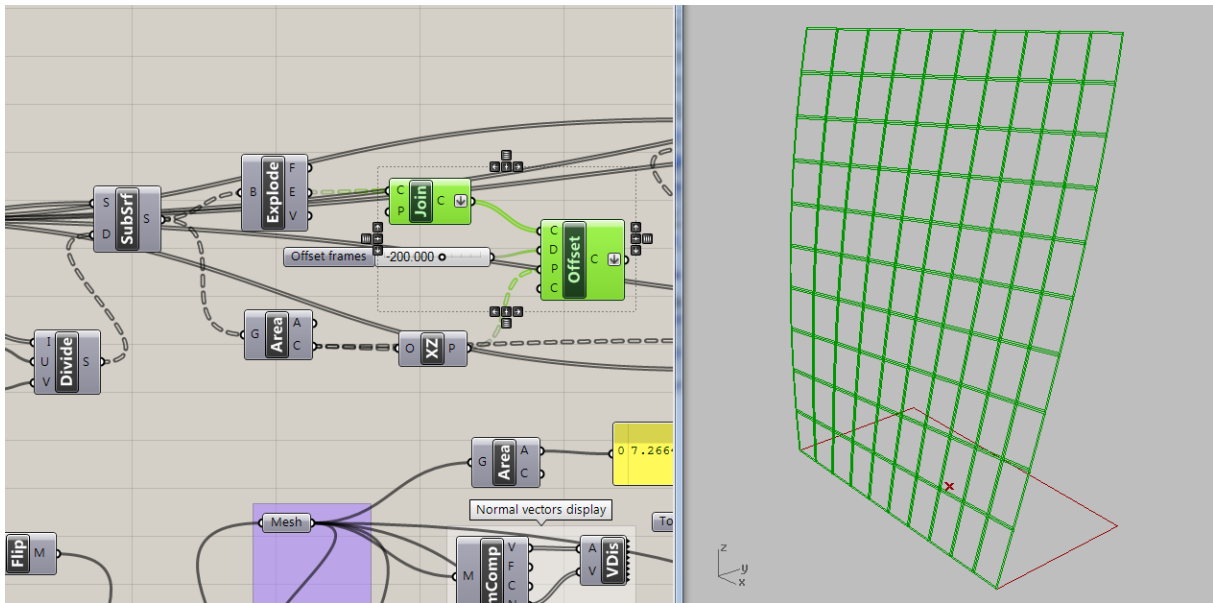


Figure 63. *Grasshopper* definition (on the left) for creating the frames for supporting the panels visualized in *Rhinceros* work environment (on the right)

For reducing the software elaboration's time, the paneling doesn't take in consideration the real dimension of the panels: in these examples the images are reported for visualizing the *Grasshopper*'s definition results.

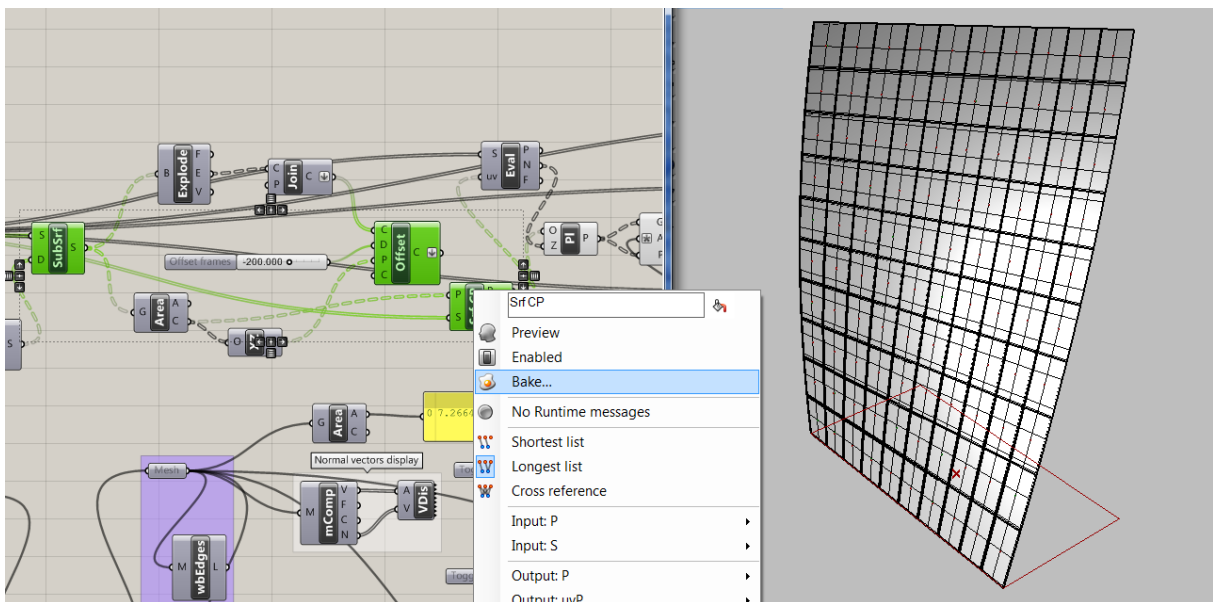


Figure 64. *Grasshopper* definition (on the left) for creating the frames for supporting the panels visualized in *Rhinceros* work environment (on the right)

At the beginning was created the structure of the panels exploding the all geometry (faces, edges, and points) and then jointed only the edges thus to have the frames. For creating the panels was done an offset of the joined edges, that is possible to change using the relative linked slider: in this way different kind of panel's sizes are tested in quick way as shown in Figure 70.

Now is possible to export the frame from *Grasshopper's* definition to *Rhinoceros* work environment and the paneling is already finish.

Another useful way to create the paneling on the surface starts from the previously definition just described now. Are defined the centres of the all panels' area and on their normal faces are drawing the panels that can have every sizes, shape and rotations assigned from by custom. In Figure 73 are chosen, for example, a panel like a polygon of 5 segments. Obviously is possible choosing any type of panels, sizes and shapes substituting the "Polygon" with desired shape. Furthermore rotate them around respective areas' centres and varying the dimension using the sliders.



Figure 65. *Grasshopper* definition (on the left) with the profile of the panels visualized in *Rhinoceros* work environment (on the right)

The next two steps are concerning the panel's creation from the profile visualized in the Figure 73. The most delicate and important aspect were to set the extrusion of the panels along the normal vector of every centre of area's panels.

Figure 66 shows the panels extruded along the normal direction of the central vector localized in the centre of every areas.



Figure 66. *Grasshopper* definition (on the left) with the extrusion of the panels visualized in *Rhinoceros* work environment (on the right)

Finally the frames of the panels are realized subtracting the panels profiles from the entire surface, as visualized in Figure 67.

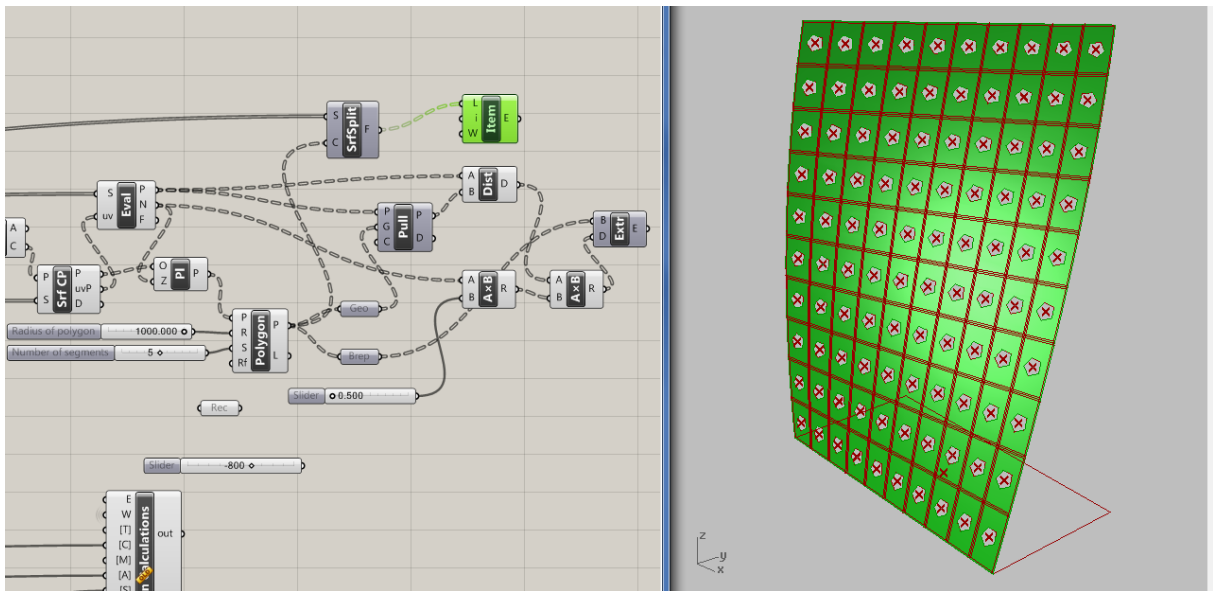


Figure 67. *Grasshopper* definition (on the left) with the frames structure of the panels visualized in *Rhinoceros* work environment (on the right)

The last step is the exportation of panels and their structure in the *Rhinoceros* work space, as shown in Figure 68.

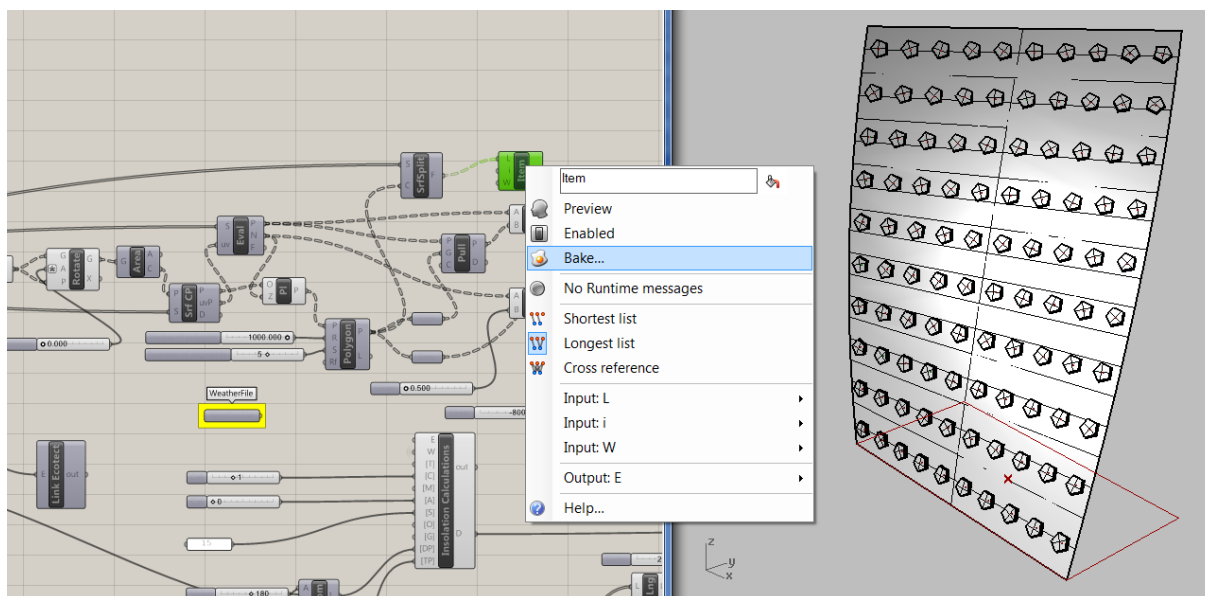


Figure 68. *Grasshopper* definition (on the left) with the paneling surface visualized in *Rhinoceros* work environment (on the right)

Following the same process just explained, all façades surface are paneling: the final result of entire building paned is reported below in Figure 70.

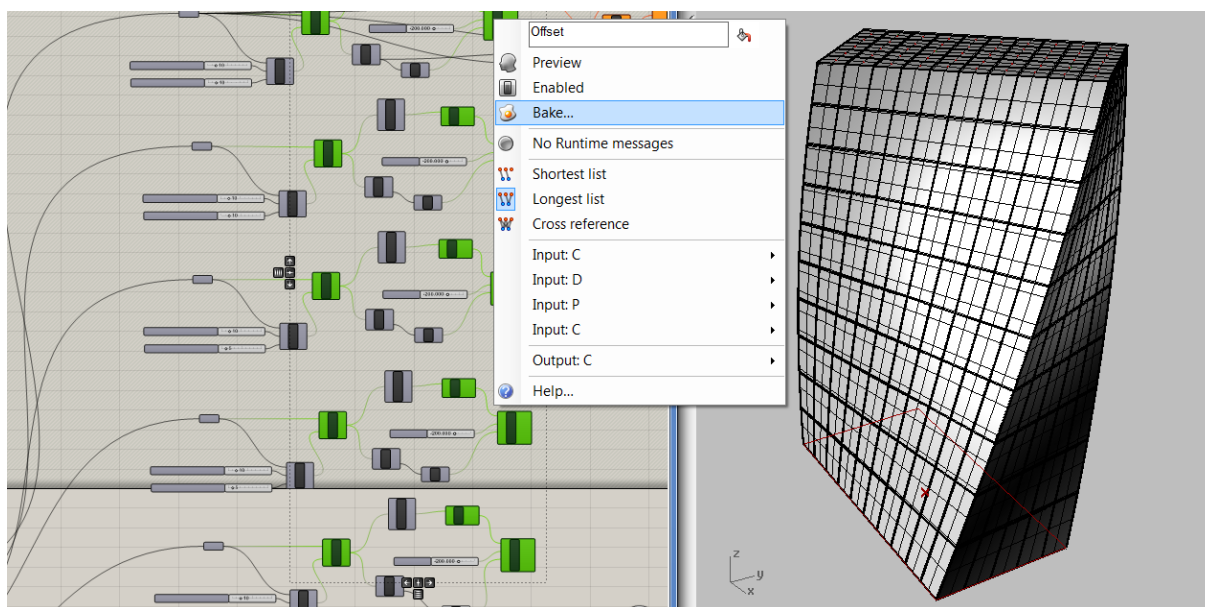


Figure 69. *Grasshopper* definition (on the left) with the entire building's surfaces paneling in *Rhinoceros* work environment (on the right)

## **5.4. Results and discussion**

In these section are presented the final results for the paneling surface and in particular using *PanelingTools* on the most irradiative surface façade and using *Grasshopper* for paneling all façades of the *Building A*.

Furthermore are presented how is possible to extract every single panel, gathering the panels with same dimensions and create a label for each of them in order to facilitate the creation of the moulds in phase of industrialization and installation in construction site.

Finally is presented an estimation of energy production using PV, thermal solar collectors and flexible solar product.

### **5.4.1. Paneling façade surfaces for installing a solar systems**

In this section is presented the sequel of the paneling process described above using *PanelingTools* in *Rhinoceros*.

For optimizing the façade was assumed that in every panel could be install a standard PV panel of size about 120 x 55 cm at least. Thus the smallest panel that constitutes the façade, can be included inside itself a standard panel. Considering the façade's size the total amount of the panels is equal to 2000, equivalent about to 1868 m<sup>2</sup> divided onto 80 number of space in u direction and onto 25 number of space in v direction. This choice was taken for obtaining the subdivision of surface based on flat panels and considering the double curvature of the surface. In fact the geometry of the surface, characterized by a double curvature, doesn't consent a subdivision with equal panels, even if many panels are similar each other: they have the same area and similar profile.

However were done two different subdivisions: the first maintaining the double curvature of the surface, and the second adopting the flat panels. The subdivision of the surface in many flat pieces with small sizes permitted a good approximation of the original surface. However the profile of the panels that follow the surface trend aren't a profile equal to the solar or PV panel, for this reason it isn't possible to use the total surfaces for installing the panels. For this reason was chosen to subdivide the surface so that the profile of a standard size panel.

While choosing to utilize a flexible solar panel the subdivision of the surface can be free and follow any kind of drawing and size for the panels. In fact the adaptability of the new innovative technology as thin film solar cell that is starting to develop consent to cover and exploit any type of surfaces.

However this new technology has advantages respect to the standard PV panels as low weight, that permits to reduce the total load of the solar systems' structure and furthermore they are not subject to wind lifting, and can be walked on (with care). The comparable disadvantages are for example the increase of the costs and the reduction of efficiency.

A silicon thin film technology is being developed for building integrated photovoltaic (BIPV) in the form of semitransparent solar cells which can be applied as window glazing. These cells function as window tinting while generating electricity.

Below is illustrated the study for extracting the flat panel and the process for integrating a standard solar or photovoltaic panel in flat frames which subdivided and approximated the surface.

Created the grid and the pattern desired, in this case was used the box one, and the panels, the next step is the creation of the structure of the panels, extruding the edges of the panels as shown in Figure 70.

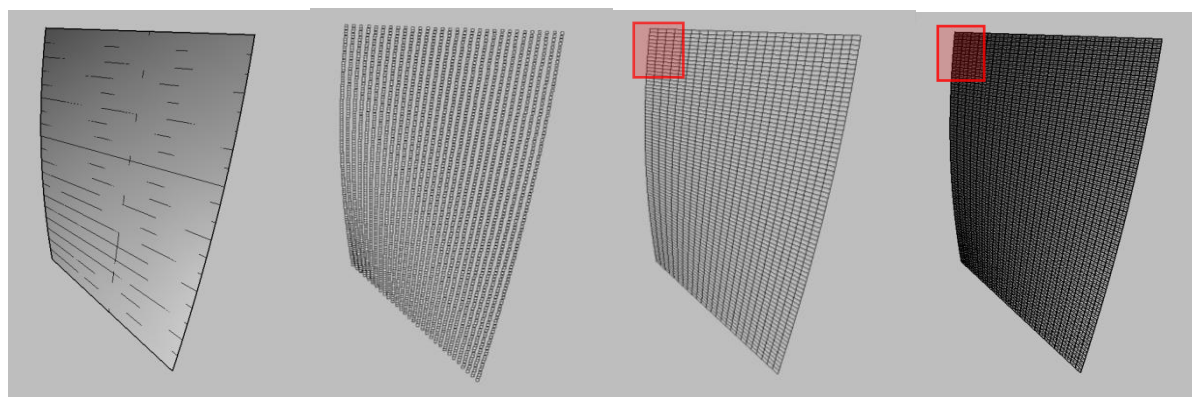


Figure 70. Process of surface's paneling: (from the right) surface, grid, structure and panels on the structure. In red the enlargement presented below

Below are shown in detail the structures of the panels the panels.

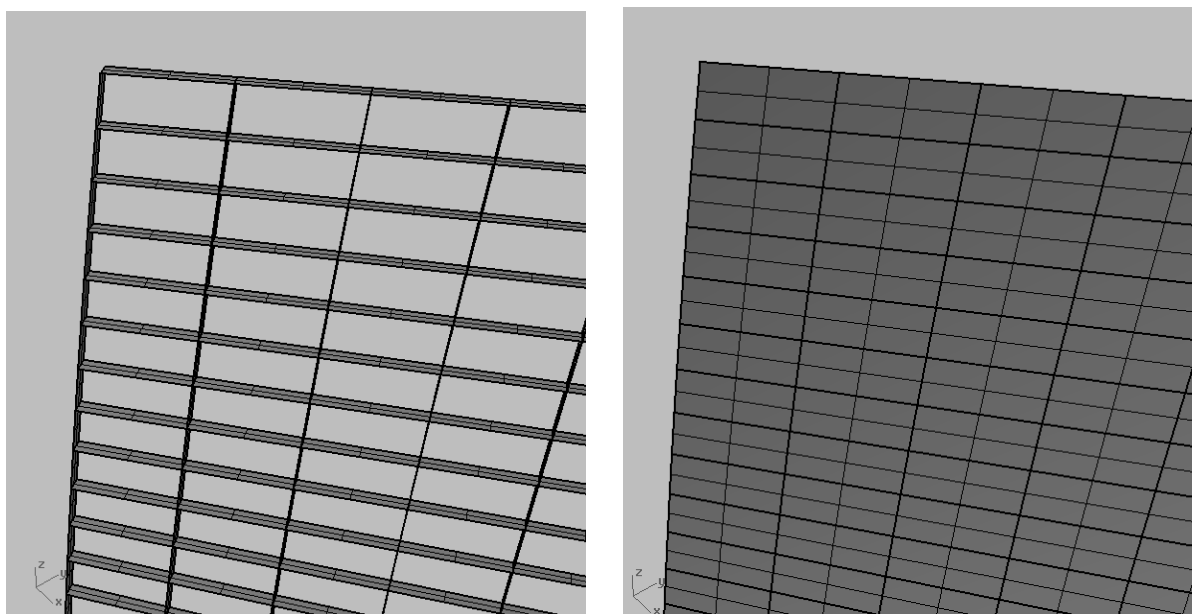


Figure 71. Enlargements of the panels' structure (on the left) and the panels (on the right)

In Figure 72 is shown the difference between non flat panels and flat panels.

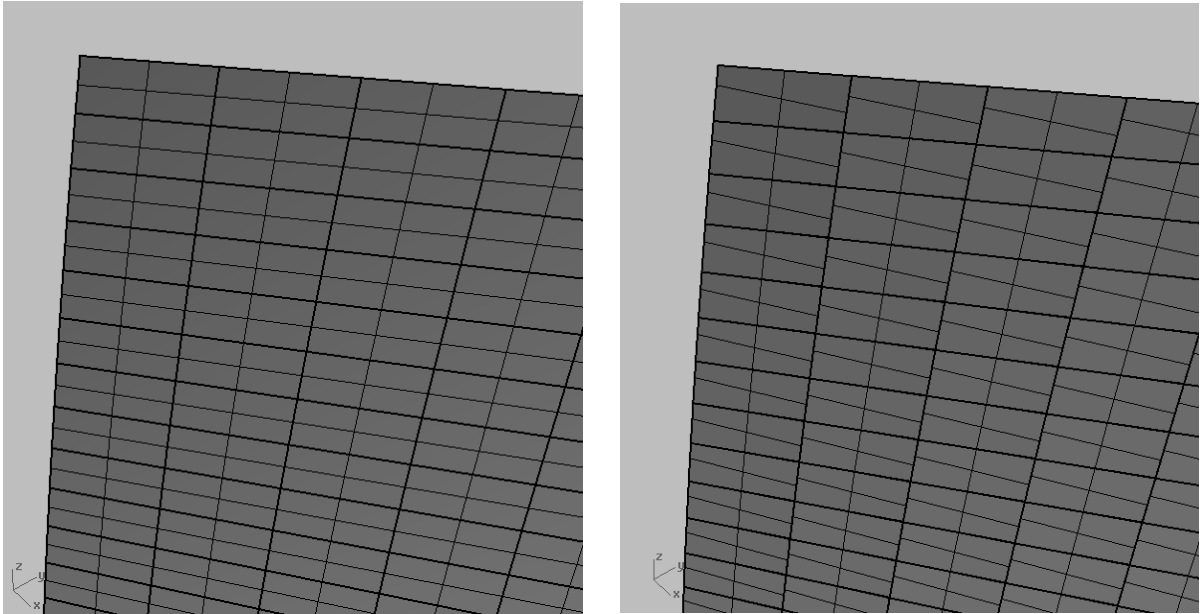


Figure 72. Enlargements of the panels' structure using no flat option (on the left) and the flat panels (on the right)

The paneling surface was thus created. Now remains the problem of the panel's production and installation.

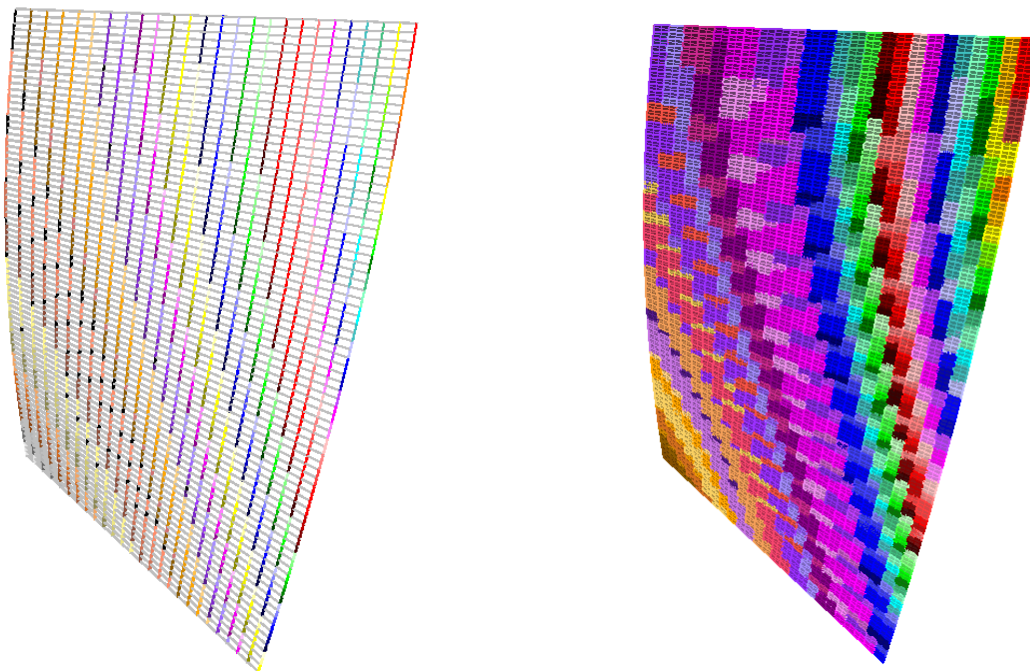


Figure 73. The groups of edges (on the left) and the groups of the faces (on the right) that compose the façade surface.

For solving this point the *PanelingTools* permits to unroll the edge and panels composed the façade and create a label of every panel. This operation allows create the groups of the similar edges and panels characterized by similar area and amount of profile. Figure 73 and Figure 74 show the different groups of edges and panels that compose the façade surface.

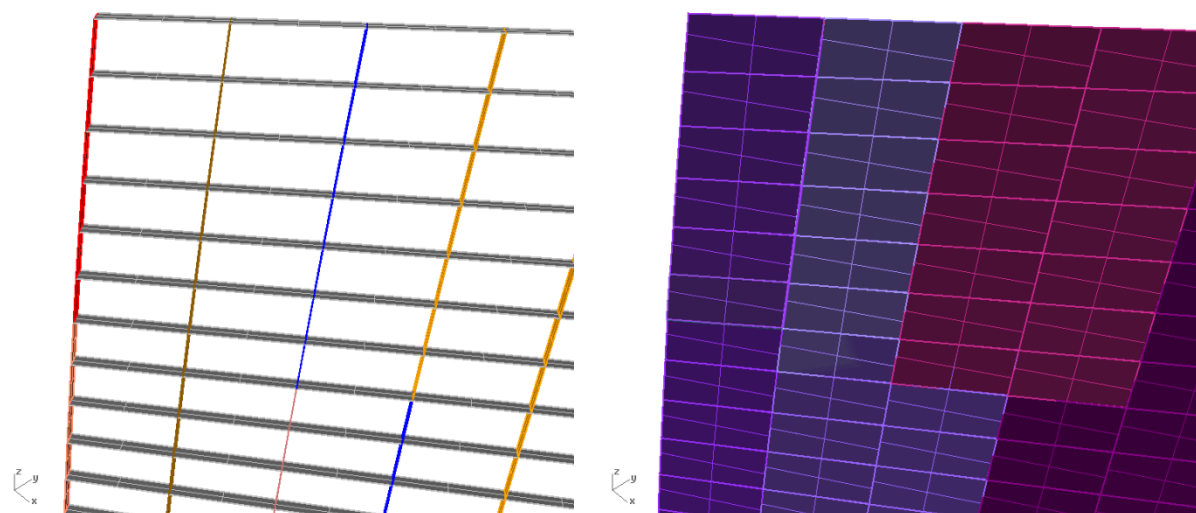


Figure 74. Enlargement of the groups of edges (on the left) and the groups of the faces (on the right) that compose the façade surface.

In Figure 73 is shown the group of the edges and the panels obtained with a specific function of *PanelingTools* that creates groups of similar panels: in this way is possible to collect the panels that have the same area and amount of the profile length with tolerance imposed by the custom (in this case equal to 5 mm). The panels that have a difference lower than 2 mm are grouped each other and coloured with the same tone. With this method the panels are collected the panels that are very similar each other, but they can have a different profile: all panels have the horizontal sides (the longer sides) equal each other and the length is equal to 1.4 m but different inclination, while the vertical sides (the smaller sides) are different each other for length as well as for inclination. These observations were provided from the unrolling operation done on the groups of the panels. Furthermore this process results to be useful for the industrialisation and installation phase, given that the extraction of the single panel consents with ease the production of the panel cutting following the panels' profile. In the Figure 75 is shown an example of unroll and the creation of the label of every panels, that results extremely useful especially during the installation activities of the façade on the construction site. In fact every panel enrolled has a label that permits to identify the panel during its process of production and to individuate its position on the façade during its installation.

Finally is presented the study of the standard photovoltaic panel insert in a panel, which thus works as a frame for the panel.

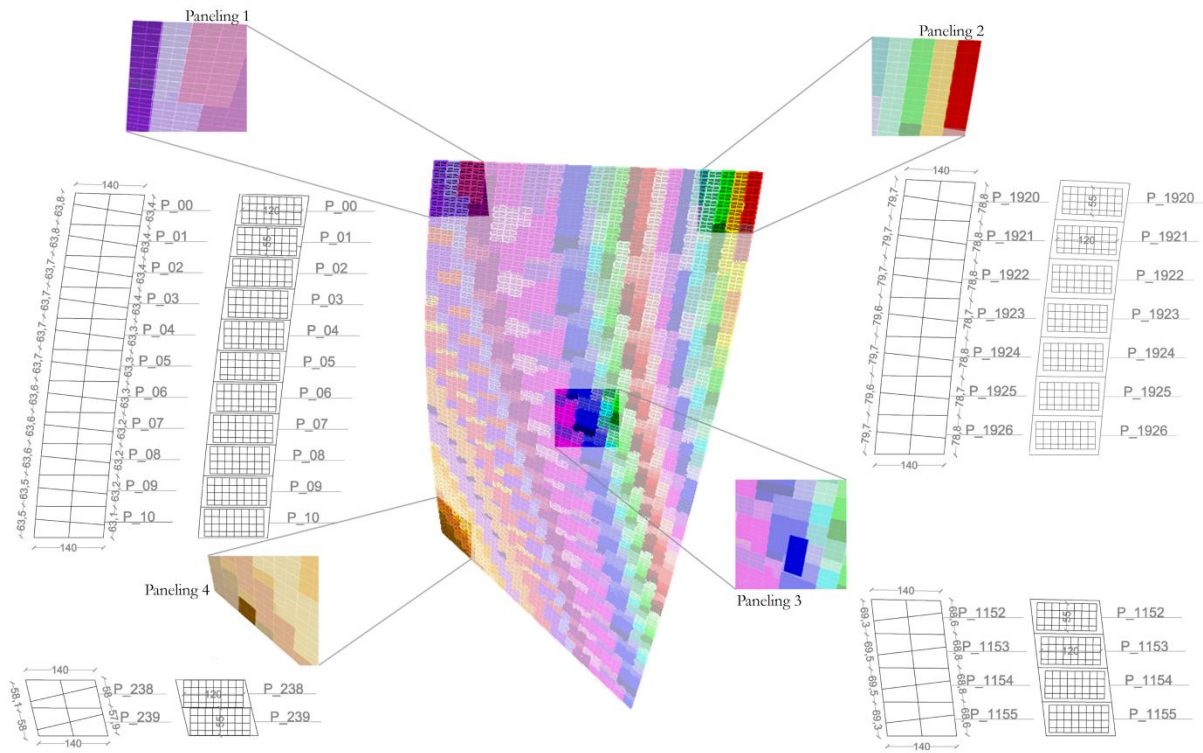


Figure 75. Example paneling unroll of four part of the groups in different areas of the façade.

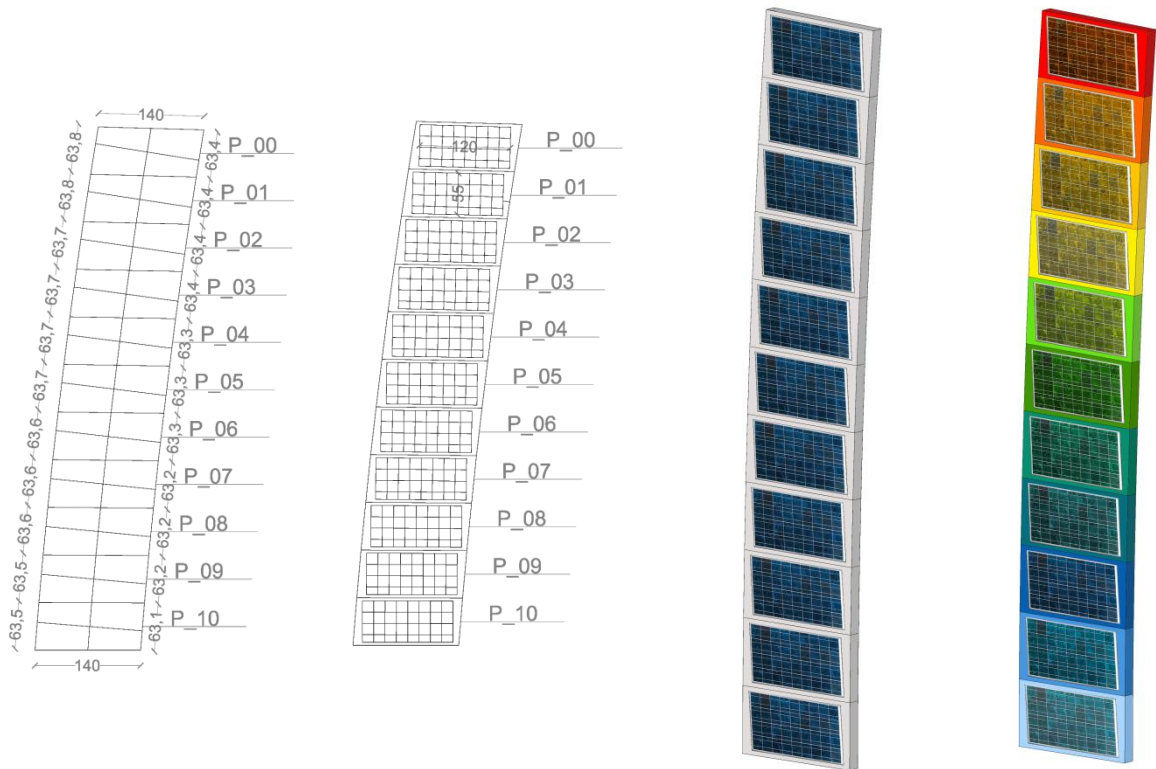


Figure 76. Particular of a one paneling's unroll and the 3D elaboration and architectural integration in a BIPV façade.

Figure 75 presented an example of unroll of the panels collocated in the top left angle of the façades and the elaboration in 3D of that part and an architectural integration with coloured panels and photovoltaic panels.

The same study can be conducted for the non flat panels.

#### **5.4.2. Estimation of the energy production**

In this last section is presented a rough estimation of the energy yield using the paneling of the surface just described, in a first stage, through a simple calculation and a comparison with different solar technologies available today in the market. For giving an estimation of energy production in order to have an idea that is possible to install and use the solar systems on a complex façade as that is examined, was chosen the calculation procedure described in one of the reports of subtask A of IEA-SHC Task 41 [88]. This method was elaborated in order to give a simple tool for architects to estimate the energy yield in the very early design phase. The calculation is resumed in the following points, where the main information needed is:

1. Location of the photovoltaic plant in order to estimate the Global irradiation on the horizontal surface “G” (many Irradiation maps are available which calculate the Global irradiance as function of the Latitude). The orientation of the modules gives then the effective radiation reaching the modules (orientation factor).
2. The adopted module technologies and the number of installed modules. With a simple multiplication of the cell efficiency (eff) and the modules area is possible to calculate the installed Power of the system.
3. The type of the installation: if the modules are integrated in the envelope and if the module are well ventilated. This information gives the Performance Ratio (PR) of the systems. As explained before, the PV modules efficiency strictly depends on the cell temperature.
4. The calculation can be done as follow:

$$FinalYield = G \text{ kWh/m}^2 \cdot a \cdot OrientationFactor \% \cdot Area \text{ m}^2 \cdot eff \% \cdot PR \% \quad \text{eq. 2}$$

Regarding the first two elements presented in the eq. 2 in this case are substituted by the data of solar global radiation that has directly been calculated on a specific façade’s geometry with solar dynamic

analysis presented previously. However considering the energy production on the same façade the differences is given by the specific efficiencies of solar technologies and the area that they occupy.

Therefore the efficiency of solar products becomes the important aspect to consider in this calculation.

For the solar systems products to apply on the façade were considered the standard average value of efficiency of each of them: 70% for the solar panels, 17% for the photovoltaic and 11% for the flexible solar panel. However their efficiency is strongly influenced by working temperature, as will shown in the chapter 6, but in this simple estimation it will considered the best conditions: good back ventilation of the modules and current maintenances are supposed (PR=80%)

In particular considering the evacuated tubes their efficiency is around 70%.

Regarding the efficiency of monocrystalline cells is currently the highest available on the market, ranging approximately from 17% to 22%, while multicrystalline cells are around 11% to 17%.

While regarding thin-film solar cells, are usually categorized according to the photovoltaic material used, the three main technologies being amorphous silicon (a-Si), Copper Indium Gallium Selenide (CIS or CIGS) and Cadmium Telluride (CdTe). For standard amorphous silicon cells the efficiency lies among 4% to 8%, but some manufacturers produce modules with combined cells (multijunctions), reaching efficiencies around 10%. CIGS cells can reach 12%.

#### *From façade's energy production to primary energy index for heating (EP<sub>H</sub>)*

Considering the presupposition that has just been done, in the Table 35 are summarized the all data necessary for the this early estimation of energy production with the solar systems installation and its conversion in primary energy for heating in order to estimate the percentage of building's energy demand it is able to cover Table 36.

The data were divided into three part: in the geometrical data are reported the total surfaces for the building envelope and the surface of most radiative façade on which is calculated the estimation of energy production. As it was shown in the paneling's study of this chapter, if are installed standard photovoltaic panels or solar panels, is not possible to cover the all façade's surface. In fact in each panel created by paneling's it can be installed a standard photovoltaic or solar panel: the 2000 of these panels cover a surface equal to 1320m<sup>2</sup>, that is equivalent to 30% less than the total façade's surface (1876m<sup>2</sup>).

For calculating the solar direct radiation were done a simulation using *Daysim* and setting the ambient bounces radiance parameter equal to 0: doing the difference with simulation which was set ambient bounces equal to 1 is possible to isolate only the direct radiation that is the solar radiation's component that is exploited from photovoltaic and solar panel. Instead for the thin-film solar cells, that have the

lowest value of performance (10%), the total global radiation ( $a_b=1$ ) has been considered, given that these kind of solar system is able to exploit the total solar radiation.

Therefore in solar radiation data are reported the total solar direct radiation on the most radiative façade for different scenario thus that is possible to compare the case of isolated building setting the ambient bounces equal to 0 and building inserted in a district setting before ambient bounces equal to 0 and than equal to 1. It is better to underline that on the values collected in a table, when the building is inserted in a district and it is considered ambient bounces equal to 0, the direct solar radiation on the most radiative façade is less than 12%. However in the same scenario, when the ambient bounces is set equal to 1, the façade resulted more radiated (+40%) respect to the isolated building's case study. This latter data could be used for calculating the energy estimation supposing to install the thin-film solar cells on the façade. Nevertheless this data is not completely correct: in spite of the ground's reflectance is set equal to 0.0 and therefore the solar reflection coming from the ground wasn't considered, the solar reflections coming from the surrounding are included in this value. This technical aspect explains in part the high difference of values: in fact the high value is also given from the global radiation's value that includes direct and diffuse radiation together when the ambient bounces is equal to 1. Unfortunately the tool doesn't permit to split the different solar radiation components and for this reason the value of solar radiation is overestimated and consequently the energy estimation calculated with thin-film solar cells.

In Table 36 are reported the results of energy estimation considering three types of technologies, the solar radiation incident on the façade and the surface considered for any solar product. The energy production is converted in primary energy for building's heating in order to compare the value calculated with the value of primary energy for this building that is equal to 49.6 kWh/m<sup>2</sup>yr, as indicated in the Figure 77.

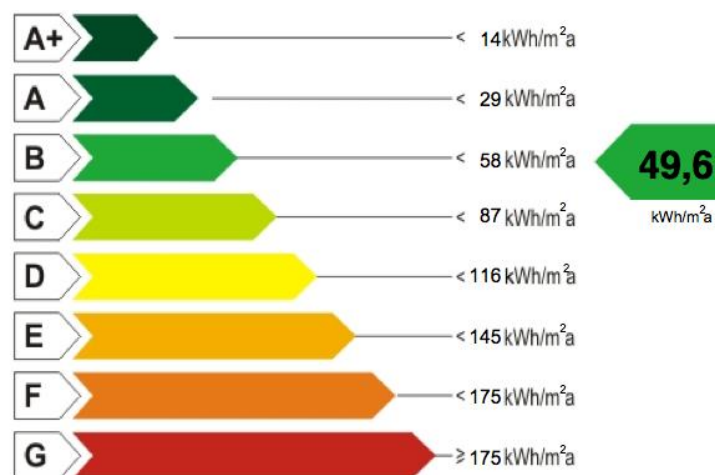


Figure 77. Value of primary energy for building's heating. The building examined belongs to energetic class "B".

The results show that, in spite of the available surface (1320 m<sup>2</sup>) for installing the solar system as solar thermal collectors and photovoltaic panels is 30% less than the total façade's surface (1867 m<sup>2</sup>), using the solar thermal collectors is possible to cover until 87% of energy demand of the entire energy demand of the building, given their high efficiency (70%), while using the photovoltaic panels only the 9.7% of primary energy demand is covered. Finally using the thin-film solar cells the percentage of energy demand of the building raises until 15%, not for their performance (10%), but for their installation area (1867m<sup>2</sup>)

Table 35. Summary of the data used for the analyses

Data of the analysis			
Geometrical data			
Total heated surface	5993 m <sup>2</sup>		
Total solar optimized façade surface for solar system's installation	1867 m <sup>2</sup>		
Area of each photovoltaic panel and solar thermal collectors	0,66 m <sup>2</sup>		
Total available area for installing photovoltaic panels and solar thermal collectors	1320 m <sup>2</sup>		
Solar radiation data	Isolated building (ab=0)	Building in the district (ab=0)	Building in the district (ab=1)
Total solar global adiation on the building envelope (façades and roof)	1325019.5 kWh	1159865 kWh	3061493 kWh
Total solar direct radiation on the most radiative façade	734016 kWh	658229.67 kWh (-12%)	1218967 kWh (+40%)
Solar radiation per unit on the most radiative façade's surface	393.15 kWh/m <sup>2</sup> yr	352.5 kWh/m <sup>2</sup> yr	653 kWh/m <sup>2</sup> yr
Performance of the solar systems			
Photovoltaics panels performance- monocrystalline cells	17%		
Thin-film solar cells performance	10%		
Solar thermal collectors performance - evacuated tubes	70%		

Table 36. Summary of the energy production's results and the conversion in the primary enegy for building's heating

Technology	Energy production (kWh/yr)	EP <sub>H</sub> (kWh/m <sup>2</sup> yr)	% Energy demand covered
Photovoltaics panels - monocrystalline cells	29097	4.8	9.7%
Thin-film solar cells	44839.5	7.4	15%
Solar thermal collectors - evacuated tubes	260568	43.5	87.6%

## **5.5. Conclusion**

This chapter has presented the initial study on processes of optimization that starting from the solar optimization of the building's shape arrives until the development of an innovative, smart kinetic shading systems integrating a photovoltaic, therefore is able to produce the energy avoiding overheating.

However are necessary a deep studies in order to improve the evaluation related to the different products that today are available on the market.

## **6. Conclusion Section 1**

The first research's objectives described in the Section 1 were to develop and test new methods and approach for efficiently optimising the environmental sustainability of urban planning and design proposals. The study was started, in the first instance, tackling the problem of optimising the shape of buildings for the improvement of solar radiation on the building envelope and its solar access. The geometric shape of the buildings was parameterised, allowing for their representation by manipulations of the building volume, initially with simple transformations create manually and then using generative modeling tools in order to impose more complex transformations, and the parameters of optimization were selected in order to maximise the solar irradiation potential. The methodology was applied successfully to study cases in the city of Milan (Italy), producing interesting results.

The first part of the research described above, has developed a new design approach starting from a new local, national and international regulations framework regarding energy consumptions and use of land, focusing on principles of sustainable development that nowadays is the only possible for the future.

Starting from the urban context, considering a new or refurbished building, maintaining some parameters fixed from the urban regulations as volume, footprint and height, the designer has two possible alternatives: the maximization of the solar potential of the building or the minimization of its impact on the urban built environment.

The first of these two design approaches has its origin in the historical urban and architectural design. In fact from always the "conscious and intelligent" designer exploit the gains come from of the environment and there are numerous examples: from the perfect orientation of Egyptian pyramids to the study of natural ventilation of "Casa Batlò", until the importance of the daylighting in the XVI century constructions. Nowadays, with the availability of new innovative technologies, that allow an active exploitation of the renewable sources, it becomes more and more important an adequate design that makes an attention on these topics, also seen the costs linked on them.

During these last years the way to do architecture is going towards dynamism, making attention to the movement through shape manipulation with parametric transformations as rotations, slopes, twists and projections. However, often these new idea of architecture is a sort of formalism of architects that design a building that is possible to insert everywhere in the world, without any relation with urban environment where is inserted.

The dynamic shape of a building must come from urban context analysis and functions that the building has in itself. Furthermore the relation between a building and urban environment is also a relation with nature and climate of the place.

Nevertheless today is fundamental to develop a conscious and intelligent design where the environment impact of a new building and its sustainability influence every scale order from urban to building component scale.

The present research in fact starts from a urban solar and thermal dynamic optimization scale analysis and in particular in the section 1, regarding the “Solar Potential in Urban Areas”, was developed a new design approach in order to provide a process for architects, urban planners and engineers focused on supporting decision making especially in early design phase.

### 6.1. A New Solar Design Approach

The new solar design approach is based on the combination of different tools that were described previously: *Rhino*, *Grasshopper*, *Galapagos* are the generative modeling tools used for volume’s transformations, *Geco* is the plug-in for linking the modeling tools with solar dynamic software as *Autodesk Ecotect Analysis*, *Daysim* and *DIVA*.

The flow chart in Figure 78 summarizes the steps of the process.

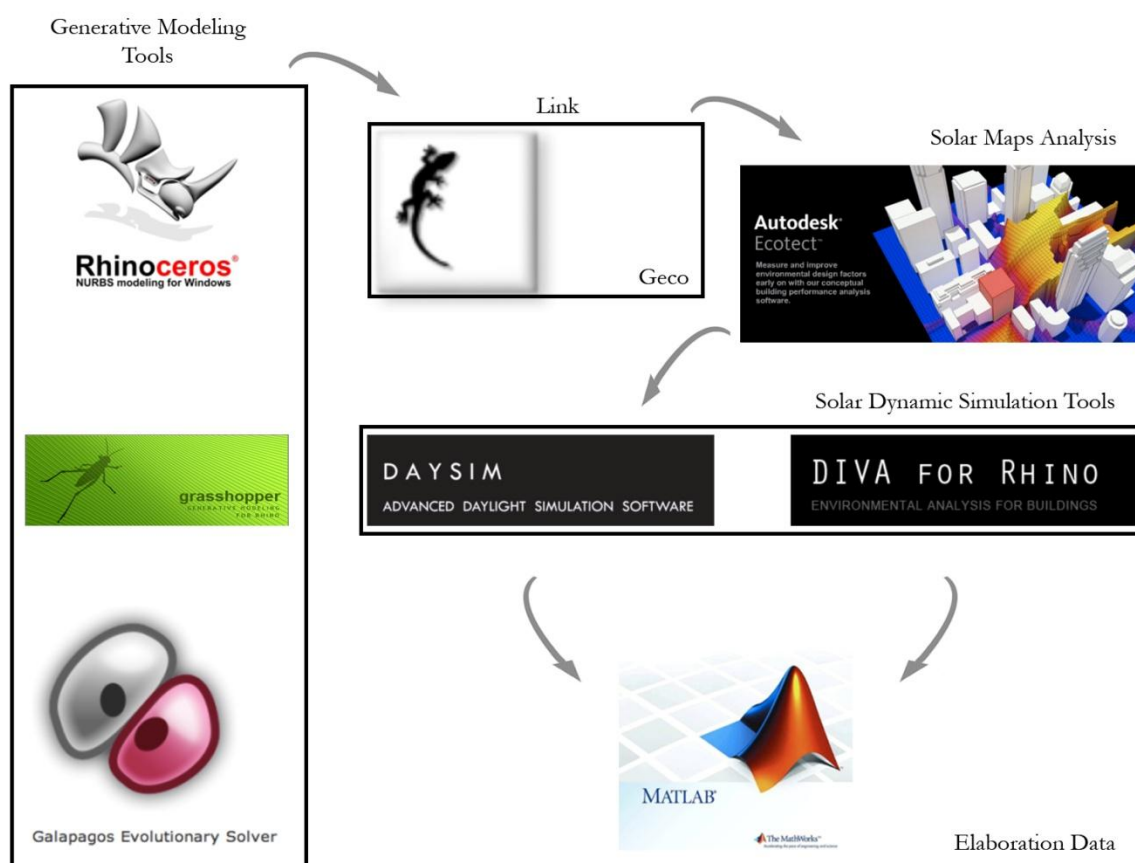


Figure 78. Flow chart of the tools used for developing the new solar design approach.

The most important and innovative aspect of this new design approach is the fact that it is composed combining different tools that usually are used alone for achieving only one specific goal and doing one unique type of analysis. Thanks for the interoperability among the tools was possible to connect all of them in order to elaborate an unique process that permit to start from the plane, modeling the shape of the building and run the simulation in order to analyse the solar access and develop the solar optimized design of the building's shape:

Moreover the other important aspect of this approach is that it isn't important the place that the building is located because is possible to upload the all weather data climate of the most important area of the world and the modeling can start from every site of construction without any limitation.

Obviously it is most important to conduct a deep previous urban analysis to define a framework in order to fix some urban data to limit the parameters to modify.

The other important aspect is related the limitation of the transformation limitation: in fact in the case study of the city of Milan, has just been presented, were fixed the rotation and the slope upper limit in order to guarantee the static balance of the structure and its construction.

Therefore the first section of the research gave the first answers related to the initial questions written at the beginning of the research and the section as well.

1. *The surfaces of the roofs are sufficient for installing the solar panels in order to produce the energy and reduce the non-renewable energy demand?*

The case study of the city of Milan demonstrated that the optimization of the building's volume and the modeling of the its surfaces in order to improve the solar radiation on themselves and a good design of the solar systems' installation joined with the best localization on the building envelope can cover a high percentage of the energy demands of the building. It depends on the solar systems' efficiency and on the facades' exposure. The tool for a new design approach created in this section could help the architects, urban planners and engineers in order to develop a more intelligent and sustainable design.

2. *Why not using the most exposed surfaces: the façade?*

The calculations and the analyses done in the first section were focused on the study that the increment of the solar exposure of the façades improves their solar access and consequently it is easier to use their surfaces in order to exploit the solar radiation for installing the solar system.

The estimation of the increments of solar radiation on the façades, conducted in the first section, demonstrated that it is useful to exploit their surfaces in order to produce the energy using the solar systems.

3. *How is possible to reduce the overshadowing among the buildings?*

Regarding this point the research gave some examples that the optimization of the building's volume can reduce the overshadowing effect on the design building, especially considering the buildings that have the same height of the nearby buildings (case study of the city of Milan). Furthermore the *SolarPW Tool* presented in this dissertation, permits to optimize the solar access considering two buildings.

Sometimes the optimization of the new building in existing urban area, can improve its solar access reducing the overshadowing effect from the nearby buildings as has been demonstrated for the Building B in the case study of the city of Milan.

4. *How is possible to increase the solar access for a new building designed in the existing urban area?*

The conception of a new solar design approach that permits to model the building's volume has been thought in order to improve the solar access for a new building. The final analysis of the new designed building inserted in a district demonstrated that its shape's optimization in isolated scenario, allows to increase its solar access when it is considered in a district.

5. *Which are the effects of solar reflections coming from the surrounding, from existing buildings, from ground reflection and sky component, on a building? How can calculate their contributions?*

This section gave some results in terms of solar reflection contributions coming from the surrounding in order to provide the different amounts of solar radiation increment that the various surfaces (buildings facades, roofs, ground, sky component) create on the new designed building. Furthermore for a simple district models were simulated the solar reflection contributions coming from the surrounding testing various colors and finishing materials applied on the facades' surfaces in order to estimate the percentages of solar radiation increment or decrement on the designed building envelope.

The study demonstrated that the surrounding's solar reflection contribution depends on the reflectance of the finishing materials and in general by their physics properties. Moreover their contribution is composed by different components that are related to the number of solar reflections are considered during their calculation: for this reason has been done an initial sensitive analysis in order to calculate the solar reflection contribution set various number of ambient bounces.

Finally the solar reflection given by ground contribution represents the highest contribution from the surrounding, as has been demonstrated in all simulations done.

## **6.2. Future developments and outcomes**

The study demonstrated that is possible to create a new design approach for optimizing the building volume in order to improve the solar access and consequently the energy production exploiting the solar potential of its building envelope.

However the study has needed more important future developments for integrating some solutions and analyses for important technical aspects:

- Analyse the impact of the costs related to the surfaces' modeling manipulations, the realization of the structure and its construction;
- Improve the tool for testing many other types of surfaces' transformations in order to optimize the volume automatically in base of the weather data climate and the surrounding context;
- Analyse the effects that the solar optimized design building could create on the surrounding area in term of overshadowing, solar access and solar reflections.
- Evaluate the internal comfort of the ambient behind the facades, as well as further analyses on the technology and the materials of shading devices that should be used in order to reduce the warming inside.



**SECTION 2**  
**MICROSCALE CLIMATE INTERACTIONS**

## 7. Micro-climate environmental analysis: surface temperatures

### Questions of chapter

1. Which are the adequate surface temperatures that permit a good efficiency the solar systems?
2. How is possible to decrease the surface temperatures on the façades?

### Abstract

When the urban planning of a new district or a design of a new building in existing urban area starts, it is important to make attention on the plan morphology and heights profile distribution of the buildings that composing the entire urban area to achieve the optimum configuration regarding exterior thermal stress at the pedestrian level and interior thermal comfort for the inhabitants.

The variety of surface cover and the use of land are always the result of the process of urbanization. Consequently, the elevated temperatures are mostly presented in the urban areas rather than non-urbanized surroundings: this phenomenon is often defined as “the urban heat island”. The impact of urban heat islands on the residents are several [89], among other: modified energy demand (higher in summer, lower in winter), thermal stress on inhabitants, especially on pedestrians, increased air pollution formation rates and temperature on the façades.

This chapter gives an overview regarding the problem of thermal stress due to the temperatures on the façades and some consideration on the benefit of the vegetation regarding the distribution of the temperatures on the façades. The analysis have been conducted by the use of micro-climate three dimensional tool *ENVI-met* [90] for the most irradiative building, inserted in a simple district to study the micro-climate scenario during the highest solar radiation day on a building’s façade (South façade) that have been obtained in the previous part of analysis have been done. The analysis conducted wants to investigate the micro-climate effects in different scenarios with many configurations of the green systems and soils set up.

Finally, have been conducted the same micro-climate analyses on the same real case study of the city of Milan analysed previously. The main aim of this part of the research has as objective the calculation of the surfaces’ temperatures to explore how is possible to reduce the effect of solar radiation on the values of temperature without reach the critical point of operative temperature in which the solar systems decrease your efficiency.

## **7.1. Introduction**

The urban developments can significantly change the image of a neighbourhood or town. In the city, the microclimatic component can unite several actors (architect, planner, landscape, political, developer, engineering firm,) advocating an interest in energy savings for the adjustment of thermal conditions of the urban space and the improvement of life. These components in fact influence largely the relationship between vegetation and the city [91].

Focalizing at the lower part of the atmosphere where we live, it is directly influenced by local exchange processes which can develop an individual local climate, different to the expected average conditions. Especially in urban areas the great variety of different surfaces and sheltering obstacles produces a pattern of distinct microclimate systems. To simulate these local systems, microscale numerical models with special extensions for typical artificial urban boundaries are needed [92].

Analysing the interactions between the environment and the atmosphere on local scale is much more complicated than looking at the same system on a regional scale. The multitude of different surface materials and sheltering objects produce a very distinct pattern of different climate conditions, especially within the building structures such as street canyons or backyards [92].

Of special interest, however, is the daytime situation, since the combination of high temperatures and intense solar radiation create severe problems of heat stress [93].

In the course of planning city expansion, urban climate simulation models are extremely useful for visualizing the impact of new buildings before construction even begins. These models re-create the atmosphere within the urban environment by representing the local environment and morphological data (buildings, roads, trees, etc.). The simulation results provide the ability to understand and predict the impact of various building configurations and surface materials on the urban atmosphere. Since the simulation process is based on the input parameters representing the structural and surface characteristics of the urban environment, the accuracy of the simulation primarily depends on the quality of input data.

Models of urban environments are extremely useful in city planning. Having a high-quality environment is central to improving urban life and is a main challenge in urban planning. An increase in urbanization has been observed during the twentieth century. This trend can be expected to continue, and the environmental impact of urban areas is a growing concern [94]. Architects, urban designers, and decision makers play an important role in this aspect. They need a tool to evaluate and analyse the environmental impacts of their projects on the urban microclimate before making decisions. This task leads to the research of computer-based approaches for storing, manipulating, managing and visualizing urban data as well as environmental properties of urban space

The micro-climate study below presented is aimed to analyse the thermal comfort of different configuration of simple districts and finally on an urban area in the city of Milan. The area selected has characterized by medium density and it is located in the north-west of Milan and it represents a very

typical operation in Milan: demolition of the existing building and reconstruction of the same volume, but with a different shape. The analysis of thermal comfort index and the Wind flow showed the influence of high buildings in the local climatic environment.

## 7.2. Material and method

### 7.2.1. Clear-sky simulations and simulation parameters

Input parameters and initial conditions are found from the sensitive analysis of the buildings façades that constituted the urban area simulated. The average value of urban albedo used for the urban district simulation is carried out from literature. Regarding urban canyon albedo model, among other, one of the most referential is the following method composed in two parts: the first carried out the results of measurements of the albedo over time (during the day and in different seasons) of concrete arrays blocks in different configurations [95] [96]. In the second part, a photon tracking 2-D model (Monte Carlo module included) is validated with measured data [97]. Figure 79 summarizes the computer simulation: it is possible to observe that for materials having half Lambertian and half specular reflection mode, the increment of the height to width ratio of the canyon causes the solar reflectance decrement with solar zenith angle. In the Figure 79, if it is considered a canyon with height equal to width, with materials that present a perfect specular reflection mode ( $\alpha = 1.0$ ), solar reflectance decreases with solar zenith angle until  $60^\circ$ , and increases again after  $60^\circ$ . There is a slight decrease until  $40^\circ$  in solar zenith angle, and then reflectance increases, for materials that have half-Lambertian, and half-specular reflection mode.

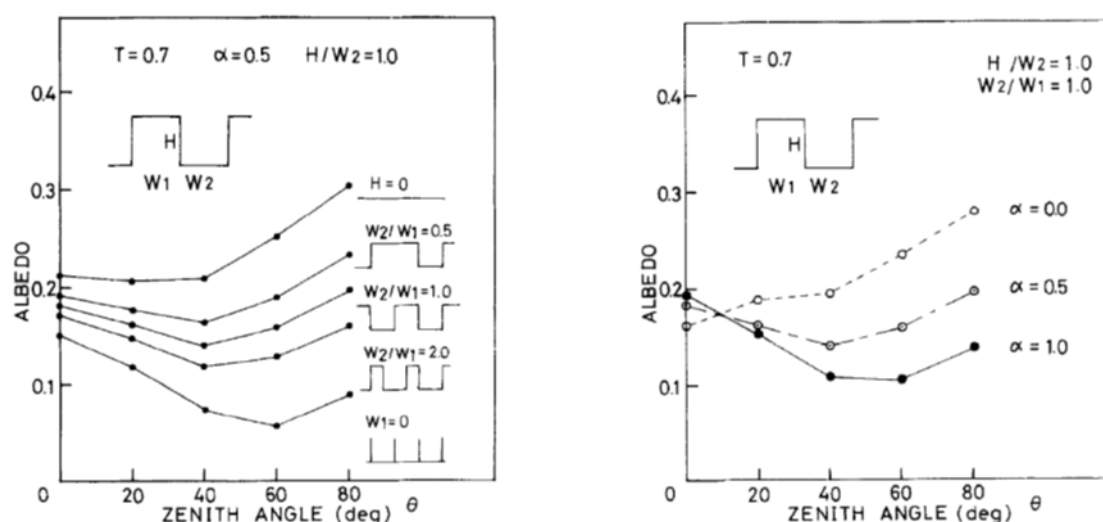


Figure 79..Analytic relationship between albedo and solar zenith angle modeled with ray-tracing simulation and assuming materials that have reflection mode half-Lambertian and half-specular: for different canyon configurations (on the left), and for a canyon having  $H/W = 1$  (on the right), specular reflection mode ( $\alpha = 1$ ), Lambertian reflection mode ( $\alpha = 0$ ), and half-Lambertian and half-specular ( $\alpha = 0.5$ ).  $T$  represents the transmissivity of the atmosphere.

The configuration of the urban district analysed with different ratios between heights and widths and the zenith angle (deg) that varies as shown in the Table 38, where data have been carried out from the Solar Tool 2011 [98] integrated in *Autodesk Ecotect Analysis* [99], for the simulation time period

considered (from 6:00am of the 16<sup>th</sup> June to 6:00am of the 17<sup>th</sup> June), indicate that could be used the albedo values from 0.1 and 0.2. Therefore it has been chosen a value of albedo walls equal to 0.2 and equal to 0.3 for roofs: these values have been inserted in the building section defined in the input area file in *ENVI-met*. According of the albedo's definition that is "the ratio of total reflected to total incoming solar radiation (i.e. averaged over all solar wavelengths)" [100], it can be seen in Figure 80 that about 30% of the annually solar radiation incident on the Earth is reflected or scattered (b,c and e), and for this the effective Earth's albedo is approximately 0.3.

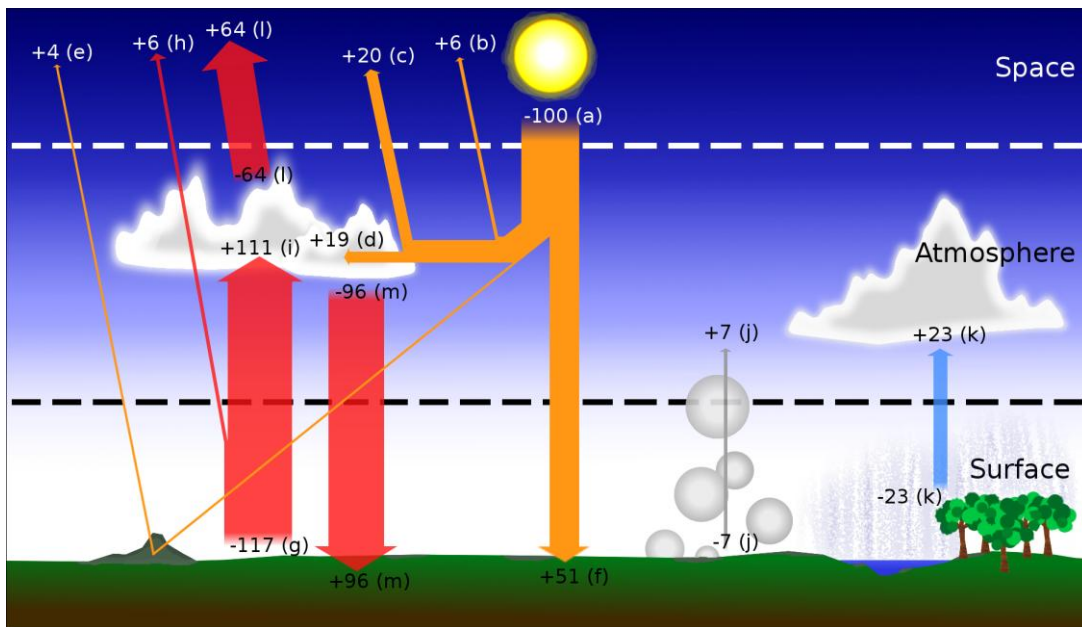


Figure 80. The annual energy balance of Earth's surface and atmosphere, showing equal input and output of energy in each zone. [101]. a) Incoming (short-wave) solar radiation at the top of Earth's atmosphere. b) Short-wave radiation scattered back into space by the atmosphere. c) Short-wave radiation reflected back into space by clouds. d) Short-wave radiation absorbed by clouds and atmosphere. e) Short-wave radiation reflected back into space by the surface. f) Short-wave radiation absorbed by the surface. g) Long-wave radiation emitted by the surface. h) Long-wave radiation emitted by the surface which passes through the atmosphere out into space. i) Long-wave radiation emitted by the surface and absorbed by the atmosphere. j) Conductive and convective heat transfer from the surface to the atmosphere. k) Latent heat transfer from the surface to the atmosphere by evapotranspiration and condensation of water. l) Long-wave radiation from the atmosphere emitted out into space. m) Long-wave radiation from the atmosphere emitted back to the surface.

From the definition, it is clear the relationship between the colour of different objects and its albedo and the consideration that the darker objects usually have a lower albedo than light coloured objects.

For this reason the simulations that have been conducted, consider three values of albedo in order to calculate the effects of reflection in different scenarios regarding the influence on the surfaces and air temperatures. Table 37 collected the different albedo's values [102].

Table 37. Albedo of surface examples [102].

Non-urban		Urban		
Surface	Albedo	Surface	Material	Albedo
Soils	0.05-0.40	Roads	Asphalt	0.05-0.2
Desert	0.20-0.45	Walls	Concrete	0.10-0.35
Grass	0.16-0.26		Brick	0.20-0.40
Agricultural crops & tundra	0.18-0.25	Roofs	Tar and gravel	0.08-0.18
Deciduous forest	0.15-0.20		Tile	0.10-0.35
Coniferous forest	0.05-0.15	Windows	Glass, zenith angle < 40°	0.08
Snow	0.40-0.95		Glass, zenith angle 40-80°	112.0°
Water, small zenith angle	0.03-0.10	Paints	Whitewash	0.50-0.90
Water, large zenith angle	0.10-0.27		Black	0.02-0.15
Mid-latitude cities in snow-free conditions	0.10-0.27	(mean:0.15)		

Therefore there are different values of albedo for substance and surfaces, but is also varies for the same surface during a day and year. In fact the albedo can double from early morning to midday and then decrease again toward the evening; this difference is caused by the changing angle of incoming solar radiation [103]. All the simulations have been carried out for the city of Milan – Italy (latitude 45.27° N, longitude 9.11° E).

Table 38. Results of daily solar position data on the 16<sup>th</sup> of June: the table summarizes the Azimuth, Zenith and Horizontal Shadow Angle (HAS) and Vertical Shadow Angle (VSA) for south orientation.

Local	Azimuth	Zenith	HSA	VSA
05:00	59.1°	2.9°	59.1°	5.6°
06:00	69.2°	12.4°	69.2°	31.7°
07:00	79.0°	22.5°	79.0°	65.3°
08:00	89.2°	32.9°	89.2°	88.7°
09:00	100.6°	43.4°	100.6°	101.0°
10:00	114.9°	53.4°	114.9°	107.4°
11:00	135.3°	62.1°	135.3°	110.6°
12:00	165.5°	67.4°	165.5°	112.0°
13:00	-158.7°	66.7°	-158.7°	111.8°
14:00	-130.6°	60.6°	-130.6°	110.2°
15:00	-111.8°	51.5°	-111.8°	106.4°
16:00	-98.2°	41.4°	-98.2°	99.2°
17:00	-87.1°	30.9°	-87.1°	85.2°
18:00	-77.1°	20.4°	-77.1°	59.1°
19:00	-67.3°	10.4°	-67.3°	25.5°
20:00	-57.1°	1.1°	-57.1°	2.1°

Simulations are conducted with clear-sky conditions on the day with the highest global incident solar radiation that carried out from the results of the dynamic simulation made using *Daysim* 3.1b and presented in the chapter 2. The sets of simulations have been organized in three different configurations following described:

Each clear-sky case consists of a 2-day simulation that begins with an observed sounding of atmospheric temperature, humidity, and wind speed representative of clear weather conditions for the season under consideration (summer, spring, winter). Clear skies and a clean atmosphere are assumed throughout the simulation, maximizing the impact of solar radiation on the surface layer climate. Simulations are conducted assuming no advective influences on the 1-D boundary layer to assess the maximum impacts of roof albedo change on the atmosphere. One additional simulation includes an estimate of cooling due to lake-breeze advection, given Chicago's proximity to Lake Michigan.

### **7.2.2. Urban climate**

The term urban climate refers to climatic conditions in an urban area that differ from neighbouring rural areas and are attributable to urban development. A microclimate is a local atmospheric zone where the climate differs from the surrounding area. The term may refer to small or large areas. There is no more important input to the success of an urban station than the appreciation of the concept of scale in Figure 82. According to [104], there are three scales of interest:

- Microscale  $10^{-2}$  to  $10^3$  m;
- Localscale  $10^2$  to  $5 \times 10^4$  m;
- Mesoscale  $10^4$  to  $2 \times 10^5$  m;

Urban areas result among the most altered environments on Earth. The humans uses determinant the finishing materials of the surfaces from the cities to suburbs, instead the humans concepts and needs such as construction cost, design and tradition, influence their geometry. Climatic variables among other temperature, wind patterns, precipitation, evapotranspiration and solar radiation are affected by the urban and humans changes. Probably the urban heat island effect (UHI) is the most known: it creates a high increment of air and surface temperatures in cities [102] which reach the temperature record be questioned in the global warming context [105]. The energy balance reported in the eq. 3 expresses the UHI effect as result of a combination of modifications. Firstly,  $Q^*$  is influenced in several ways; urban areas often are characterized by low average albedo and emissivity, the cloud cover altered the air pollution.

$$Q^* + Q_F = Q_H + Q_E + \Delta Q_S + \Delta Q_A \quad \text{eq. 3}$$

Where:

- $Q^*$  is radiation;
- $Q_F$  is anthropogenic heat release;
- $Q_H$  and  $Q_E$  are sensible and latent heat transfer;
- $\Delta Q_S$  is the change in stored energy, seen as changes in the temperature of the air and surfaces within the volume;
- $\Delta Q_A$  is the effect of advection, or horizontal winds, transferring e.g. latent heat in and out through the sides of volume [102].

As written above, the urban materials and surface geometry, affect the low albedo and emissivity, and the multiple reflections within spaces between buildings, defined as urban canyons, are important for the urban energy balance, as the contribution of forest canopies, trapping both incoming short-wave and outgoing long-wave radiation.

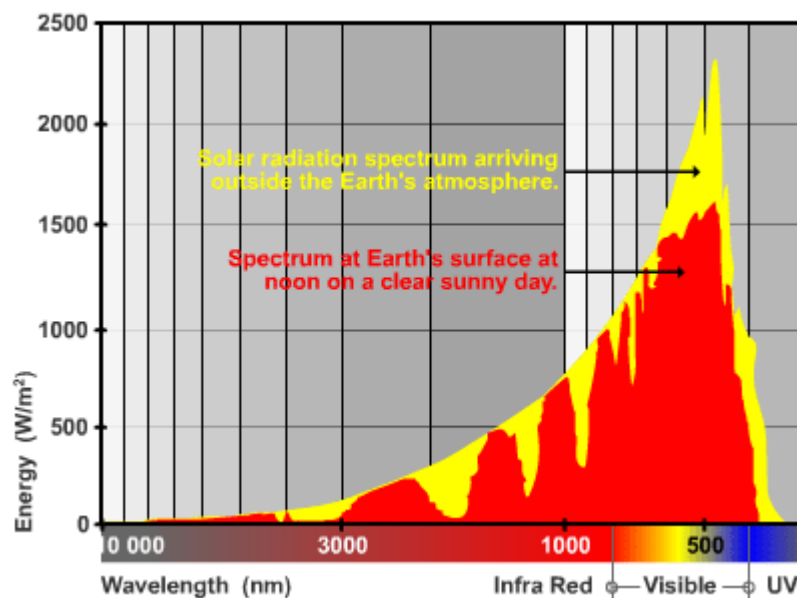


Figure 81. Spectral content of incident solar radiation.

Figure 81 clearly shows that the majority of solar radiation occurs in the short-wave visible and ultraviolet portions of the electromagnetic spectrum. There is some long-wave component of infrared, however large bands of this are absorbed by gasses and particles within the upper atmosphere

Unfortunately the urban effects, that determinate the global temperatures increment, are still not completely understood.

#### *Effects of urban climate*

The urban canopy generally increases surface roughness and exerts a frictional drag, reducing wind speeds [102]. The UHI create closed circulations, with surface winds converging toward the city centre where air rises and diverges, under weak synoptic (large-scale) wind conditions [106].

It has been analysed that the surface skin temperatures,  $T_{\text{skin}}$ , are on average 1-5 °C higher in urban areas than in adjacent crop-lands [107]. With MODIS version 4 (Moderate-Resolution Imaging Spectroradiometer) analyses [108] [109] has been defined, for the all cities, globally, the land cover data, the albedo and the UHI effect for different latitude. Other analysis presented in literature have been modeled the effect of urban areas on climate in Europe with a resulting average reduction in diurnal temperature range by  $1.26 \pm 0.71$  °C in summer and winter respectively [110], and the same analyses has been conducted in the continental U.S [111].

#### *Effects on albedo in urban areas*

The different values of albedo assigned for the same surface could give a variety of results in term of surface and air temperatures. Many studies report the values of albedo calculated in urban, suburban and rural areas [112]. From early results, have shown that the urban development consistently reduces the albedo and probably the representative average albedo, should become 0.14 and 0.15 for urban and suburban areas, respectively.

Nowadays in urban context the introduction of dark surfaces as impervious or solar system is more and more diffuse. The Table 37 shown that many construction materials have lower albedo than non-urban surfaces and it is confirmed in many studies of cities situated in rural or desert areas [108] [113]. In many other examples have been presented the large effects on urban temperatures in case studies where much percentage of roofs and asphalt paving has covered by dark materials [114] [115].

There are also some case studies where have been conducted simulations increasing the surface and surrounding albedo, shown that the high-albedo decrease the surface's temperature in summer as well as in winter, giving significant energy reduction [116].

Furthermore the albedo of surface materials changes with time: diurnal change due to solar angle, seasonal change due to e.g. shedding of leaves in deciduous forest canopies and considering on longer time scales, the variations of many materials as asphalt, that for example increase two or three times its albedo after years of use from an albedo equal to 0.05-0.10 for fresh asphalt to an albedo equal to 0.15-0.20 for worn asphalt.

Generally, the dark surfaces are used for covering a huge part of the urban surface and its low albedo reduces the total urban albedo.

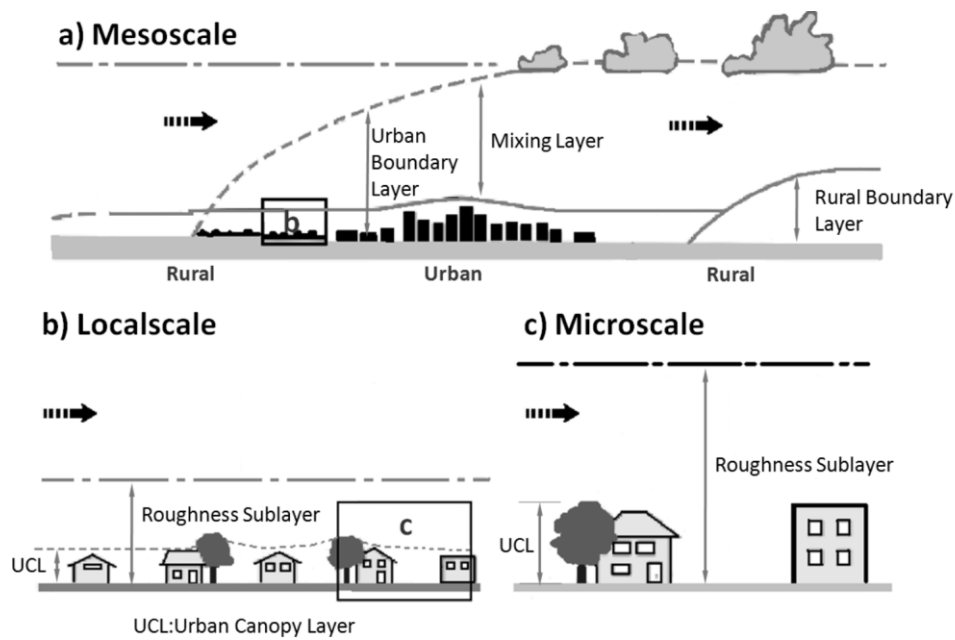


Figure 82. Schematics of Climatic Scales and Vertical Layers Found in Urban Areas [89]

Furthermore, the local microclimate and site factors will affect the actual environmental conditions of the building. The following site-related factors should be considered when making climate analysis:

- Topography – Elevation, slopes, hills and valleys, and ground surface conditions
- Vegetation – Height, mass, texture, and location
- Built forms – Nearby buildings and surface conditions

## 7.3. Theory and calculation

### 7.3.1. Description of the micro-climate tool ENVI-met

*ENVI-met* is a free microclimate modeling software and is an example of widely used urban climate simulation program. *ENVI-met* does not support data exchange format (.dxf) or shape files (.shp), and this makes data entry more difficult for the user. Building locations, plants, and surface types are among the items that require manual work with a digitized graphic background.

The 3D model *ENVI-met* is free software that is used to calculate all the meteorological factors as well as comfort quality within an urban area [92] [117]. A major advantage of using *ENVI-met* is that it is one of the first models to reproduce the major processes in the atmosphere - including air flow, turbulence, radiation fluxes, air temperature, and humidity - on a well-founded physical basis. *ENVI-met* simulates the microclimatic dynamics within a daily cycle in complex urban structures (i.e., buildings of various shapes and heights) as well as vegetation. Its high spatial and temporal resolution enables a fine understanding of the microclimate at street level.

This description of the tool is free and available on its website [118]. A micro-climatic *ENVI-met* was used to simulate the interaction surface-atmosphere in the urban environment. The model resolution is between 0.5 and 10m. This model was developed by [119] [120]. Through the thermal comfort index PMV (predicted mean vote) and MRT (mean radiant temperature) provided by the model, it revealed that the State Park displays PMV values close to comfortable compared to the other studied area.

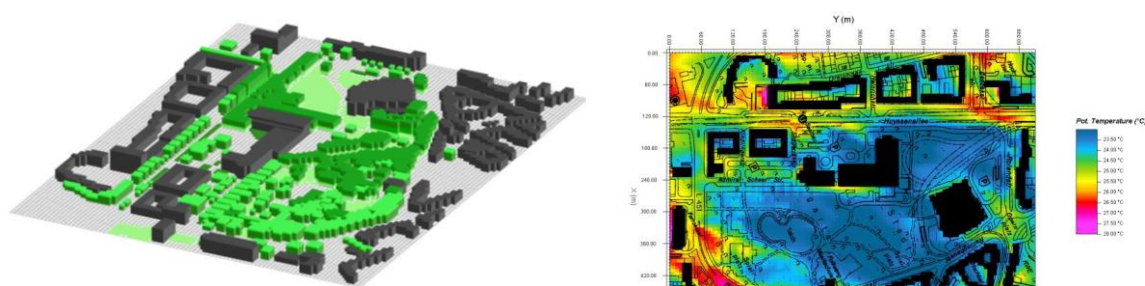


Figure 83. 3D View of an example urban area modeling in *ENVI-met* (on the left) and temperature distribution (on the right)

*ENVI-met* is a three-dimensional, non-hydrostatic numerical model that calculates exchange processes in, at, and between urban elements with a high spatial (0.5 to 10 meters) and temporal (10 seconds) resolution [120]. *ENVI-met* provides detailed climate information including speed, air temperature, and radiative fluxes for each point inside the model domain as shown in Figure 83. *ENVI-met* calculates dynamically over at least one diurnal cycle to simulate different surface heating and cooling processes and their effects on the microclimate. *ENVI-met* enables the user to simulate microclimates in urban structures through the solution of the physical basic equations for wind current, thermodynamics, and the

radiation balance of surfaces. *ENVI-met* has been developed by Dr Bruse and is freeware; its name derives from the term environmental meteorology. Typical areas of *ENVI-met* application are urban climatology, architecture, building design, and environmental planning. It is an innovative tool that offers great potential for urban planning.

The main aim of microclimate modeling is to make use of the new ability to observe and analyse consequences of different planning scenarios as well as study the impact of the probable increase or decrease of buildings or vegetation due to urban planning. This makes *ENVI-met* a powerful decision support system for urban master planning that takes into account contemporary demands of energy efficiency. Figure 84 presents the flow diagram of *ENVI-met*.

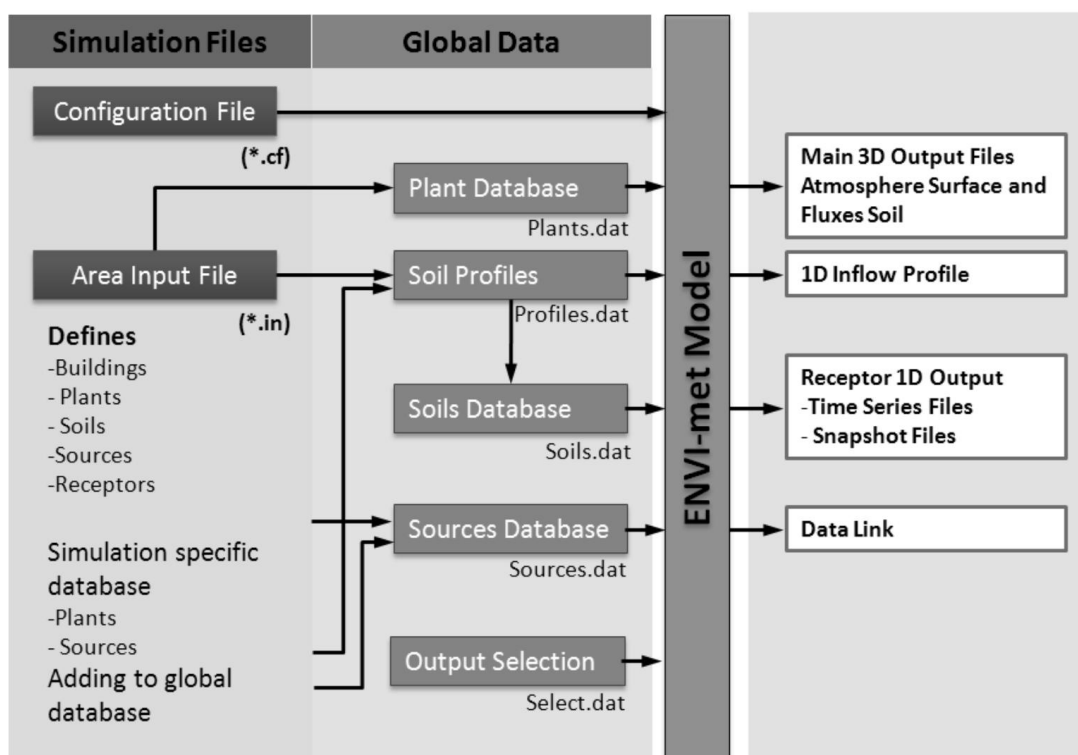


Figure 84. Flow diagram of *ENVI-met* micro-climate tool.

The microscale model *ENVI-met*, which is able to simulate the interactions between different urban surfaces, vegetation and the atmosphere. *ENVI-met* allows to analyse the effects of small scale changes in urban design (e.g. trees, backyard greening, new building constellations) on microclimate under different mesoscale condition [117].

The model is used to study the interactions between environment and the atmosphere in the CBD of Sydney, Australia. The Sydney CBD Area, including the harbor districts and the Botanical Gardens, build a system of very different urban elements forming the local climate by interacting in a complex way. Very tall buildings in the main CBD create a strong modification of the atmospheric boundary up to a height

of more than three hundred meters. This area of high roughness is surrounded by the Botanical Gardens with grass and occasional trees as well as by the Pacific Ocean. Both systems have a moderate daily surface temperature amplitude, high transpiration rate and reduced wind friction offering good ventilation properties.

*ENVI-met* is a Freeware program [A] based on different scientific research projects and is therefore under constant development. *ENVI-met* comes along with a number of additional software ranging from an editor up to graphical visualization tools for the model results. You can use it for any purpose you want, research or commercial without paying. All they ask for is to register to their e-mail list so that they can contact you if serious errors have been found or new versions are available. In addition, *ENVI-met* Professional edition comes along with a more sophisticated object model, more model sizes and advanced analysis tools.

Multiple-Processors Systems are not supported. The exact memory requirements depend on the number of grid points used. A rough overview of the memory requirements is:

- 100 x 100 x 30 Grids 128 Mbytes;
- 180 x 180 x 30 Grids 128 Mbytes;
- 250 x 250 x 30 Grids 1 GByte.

### **7.3.2. The physical model**

*ENVI-met* is a prognostic model based on the fundamental laws of fluid dynamics and thermodynamics.

The model includes the simulation of:

- Flow around and between buildings;
- Exchange processes of heat and vapour at the ground surface and at walls;
- Turbulence;
- Exchange at vegetation and vegetation parameters;
- Bioclimatology;
- Particle dispersion.

*ENVI-met* is a three-dimensional non-hydrostatic model for the simulation of surface-plant-air interactions not only for but especially inside urban environments. It is designed for microscale with a typical horizontal resolution from 0.5 to 10 m and a typical time frame of 24 to 48 hours with a time step of 10 sec at maximum. This resolution allows analysis of small-scale interactions between individual buildings, surfaces and plants.

The model calculation includes:

- Shortwave and longwave radiation fluxes with respect to shading, reflection and re-radiation from building systems and the vegetation;
- Transpiration, Evaporation and sensible heat flux from the vegetation into the air including full simulation of all plant physical parameters (e.g. photosynthesis rate);
- Surface and wall temperature for each grid point and wall;
- Water- and heat exchange inside the soil system;
- Calculation of biometeorological parameters like Mean Radiant Temperature or Fanger’s Predicted Mean Vote (PMV) - Value;
- Dispersion of inert gases and particles including sedimentation of particles at leaves and surfaces
- Buildings, vegetation, soils/ surfaces and pollutant sources can be placed inside the model area. Besides natural and artificial surfaces, the model is also able to handle water bodies.

Below are presented the basic equations and variables of the atmospheric model. Wind flow, temperature, humidity and turbulence are the main variables in the model [92].

### 7.3.3. The atmosphere

#### Wind Field: mean air flow.

The three-dimensional Navier-Stokes equations are used in the Boussinesq approximated non-hydrostatic form including sink terms for drag forces at vegetation elements. The pressure perturbation is removed from the equations and an auxiliary velocity field is computed. Mass conservation is satisfied by correcting the auxiliary field by an iterative solution of the Poisson-Equation and correction at the outflow boundaries. The flow is updated at given time intervals. *ENVI-met* also supports a real-time flow calculation which means that the flow field is treated as a normal prognostic variable and calculated each step. Due to the very small time steps needed here, this way of calculation needs very powerful computers.

The non-hydrostatic incompressible Navier-Stokes equations in the Boussinesq- approximated form (eq. 4, eq. 5, and eq. 6) and the continuity equation (eq. 7) presented below, give the basic concept to describe three-dimensional turbulent flow [92]:

$$\frac{\partial u}{\partial t} + u_i \frac{\partial u}{\partial x_i} = -\frac{\partial p'}{\partial x} + K_m \frac{\partial^2 u}{\partial x_i^2} + f v - v_g - S_u \quad \text{eq. 4}$$

$$\frac{\partial v}{\partial t} + u_i \frac{\partial v}{\partial x_i} = -\frac{\partial p'}{\partial y} + K_m \frac{\partial^2 v}{\partial x_i^2} + f u - u_g - S_v \quad \text{eq. 5}$$

$$\frac{\partial w}{\partial t} + u_i \frac{\partial w}{\partial x_i} = -\frac{\partial p'}{\partial z} + K_m \frac{\partial^2 w}{\partial x_i^2} + g \frac{\theta - \theta_{ref}}{\theta_{ref}} - S_w \quad \text{eq. 6}$$

$$\frac{\partial u}{\partial t} + \frac{\partial v}{\partial y} + \frac{\partial w}{\partial z} = 0 \quad \text{eq. 7}$$

Where:

- $f$  ( $=10^{-4} \text{ sec}^{-1}$ ) is the Coriolis parameter;
- $p$  is the local pressure perturbation;
- $\theta$  is the potential temperature at level  $z$ .

The reference temperature  $\theta_{\text{ref}}$  represents the larger scale meteorological conditions and is calculated as an average temperature over all grid cells of height  $z$ , excluding those occupied by buildings.

The air density  $\rho$  was removed from the original compressible Navier-Stokes equations using the *Boussinesq-Approximation*, which leads to one additional source term in the  $w$ -equation to include thermal forced vertical motion and one continuity (filter) equation (eq. 7) which has to be satisfied for each time step in order to keep the flow field mass conserving. (Note that all three-dimensional advection and diffusion terms are written in Einstein summation ( $u_i=u,v,w$ ;  $x_i=x,y,z$  for  $i=1,2,3$  to save place).

The local source/sink terms  $S_u$ ,  $S_v$  and  $S_w$  describe the loss of wind speed due to drag forces occurring at vegetation elements. This effect can be parameterized as [121] [122]:

$$S_{u_i} = -\frac{\partial p'}{\partial x_i} = +c_{d,f} \text{LAD}(z) \cdot W \cdot u_i \quad \text{eq. 8}$$

Where:

- $W=(u^2+v^2+w^2)^{0.5}$  is the mean wind speed at height  $z$ ,
- $\text{LAD}(z)$  is the leaf area density in [ $\text{m}^2\text{m}^{-3}$ ] of the plant in this height.

The mechanical drag coefficient at plant elements  $c_{d,f}$  is set to 0.2.

### Temperature and Humidity.

Advection and diffusion of temperature and humidity is calculated using the previous calculated wind field. The ground surface and vegetation is incorporated using a source/sink term in both equations, building walls are only acting as a source/sink for temperature.

The combined advection-diffusion equation with internal source/sinks reported below, give the distribution of the air temperature  $\theta$  and specific humidity  $q$ :

$$\frac{\partial \theta}{\partial t} + u_i \frac{\partial \theta}{\partial x_i} = -K_h \frac{\partial^2 \theta}{\partial x_i^2} + \frac{1}{c_p \rho} \frac{\partial R_{n,lw}}{\partial z} + Q_h \quad \text{eq. 9}$$

$$\frac{\partial q}{\partial t} + u_i \frac{\partial q}{\partial x_i} = K_q \frac{\partial^2 q}{\partial x_i^2} + Q_q \quad \text{eq.10}$$

Where:

- $Q_h$  and  $Q_q$  are used to link heat and vapour exchange at plants with the atmospheric model, similarly to the momentum equations, and their quantity is supplied by the vegetation model described in the specific section below;
- $\partial R_{n,lw} / \partial z$  represents the vertical divergence of longwave radiation taking into account the cooling and heating effects of radiative fluxes.

*Turbulence and Turbulent Kinetic Energy (TKE).*

The pressure of the air flow on the building walls or vegetation elements creates the turbulence effect. Under windy conditions, the magnitude of local turbulence production normally surpasses its dissipation: in this state the turbulent eddies are transported by the mean air flow. This leads to an increased turbulence away from the original source of disturbance, depending on the structure of the flow [92].

The turbulence is calculated using the E-epsilon 1.5 order closure ("E-epsilon" or "K-epsilon" model). Two prognostic equations for turbulent energy production (E) and its dissipation ( $\epsilon$ ) are used to simulate the distribution of turbulent energy. Exchange coefficients in the air are calculated using the Prandtl-Kolmogorov relation. For low wind situations, the 1st order mixing length model can be used instead of the E-epsilon model (which often fails in this situations).

$$\frac{\partial E}{\partial t} + u_i \frac{\partial E}{\partial x_i} = K_E \frac{\partial^2 E}{\partial x_i^2} + P_r - T_h + Q_E - \epsilon \quad \text{eq. 11}$$

$$\frac{\partial \epsilon}{\partial t} + u_i \frac{\partial \epsilon}{\partial x_i} = K_\epsilon \frac{\partial^2 \epsilon}{\partial x_i^2} + c_1 \frac{\epsilon}{E} T_h - c_2 \frac{\epsilon^2}{E} + Q_\epsilon \quad \text{eq. 12}$$

Where:

- $P_r$  and  $T_h$  describe the production and dissipation of turbulent energy due to wind shear and thermal stratification;
- $Q_e$  and  $Q_\epsilon$  are the local source terms for turbulence production and dissipation at vegetation.

The three-dimensional deformation tensor of the local wind field parameterizes the mechanical production  $P_r$ :

$$Pr = K_m \frac{\partial u_i}{\partial x_j} + \frac{\partial u_j}{\partial x_i} \frac{\partial u_i}{\partial x_j} \text{ with } i,j=1,2,3. \quad \text{eq. 13}$$

The Th buoyancy production is given by:

$$Th = \frac{g}{\theta_{ref}(z)} K_h \frac{\partial \theta}{\partial z} \quad \text{eq. 14}$$

The standard values  $c_1=1.44$ ,  $c_2=1.92$  and  $c_3=1.44$  to calibrate the  $\epsilon$ -equation have been provided by Launder and Spalding [123]. The application of the 1.5 order closure model to the atmospheric layer presents certain uncertainties. The different calibration values and the production of the turbulent energy could normally to be limited in the higher layers of the atmosphere, in base on the specific situation.

Two extra source terms are considered to the E- $\epsilon$  System to evaluate the additional turbulence created from vegetation and also the turbulence destruction due to the cascade from larger shear-induced eddies to smaller and waker eddies [121] [124]:

$$Q_E = c_{d,f} LAD z \cdot W^3 - 4c_{d,f} LAD z \cdot W \cdot E \quad \text{eq. 15}$$

$$Q_\epsilon = 1.5c_{d,f} LAD z \cdot W^3 - 6c_{d,f} LAD z \cdot W \cdot \epsilon \quad \text{eq. 16}$$

Where:

–  $W$  is the mean wind speed like in eq. 8.

The dissipation equation (eq. 16), that should be regulated by measured data if available [121], is provided from the Kolmogorov relation [123].

The calculation of the turbulent exchange coefficients from the E- $\epsilon$  field, are evaluated assuming local turbulence isotrophy with the follow relationships:

$$K_m = c_\mu \frac{E^2}{\epsilon}; K_H, K_q = 1.35 \cdot K_m; K_E = \frac{K_m}{\sigma_E}; K_\epsilon = \frac{K_m}{\sigma_\epsilon} \text{ with } c_\mu=0.09, \sigma_E=1 \text{ and } \sigma_\epsilon=1.3. \quad \text{eq. 17 a-d}$$

### 7.3.4. The soil system

In the urban environments is possible to consider a wide range of different soil and surface type and evaluate the effects of the natural soil and artificial materials. To evaluate these heterogenous scenarios, *ENVI-met* permits to assign individual soil properties such as thermodynamic and hydraulic conductivity or albedo, for each grid cell of the surface of the soil model.

*Temperature and Water flow inside the soil.*

The vertical distribution of temperature and water is calculated for natural soils as well as for artificial seal materials. For each vertical grid box a different soil material can be chosen in order to simulate different urban soils. The soil model is composed by 14 layers, from the surface and its lower boundary in 2 m depth: the vertical variation resolution is constituted by layer of 0.01 m close to the surface and 0.5 m in the deeper layers. The flow of water inside natural soils is calculated using the formulae from Clapp and Hornberger and is simulated in terms of heat and water transfer between the layers. The hydraulic equations include a sink term for water uptake by plant roots. The thermodynamic properties of the soil are estimated by means of the actual water content. The one dimensional prognostic equations, presented below, give the distribution of the heat  $T$  and soil volumetric moisture content  $\eta$ :

$$\frac{\partial T}{\partial t} = K_s \frac{\partial^2 T}{\partial z^2} \quad \text{eq. 18}$$

$$\frac{\partial \eta}{\partial t} = D_\eta \frac{\partial^2 \eta}{\partial z^2} + \frac{\partial K_\eta}{\partial z} - S_\eta z \quad \text{eq. 19}$$

Where:

- For natural soils, the thermal diffusivity  $K_s$ , is a function of the available soil moisture  $\eta$  [125];
- $\eta$  is a volumetric water content:  $\eta_s$  its saturation values,  $K_\eta$  the hydraulic conductivity,  $D_\eta$  the hydraulic diffusivity [126].

#### Water Bodies.

Water bodies are represented as a special type of soil. The calculated processes inside the water include the transmission and absorption of shortwave radiation inside the water. No second energy balance is used for the ground surface of the water pool, so that heating of shallow systems is lower than under real conditions where the main source of energy is the convection from the water ground surface rather than the absorption of radiation. In addition, no turbulent mixing is included in the model so that the use is restricted to still waters (e.g. lakes). The water parameterisation will be extended to turbulent mixing (oceans) later on. Special water usage (e.g. fountains) cannot be calculated with the model at the moment.

### **7.3.5. The vegetation**

*ENVI-met* assumed the vegetation as a one-dimensional column with height  $z_p$  and the amount and the distribution of leafs describe the profile of leaf area density (LAD). The soil uses the same concept: the root area density (RAD) profile extending from the surface down to the root depth  $-z_r$ , represents the distribution of roots. This universal conceptualisation is used for all type of trees, from small like grass to huge trees if  $z_p$  and  $-z_r$  are adjusted accordingly.

Foliage Temperature.

The average temperature of the leaves in one grid box is calculated by solving the energy balance of the leaf surface with respect to the actual meteorological and plant physiological conditions. Turbulent fluxes of heat and vapour are calculated from the given wind field and the geometry of the plant (see next section). The calculation of radiative fluxes includes the shading, absorption and shielding of radiation as well as the re-radiation from other plant layers.

Heat, Water and Vapor exchange with in-canopy air

The gas and heat exchange between the vegetation and the atmosphere is controlled by the local energy balance steering the leaf temperature and by the stomata conductance controlling the gas exchange (vapour and CO<sub>2</sub>). The actual stomata conductance of a plant is a complex function depending on external meteorological conditions (air temperature, available solar radiation PAR and many others) as well as on the plants physiological processes (Photosynthesis rate, CO<sub>2</sub> demand, CO<sub>2</sub> fixation). *ENVI-met* uses a sophisticated model to simulate the stomata behaviour of the vegetation.

In particular the interactions between the surrounding air and the plant leafs can be expressed in terms of sensible heat flux ( $J_{f,h}$ ), evaporation flux of liquid water on the leafs ( $J_{f,evap}$ ) and transpiration flux controlled by the leaf stomata ( $J_{f,trans}$ ):

$$J_{f,h} = 1.1r_a^{-1} T_f - T_a \quad \text{eq. 20}$$

$$J_{f,evap} = r_a^{-1} \Delta q \delta_c f_w + r_a^{-1} (1 - \delta_c) \Delta q \quad \text{eq. 21}$$

$$J_{f,trans} = \delta_c r_a + r_s \quad r_a + r_s \quad^{-1} (1 - f_w) \Delta q \quad \text{eq. 22}$$

Where:

- $T_a$  and  $q_a$  represent the temperature and specific humidity of the air around the leaf;
- $\Delta q$  is the leaf to air humidity deficit with  $\Delta q = q^*(T_f) - q_a$ ;
- $T_f$  is the foliage temperature;
- $q^*$  is the saturation value of  $q$  at the leaf surface.

The aerodynamic resistance  $r_a$  is a function of the leaf geometry and wind speed [127]:

$$r_a = A \frac{D}{\max(W, 0.05)} \quad \text{eq. 23}$$

Where:

- $W$  is the wind speed at the leaf surface;
- The parameter  $A$  is  $87 \text{ sec}^{0.5}\text{m}^{-1}$  for conifers and grass and  $200 \text{ sec}^{0.5}\text{m}^{-1}$  for deciduous trees;
- $D$  is the typical leaf diameter ranging from 0.02 m for conifers up to 0.5 or more for tropical plants [128].
- The max condition ensures that no invalid values appear in the case of very low winds;
- The factor  $\delta_c$  is set to 1 if evaporation and transpiration can occur ( $\Delta q \geq 0$ ), otherwise  $\delta_c$  is 0 and only condensation is possible.

Assuming that only wet parts of the vegetation can evaporate eq. 21 and, on the other side, only dry parts will transpire eq. 22, the fraction of wet leaves inside one grid box is needed. The wet fraction can be calculated as [129]:

$$f_W = \frac{W_{\text{dew}}}{W_{\text{dew,max}}}^{2/3} \quad \text{eq. 24}$$

Where:

- $W_{\text{dew}}$  is the actual amount of dew on the leave surfaces;
- $W_{\text{dew,max}}$  is the maximum possible value ( $0.2 \text{ kgm}^{-2}$ ).

#### Water interception and transport

Liquid water on the leaves influences highly the evaporation of the plant. The condensation of water on the leaves, the absorption of rain and the transport between different layers or the ground surface due to gravity is treated as an independent system inside the model.

### **7.3.6. Ground surface and building surface**

The ground surface's temperature,  $T_0$ , is calculated from the energy balance in equilibrium condition.

$$0 = R_{\text{sw,net}} + R_{\text{lw,net}} - c_p \rho J_h^0 - \rho L \cdot J_v^0 - G \quad \text{eq. 25}$$

Where:

- $R_{\text{sw,net}}$  and  $R_{\text{lw,net}}$  are the net radiative energy fluxes;
- $J_h$  and  $J_v$  are the turbulent fluxes of the heat and vapour;
- $G$  is the soil heat flux.

When are considered a building surfaces, as walls or roofs, the soil heat is substituted by the heat transmission through the wall or the roof ( $Q_w$ ).

### 7.3.7. Radiative fluxes

$R_{sw,net}$  and  $R_{lw,net}$  represent the net shortwave and longwave radiation adsorbed by the surface calculated with respect to the temperatures of surfaces and walls with the normal vector direct towards on the ground.

$$R_{sw,net} = R_{sw,dir} \cos \beta + R_{sw,dif} (1 - a_s) \quad \text{eq. 26}$$

Where:

- $R_{sw,dir}(z)$  is the direct shortwave radiation fluxes at any point, and it can be calculated as:

$$R_{sw,dir} = \sigma_{sw,dir} R_{sw,dir}^0 \quad \text{eq. 27}$$

$$R_{sw,dif} = \sigma_{sw,dif} R_{sw,dif}^0 + (1 - \sigma_{svf}(z)) R_{sw,dir}^0 \cdot a \quad \text{eq. 28}$$

Where  $R_{sw,dir}^0$  and  $R_{sw,dif}^0$  are the direct and diffuse shortwave radiative fluxes at the model top.

The reflection of shortwave radiation inside the environment that use the average wall albedo ( $a$ ) as reflectivity indicator is inserted as a last term in the diffuse component.

And the other terms presented in the eq. 26 are:

- $R_{sw,dif}(z)$  is the diffuse shortwave radiation fluxes at any point;
- $\beta$  is the angle of incidence of the incoming shortwave radiation to the surface exposition;
- $a_s$  is the surface albedo.

The influence of potential vegetation layers above the surface as well as the longwave fluxes from buildings and the reflection of radiation among buildings and surfaces, must to be considered for the longwave's calculation. The longwave balance is split into two contributes: a fraction that unshielded by buildings ( $R_{lw,net}^{us}$ ) and a fraction obstructed by buildings ( $R_{lw,net}^s$ ):

$$R_{lw,net} = \sigma_{svf} R_{lw,net}^{us} + (1 - \sigma_{svf}) R_{lw,net}^s \quad \text{eq. 29}$$

Where:

- $\sigma_{svf}$  represent the sky-view factor and it is used to weight the energy budget for the shielded and unshielded fraction according to the situation.

For the calculation of the radiative fluxes on building walls, the effect of vegetation is not considered due to the availability of only few information regarding the horizontal longwave fluxes from the vegetation layers. Instead for the vertical walls it is considered, that the unshielded fraction will receive 50% of the longwave radiation from the sky and other 50% from the ground. Considering the shielded fraction, 2/3 of the longwave radiation are supposed to come from the emission of other walls and remaining 1/3 of the radiation is assumed to be radiation from the ground reflected by the walls.

The radiative components on the roofs are the same as for the ground surface except that  $z \neq 0$  and that additional vegetation layers above the roof are not taken into account.

### 7.3.8. Turbulent fluxes of sensible heat and vapour

The heat  $J_h^0$  and vapour turbulent fluxes at the ground surface and at building walls and roofs are calculated as:

$$J_h^0 = -K_h^0 \frac{\partial T}{\partial z} \Big|_{z=0} = -K_h^0 \frac{T(k=1) - T_0}{0.5\Delta z(k=1)} \quad \text{eq. 30}$$

$$J_v^0 = -K_v^0 \frac{\partial q}{\partial z} \Big|_{z=0} = -K_v^0 \frac{q(k=1) - q_0}{0.5\Delta z(k=1)} \quad \text{eq. 31}$$

Where:

- $K=1$  indicates the first calculation layer above or adjacent to the surface and  $K_h^0$ ,  $K_v^0$  are the exchange coefficients for heat and vapour between the surface and the air, that are calculated with respect to the thermal stratification between the surface and the overlying air layer [130].
- The notation in eq. 30 and eq. 31 must to be arranged in base to the orientation of the wall.

### 7.3.9. Soil heat flux and heat flux through building walls

The soil heat flux is calculated from the surface temperature and the temperature of the first level of the soil model below the surface:

$$G = \lambda_s(k=-1) \frac{T_0 - T(k=-1)}{0.5\Delta z(k=-1)} \quad \text{eq. 32}$$

Where:

- $\lambda_s$  is the heat conductivity of the first soil layer which depends on the soil material and the water content;
- For buildings,  $G$  is replaced by  $Q_w$ :

$$Q_w = k(T_w - T_{a,i}) \quad \text{eq. 33}$$

Where:

- $K$  is the heat transmission coefficient of the wall material;
- $T_{a,i}$  is the air temperature inside the building.

This simple approach does not take into account the heat storage inside the wall material.

### 7.3.10. Numerical aspect: solution techniques

The numerical method used for solving on a staggered grid system, the differential equations in the model, is the finite difference method. The Alternating Directions Implicit (ADI) method in combination with an upstream advection scheme is used to de-couple the three dimensional advection-diffusion equations. Although implies a relatively high numerical diffusion, this scheme allows a quick and implicit solution of the equations and for this reason has been chosen in the *ENVI-met* model calculation.

A splitting method [131] is used for solving the Navier-Stokes equations. The following equation that represents the prognostic equations for a mass-conserving wind field  $u_i^{t+\Delta t}$ , are split into an auxiliary flow field ( $u^{aux}$ ) and a pressure field ( $p$ ):

$$\frac{\partial u_i^{t+\Delta t}}{\partial x} = \frac{\partial u_i^{aux}}{\partial t} + \frac{1}{\rho} \nabla p \quad \text{eq. 34}$$

The pressure variable is then removed from the prognostic equations (eq. 4, eq. 5 and eq. 6) leading to a set of three prognostic equations for an auxiliary flow field:

$$\frac{\partial u^{aux}}{\partial t} + u_i \frac{\partial u^{aux}}{\partial x_i} = K_m \frac{\partial^2 u^{aux}}{\partial x_i^2} + f v - v_g - S_u \quad \text{eq. 35}$$

$$\frac{\partial v^{aux}}{\partial t} + u_i \frac{\partial v^{aux}}{\partial x_i} = K_m \frac{\partial^2 v^{aux}}{\partial x_i^2} + f u - u_g - S_v \quad \text{eq. 36}$$

$$\frac{\partial w^{aux}}{\partial t} + u_i \frac{\partial w^{aux}}{\partial x_i} = K_m \frac{\partial^2 w^{aux}}{\partial x_i^2} + g \frac{\theta z}{\theta_{ref} z} - S_w \quad \text{eq. 37}$$

This flow field contains the correct vorticity, but is not mass conserving, which means that it does not fulfil the filter condition (eq. 7).

The matching pressure field can be obtained by solving the Poisson equation:

$$\nabla^2 p = \frac{\rho}{\Delta t} \nabla u_i^{\text{aux}} \quad \text{eq. 38}$$

with the iterative Simultaneous Over Relaxation (SOR) method. Finally, the mass-conserving flow field can be calculated correctly and approximately from

$$u_i^{t+\Delta t} = u_{\text{aux}}^i - \frac{\Delta t}{\rho} \frac{\partial p}{\partial x_i} \quad \text{eq. 39}$$

The all obstacles presented in the urban environment create the steep pressure gradients in microscale simulations and for this reason it is required a very small time steps to solve the set of wind field equations. Therefore, the wind in *ENVI-met* is updated after a small time step to consider the changes in turbulence and thermal stratification, and not as a “normal” prognostic variable, even if it should be technically possible, but the process would take too much time.

### 7.3.11. Computational domain and grid structure

The domain of the model is subdivided in finite volumes, for modeling the area of simulation and solving the balance equations. The resolution of the grid and the total size of the three dimensional model X,Y and Z, depends by the case study that it must be analysed. However, it could be possible to create a wide range of the grid. In the default grid the spacing  $\Delta x$ ,  $\Delta y$  and  $\Delta z$  is equidistant in each direction, except the lowest part of the grid, above of the ground, is divided into 5 sub-cells with size  $\Delta z_s = 0.2\Delta z$  to increase accuracy in calculating surface process. The boundary condition for each finite volume, are those calculated for the adjoining one. A big number of non-linear equations solving create long time of simulation and risks of divergence of the simulation parameters presented in the equations. Therefore the system has needed simplifications and boundary conditions for limiting the possibility of divergence, without lose important information or data accuracy. As every numerical model, especially 3D models such as *ENVI-met* are not working reliably at their model borders and at the grids very close to them, because in those points the equations can't be solved. The reason for these problems is resulting from the fact, that the model can't calculate real values for grid points along the borders (and especially not for grid points that are the border). As these points are missing at least one neighbour grid, only simple assumptions can be used here to obtain values that can be used in the model. This simple assumption can be that the values are constant at these grid points (so called closed boundary conditions or forced boundary conditions) or that values from inner grid points are copied to the grids on the border (open boundary conditions). A third method also offered in *ENVI-met* is to copy the values from the outflow boundary back to the inflow boundary (cyclic boundary conditions). Therefore, it is necessary to fix

hypotheses for solving the calculation and one of the three lateral boundary conditions that *ENVI-met* permits to choose:

- Open Boundary Conditions: the values of the next grid point close to the border are copied to the border for each time step;
- Forced (or closed) Boundary Condition: the values of the one dimensional model are copied to the border;
- Cyclic Boundary Condition: The values of the downstream model border are copied to the upstream model border.

The choice of boundary conditions is fundamental for the incidence of the borders on the calculated data inside the model area. For the same reason are introduced the “Nesting Grids”. Practically they are not necessary: if the simulation area is restricted to the main (core) area, it is possible to run the analysis without adding any grids as nesting area.

So the best you can do is to move these borders as far as possible away from your area of interest in the core area.

Moreover *ENVI-met* allows two different types for dividing the vertical grids: an n equidistant grid (A), where all grids, except the lowest five, have an identical vertical extension  $\Delta z$ , and a telescoping grid (B1,B2 and C) where the grid size expands with the height. The Figure 85 below shows the differences of the different types of vertical grid generation method.

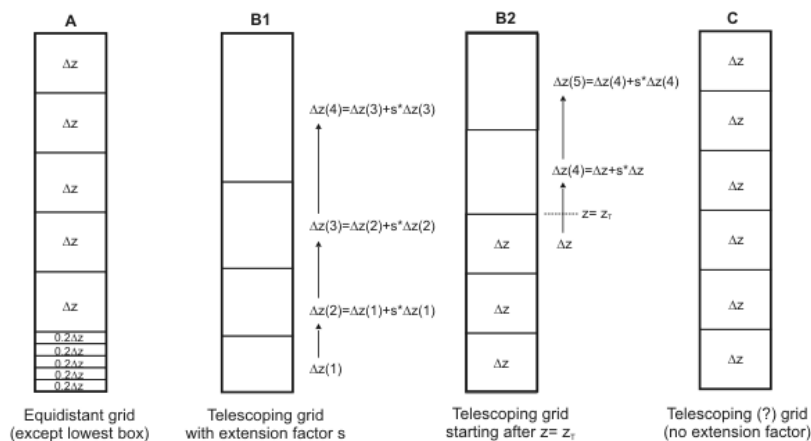


Figure 85. Different types of vertical grids in *ENVI-met*

The equidistant grid method (A), has just been presented above, has the same spacing over all vertical layers. Only the lowest box is split in 5 sub-boxes with  $\Delta z_s=0.2 \Delta z$ .

The telescoping grid allows covering much more height without running out of grid points. This grid should be used if the model domain has high objects (e.g. skyscrapers) that should be included, but the processes at the upper parts of the model are of less interest.

Although grid C was generated with the telescoping grid method, it is the least telescoping grid available. To generate a vertical grid without splitting the lowest box into 5 sub-boxes, use the telescoping grid method with an extension factor of  $s=0$ .

A one-dimensional model that extends up to 2500 m height has nested in itself the three dimensional model, and its values are used as reference values as well as inflow profiles and top boundary conditions for three-dimensional model [119].

### **7.3.12. Limits of the Tool**

The *ENVI-met* works with two physical systems (land surface and atmospheric) up to an altitude of 2500 m. The terrestrial surface is treated as a multilayered, where the vegetation and soil are treated separately. The model for the soil is composed of 14 layers, narrower near the surface and larger to a depth of 2.0 m. Due to the simplicity, only on the exchange of heat and moisture the equations of Fourier and Richards are used.

In the calculations of soil hydraulic parameters are used the classifications by Clapp and Hornberger (1978). Thermal conductivity and diffusivity are calculated using the formalism of Pielke (1984) and Tjernström (1989), respectively, in Bruse (2004). The turbulent fluxes at the soil (2004). The turbulent fluxes at the soil surface are determined by the theory of similarity of Monin/Obukhov, which takes into account the atmospheric stability.

Also the vegetation is treated as a system of multiple layers, with their own radioactive exchanges, energy balance and average temperatures. It is also important to mention that the first layer above the surface is divided into five sub-layers in order to best represent the radioactive exchange and turbulence near the surface. Because it is a model for urban areas, the radiation transfer in vegetation is very simple, several assumptions are made, for example, the diffuse radiation is not attenuated by the leaves.

The initial vertical distribution of leaves is described by the leaf density (LAD), given as medium values. The model does not consider a canopy and the vegetation takes as homogeneous, which means that only one type of vegetation can be considered vertical. In the horizontal direction can be used various kinds of vegetation.

The latent heat influx produced by the turbulence and the radiant energy available at each layer are calculated based on stomata and aerodynamic resistance, as well as temperature and humidity in the environment. In the leaves are considered only the exchange of heat and humidity, which means that the flow of CO<sub>2</sub> are not represented.

The CO<sub>2</sub> in the integration soil-atmosphere and soil-vegetation, is also neglected.

The atmospheric system is very complex compared to soil and vegetation, as it involves Reynolds and Navier-Stokes equations average. Three main variables are calculated with these equations: wind

speed, air temperature and humidity. The calculation of the turbulence is based on the E-e model (Launder, Spalding, 1974), which calculates the turbulent kinetic energy (E) and its dissipation rate (e). Note that all these equations are used for vegetation, using source/sink in the calculation of heat, moisture and momentum exchange. These “sources” take into account mainly the LAD and the gradient of the variables involved (wind speed, humidity and temperature). The initial conditions of the atmosphere and soil profiles consist of constant or linear dependent variable predicted and calculated in accordance with the work of Bruse and Fleer (1998) and Samaali (2002) [132].

### **7.3.13. Method of data extraction**

The *ENVI-met* software analyses tridimensional modelling of building’s volumes in order to study lots of parameters in which the temperature variation and the wind speed in a certain period of simulation.

The envelope’s model is discretized in a certain number of two-dimensional elements, each one characterized by one point of measure.

The program output is organized in seven folders, each one related to a specific simulation; each folder contains several files, that is possible to analyze separately. The program also permit to view the output files using two interfaces programs, Leonardo and Xtract, that allow to transfer the previous files into a graphical form.

From the singles folders we can obtain information, for example (folder ‘Atmosphere’), on wind velocity in every direction in addition to wind general velocity and resulting direction, relative and absolute humidity, air temperature, surfaces temperatures and others, even for the single model cell than for plane sections, using the reading interfaces. Furthermore is possible to have the data resulting from the analysis of a specific point of view, identified by an element called ‘receptor’, located in a chosen point of the model. The receptor gives back the data of all the volumes’ column that is located on the receptor, in addition to the data of the portion of the soil under this particular point of view. In this folder (‘Receptor’) we can also find the information on the radiant energetic fluxes related to the soil surface identified by the receptor. These files are very useful, because they permit to have instant information on a single point and on all its height. Nevertheless one big limit is given from the impossibility to locate the sensor on a building or on a vertical surface. In order to have the roof or the walls temperatures, in fact, we have to use vertical or horizontal sections of the three-dimensional output files. Unfortunately, sometimes these sections cannot be easy to do, depending on eventually different heights of the buildings.

Using the interface lecture programs, whatever, is possible to have a clearer idea of the analysis result, even if this kind of output is qualitative and not numerical as accurate as the data files.

#### **7.3.14. Leonardo**

Leonardo is software that provides a graphical representation of the data contained in output File "three-dimensional", that are those files that can not be read except through these interfaces provided by the software itself. Importing one of these files in Leonardo interface, you can view the list of output parameters present in it

and select the most appropriate method of representation for each. Leonardo allows display data through four main graphical methods: data, vectors, isoline, special. They represent layers in the drawing and can be viewed individually or simultaneously depending on the type of representation that is desired, or is possible to perform operations between them.

The layer 'Data' displays data in a chromatic scale, flanked by legend to the map. It is useful, for example, for the representation of the temperature gradient.

The layer "Vector" displays the data by the arrows (vectors) and directed with form proportional to the value. It is a good way of representing the flow air and wind since the arrows are able to express the direction and also the points at which speed becomes greater.

The layer "Special" lets you view the data with a single value or meaning. It is used primarily for the display of buildings and vegetation within the graphical representation of the other parameters.

The layer "Isoline" allows you to display very effective parameters such as the view factor of the sky, temperatures, radiant fluxes incident, factors related to air turbulence and wind speed. Alongside the curves is indicated the parameter value that it represents.

The representation of data through the interface Leonardo is very useful to get an idea immediate and clear data, to identify the incidence of some factors on the model and for understand the variations that some parameters have in time or in space. It is useful primarily to identify also the critical zones of the model depending on the type of analysis that you want to make. The representation, however, is purely graphical and qualitative. The legend, although it may help to make the data readable, allows only a qualitative analysis. By Leonardo in fact you do not get the actual values of the parameters represented and cannot make more detailed numerical analysis on the data contained in three-dimensional and two-dimensional files (folders Atmosphere and Surface). To this is present another interface for reading the output: Xtract.

#### **7.3.15. Xtract**

Xtract is useful to extract, from the two-dimensional and three-dimensional files output from the simulation, some readable text files to extract the output data. The interface is extremely intuitive: chosen

the output file to be analyzed, it is imported into the software; then, using coordinates, selecting the section plane you can make the "cut". You can also obtain an additional file containing the data that you want in a readable format and you can be imported it into other programs for data analysis. However easy, a section made in this way presents some limits. Firstly, the section of data is performed only on a "DataField". It was therefore forced to choose only one parameter among all the output that the program offers. In addition, the "cut" is carried out on a file, later the data will be related only to that moment of the day. For this reason, in order to perform a numerical analysis, such as that of daily variation of a parameter (which, as we have seen, it is not possible to perform with Leonardo), it is necessary to extract several files and then import them all together in a spreadsheet

calculation or in another system of numerical analysis. In addition, the extrapolated values from the section are

related to the whole model and it is not possible to distinguish the areas of interest if not manually using a spreadsheet.

### **7.3.16. Type of analysis and aim**

This part of the research is related the evaluation of microclimate of the district and the relationship from the atmosphere components and the surrounding. The phenomenon of "the urban heat island" is the most influent and evident effect that happens at the urban scale. However in this section of the study, it wants to investigate which are the consequences that the urban planning and the surrounding morphology and components in terms of soil materials, finishing materials of the building, presence of vegetation and water, as lake, sea, river etc. contribute to affect the microclimate comfort at the building scale and pedestrian level. In particular it will be analysed the wall temperatures in order to estimate which is the best urban planning scenario that minimizes the operative temperature on the facades if it wants to install the solar systems as photovoltaic panels or solar thermal collectors and finally have a qualitative analysis regarding the air temperature and the wind speed at the ground level to minimize the thermal stress and guarantee a certain thermal comfort to the pedestrians. It is obvious that these aspects deserve to have a deeply discussion for having an entire resolution of scientific treatment, but the main goal of this part of the research it gives a consciousness knowledge about the different aspects that it needs to consider for a sustainable urban planning for engineering, architects and urban planners.

Therefore, it has been decided to use the software *ENVI-met*, deeply described above, to simulate the effects of different urban design scenarios on air and surface temperatures, as well as on outdoor thermal comfort. The latter is expresses as the physiologically equivalent temperature (PET), an index based on air and radiant temperatures as well as wind and humidity. The selection of software *ENVI-met* as the numerical model to analyse the effect of mitigation of atmosphere has been done from vary widely urban

microclimate models, based on their physical basis and spatial/temporal resolution. The literature provides a detailed critique of the most popular models for the microscale analysis with fine temporal resolutions [133]. They inferred that *ENVI-met* [92] is the most suitable model for analysing the thermal comfort regime within the street canyon at fine resolutions (down to  $0.5 \times 0.5$  m). It is a three dimensional non-hydrostatic model for the simulation of surface-plant-air interactions, especially within the urban canopy layer. It is designed for micro-scale with a typical horizontal resolution from 0.5 to 10 m, and a typical time frame of 24 - 48 h with a time step of 10 s at maximum. This resolution allows the investigation of small-scale interactions between individual buildings, surfaces and plants [119]. It has been chosen, therefore, selected *ENVI-met*.

Input data required to initiate *ENVI-met* simulations are:

- Wind speed and direction at 10 m above ground level;
- Roughness length ( $Z_0$ );
- Initial temperature of atmosphere;
- Initial temperature and humidity of the soil;
- Specific humidity at 2500 m;
- Relative humidity at 2 m.

The model calculation includes:

- Short-wave and long-wave radiation fluxes with respect to shading, reflection and re-radiation from building systems and the vegetation;
- Transpiration, evaporation and sensible heat flux from the vegetation into the air, including full simulation of all plant physical parameters (e.g. photosynthesis rate);
- Ground surface and wall temperature for each grid point and wall;
- Water- and heat-exchange within the soil system;
- Calculation of bio-meteorological parameters such as, MRT and PMV [134].

A major shortcoming with *ENVI-met* is that buildings, which are modeled as blocks where width and length are multiples of grid cells, have no thermal mass.

Moreover, all buildings have constant indoor temperature and albedo. The thermal transmittance, or U-value, for walls and roofs are the same for all buildings (U-value is defined as the heat flow per unit area under steady conditions from warm to cold side of a building element, per unit temperature difference).

*Assumptions for vegetation and climatic input*

Starting from the observation that the climatic conditions of a locally have a consequences on the behaviour of its inhabitants. The use of asphalt as finishing material of soil, creates an absence of evaporative cooling and causes consequently the increment of temperature on the ground level and of the air temperature. This phenomenon induces high radiative exchanges wavelength greater than in the case of a surface plant. Asphalt and similar concrete and granite materials are inert coatings which accumulate heat during the day and return during the night. Furthermore these materials are usually dark surface and therefore with low albedo value, that contribute to increase the heat accumulation and the consequently surface temperature. The vegetation, with trees and green areas, participates to balance the outside temperature: plants absorb water through their roots and reject it by the leaf canopy, the presence of green roof acts to cool air thank to the effect of evaporation and evapotranspiration. Furthermore by providing a cooler surface at roof level the green roof reduces the need for air conditioning during periods of higher than normal temperatures and this means a reduction of energy demand of the building. The Combined effect is to reduce the UHI.

*Objectives*

The main aim of this part of research, as written above, concerns the evaluation of surface temperatures in order to calculate:

- How is the operative temperature which the solar systems work in different scenarios that have been analysed;
- How the vegetation effect can reduce the surface temperatures improving the solar systems efficiency.

Other evaluations regarding air temperature and wind speed, which are most important for urban planning strategies, are treated marginally for giving a new design approach for urban planner and architects. The microclimate tools *ENVI-met*, used for these analyses, as described before, gives output data for calculating many aspects that influence the atmosphere at microclimatic scale. However the qualitative analyses regarding other objectives are:

- Evaluation of the air temperatures at the ground level in order to estimate the vegetation effect reducing the thermal stress for inhabitants and pedestrians;
- Evaluation of the wind speed on the façades;
- Evaluation of the wind speed at the ground level

Furthermore other mitigation options for reducing the air and facades temperature are possible and some of them have been tested in this parametric analysis for studying:

- The influence of albedo wall values in term of increment of surface and air temperatures;

- The influence of green roof for reducing the roof's temperature and energy consumption and consequently the energy demand.

### **7.3.17. Methodology**

As said above, the impact of vegetation in urban area, can be quantified at different level. Certainly, the presence of the vegetation influences the microclimate of urban area in terms of quantity of transmitted radiation, temperature of the air and plant leaves, humidity of the air and wind speed.

Two sets of simulations have been conducted: the first one on a simple district, SQ\_25\_NS, previously analysed for the solar radiation analysis and the second one on a real case study of the city of Milan presented in the last section of this dissertation.

Among other simple models analysed, has been chosen the SQ\_25\_NS because is resulted the most irradiative model related the amount of solar radiation on the south façade. All scenarios analysed are compared with the isolated building case study. The main aim of this parametric analysis is to estimate the influence that different soils, wall albedo and vegetation can have on the surface wall temperatures, therefore mitigating the urban heat island effect especially in the city centres, where the temperatures are higher than the surrounding countryside. The all aspects written above affect the microclimate of the existing open space as well as the energy use of the existing buildings for heating, sooling and lighting, through shading, evapotranspiration, etc. In particular the vegetation mitigates the heat island effect not by cooling the air, but by warming the air less [135].

The influence of high buildings in the local climatic environment is analysed from the thermal comfort index and the wind flow.

Table 39 reported below summarized the most important setting parameters of the *ENVI-met* model.

All the simulations have been carried out for the city of Milan –Italy (latitude 45.27° N, longitude 9.11° E). The parametric study on a simple model have been conducted for studying the effects that different strategies adopted, create on the building's surface temperatures trend, air temperature and wind speed at the ground level. Below are presented the all scenarios analysed with respectively description of soil, vegetation, wall and roof albedo and roof finishing material.

The simple chosen for the microclimate parametric study is the district with the most radiative building that carried out from the solar radiation parametric study on a geometric district described in the chapter 4.

Table 39. Input data for the *ENVI-met* simulations.

<b>Main data</b>	
Date of start of simulation	16 <sup>th</sup> June
Time of start of simulation	24:00
Wind speed at 10 m height (m/s)	2.5
Wind direction	West/South-west
Roughness length	0.4 (simple district model) 0.8 (case study)
Initial air temperature (°C)	20
Specific humidity at 2500 m (g/kg)	7
Relative humidity at 2 m height (%)	50
<b>Position</b>	
Longitude (°)	9.11
Latitude (°)	45.29
Time zone	15.0
<b>Soil data</b>	
Initial temperature in layer 0–0.2 m (°C)	18
Initial temperature in layer 0.2–0.5 m (°C)	18
Initial temperature in layer >0.5 m (°C)	18
Relative Humidity Upper Layer (0-20 cm)	50
Relative Humidity Middle Layer (20-50 cm)	60
Relative Humidity Deep Layer (below 50 cm)	60

The simulation time is about 24 hours: it starts on the 16<sup>th</sup> of June from the 6:00 a.m. and finishes on the 17<sup>th</sup> of June at 6:00 a.m. with time step of 2 second. It means that the wind turbulence is calculated every to second. The simulation has been done during this day because from the annual daily solar radiation data carried out from the previous solar radiation simulation run with *Daysim* 3.1 b, the highest value of solar radiation on the most irradiative façade (South façade) is resulted on the 16<sup>th</sup> of June. During this day has been chosen the hour after the hours have the highest solar radiation values, given that *ENVI-met* considers the heat stored during the hours. This is one of the most important settings of the tool before run the simulation. Before starting the set of simulations have been done the previous simulations to set up the configuration file in order to know if was possible to limit the time simulation, but the results and the support of literature have confirmed that a limited time simulation gives incorrect data output. Every example in literature underlines that the minimum time simulation that is possible to set is 24 hours: therefore has been decided to set this value. The time of entire simulation it depends by the complexity and the dimensions of the three-dimensional grid of the model analysed: in this case the simulation on a simple district has taken 12 hours (grid dimension: x-grids 60, y-grids 60, z-grids 30. Size of grid cell:  $\Delta x$  equal to 1m,  $\Delta y$  equal to 1m and  $\Delta z$  equal to 3m), while the simulation conducted on entire district of the case study of Milan, are gone on for 48 hours each (grid dimension: x-grids 125, y-

grids 125, z-grids 30. Size of grid cell:  $\Delta x$  equal to 2m,  $\Delta y$  equal to 2m and  $\Delta z$  equal to 3m). The grid dimensions and the morphology of the district analysing, vary the time of simulation considerably. However it also depends from the kind of analysis that it wants to conduct and which data that it would extract. For example for this study was necessary having the thickest grid in order to extract as much as possible data of temperature on the wall surfaces, compatibility with the limits of model settings. Nevertheless it can be possible to set a bigger size of grid cell in order to reduce the time simulations and consequently the accuracy of the analysis in term of quantities of data. Moreover when the simulation area is very big is almost obliged to increase the size of grid cell if it wants to analyse the entire area.

Related to the U values of the different parts of the building envelope have been used the standard values regulated by local law [136].

In the creation of model domain have been set the dimensions of the grid, and other parameters as boundary conditions, nesting grids and soil profil, grid size, vertical grid method and geographic properties. The “open boundary conditions” have been set for all simulations. Three nesting grids have been set: they add about 45m from the borders of the model in all directions. This means that the total area dimensions are 150 mx150m (22500m<sup>2</sup>) for the simple models and 205 mx205m (42025m<sup>2</sup>) for the case study of the city of Milan. Regarding the vertical grid generation has been chosen the equidistant method for maintaining a regular grid to extract the wall temperatures values always at same interval from one to the next. It could be possible to set the telescoping vertical grid without extending, but it has been chosen the equidistant way because permits to subdivide the lowest box in 5 sub-boxes with  $\Delta z_s = 0.2 \Delta z$  and it could be result important for analysing the data differences of air and wall temperatures or wind speed especially at the ground level, where the eventual difference could be relevant in term of thermal comfort.

### **7.3.18. Parametric microclimate analysis on simple models**

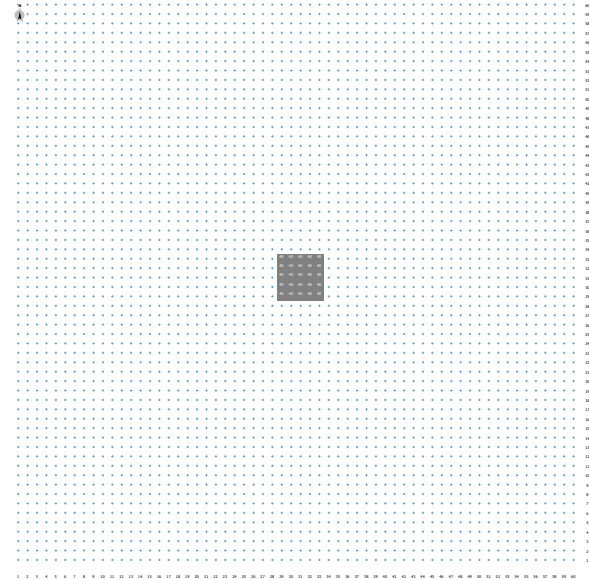
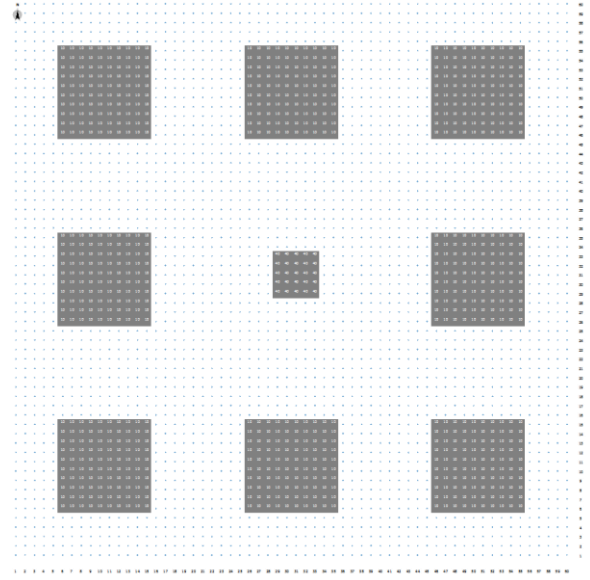
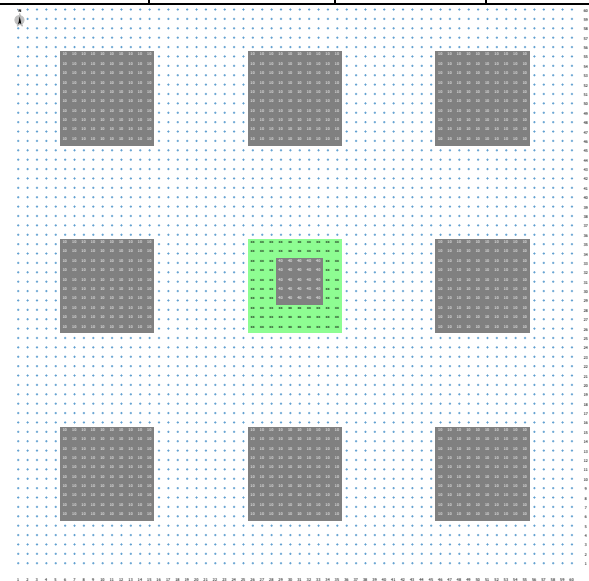
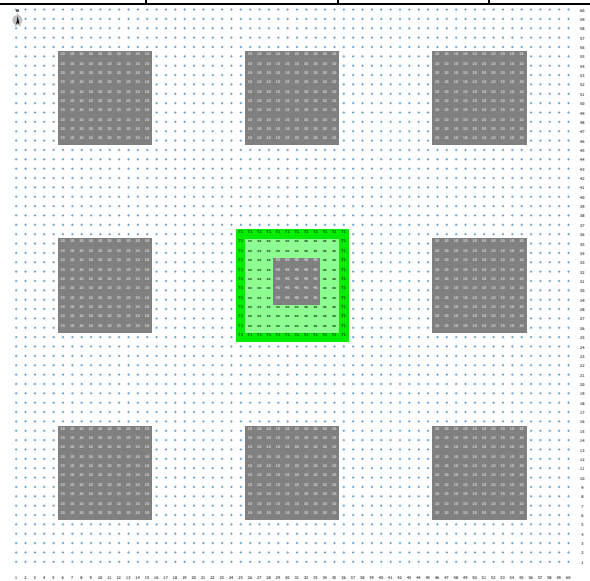
The first set of simulations has been done on simple models in order to study the different effects on wall temperatures and qualitative analysis of air temperature and wind speed.

The district analysed is composed by nine buildings which have 1000m<sup>3</sup> of volume each: eight buildings have 100m<sup>2</sup> of foot print (10 m x 10m) and 10 m of height, the central building, which the south façade is object of this analysis since it resulted the most irradiative façade, is characterized by a 25 m<sup>2</sup> of foot print (5 m x 5 m) and 40 m of height. Therefore the width of the street between buildings varying from 10 m to 12.5 m, the height to width ratio for the street canyon is 1.0.

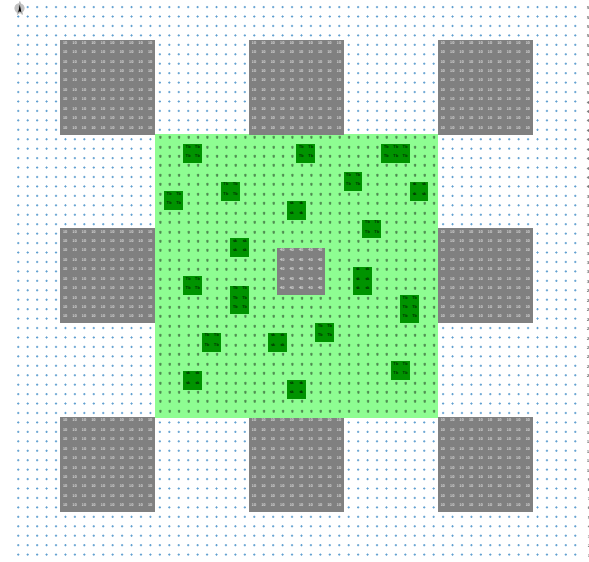
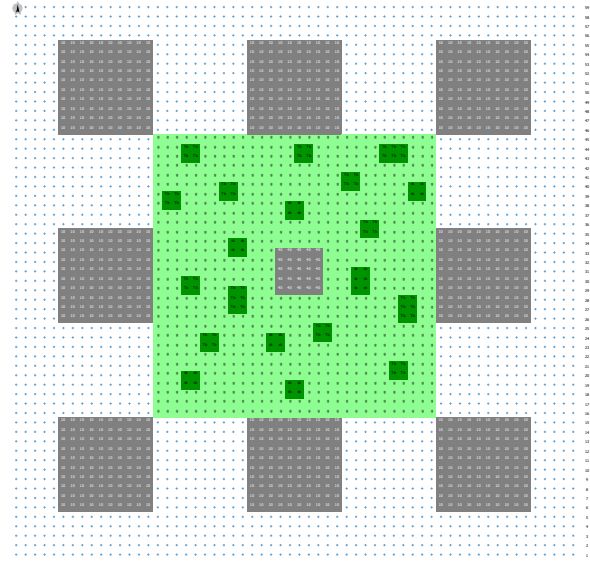
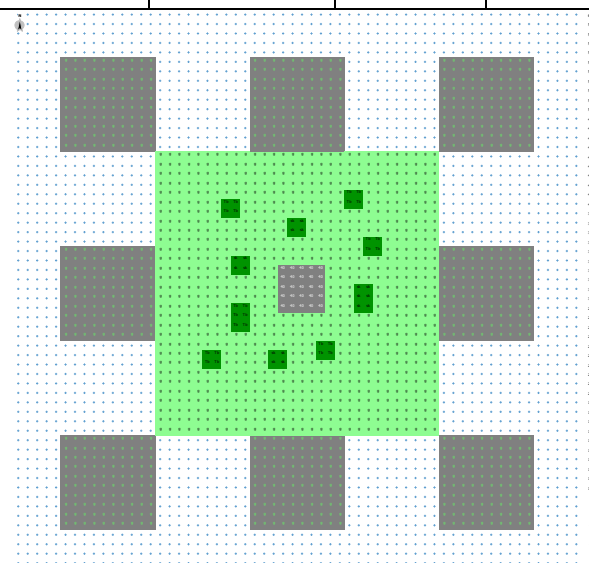
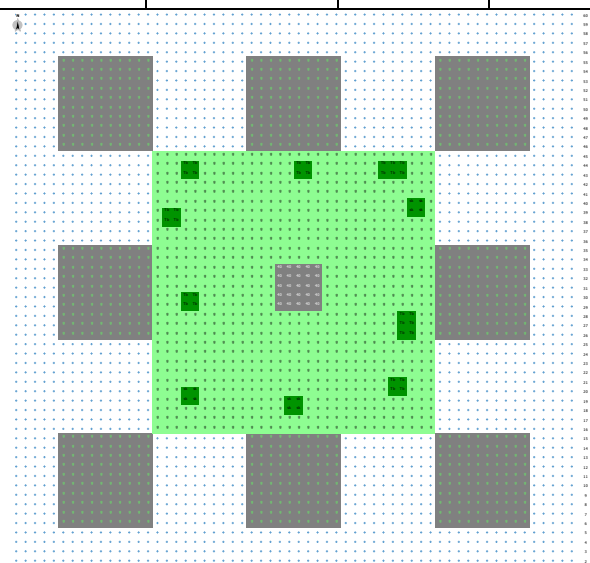
Different analysis have been done on the same district varying the soil, setting asphalt and/or loamy, the wall albedo, sitting three values (0.2, 0.5, 0.8), the roof's finishing material, setting gravel or green and vegetation's configuration and species.

The first three simulations have been conducted on isolated building varying the value of wall albedo in order to analyse how the different colour of material can influence the temperature on the façades, without the benefit given from the vegetation or any other process element.

The basic morphology of the parametric studies on analysed district is presented in the tables of the following pages on the top view. All figures have been extracted from the area editor of *ENVI-met*: buildings are coloured in grey, the grass is in pale green, the trees in shade of green (light green for trees of 10 m, dark green for trees of 15 m and 20 m).

Scenarios: 1 – I (wall albedo 0.2); 2 – I (wall albedo 0.5); 3 – I (wall albedo 0.8)				Scenarios: 1 – A (wall albedo 0.2); 2 – A (wall albedo 0.5); 3 – A (wall albedo 0.8), 4 – A (wall albedo 0.2 - green roof)			
Soil	Vegetation	Albedo	Roofs	Soil	Vegetation	Albedo	Roofs
Asphalt	Ground: -	Wall: various	Gravel	Asphalt	Ground: -	Wall: various	Gravel
	Trees: -	Roof: 0.3			Green		
							
Scenarios: 1 –G (gravel roof); 2 – G (green roof)				Scenario 3 - G			
Soil	Vegetation	Albedo	Roofs	Soil	Vegetation	Albedo	Roofs
Asphalt	Ground: grass	Wall: 0.2	Gravel	Asphalt	Ground: grass	Wall: 0.2	Gravel
	Trees: -	Roof: 0.3	Green	Loamy	Trees: 10m very dense crown	Roof: 0.3	
							

Scenario 4 –G				Scenario 5 - G			
Soil	Vegetation	Albedo	Roofs	Soil	Vegetation	Albedo	Roofs
Asphalt	Ground: grass	Wall: 0.2	Gravel	Asphalt	Ground: grass	Wall: 0.2	Gravel
Loamy	Trees: 15m very dense crown	Roof: 0.3		Loamy	Trees: 20m very dense crown	Roof: 0.3	
Scenarios:1 – P (gravel roof); 2 – P (green roof)				Scenarios: 3 – P (gravel roof) ; 4 – P (green roof)			
Soil	Vegetation	Albedo	Roofs	Soil	Vegetation	Albedo	Roofs
Asphalt	Ground: grass	Wall: 0.2	Green	Asphalt	Ground: grass	Wall: 0.2	Gravel
Loamy	Trees:	Roof: 0.3		Loamy	Trees: 10m very dense crown	Roof: 0.3	

Scenario 5 – P (Gravel roof) – Scenario 6 – P (Green roof)				Scenario 7 – P (Gravel roof) – Scenario 8 – P (Green roof)			
Soil	Vegetation	Albedo	Roofs	Soil	Vegetation	Albedo	Roofs
Asphalt	Ground: grass	Wall: 0.2	Gravel	Asphalt	Ground: grass	Wall: 0.2	Gravel
Loamy	Trees: 15m very dense crown	Roof: 0.3	Green	Loamy	Trees: 20m very dense crown	Roof: 0.3	Green
							
Scenario 9 – P				Scenario 10 - P			
Soil	Vegetation	Albedo	Roofs	Soil	Vegetation	Albedo	Roofs
Asphalt	Ground: grass	Wall: 0.2	Green	Asphalt	Ground: grass	Wall: 0.2	Green
Loamy	Trees: 15m very dense crown	Roof: 0.3		Loamy	Trees: mix very dense crown	Roof: 0.3	
							

Scenario 11 – P				Scenario 12 - P			
Soil	Vegetation	Albedo	Roofs	Soil	Vegetation	Albedo	Roofs
Asphalt	Ground: grass	Wall: 0.2	Green	Asphalt	Ground: grass	Wall: 0.2	Green
Loamy	Trees: mix very dense crown	Roof: 0.3		Loamy	Trees: -	Roof: 0.3	

In order to analyse the different possible effect of vegetation and wind in reducing air temperatures in the urban context, the following assumptions have been made:

- The park has been inserted in three different sizes: the first, sizes 10x10m, has been limited at the site construction of a central building (from 1-G to 5-G), the second, sizes 30x30m, limited until the sides of the other buildings constituted the entire district analysed (from 1-P to 11-P), the latter, sizes 50x50m, covers the entire soil of the district covered by grass (12-P);
- The scenarios with green roofs have been considered in different configurations of the park as well as for the scenarios with asphalt assigned for the soil (from 1-A to 3-A, and from 1-G to 4-G);
- Different sizes (10m, 15m and 20m of height with very dense crown) and configurations (dispersedly or orderly) of threes inserted in the model have been chosen in order to calculate their respectively effects;
- The wind speed, at the limit of boundary layer, at a height of 10 m, is 2.5 m/s, resulting to near calm condition near the ground, and direction from west/south-west. The wind data has been collected from a statistic weather data climate of meteorological station of Milan-Linate airport [137].
- The air is introduced in the model at the temperature of 20°C.

The presence of the park close to the city or in a city has a high benefit effect to mitigate the urban heat island and surface temperatures. Some literature results indicate that the cooling effects of a park's presence are influent not only at the green areas but also at the surrounding built environments [138]. Furthermore the choice of species is very important because their shade depends on their density and crown shape. The foliage of a tree can filter from 60% to 90% of solar radiation as well as the crouching vegetation can reduce the solar radiation reflected by the ground.

### **7.3.19. Case study of the city of Milan: current scenario**

The analysis of the case study of the city of Milan is started from its current situation. The entire district has been modelled in *ENVI-met* from plan reconstruction elaborated by Autodesk Autocad 2011 starting from google earth image: in fact it is possible to load the bitmap as background behind the editor area. Digitizing a bitmap on the screen is a very helpful feature to construct an area based on a map in the editor: it is important to import a bitmap with exact size or in scale of the district it would be simulated and set the grid area conveniently, because *ENVI-met* will adjust the map to the area of your selected model and does not care what the bitmap actually shows. The top view of the district is presented below:



Figure 86. Top view of the district analysed: picture extract from Google Earth.

The bitmap, elaborated by Autodesk Autocad 2011, simplified the district drawing and has been very useful for modeling it in *ENVI-met* editor area.

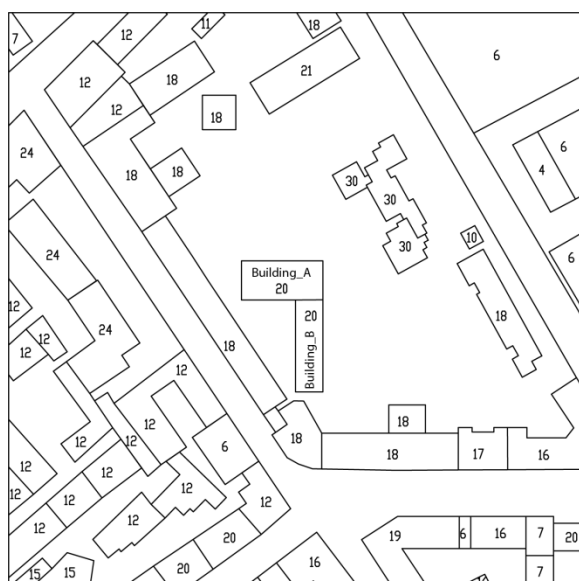


Figure 87. Bitmap of the district used from modeling it in *ENVI-met* editor area. The numbers represent the height of the buildings

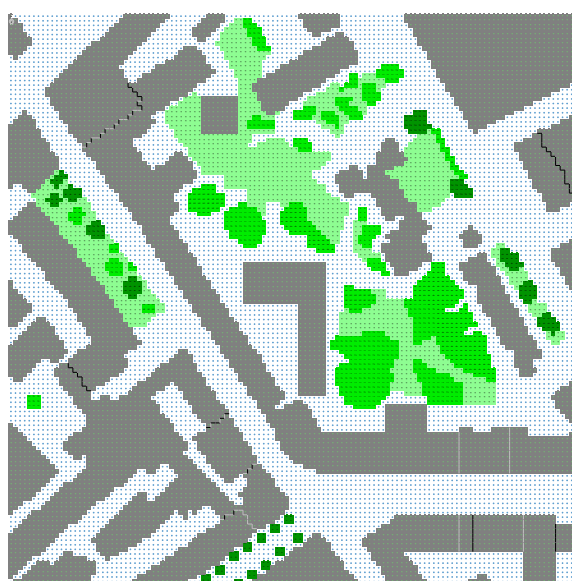


Figure 88. Area model created in *ENVI-met*. In grey the buildings, in pale green the grass, in shade of green the trees (light green for trees of 10 m, dark green for trees of 15 m)

The combination of bitmaps permitted to modeling the area in *ENVI-met* editor, drawing the vegetation actually presented in the area. The result of the *ENVI-met* modeling is shown in Figure 9.

The setting parameters of the model, written in *ENVI-met* Configuration Editor, are summarized in the Table 39. For the current situation two different scenarios have been analysed: first the current state of the district and then applying green roof for all buildings in order to estimate how the roofs temperatures and the air temperature change.

### 7.3.20. Case study of the city of Milan: actual design scenario

The next step of the case study of the city of Milan has been the analysis of the actual design scenario. The modeling area and the setting parameters are the same than the current design scenario, but the analysis part of the district has been modified in accordance with actual design scenario where *Building A* is 50 m high and *Building B* 30m have been inserted (Figure 89). Also for the actual design scenario two different configurations have been analysed: the first inserting *Building A* and *Building B* in the current district, the second adding the vegetation at the ground level with grass and tree in the district, tree-lined roads and green roof for all buildings.

The main purposes of this scenario are:

- Calculate the wall temperatures of the most irradiative façades of the *Building A* and *Building B*;
- Qualitative analysis for the air temperature and wind speed at the ground level.

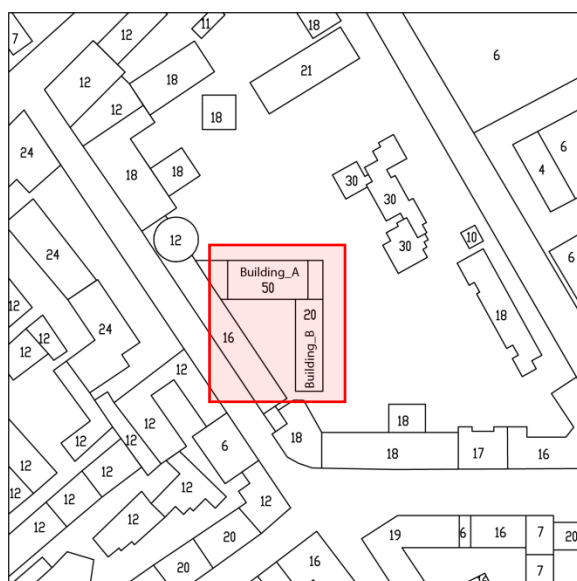


Figure 89. Bitmap of the district used from modeling it in *ENVI-met* editor area. The numbers represent the height of the buildings (actual design scenario – red rectangle)



Figure 90. Area model created in *ENVI-met*. In grey the buildings, in pale green the grass, in shade of green the trees (light green for trees of 10 m, dark green for trees of 15 m)

Regarding the temperatures analysis on the walls, for splitting the influence that one building creates on the other, have been done other two simulation in the current scenario of the district without add the vegetation: the first without *Building B*, and the second without *Building A*.

Therefore, isolating the examined building is possible to calculate the wall temperatures, without considering the solar reflection from one building to the examined one that affects the temperature on the façade.

### 7.3.21. Case study of the city of Milan: solar optimized scenario

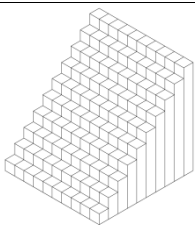
In the last step of the case study of the city of Milan the same set of simulations has been conducted for the *Solar\_Optimized\_Scenario*. The complexity of the model presents in this last scenario underlines the *ENVI-met* modeling issue regarding geometry.

As mentioned above the building modeling in *ENVI-met* is very complicated: it can be possible to create a simple shape with relative accuracy that depends from the grid spacing  $\Delta x$ ,  $\Delta y$  and  $\Delta z$ . *ENVI-met* can't offer many possibilities to work with complicated geometry, nonetheless there are some reasonable ways for modeling the non-linear surfaces. For example if it wants modeling a building within clined roof

or a complex surface façade at the moment is not possible, because the tool doesn't permit to construct inclined surface. In fact is not possible to define an inclined roof with a kind of step as well as for a complex façade, because the values could be affect by errors of calculation. In *ENVI-met* the topography is also always flat: is not possible to modeling a slope, hill or valley. Otherwise, considering the modeling limit of the tool and the poor accuracy of calculation, a set of simulations have been done in order to estimate the relative error of the wall temperatures' calculation.

The process started from simple models of a building composed by ten storeys and has been assumed that it is characterized by a 45° slope surface. The model has been built creating by ten steps of one grid spacing  $\Delta x$  and  $\Delta y$  each, as a stairs shown in the 3D model in the Table 40. This concept of the model creates some solar reflection radiation and heat flux exchange that a perfect surface modeling wouldn't have created. For minimizing these effects the model has been tested in three different configurations assigning different values of roof albedo and maintaining the same values of wall albedo set previously in order to simulate the solar systems. The first model has albedo roof equal to 0.0, the second equal to 0.3 and the latter equal to 1.0.

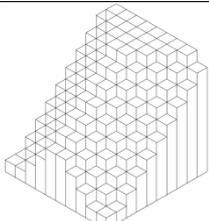
Table 40. Average temperatures values and  $\Delta T$  for a 3D simple model on the right.

	Roof albedo 0.0	Roof albedo 0.3	Roof albedo 1.0	
Average temperature on the façade (°C)	37.21	37.09	36.80	
$\Delta T$ (°C)	-	-0.12	-0.41	

The results show that roof albedo value, that minimizes the effect of solar reflection radiation and the heat flux exchange, is equal to 1.0.

The second set of simulations conducted on simple models, consider a different shape. This time the grid spacing  $\Delta x$  and  $\Delta y$  varies along x and y axes always of one grid point, in order to create the shadow effect also. The model has been set by the same values of roof and wall albedo. Table 41 reported below summarizes the simulations' results:

Table 41. Average temperatures values and  $\Delta T$  for a 3D simple model on the right.

	Roof albedo 0.0	Roof albedo 0.3	Roof albedo 1.0	
Average temperature on the façade (°C)	40.80	40.68	40.60	
$\Delta T$ (°C)	-	-0.12	-0.20	

The results show again that the roof albedo value for minimizing the effect of the solar radiation reflection and heat flux exchange is 1.0, but  $\Delta T$  is not more relevant than the previous analysis. This could mean that the shadowing effect reduces the  $\Delta T$  decrement due to the roof albedo, and that so it is possible not considered. Furthermore the average temperatures are higher in the last simple model, than the first and this effect could be created by the multiple solar reflections among the façades. This approach has been done according to find the best set up configuration of entire district model in order to run the microclimate simulation with the solar optimized design scenario.

However, the most important aspect that it wants to analyse on this section is the variation of values of wall temperatures: therefore the most important thing has been to use the same set of parameters for all simulations conducted in order to compare the output values, conscious that the data are affected from the approximated modeling and calculations.

After having analysed the set up configuration of the model, the problem of surfaces modeling of the solar optimized design building has been solved as described below. The surfaces created in *Grasshopper*, with the script that generated the parametric deformations of the volume described in the chapter 4, have been baked for exporting in *Rhinoceros*, and finally saved in .dwg file and imported in Autodesk Autocad space modeling. The footprints of the *Building A* and *Building B* have been divided according the *ENVI-met* grid subdivision  $\Delta x$  and  $\Delta y$ . Every single grid piece on footprints has been extruded to rebuild the entire volume of the *Building A* and *Building B* following approximately the shape of the volume surfaces. The Figure 91 shows the final result of volumes of the buildings rebuilding.

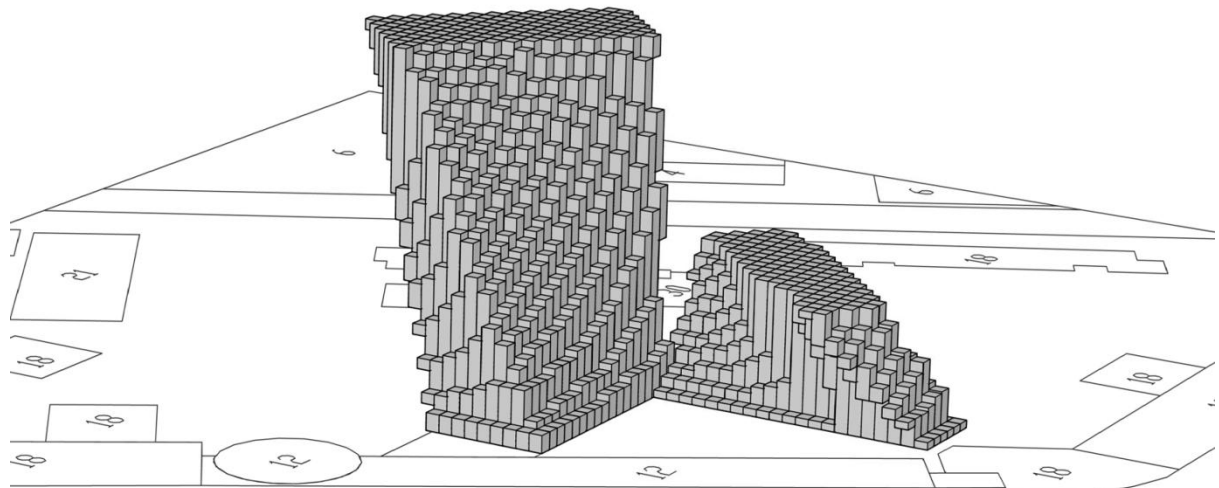


Figure 91. Image of the reconstruction of entire complex buildings' volume. It is clear the subdivision of the volumes.

This process has been necessary to extract the height of single piece inserting in *ENVI-met* Eddi, the *ENVI-met* 2D modeling space. Many pieces have a top and bottom height to rebuild faithfully shape of the volumes. The rebuilding is extremely approximate, but the subdivision of the model has been thought to have always the best approximation of the volume and value of the temperature on the façade.

The modeling result is shown in the following Figure 92: from the top view of model is possible to recognize the buildings twisted inserted in the entire district.

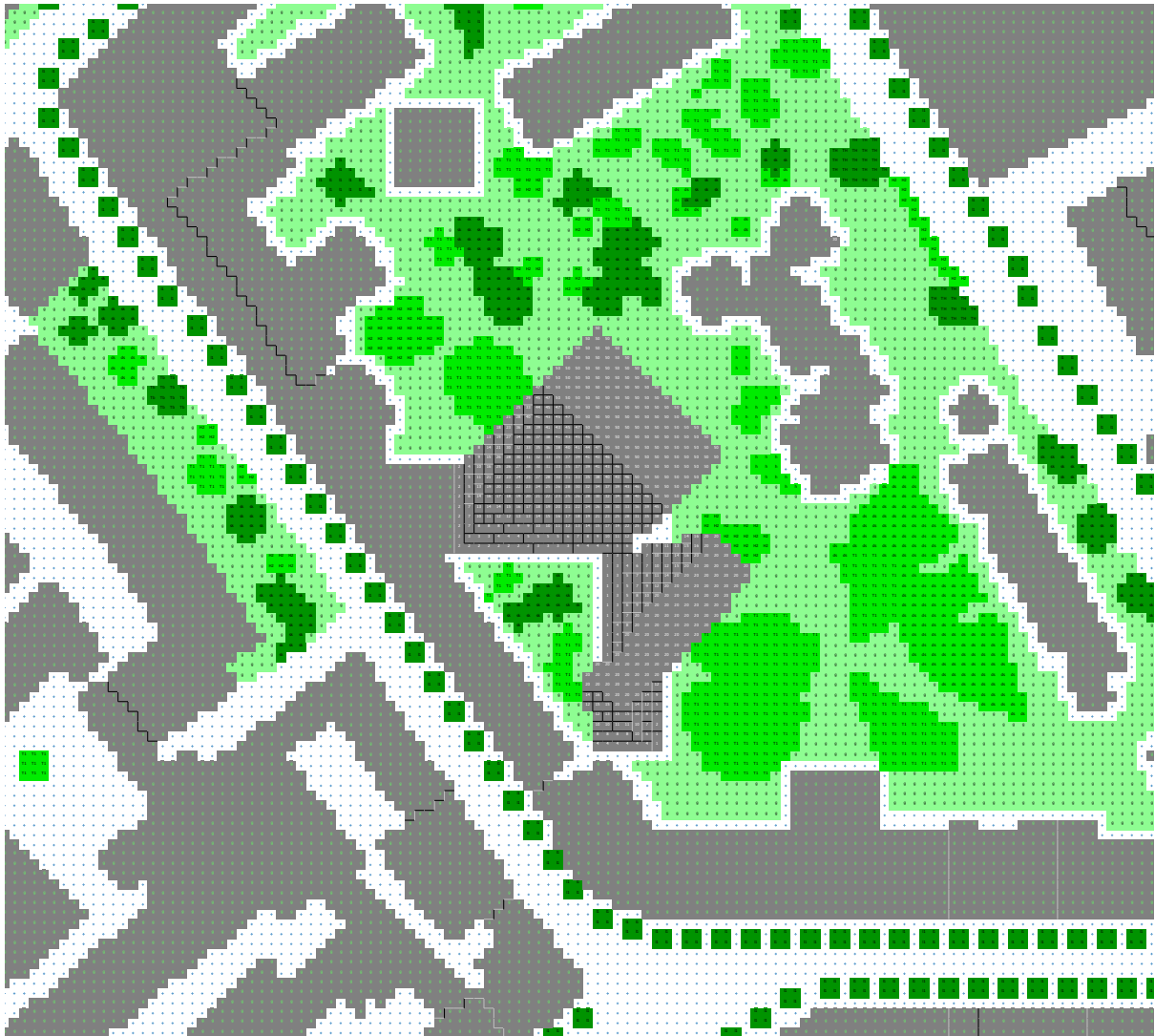


Figure 92. Top view of the district and the Building A and Building B with optimized shape. It is clear the subdivision of the entire buildings' volumes in small simple volumes.

## 7.4. Results and discussion

The results, carried out from the models simulated in *ENVI-met*, have been extracted using Leonardo tools and Extract *ENVI-met* Data.

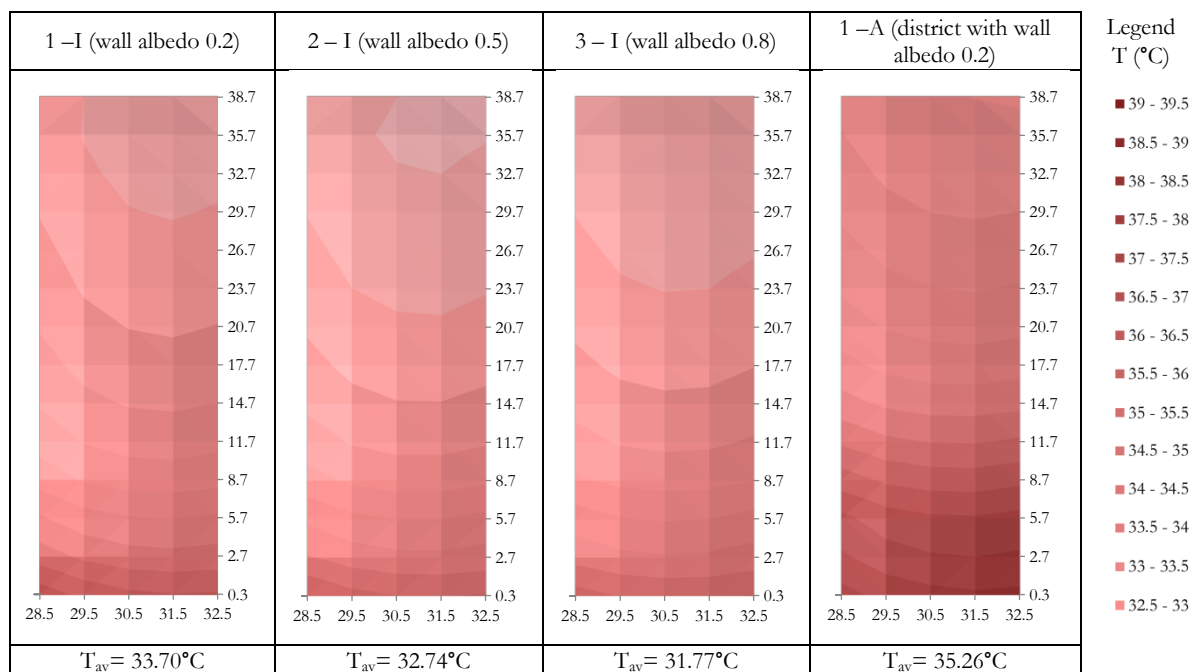
### 7.4.1. Parametric Microclimate analysis on simple model: results

The parametric study on the simple models has been done for studying the different aspects of microclimate behaviour.

#### Wall temperatures

Regarding the wall temperatures analysis have been extract the values of the south façade (most irradiative façade) from the all simple models analysed. Below are reported the data of average temperature on the façade and the temperature map.

Table 42. Temperatures maps of the simple models with different wall albedo values (1 – I, 2 – I, 3 – I) and the simple model of analysed building inserted in a district (1 – A)

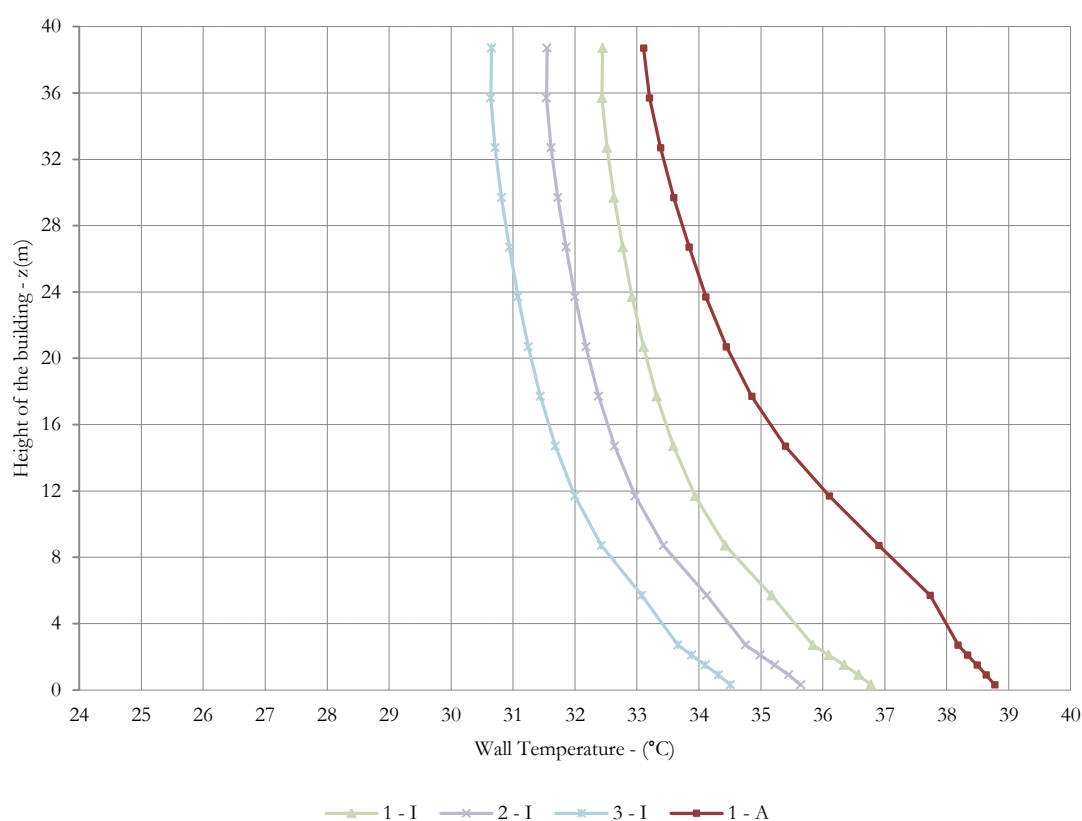


These first results underline that the temperature distribution on the façade is radial (visible on the temperature maps trend) and they vary from higher value on the bottom of the façade to the lower on the top. The variation of wall albedo values influences temperatures distribution: a high value of albedo (3 - I) can reduce the average temperature of the façade until 2°C than low one (e.g. solar system 1 - I).

The same building with the same wall albedo value (0.2) inserted in a simple district increases your average temperature on the most irradiative façade about 1.5°C due to the solar reflection from the neighbourhood buildings and for the heating of air temperatures.

This effect is easily visible on the Graph 12 that shows the trend of average temperature on the south façade: the difference of the temperature from simple model 1 – A, than the others is major on the bottom part of the façade rather than on the top. It means that the increment of the temperature is influenced by the solar reflection and the distance of the neighbourhood buildings.

Graph 12. Trends of average temperatures on the south building façade simple models 1 - I, 2 - I, 3 - I and 1 - A.

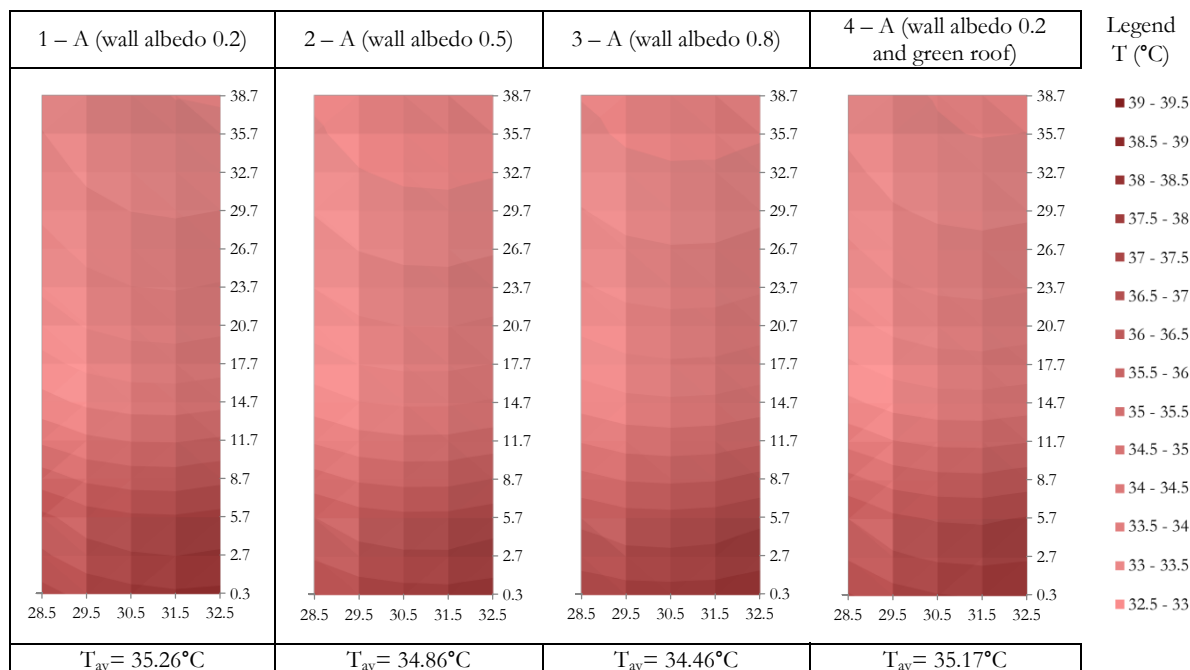


The effect of different wall albedo values has been analysed also on the simple models 1 - A, 2 - A, 3 - A, where the building is inserted in a simple district: temperature maps and average façade temperature are shown on the Table 43.

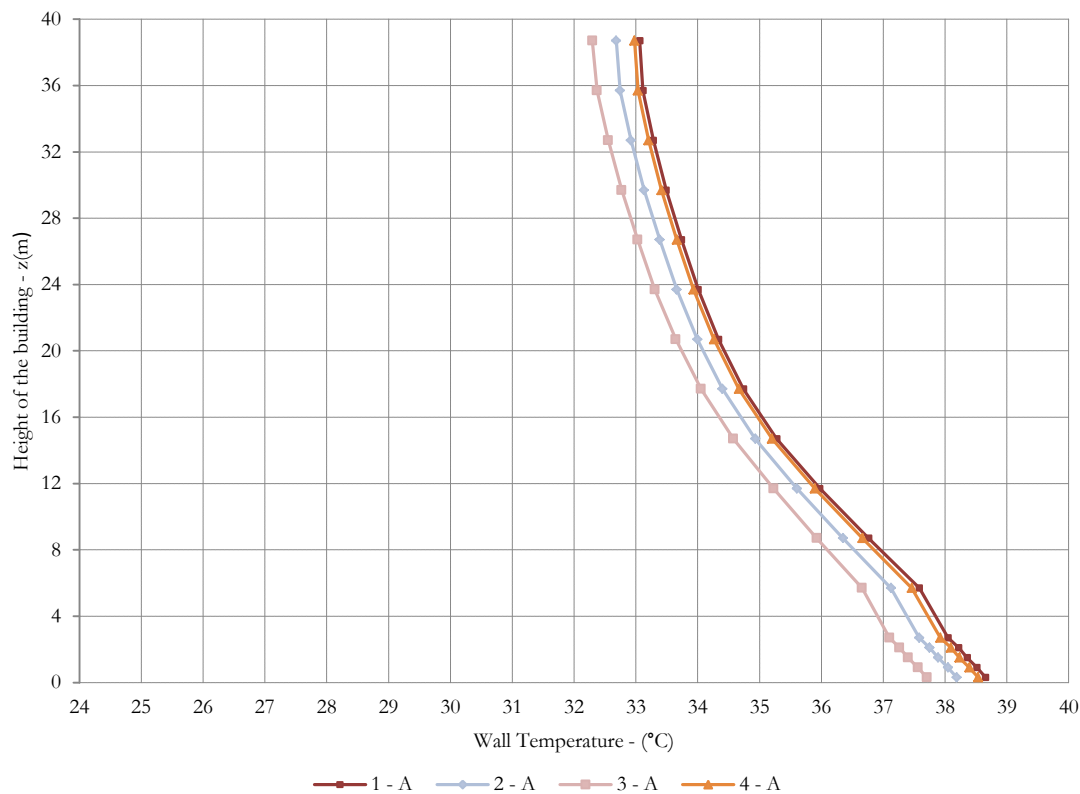
Also these results show that the temperature distribution on the façade is radial and they vary from higher value on the bottom of the façade to the lower on the top.

In these models the variation on the wall temperature caused by different wall albedo values doesn't have a high influence on temperatures distribution: in fact the average temperatures vary much less than the models analysed before

Table 43. Temperatures maps of simple models with different wall albedo values (1 - A, 2 - A, 3 - A) and green roof (4 - A).



Graph 13. Trends of average temperatures on the south building façade simple models 1 - A, 2 - A, 3 - A, 4 - A.



Furthermore the last model (4 - A) of these set of simulations is characterized from the same wall albedo value and district morphology of the previous model (1 - A), with green roof set on all buildings.

The results show that temperatures distribution and the average temperature are practically the same in both scenarios 1 - A and 4 - A, as predictable.

Regarding the roof's temperature the presence of green roof reduces the average temperature about 2°C: from 50.27°C with gravel roof (1 - A) to 48.37°C with green roof (4 - A). In literature a case study demonstrates the benefit of green roofs in term of air temperature reduction: at the roof level the temperature decrease until about 2.4°C [139].

Graph 13 shows the trend of average temperature on the south façade and the results commented above: it is possible to see that the differences of temperatures are constant along all building's height.

All following analysis have been done in order to estimate the effect of vegetation in different scenarios: first setting the grass and trees with different heights only on the site construction of the central analysed building (1 - G, 2 - G, 3 - G, 4 - G, 5 - G) and then extending the grass and trees (1 - P, 2 - P, 3 - P, 4 - P, 5 - P, 6 - P, 7 - P, 8 - P, 9 - P, 10 - P, 11 - P) and finally setting the grass for the entire district (12 - P).

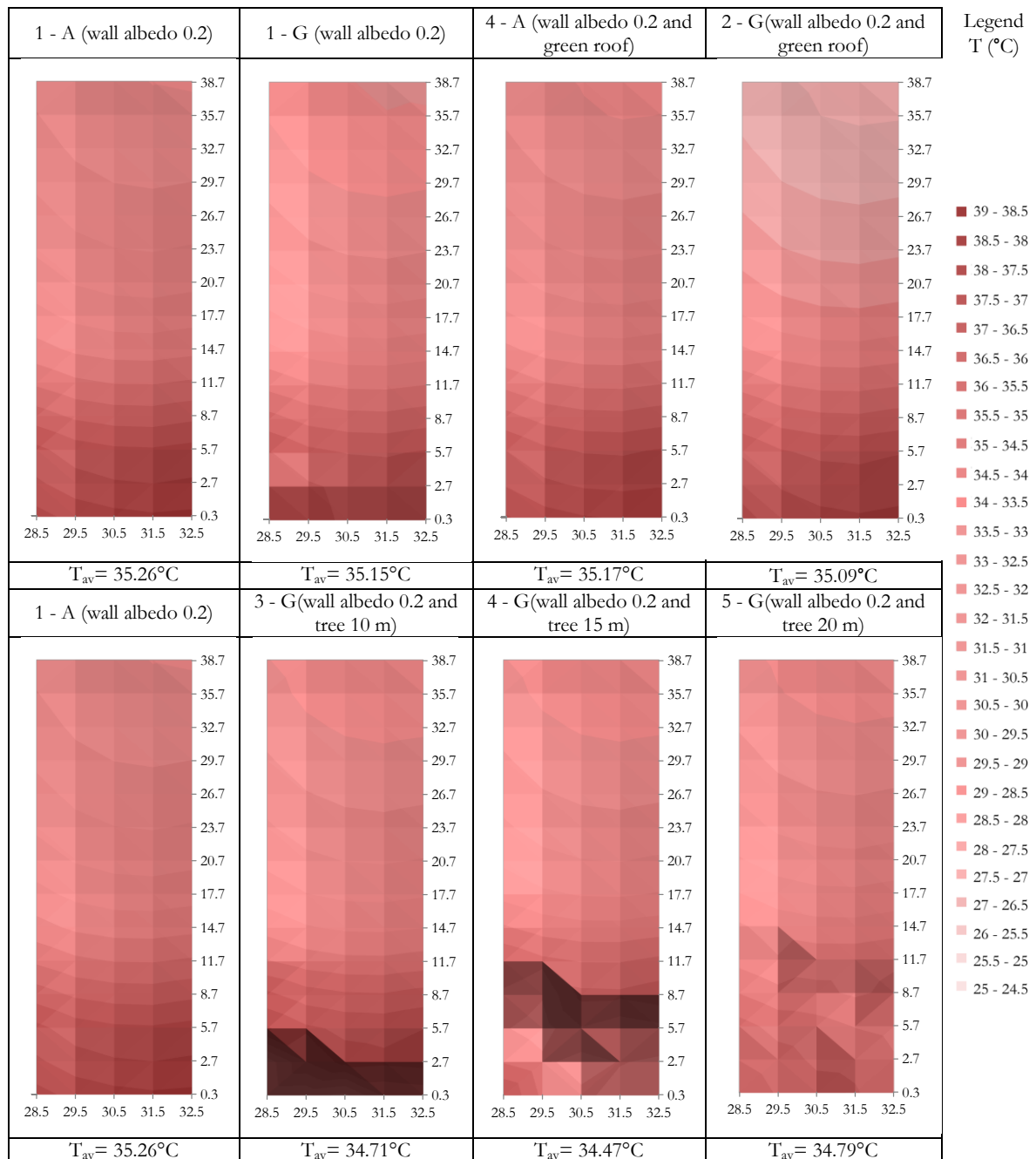
In Table 44 are summarised the results of this section of the parametric study and the first trend of the vegetation effect on the wall temperature. The limited vegetation area has given interesting results already in this phase: it is possible to see that in comparison with the base case study 1 - A, taken as reference, the 1 - G scenario hasn't practically any difference regarding average temperature on the wall. Also the comparison from scenario 4 - A to scenario 2 - G presents a very little difference always regarding the average temperature. The trend of temperatures distribution is also almost the same, except the low part of the façade, where is presented the grass.

In other scenarios analysis on the temperatures maps of south façade is easily visible the effect of shadows. Scenario 3 - G, with trees about 10 m heights distributed along the border of the site construction, the shadow effect is visible on the bottom part of the façade. In scenario 4 - G the shadow effect of trees about 15 m of heights, is distributed in the zone from 3 m and 12 m, and the bottom part has a higher temperature. This fact is probably given from crown's density and shape: different species of the trees have been chosen in order to estimate which should be the effect on the façade. Similar effect it can be seen in scenario 5 - G which the trees of 20 m of heights create another different shadows affect from ground level to 14.7 m.

Regarding the comparison from case study of reference, 1 - A, the difference of average temperature on the façade are more relevant than the other scenarios (1 - G and 2 - G). The presence of the trees reduces the average temperature on the façade from about 0.5°C (3 - G and 5 - G) to 0.8°C (4 - G). The differences from one scenario and other are also caused by crown's density and shape and their effect on the façade.

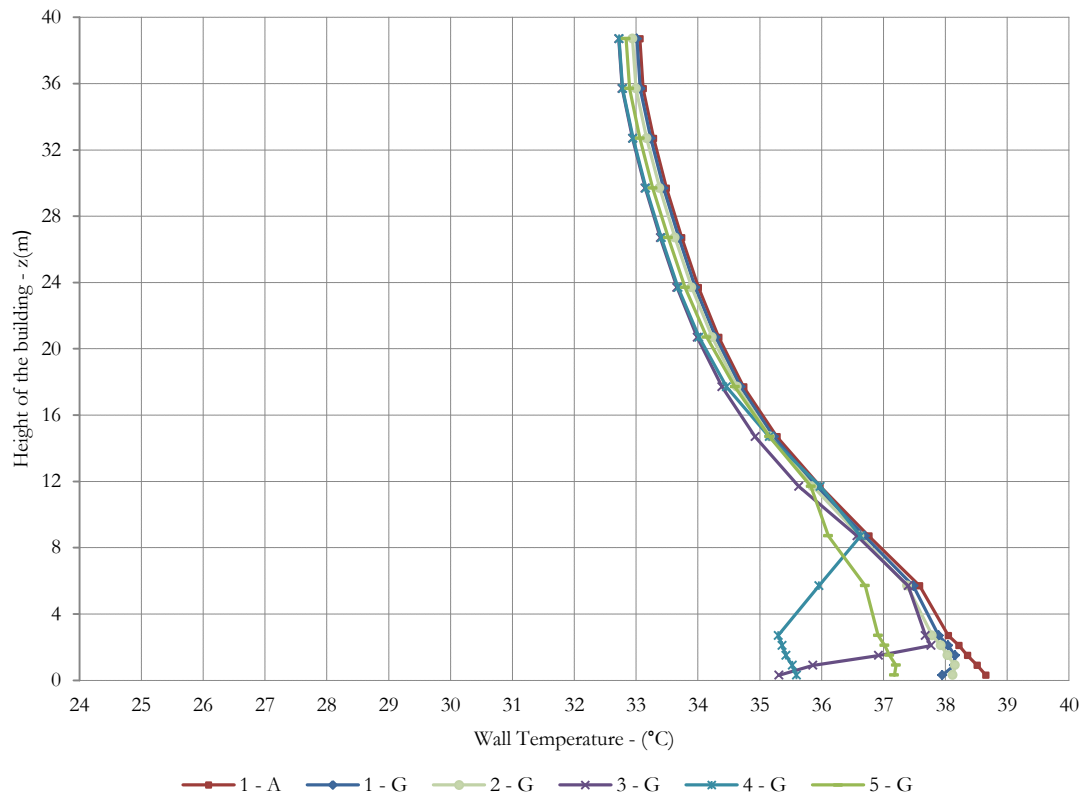
Graph 14 shows well the different effects that the trees caused on the bottom part of the façade: Scenario 1 - G and 2 - G, as analysed before, have a similar trend to the simple reference model 1 - A, while simple model 3 - G (trees of 10 m heights), 4 - G (trees of 15 m heights) and 5 - G (trees of 20 m heights) have a unstable trend from the ground level to 15 m approximately due to shadows effects.

Table 44. Comparison from temperatures maps of simple models with grass on the site construction (1 - G) and green roof (2 - G) and previous with the same settings (top). Comparison from base case without grass (1 - A) and simple models with grass and trees on the site construction (3 - G, 4 - G and 5 - G)



The vegetation reduces the wall temperature by direct shading of surfaces as well as by moderating solar heat gain through evapotranspiration of the plants, and conversion of incident solar radiation to latent heat.

Graph 14. Trends of average temperatures on the south building façade simple models 1 – A (reference case study), 1 - G, 2 - G, 3 - G, 4 - G, 5 - G.



The last part of parametric study has been conducted in order to analysis the influence of vegetation when the grass is extended and the number of trees is thickened.

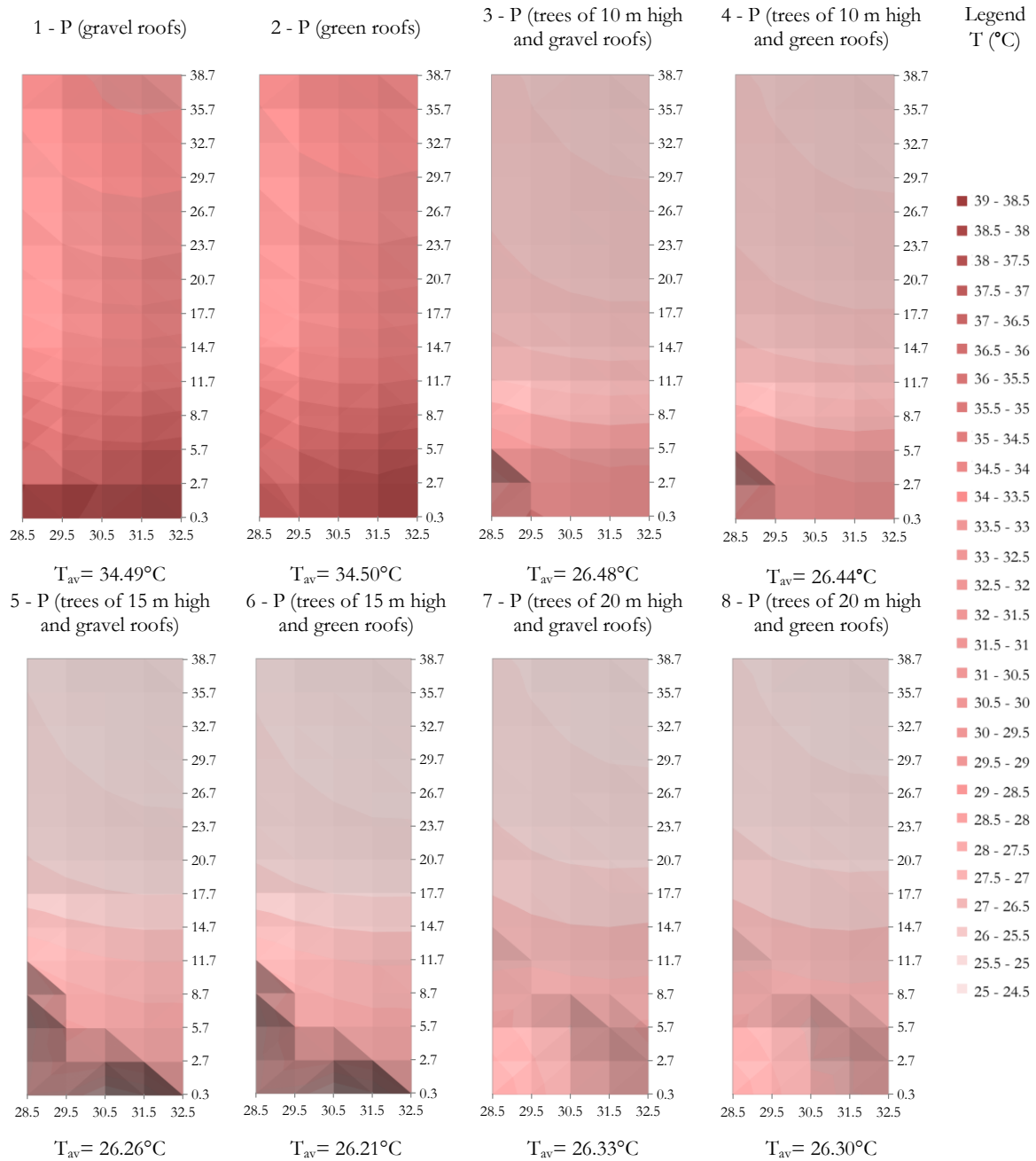
Different scenarios have been simulated starting from the extension of grass area from the central building to the internal sides of neighbourhoods building, to constitute a park of 30 x 30 m dimension (1 - P) and green roofs (2 - P).

In the other scenarios, trees characterized from different heights (trees of 10 m high scenarios 3 - P and 4 - P, trees of 15 m high scenarios 5 - P and 6 - P, trees of 20 m high scenarios 7 - P and 8 - P) and crown density, have been inserted in the model and tested in order to estimate how the park with vegetation influences the microclimate of the district and in particular the trend of wall temperatures.

Furthermore different dispositions of vegetation have been simulated for studying if the arrangement of the trees and their quantities in the same park area 30 x 30m, can influence the atmosphere and façades

temperatures. Ten trees disposed in the inner part of the park close to the central building (scenario 9 - P) and then along the borders in the external part of the park far from the central building (scenario 10 - P) have been tested as well as a regular disposition of the trees characterized by different high and crown density (scenario 11 - P) and finally the last scenario with grass area of 50 x 50 m (scenario 12 - P).

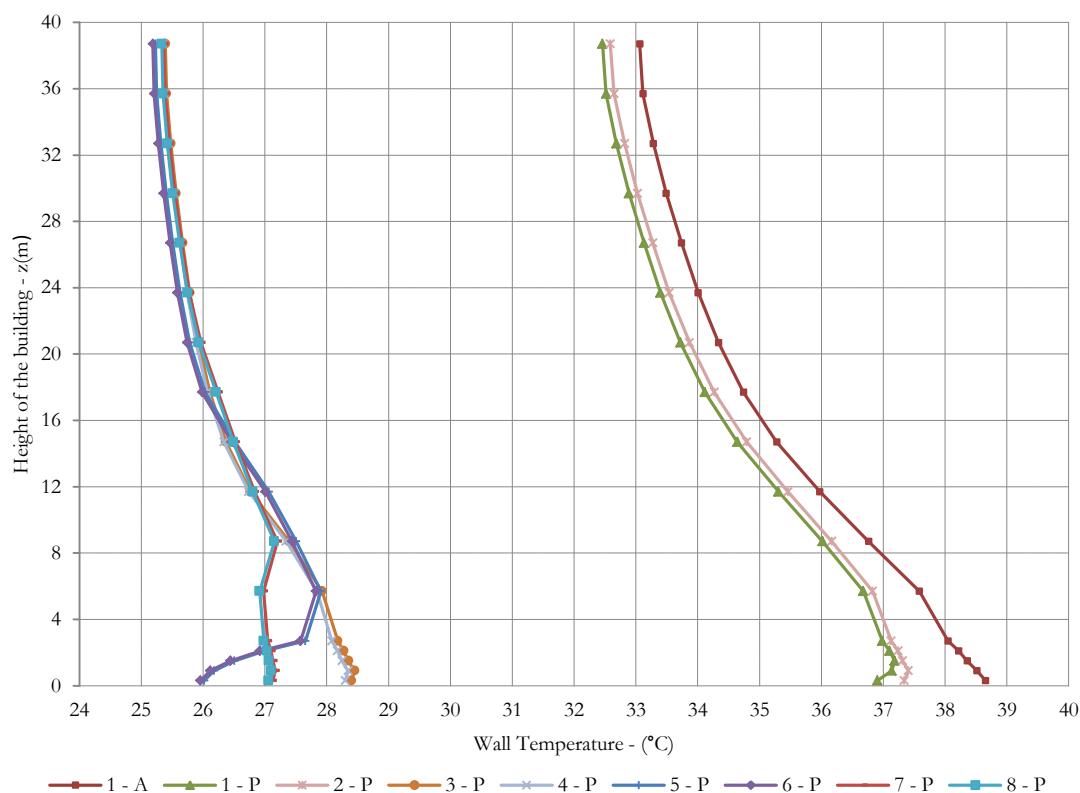
Table 45. Temperatures maps of scenario with park of 30 x 30 m (1 - P) and green roof (2 - P), with trees of 10 m high (3 - P) and green roof (4 - P), with trees of 15 m high (5 - P) and green roof (6 - P), with trees of 20 m high (7 - P) and green roof (8 - P)



The temperatures maps and the Graph 15 show that all case studies have lower values of temperatures than the reference case study (1 - A). The case studies 2 - P, 4 - P, 6 - P and 8 - P (gravel roofs) have practically the same temperatures' distribution respectively of the case studies 1 - P, 3 - P, 5 - P, 7 - P (green roofs) and this demonstrate that the green roofs don't have an influent effect on the wall temperatures. Also the values of average temperatures confirm this fact.

In scenario 1 - P the bigger presence of grass area gives a good effect in term of temperatures' reduction: in fact it is easily to observe on the Graph 15 that the temperature difference is equal to 1°C than the reference scenario (1 - A) along all height of the façade. A higher difference is on the bottom of the façade where the presence of the grass decreases the solar reflection and the heat transfer from the ground.

Graph 15. Trends of average temperatures on the south building façade simple models 1 – A (reference case study), 1 - P, 2 - P, 3 - P, 4 - P, 5 - P, 6 - P, 7 - P, 8 - P.



Adding the trees on the park, the vegetation effect became more influent: in fact the average temperatures decrease about 8/9°C than scenarios 1 - A and 1 - P that has only the presence of the park. This effect is extended on the all façade surface as shown on the Graph 15. It is important to underline that on the bottom of the façade the shading effect reduces more the wall temperature until 10/11°C and furthermore the crown density create unstable trend of the temperatures from the ground level

until 10/15 metres of the façades as it is possible to see on the maps temperatures in Table 45 and average temperature trend on the Graph 15.

In literature there are [140] many case studies that confirmed these results: the massive presence of vegetation close to the city can reduce the air temperature and wall temperatures more than 8°C as well as the installation of green wall [141].

The last set of simulations has been conducted on different scenarios focused on the effect of vegetation's disposition (9 - P, 10 - P and 11 - P) and on a case study where the park covered entire district (12 - P).

Table 46. Temperatures maps of scenario with park of 30 x 30 m and 10 trees disposed in the inner part of the park close to the central building (9 - P) and then along the borders in the external part of the park far from the central building (10 - P) a regular disposition of the trees characterized by different high and crown density (11 - P) and finally the last scenario with grass area of 50 x 50 m (12 - P).

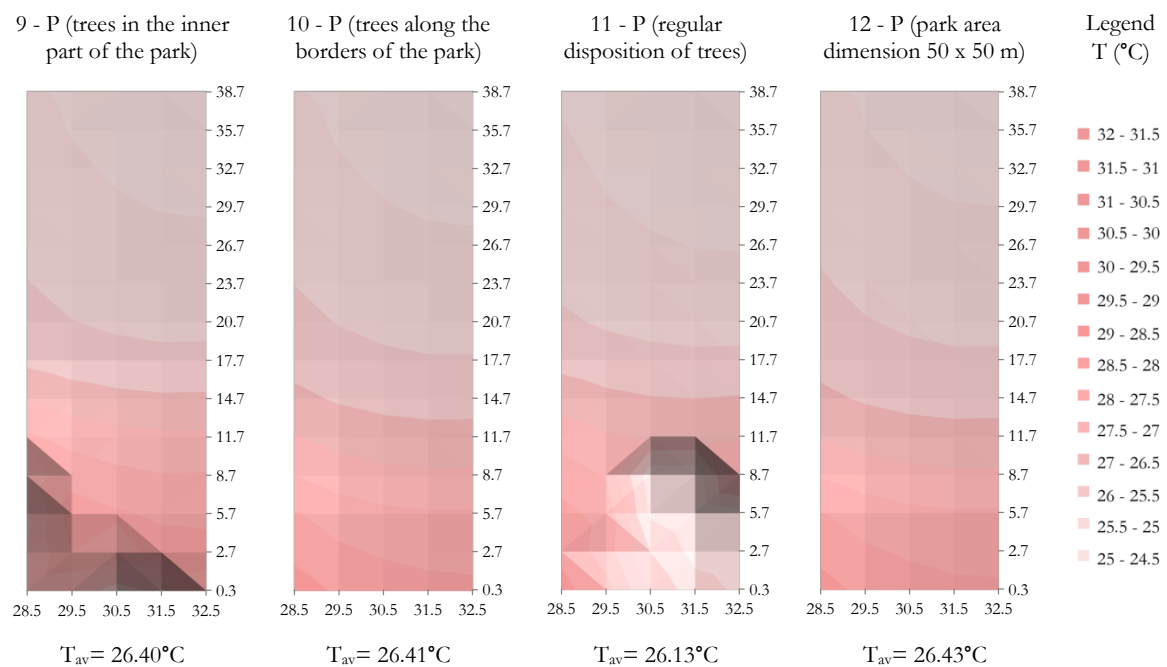
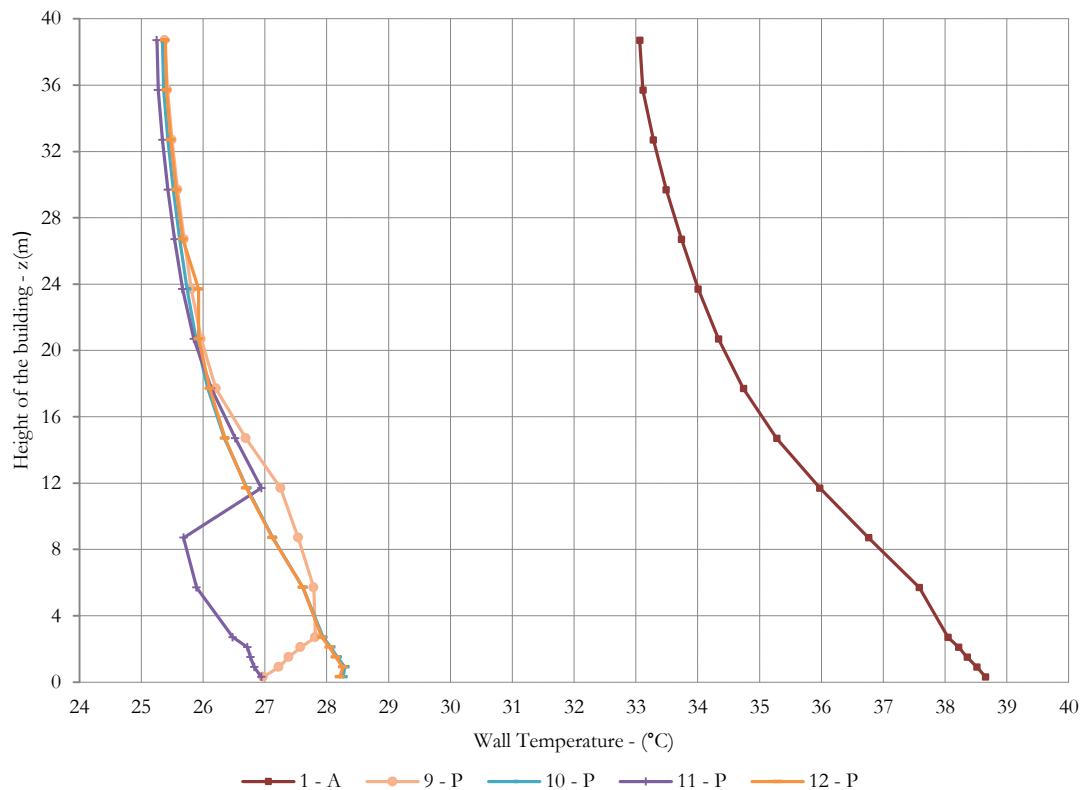


Table 46 and Graph 16 show the results of these scenarios: the reduction of wall temperatures due to the vegetation presence is almost the same than the other scenarios, even if the number of trees is decreased. Furthermore the disposition of the trees in the park doesn't influence the reduction of average temperature on the façade, but the shading effect creates different trend of temperatures on it as shown on the map temperatures and in the Graph 16 (9 - P, 10 - P, 11 - P).

The final scenario (12 – P) has given an interesting result: if the soil of the entire district is completely constituted by grass, the effect of temperatures’ reduction is almost the same than the scenarios with the presence of the trees.

Graph 16. Trends of average temperatures on the south building façade simple models 1 – A (reference case study), 9 - P, 10 - P, 11 - P, 12 - P.



Summarising, the results obtained from the parametric study on simple models are:

- The wall albedo values can reduce the average temperature on the façade until 2°C;
- The presence of a medium park area with trees in the middle of a district decreases the wall temperatures of about 8/9 °C;
- The different species of tree and their crown density create the shading effect on the bottom part of the façade reducing the wall temperatures more and the thermal stress at the ground level;
- The disposition of vegetation doesn't influence on the average wall temperature;
- The presence of large park area in a district contributes to decrease the temperature of the most irradiative façade (south) of the building of about 8/9 °C;

### 7.4.2. Case study of the city of Milan: actual design scenario

The results of microclimate aspects of case study of the city of Milan are presented below. In particular in this part of the study are treated the results regarding the actual design scenario.

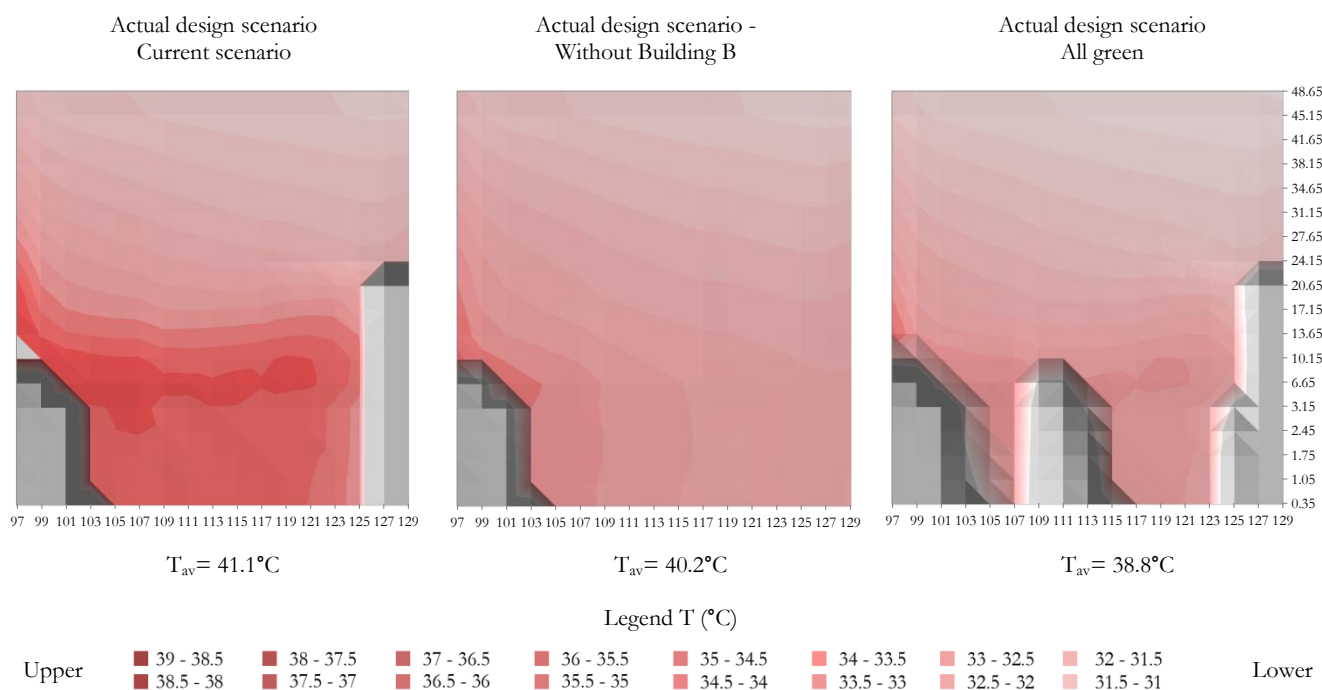
#### Wall and temperatures

The purpose of this part of the study is the calculation of wall temperatures in order to estimate the benefits of vegetation in a real case study. Furthermore the analysis is focused on the *Building A* and *Building B* for calculating the increment of temperatures on the façades given by the solar reflection from *Building A* on *Building B* and vice versa.

The specific photovoltaic albedo value equal to 0.2 has been fixed for wall albedo value in order to simulate the installation of solar systems on the façades.

The set of simulations analysed the wall temperature of both designed building (*Building A* and *Building B*). The results are reported in Table 47: are presented the wall temperatures maps of south façade of *Building A* in the actual design scenario maintaining the existing green system of the district (*Current scenario*), without *Building B* in order to calculate its solar reflection influence on the *Building A* and in the scenario with green roofs set for all buildings that compose the entire district, the park in a district and the tree-lined roads (*All green*).

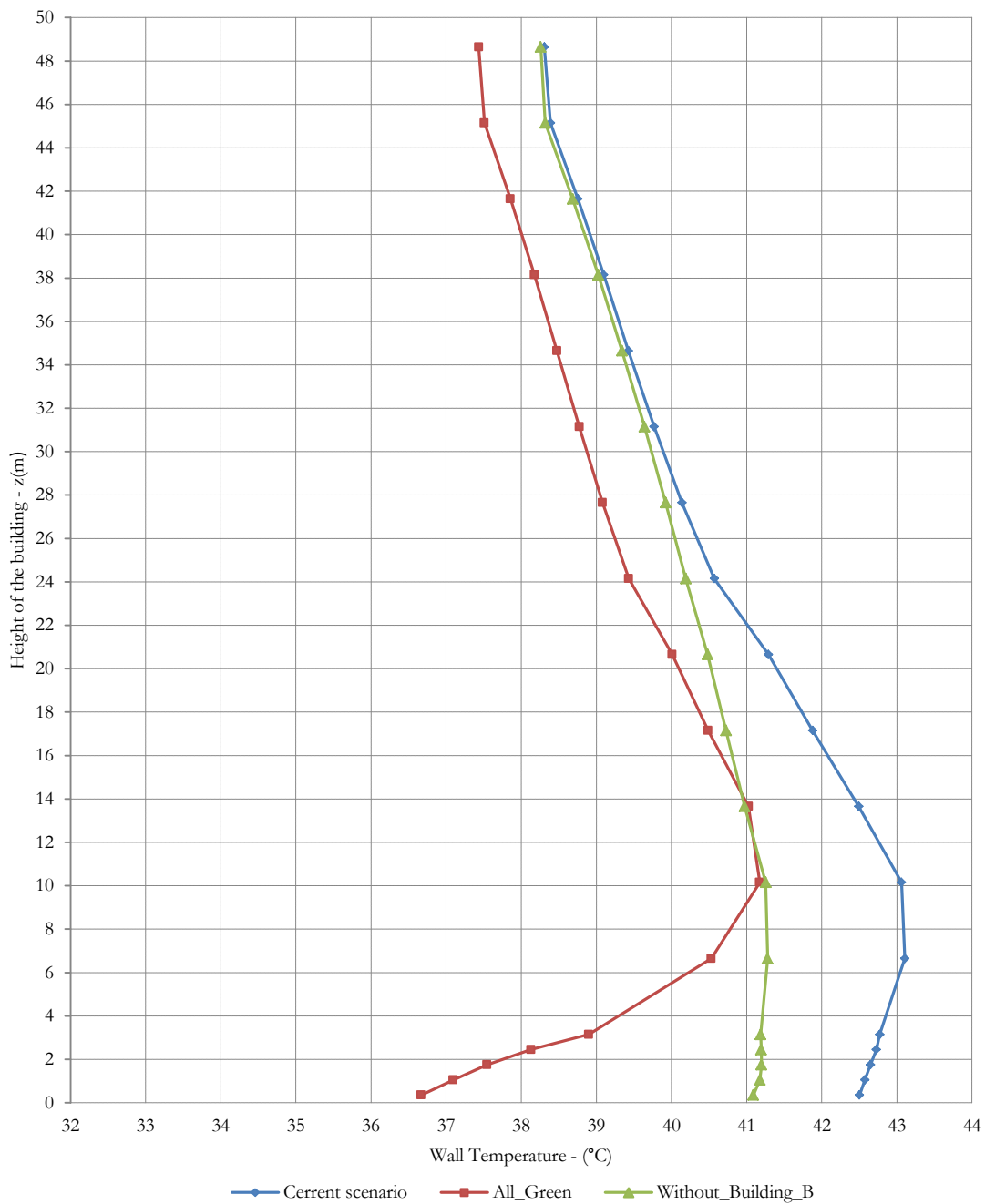
Table 47. Temperatures maps of Actual design scenario - *Current scenario*, *Without Building B* and *All Green*. In the primary horizontal axes the x-coordinates of the south façades of *Building A* in the model, in the primary vertical axes the z-height of the sensors on the façade.



In the wall temperatures maps in the Table 47 the effect of solar reflection and the increment of temperature caused by *Building B* is clearly evident from the maps temperature of current scenario, compares to the others.

The average temperature values confirm the benefit of the presence of vegetation: the façade' temperature reduction is about 2.3°C, while the effect of solar reflection by *Building B* on the *Building A* increases the wall temperature about 1°C.

Graph 17. Trends of average temperatures on the south *Building A* façade in the different actual design scenarios analysed.



Graph 17 shows the trend of average temperature on the analysed façade in the different simulated scenarios. Many important aspects from these analyses have been carried out: if it considers the *Without Building B* scenario and *Current* scenario it can be easily seen that the temperatures' trend is almost similar than the others analysed in the parametric study. It confirms that the temperatures are very high at the ground level and decrease along the height of the building for the wind effect.

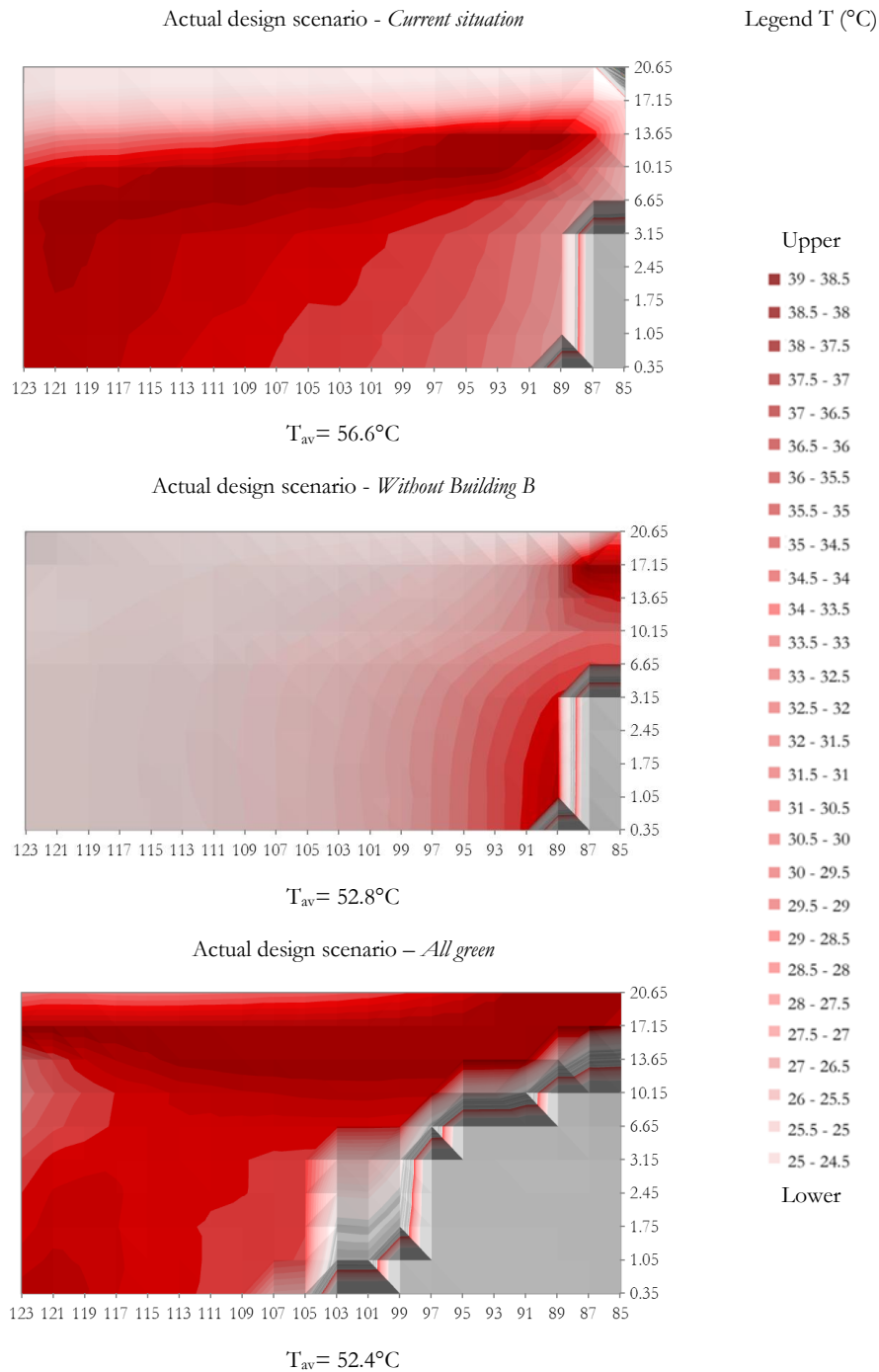
The current scenario presents a very interesting trend of temperatures: in fact the values of average temperatures along the height of the *Building A* are higher than the scenario *Without Building B* until the 22 metres. These high differences are caused only by the solar reflection coming from the *Building B* that consequently increase the wall temperatures: the highest value of temperature variation at a height 10.5 metres is about 2.5°C, while the highest value of average temperature variation is equal to 1.8°C at a height 6.65 metres. On the temperatures map in Table 47 is possible to see that the warmer part of the *Building A*'s façade is concentrated on its bottom part. The differences from the temperatures between *Without Building B* scenario and current scenario remain high also after a height of 20 metres that is respectively the height of the *Building A*. This effect is caused by the solar reflections coming from the roof of the *Building B*. After this level the temperatures' trend is practically the same of the temperatures trend extracted from the *Without Building B* scenario, as expectable. However the average reduction of global warming on the façade is about 1°C.

Regarding the *All Green* scenario there are some results to comment: firstly the general trend of the average temperatures is the same already seen on the parametric analysis in scenarios with presence of vegetation. Secondly the presence of vegetation on the ground level contributes for reducing the wall temperature on the bottom part of the façade. In particular the shading effect reduces the wall temperatures until about 14°C in some points, even if the average decrement of the temperature is more than 5°C until at a height 1.75 metres, 4.50°C at a height 2.50 metres, 3.80°C at a height 3.15 metres, more than 2.50°C at a height 6.65 metres and about 1.50°C until at a height 17.15 metres. The average value of temperatures reduction considering the entire façade is about 2.3°C. The shift of the entire average temperature trend's line visible on the Graph 17, confirmed that the effect of vegetation is local for the highest values of reduction where the shading effect is strong but its benefit is global because the temperatures decrease along all height of the *Building A*'s façade.

However the most important aspect that this set of simulation demonstrated is that the vegetation limits the effect the wall temperatures' increment, rather it gets better the wall temperatures' values, reducing the global warming of the façade maintaining the same boundary condition in term of walls and roofs albedo and morphology of the district. This aspect results very important especially if it considers the initial purposes of this part of the study that were to find a new design approach for planners, engineers and architects for sustainable development in existing urban area and to estimate the vegetation effect on the wall temperatures when solar systems are installed on them.

The same analysis has been done on the east façade of the *Building B*. Following are reported the results: the Table 48 collected the temperatures maps in the different scenarios analysed.

Table 48. Temperatures maps of Actual design scenario - *Current situation*, *Without Building A* and *All green*. In the primary horizontal axes the y-coordinates of the east facades of *Building B* in the model, in the primary vertical axes the z-height of the sensors on the façade.



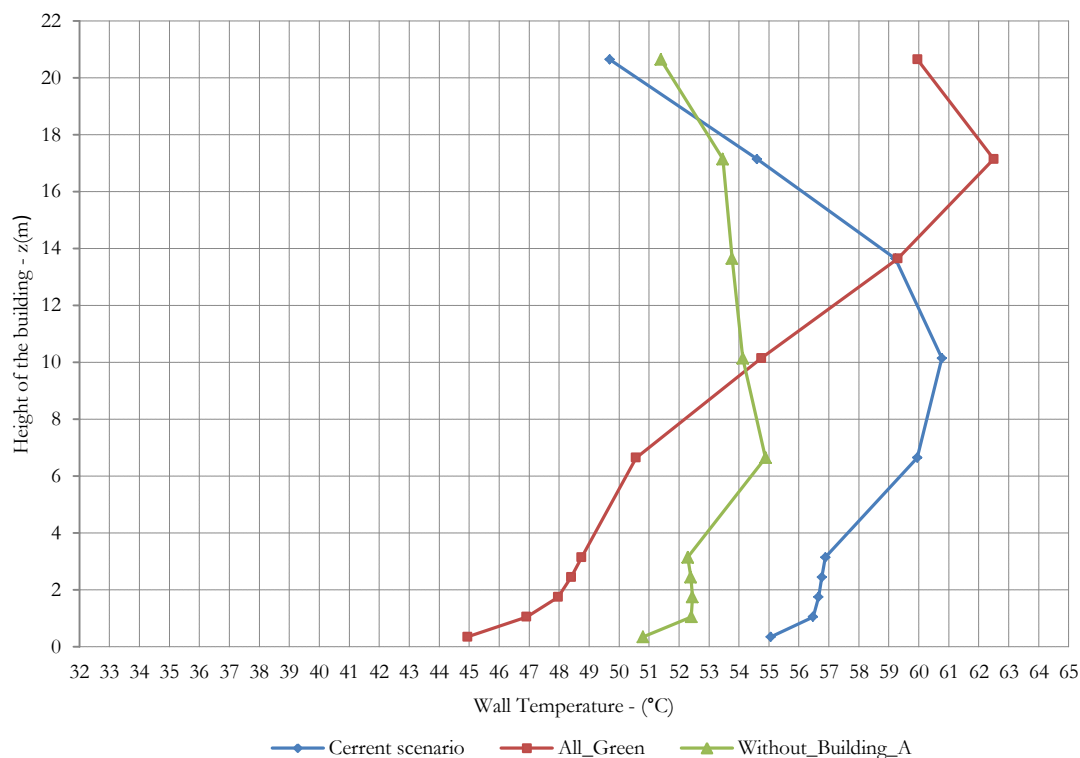
As the previous approach used for analysing the *Building A*, the results reported in Table 48 show the wall temperatures maps of east façade of *Building B* in the actual design scenario maintaining the existing green system of the district (*Current scenario*), *Without Building A* in order to calculate its solar reflection influence on the *Building B* and in the scenario with green roofs set for all buildings that compose the entire district, the park in a district and the tree-lined roads (*All green*).

The first information derivable from the analyses is that the average temperature on the façade is higher than the average temperatures measured on the *Building A*'s façade. The values are very high due to the solar reflection coming from the *Building A* that is exposed perfectly on the south and the configuration of design as a court that facilitates the mutual solar reflection especially on the *Building B*. Furthermore also the average height of *Building B* contributes to increase the global warming on its façade. The average temperature on the façade arrived until 56.6°C in the current scenario.

In the wall temperatures maps presented in the Table 48 it is possible to see the effect of solar reflection and the increment of temperature caused by *Building A* is clearly evident from the maps temperature of current situation, compares to others.

The high benefit of the presence of vegetation is confirmed from the average temperatures' trend: the façade' temperature reduction is about 4.2°C. Also the effect of solar reflection on the *Building B* coming from *Building A* is much high: the increment of the wall temperature is about 3.8°C.

Graph 18. Trends of average temperatures on the east *Building B* façade in the different scenarios analysed



Graph 18 shows the trend of average temperature on the analysed façade in the different simulated scenarios. Some interesting information can be deduced from the results of these analyses: already in the scenario *Without Building A* it can be easily seen that the temperatures' trend is quite different than the others analysed on the parametric study. This fact is probably due to the orientation of the façade and the presence of other buildings in front of the analysed façade. However the lower temperatures are again distributed on the top part of the building's façade where the wind speed contributes to decrease the temperatures.

The *Current scenario* presents the same interesting trend of temperatures than the current scenario of *Building A*: in fact the values of average temperatures along the height of the *Building B* are higher than the scenario *Without Building A*. These high differences are caused only by the solar reflection coming from the *Building A* that consequently increase the wall temperatures: the highest value of temperature variation at a height 6.65 metres is about 9.5°C, while the highest value of average temperature variation is equal to 6.6°C at a height 10.15 metres. However in the *Without Building A* scenario the temperature distribution is quite homogeneous on the entire façade as the temperature map shows: the values of temperature increase only next to the other buildings.

Regarding the temperatures distribution in Table 48 it is possible to see that the warmer part of the *Building B*'s façade is well distributed along all its central part in the current scenario, and on the upper part of the façade in the *All Green* scenario. The presence of the vegetation in fact produces a movement of the warmer part of the façade from a lower level to an upper one, as also shown in the Graph 18.

Regarding the *All Green* scenario there are some aspects that need a deeper discussion: firstly the general trend of the average temperatures is completely different from the analyses done in all previous scenarios with the presence of vegetation. The average reduction of temperature is about 10°C at the ground level and from that level the reduction continues to decrease until at a height 14.0 metres. After 14 metres the values of average temperatures of the *All Green* façade are higher than the values at the same level in the current scenario. This is caused from the disposition of the vegetation that is very thick on the right side of the façade, and practically absent on the other side. Secondly the presence of vegetation on the ground level contributes to reducing the wall temperature on the bottom part of the façade. In particular the shading effect reduces the wall temperatures also until about 27°C in some points, even if the average decrement of the temperature is more than 8.5°C until at a height 1.75 metres, more than 8.0°C at a height 2.50 metres and at a height 3.15 metres, more than 9.0°C at a height 6.65 metres and about 6.0°C until at a height 10.15 metres. After at a height 10.15 metres the average temperature presents higher values than the current scenario. The average value of temperatures reduction considering the entire façade is about 4.2°C. This latter data represents the most important aspect of this set of simulation: it has been demonstrated that the vegetation limits the effect of the wall temperatures' increment, rather it gets better the wall temperatures' values, reducing the global warming of the façade while maintaining the same boundary

condition in term of walls and roofs albedo and morphology of the district. As just said before this aspect results very important especially considering the goals of this part of the study.

The last results regarding roof temperature on the *Building A* and *Building B* have been extracted from these analyses. Both buildings present a considerable decrement of roof temperatures from Current Scenario, where the roofs are covered by gravel and *All Green* scenario, with green roofs. Reported the values of roofs' temperatures relative to the analysed scenarios:

Table 49. Values of average temperature on the *Building A* and *Building B*'s roofs in the *Current* and *All Green* scenario.

Scenario	Roof temperature - Building_A [°C]	Roof temperature - Building_B [°C]
Current scenario	49.5	52.2
All-Green	47.1	53.3
$\Delta T$ [°C]	2.4	1.1

The values demonstrated the benefit of green roof: in both buildings the decrement of average temperature of the roof decreases about 2.4°C for *Building A* and 1.1°C for *Building B*. The difference between the values is given by the wind speed at the roof level that is equal to 3.5 m/s for *Building A* (50m of height) and 2.5m/s for *Building B* (20m of height).

Summarising, the results obtained from the actual design scenario are:

- The average temperature on the façade increases about 1°C on the *Building A* due to the solar radiation coming from *Building B* and about 3.8°C on the *Building B* due to the solar radiation coming from *Building A*;
- The presence of vegetation reduces the average temperatures' trend about 2.3°C on the *Building A*'s façade and about 4.2°C on the *Building B*'s façade;
- The shading effect reduce considerably the temperature at the ground level: the average reduction of temperature on the pedestrian level is about 5°C on the *Building A* and about 10°C on the *Building B*;
- The average of roof temperature decrease about 2.4°C on the *Building A* and 1.1°C on the *Building B* installing the green roof.

### 7.4.3. Case study of the city of Milan: solar optimized design scenario

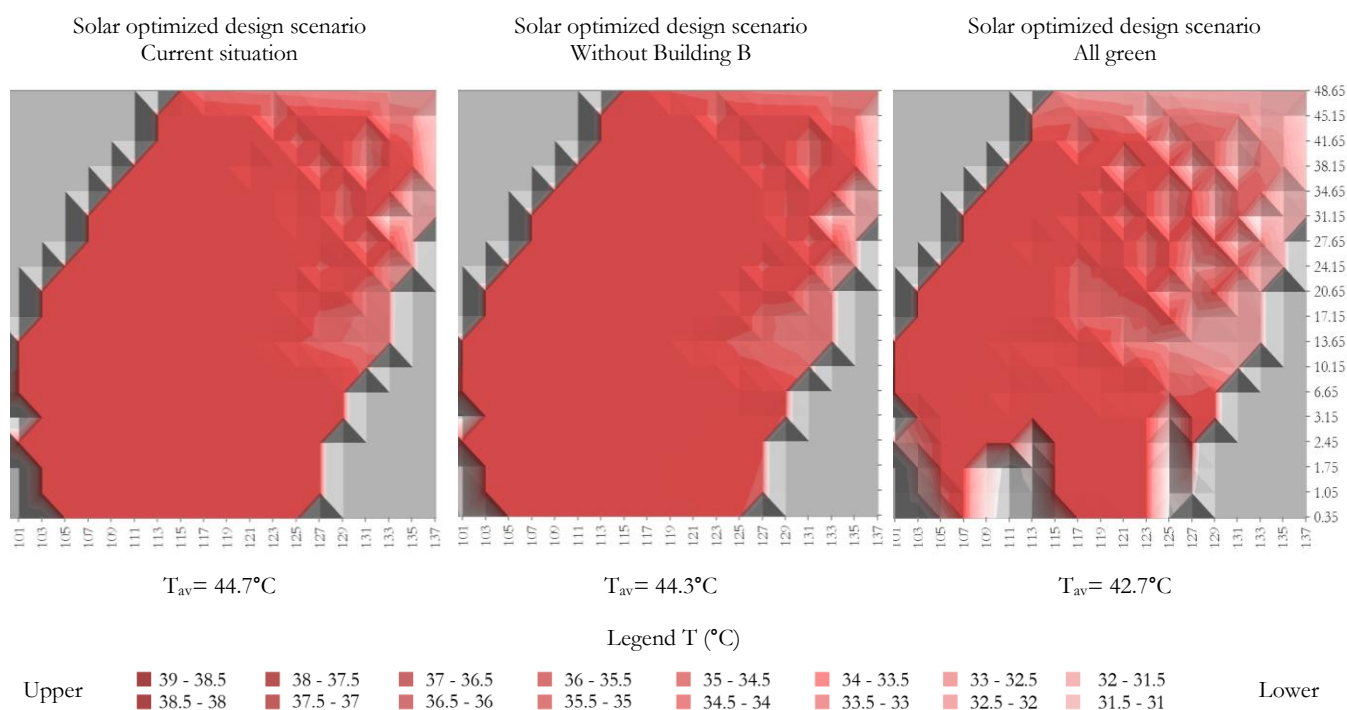
In this section are presented the results regarding the solar optimized design scenario, obtained from solar dynamic analysis.

#### Wall and temperatures

The purpose of this part of the study is the calculation of wall temperatures in order to estimate the benefits of vegetation in the optimized scenario started from the real case study. The purpose of the analysis is always the same: calculate the increment of temperature on the most radiative façades of the *Building A* and *Building B* given by the solar reflection from each other.

It was used the same specific photovoltaic albedo value equal to 0.2 in order to simulate the installation of solar systems on the façades.

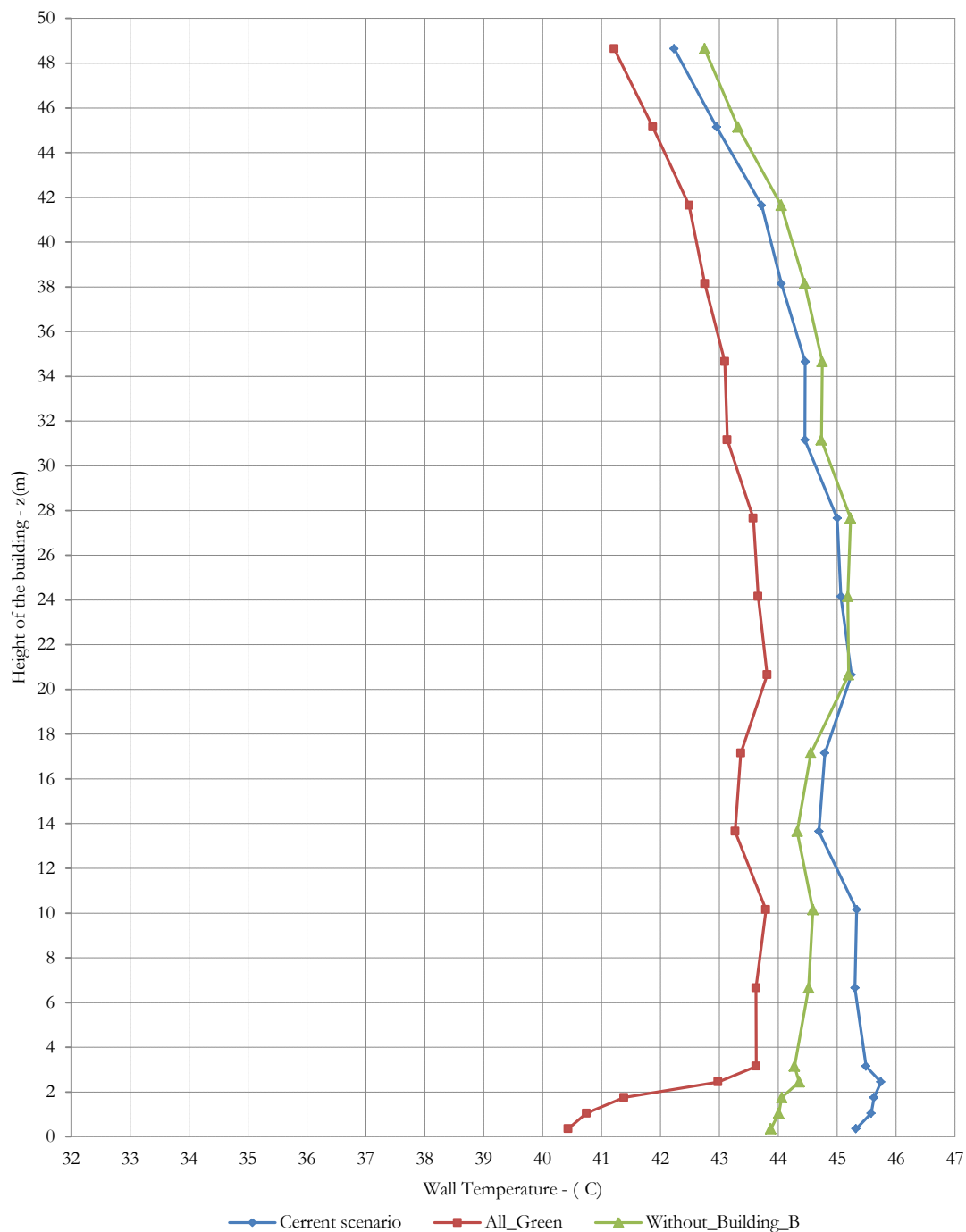
Table 50. Temperatures maps of Solar optimized design scenario - *Current situation*, *Without Building B* and *All Green*. In the primary horizontal axes the x-coordinates of the most radiative façades of *Building A* in the model, in the primary vertical axes the z-height of the sensors on the façade.



The results of set of simulations of the wall temperature of both optimized building (*Building A* and *Building B*), are reported in Table 50. Are presented the wall temperatures maps of most radiative façade of *Building A* in the solar optimized design scenario maintaining the existing green system of the district (*Current scenario*), without *Building B* in order to calculate its solar reflection influence on the *Building A* and in the scenario with green roofs set for all buildings that compose the entire district, the park in a district

and the tree-lined roads (*All green*). This latter scenario has been analysed in order to estimate the benefit of the vegetation in term of the wall temperatures' reduction.

Graph 19. Trends of average temperatures on the most radiative *Building A*'s façade in the different solar optimized scenarios analysed.



The wall temperatures maps in the Table 50 demonstrates that in this case the effect of solar reflection and the increment of temperature caused by *Building B* is lower than the actual design scenario, analysed previously. The increment of average temperature on the wall between *Current scenario* and *Without Building B* scenario is equal to 0.4°C. However the average temperature value in the *All Green* scenario confirm the benefit of the presence of vegetation: the façade' temperature reduction is about 2°C.

However the average temperatures on the façade result higher than the actual design scenario: it was predictable, given that the façade has the result of parametric transformations in order to obtain the most irradiative surface. Furthermore the modeling of the buildings, as was explained above, contributes to increase the wall temperature.

Graph 19 shows the trend of average temperature on the analysed façade in the different simulated scenarios. Regarding the *Without Building B* scenario and *Current* scenario the temperatures' trend is still similar than the others analysed in the parametric study and in the actual design scenario. It confirms one time more that the temperatures are very high at the ground level and decrease along the height of the building for the wind effect.

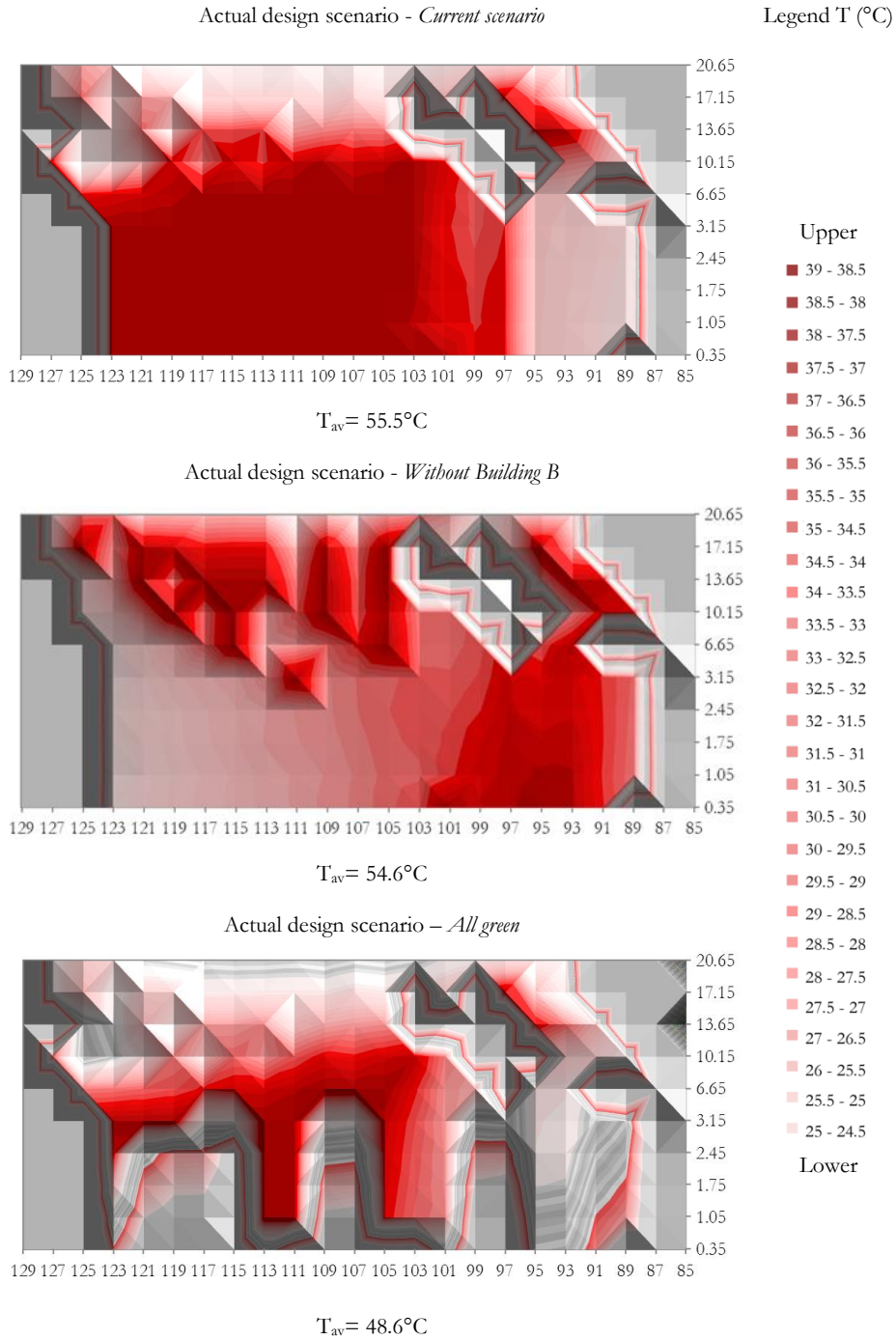
The *Current scenario* presents a very interesting trend of temperatures: in fact the values of average temperatures along the height of the *Building A* are higher than the scenario *Without Building B* until the 22 metres. These high differences at the bottom of the façade are caused only by the solar reflection coming from the *Building B* that consequently increase the wall temperatures. It is interesting to observe that the the temperature trend is almost the same after the *Building B*'s height in both scenarios.

Regarding the *All Green* scenario is better to underline that the general trend of the average temperatures demonstrates that the presence of vegetation on the ground level contributes for a relevant reducing of the wall temperature on the bottom part of the façade. In particular the shading effect reduces the wall temperatures until about 7°C in some points at the bottom of the façade, even if the average decrement of the temperature is more than 3°C until at a height 1.75 metres, about 1.5°C from the height 3.15 metres to 27.65 metres and about 1.00°C until at a height 50.00 metres. The average value of temperatures reduction considering the entire façade is about 1.9°C. The shift of the entire average temperature trend's line visible on the Graph 19, confirmed that the effect of vegetation is local for the highest values of reduction where the shading effect is strong but its benefit is global because the temperatures decrease along all height of the *Building A*'s façade.

However the most important aspect that this set of simulation demonstrated is that the vegetation limits the effect the wall temperatures' increment, rather it gets better the wall temperatures' values, reducing the global warming of the façade maintaining the same boundary condition in term of walls and roofs albedo and morphology of the district. As written above this aspect demonstrates one more time, how much is important the presence of vegetation in existing urban area and to its benefit on the wall temperatures in spite of the installation of solar systems on the façades.

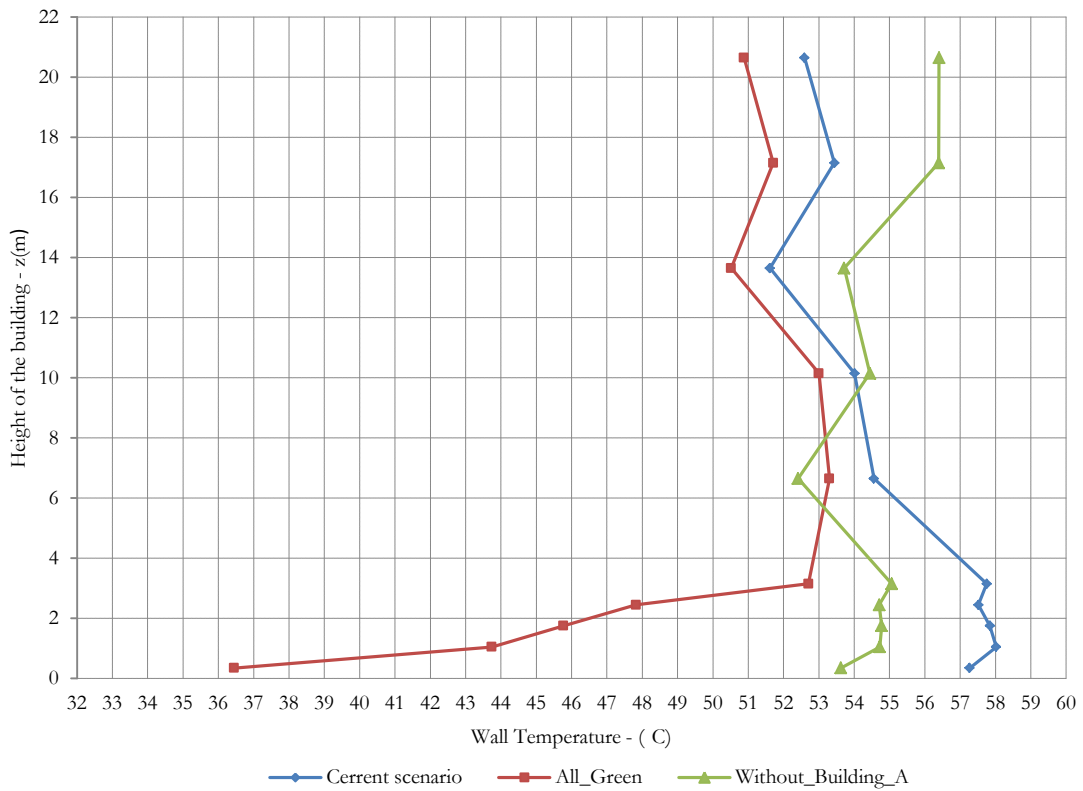
The same analysis has been done on the east façade of the *Building B*. Following are reported the results: the Table 51 collected the temperatures maps in the different scenarios analysed.

Table 51. Temperatures maps of Solar optimized design scenario - *Current scenario*, *Without Building A* and *All green*. In the primary horizontal axes the y-coordinates of the east facades of *Building B* in the model, in the primary vertical axes the z-height of the sensors on the façade.



The results reported in Table 51 show the wall temperatures maps on the most radiative façade of *Building B* in the solar optimized design scenario maintaining the existing green system of the district (*Current scenario*), *Without Building A* in order to calculate its solar reflection influence on the *Building B* and in the scenario with green roofs set for all buildings that compose the entire district, the park in a district and the tree-lined roads (*All green*).

Graph 20. Trends of average temperatures on the most radiative *Building B*'s façade in the different solar optimized scenarios analysed.



As in the actual design scenario, also in the solar optimized design scenario the average temperature on the façade is higher than the average temperatures measured on the most radiative *Building A*'s façade. Also in this case the values are high due to the solar reflection coming from the *Building A* that is exposed to exploit as solar radiation as possible on the most radiative façade and the configuration of design as a court that facilitates the mutual solar reflection especially on the *Building B*. However in this scenario the configuration of the two design buildings is such that the *Building A* reflects the rays of sunshine in different way respect to the actual design scenario. Nevertheless the average temperature on the façade arrived until 55.5°C in the current scenario. This results demonstrates that the average temperature is lower than the actual design scenario about to 1.1°C as summarized in Table 52.

In the wall temperatures maps presented in the Table 51 it underlines that the effect of solar reflection and the increment of temperature caused by *Building A* is clearly evident from the maps temperature of current situation, compares to others and it is equal about to 1°C.

The benefit of the presence of vegetation is relevant as confirmed the average temperatures' trend: the façade' temperature reduction is about 7°C respect to the *Current scenario* and about 6°C respect to the scenario *Without Building A*.

Graph 20 shows the trend of average temperature on the analysed façade in the different simulated scenarios. Some interest information can be deduced from the results of these analyses: already in the scenario *Without Building A* the temperatures' trend is different to the other scenarios. This fact is probably due to the orientation of the façade and the presence of other buildings in front of the analysed façade. In fact the trend shows that the temperature increases in the central part of the façade, where the solar radiation reflected from the others buildings comes. However the lower temperatures are again distributed on the top part of the building's façade where the wind speed contributes to decrease the temperatures. For this reason, as will show forward, the mutual configuration of the *Building A* and *Building B* create a Venturi effect that contributes to increase the wind speed between them and in particular on the buildings' walls.

The trend of average temperatures in the *Without building B* scenario, is extremely different than the other scenarios. In fact both, the *Current scenario* and the *All Green* scenario, present the same trend of average temperatures from height 7 metres until the top of the *Building B*. Regarding the *Current scenario* is interesting to underline that the difference of the temperature from the ground level (57.3°C) and the top (52.6°C) of the building is more than 5°C. Instead in *All Green* scenario the presence of the vegetation on the bottom of the building increases the difference from the temperature between the bottom (36.4°C) and the top (50.9°C), that is equal to 14.5°C. After the height of 7 metres, the trends of *Current scenario* and *All Green* scenario have an unusual trend due to the complex shape of the building.

This latter data represent the most important aspect of this set of simulation: has been demonstrated that the vegetation limits the effect the wall temperatures' increment, rather it gets better the wall temperatures' values, reducing the global warming of the façade maintaining the same boundary condition in term of walls and roofs albedo and morphology of the district.

Below in the Table 52 and Table 53 are summarized the results of two scenarios in order to compare the mutual interactions between the shape transformation of the building's volume and the presence of the "green system" in the district.

The results underline that the presence of the vegetation have a high benefit in terms of temperature's reduction in both scenarios and for both buildings as has been just discussed extensively above.

Regarding the *Building A*, as would be easily to expect, the average temperature on the most irradiative façade is higher in the solar optimized scenario, than in the design scenario: the difference between the two scenarios is more than 3.5°C in all scenarios (*Current, Without building B and All green*). This demonstrates that the optimized shape for installing the solar systems on the façade, increase the average wall's temperature considerably.

Table 52. Summary of the Building A average wall's temperature

Building and Scenario	Current scenario	Withou building B	All Green
Building A - Design scenario	$T_{av} = 41.1^{\circ}\text{C}$	$T_{av} = 40.2^{\circ}\text{C}$	$T_{av} = 38.8^{\circ}\text{C}$
Building A - Solar optimized scenario	$T_{av} = 44.7^{\circ}\text{C}$	$T_{av} = 44.3^{\circ}\text{C}$	$T_{av} = 42.7^{\circ}\text{C}$
$\Delta T$ [°C] (Solar optimized scenario-Design scenario)	3.6°C	4.1°C	3.9°C

This latter effect is not present on the *Building B*: in fact in this case the most irradiative façade has lower temperature in the *solar optimized scenario*, except for the scenario *Without building A*. This is caused by the turned shape of the building that projects the shadows on itself reducing the surface temperature on the façade.

Table 53. Summary of the Building B average wall's temperature

Building and Scenario	Current scenario	Withou building B	All Green
Building B - Design scenario	$T_{av} = 56.6^{\circ}\text{C}$	$T_{av} = 52.8^{\circ}\text{C}$	$T_{av} = 52.4^{\circ}\text{C}$
Building B - Solar optimized scenario	$T_{av} = 55.5^{\circ}\text{C}$	$T_{av} = 54.6^{\circ}\text{C}$	$T_{av} = 48.6^{\circ}\text{C}$
$\Delta T$ [°C] (Solar optimized scenario-Design scenario)	-1.1°C	1.8°C	-3.8°C

## **7.5. Conclusion and outcomes**

Regarding a parametric study on a simple model, one of interest development could comprehend simulation with different ratios between heights and widths characterized urban canyon.

In general vegetation can reduce wall and air temperature by direct shading of surfaces as well as by moderating solar heat gain through evapotranspiration of the plants, and conversion of incident solar radiation to latent heat.

Furthermore the reduction of temperatures lead to reduced long-wave radiation emitted from the ground and leaves, as opposed to the surrounding artificial hard surfaces, thus subjecting people to a reduced radiant load. In particular the microclimatic effect of trees is obtained through several processes:

- Shading effect reduces solar heat gains on windows, walls, and roofs;
- Reduction of the building long-wave exchange with the sky as building temperatures are lowered – through shading;
- Reduction of the conductive and convective heat gain by lowering dry-bulb temperatures through evapotranspiration during summer;
- Increase of latent cooling by adding moisture to the air through evapotranspiration.

Estimation of the decrease of ambient temperature, below the urban canopy, due to vegetation is therefore, critical [142].

The set of simulations that have been conducted underline the vegetation effects listed above. The presence of trees leads to cooler areas in the urban environment as the results of simulation shown. The park contributes significantly for reducing air temperature with three specific effects: vegetation shade, evapotranspiration and natural ventilation. The trees create a sort of screen for sun and wind and as a source of control the air temperature and the temperature of the surrounding surfaces. Density, shape, size and position of the trees in the urban space create different effects on the urban environment. Decrement of surface temperature that induces a lower air temperature can be explained by the mitigation of air temperature in the presence of tree [21].

These results are most important if it considers the installation of the solar systems on the façades and their tight relation with the operative temperature on them.

In one of the deliverables published in the Subtask A of the IEA-SHC Task 41 “Solar Energy and Architecture” were collected the solar systems product available in the market nowadays [88].

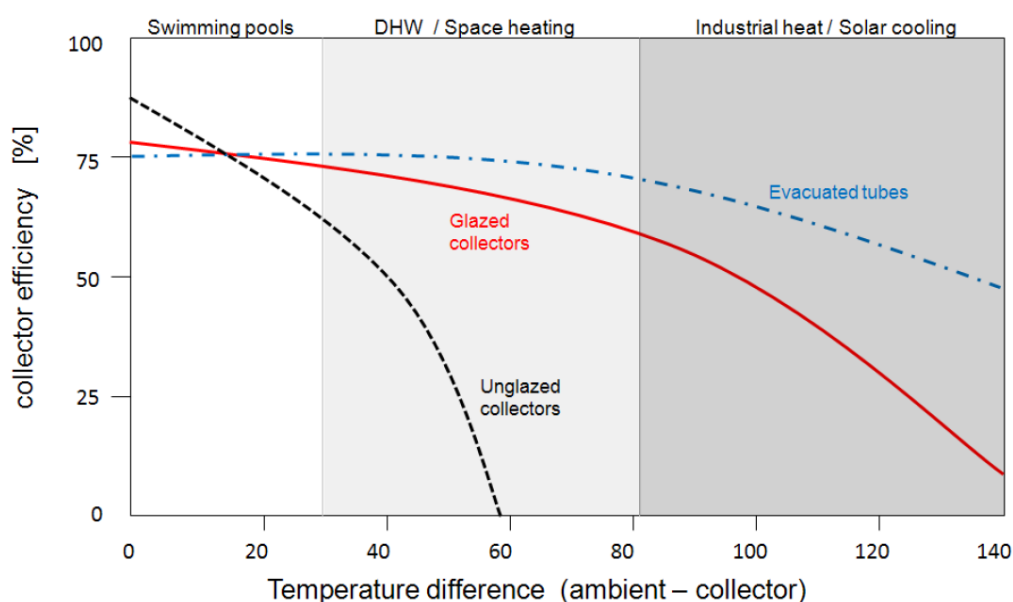
The solar thermal technologies available are divided in passive (that store the gains in the building mass itself) and active (on the surfaces optimized for heat collection placed on the outside of the building envelope) systems and among this latter type of technology two main families can be identified according to the medium used for the heat transport: air collectors systems and hydraulic collectors systems. While

the air systems are characterized by lower costs, but also lower efficiency mainly due to air low thermal capacity, the hydraulic ones represent the bulk of solar thermal systems for buildings and they allow an easy storage of solar gains and are suitable both for domestic hot water (DHW).

The hydraulic solar thermal systems are distinguished into three technologies:

- Evacuated tubes collectors;
- Glazed flat plate collectors;
- Unglazed flat plate collectors.

Graph 21. Comparison of the different solar thermal technologies relevant for DHW and space heating production in relation to their efficiency, cost, specific working temperatures, suitable applications.



In the Graph 21 is shown the efficiencies and favored application domains of three different technologies, as a function of the temperature differences between the collector and the ambient air.

In particular from that graph is interesting to underline that the characteristics of these systems depend on the working temperature:

- Glazed flat plate collectors: used for DHW production and space heating, are the most diffused in the EU. Their usual working temperatures are between 50°C and 100°C, but they can rise up to more than 150°C in summer. Therefore, measures should be taken to avoid overheating risks which can damage sensible parts as rubber jointing for instance.;
- Unglazed flat plate collectors: are used for swimming pools, low temperature space heating systems and DHW pre-heating. They are composed of a selective metal plate (the absorber) and a hydraulic

circuit connected to this absorber. When used for DHW or space heating they also need a back insulation, but differently from glazed collectors, the front part of the absorber is not insulated by a covering glass. Consequently, working temperatures are lower, reaching 50-65°C. When used for swimming pool water heating, the back insulation is not needed. For this specific application, polymeric absorbers can also be used to replace the more performing -and more expensive selective metal plates (most often black polymeric pipes systems).

- Evacuated-tube collectors: Evacuated tubes are especially recommended for applications requiring high working temperatures such as industrial applications and solar cooling, but are also used for domestic hot water (DHW) production and space heating, particularly in cold climates. They are composed of several individual glass tubes, each containing an absorber tube or an absorber plate bound to a heat pipe, surrounded by a vacuum. The very high insulation power of the vacuum allows reaching very high temperatures (120-180 °C) while keeping losses to a minimum even in cold climates.

In order to maintain the temperature of the module as low as possible, it is important not to have the module in direct contact with another surface. Ventilation allows avoiding overheating of the module and can enhance the PV efficiency.

In fact, when PV modules are not ventilated, their temperatures can reach up to 70°C leading to a system efficiency reduction up to 25%.

## **8. Qualitative microclimate analysis: air temperature, leaf temperature and wind speed on the facades**

### *Questions of the chapter*

1. How the vegetation can give a benefit in term of air temperature in a district?
2. How is the wind speed on the façades and in the urban canyons?
3. How the vegetation can affect the wind speed?

### *Abstract*

After second war world the urban areas are dramatically expanded very fast and faster than the previous evolutionary periods. Nowadays the modern cities are spread, are characterized by many different finishing materials, types of structures and the general lack of vegetation have altered their climatic peculiarities [143].

These changes affect directly on the local climate of urban spaces, in particular the central parts of the city, increasing the urban temperature that creates a typical phenomenon of urban heat island.

This creates unpleasant local climatic conditions as well as could be very dangerous for human health especially in the cities with a very hot season [144] [145].

The lack of vegetation in existing urban areas is one of the most important factors that influence the increment of urban temperatures. However it is possible to find the appreciable presence of vegetation in the parks or recreational spaces. In spite of their presence can mitigate the temperatures within their vicinity [61] [146] [120] [147], they can't thermally affecting on the urban areas characterized by high density where the people live, work and spend most part of their life.

The distribution of vegetation within the built space of the urban fabric, can decrease the values of temperatures also in the urbanized area far from the parks. In fact the trees-lined road, spaces with grass, parks and also the green wall and roofs, could easily alter the microclimate of the built environment as well as the local climate of the city. The benefit of the vegetation on the decrement of urban temperature also depends on the climatic characteristics, the amount of vegetation and urban geometry [143].

A high-resolution numerical model set with a microclimate three-dimensional non-hydrostatic urban climate model, *ENVI-met* [120], was used in order to evaluate the effect of introducing vegetation in a district, as lined-trees roads, grass areas and green roofs.

Results present the effect on the most irradiative day in the case study in a medium density area of the city of Milan. The analysis show which is the benefit of the addition of vegetation in term of reduction of surface temperatures, mean radiant temperatures, air temperatures, leaf temperatures and wind speeds on the façades and in the urban canopies.

## **8.1. Introduction**

Trees and soil influenced the atmosphere of the places where we live, especially in the urbanized areas. When the vegetation is removed and substituted with buildings and paved surfaces, the energy balance near the earth's surfaces changes: less solar radiation can be dissipated in the form of latent heat rather than sensible heat [148] [149]. The vegetation areas create a higher level of latent heat exchanges, while the large presence of impervious areas increases the sensible heat exchanges and consequently the increment of temperatures [150]. Furthermore the surface materials, characterized by physical thermal properties, as heat capacity, thermal conductivity and inertia, have a high influence on the interaction between surface temperatures and operative temperatures perceived by the human body. The thermal effects vary with soil type and its moisture content [151], and the emissivity of soils that is a function of moisture conditions, and soil density [152]. In these conditions the rising of temperatures represent one of the most important factors to the urban heat island effect.

In the high and medium density urban areas, the built environment contributes to increase the temperatures and the roofs, commonly covered by dark finishing materials, constitute the surfaces where is mainly concentrated the absorption, reflection and emission of solar radiation.

In this scenario the use of roofs' surfaces could be the only practicable way to give back the green spaces to the cities and reduce the energy consumptions and building's energy demands as well as improve the inhabitants comfort indoor [153]. All energy balance of the district and of the whole city can improved through adding more evaporating surfaces [149].

Many examples have studied the impact of vegetation on urban climates and it has been demonstrated that its benefit improved thermal comfort, in particular in hot dry climates [153] [154] [155]. Furthermore large-scale analysis has been shown the reduction of urban heat island's effect and also a lot of studies describe the micro-climatic effect of green roofs [156] [157] [158]. It is also clear that the application of green roofs in a large scale could reduce the ecological footprint of the cities [148].

Furthermore the increment of heating in the city changes the movement of wind, humidity and rain.

This chapter gives an overview regarding the problem of thermal stress at the ground level, with micro-climate analysis extracting the data of surface temperature, mean radiant temperature, potential temperature, leaf temperature and wind speed on the façades and in the urban canyon.

The analysis are conducted in a medium density district of the city of Milan where, respect to the current scenario, has been improved the "green system" (*All Green* scenario), creating an "oasis effect" in order to mitigate the urban warming at macro and micro level.

The final aim is to provide a new design approach for urban planning in order to minimize or decrease the micro-climate exterior thermal stress and to guarantee a comfort condition for pedestrians at the ground level, as well as some considerations on the vegetation' benefit on the urban heat island's mitigation.

## **8.2. Material and method**

Some studies of urban microclimate analysis, using *ENVI-met* model, simulated the effect of different design areas, considering in temperature and thermal comfort. Different ratios of height/width, called urban canyon, have been studied: the results demonstrated that the daily maximum temperature decreases with the increase in the ratio height/width [159]. The distribution of green areas and street orientation can influence the urban geometry and thermal comfort, decreasing or increasing the temperatures and the wind flow [160].

Other case studies evaluated the attenuation of solar radiation by different species of trees and the thermal comfort provided by trees [161] [162] as well as the thermal comfort in urban space in the city, which were defined areas of comfort with data of dry bulb temperature and wet bulb. The areas with vegetation were shown to be thermally comfortable compared to those without vegetation [163].

Many other studies have demonstrated that regarding the urban geometry and the width of the urban canyon, the benefit coming from the installation of the green roofs and green walls on temperature decrement is weak and the green walls have a stronger effect than the green roofs inside the urban canyon. However the green roofs have a greater effect at the roof level as well as at the urban scale. The combination of the benefits of the green walls and roofs permit the highest mitigation of temperatures inside the canyons [143]. In previous chapter have already been reported some results on the benefits of the green roofs at the roof level and in this chapter are presented some other results that consider the combination of green roofs and lined-trees road on the temperatures' mitigation of the urban canyon as well as on the wind speed.

Finally there are also examples where are compared the thermal comfort onto two areas of a city, characterized by different construction and vegetation density. With *ENVI-met* have been calculated the thermal comfort index PMV (Predicted Mean Vote) and medium radiant temperature and marked out the vertical profiles of air temperature and wind speed [132].

It is decided to analyse and present the data for the case study of the city of Milan presented in the chapter 5. It's more interesting and useful studying the effects of the vegetation in a real case study for giving a new design approach for planner and architects. In fact the case study has been simulated in two different scenarios: the current scenario (Figure 93), that considers the entire district with the new actual design of the *Building A* and *Building B*, and the *All Green* scenario (Figure 94), that considers that same geometry of the district setting the green roofs on the top of all buildings and inserting some lined-trees road and grass areas.

The choice to consider the entire district has been done for analysing the global effect of the vegetation on the mitigation of urban heat island. In fact if considers the installation of green roof only in one block, green roofs can give a small local benefit in term of temperature decrement, while applying the

green roofs on the whole city scale, they create a global mitigation's effect that reduces considerably the urban temperature until to achieve energy saving for cooling buildings from 32% to 100% [143].

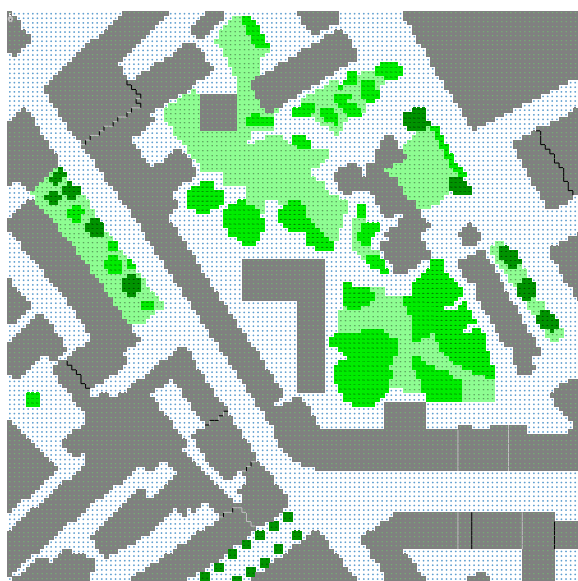


Figure 93. *Current scenario* - Area model created in *ENVI-met*. In grey the buildings, in pale green the grass, in shade of green the trees (light green for trees of 10 m, dark green for trees of 15 m)



Figure 94. *All Green scenario* - Area model created in *ENVI-met*. In grey the buildings, in pale green the grass, in shade of green the trees (light green for trees of 10 m, dark green for trees of 15 m): visible the huge grass area and lined-trees road

Regarding the presence of tree in then green spaces and in particular in the lined-tree roads a presence of single tree can already mitigate the climate, but its benefit is limited to the local microclimate [164]. Large green areas, as parks, can extend the positive effects to the whole district or city.

From microclimate simulation have been extracted the data of thermal index as surface temperatures, mean radiant temperatures, potential temperatures in order to calculated operative temperatures for giving an evaluation of thermal comfort at the pedestrian level.

Also the wind flow data are carried out from the simulations in order to analyse the wind speed in the urban canyon and the wind profile on the façades onto two scenarios presented above. These kinds of analysis were useful to estimate the comfort at the pedestrian level and to evaluate the wind benefit in term of temperatures' reduction on the façades.

All simulations were conducted by a three-dimensional non-hydrostatic urban climate model, *ENVI-met* 3.1 version [120], setting the same parameters used for the analysis presented in the chapter 5.

The maps and the results were extracted using Leonardo 3.75 version and Extract *ENVI-met* Data. All simulations and results have been done in order to analyse whether the vegetation distributed in the district can be used to tackle the heat island effect, depending on all these parameters taken into consideration.

### 8.3. Results and discussion

In the following pages are presented the results extracted for the simulations using the graphic server Leonardo 3.75 version. From the analysis have been derived the distribution on the horizontal plane of the district, the values of surfaces temperatures, mean radiant temperatures, potential temperatures and leaf temperatures.

Furthermore the wind speed in the urban canyons and the vertical wind profiles on the façades of the designed building (*Building A* and *Building B*) have been analysed.

All simulations have been done in two different scenarios: current scenario and *All Green scenario* on the most irradiative day of the year, carried out from the previous solar radiation analysis and presented in the chapter 4.

#### 8.3.1. Distribution of surface temperatures

Data of surface temperatures at the ground level (height equal to 2 m) have been extracted in order to calculate the global average surface temperature in both scenarios. This data is very useful for calculating the operative temperatures of the most interesting parts of the district.

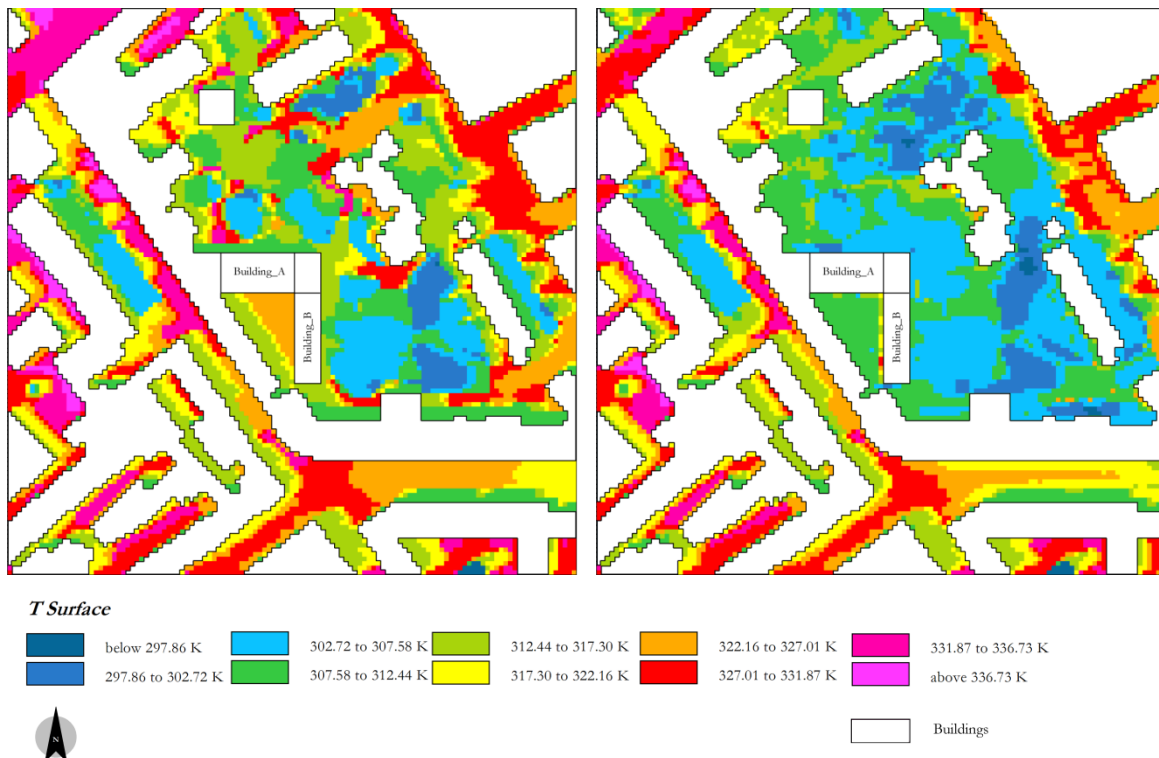


Figure 95. *Current scenario*: horizontal section at ground level, surface temperatures at 3:00 p.m. on the 16th of June

Figure 96. *All\_Green scenario*: horizontal section at ground level, surface temperatures at 3:00 p.m. on the 16th of June

Above are presented the surface temperatures' maps of the two scenarios at 3:00 p.m., when temperatures were resulted higher and the global solar radiation has the highest value.

The results of the entire district with actual design of *Building A* and *Building B* in the current scenario, show that the highest surface temperature is registered on asphalt in the area located on the top left angle of the Figure 95 and is equal to 68.44 °C (341.59 K), while the lowest surface temperature is registered on the vegetation area behind the *Building B* and is equal 24.63 °C (297.78 K).

The average surface temperature in the entire district is equal to 46.19 °C (319.34 K).

However all these values could be considered as representatives of real surface temperatures' values because they didn't consider the thermal capacity of the soil: the heat in fact can be accumulated and transferred to the atmosphere with thermal and wavelength's phase shift. This effect is more incident, considering asphalt that has a thermal conductivity equal to 920 J/KgK, and the dry soil equal to 800 J/KgK. Furthermore the vegetation has been considered as obstacle of solar radiation. In spite of this limitation the calculated values these values are representatives of surface temperatures and will be used for calculating the operative temperatures, which are characteristics of a qualitative analysis of thermal comfort at pedestrian level.

The results of the entire district with actual design of *Building A* and *Building B* in the *All Green* scenario, show that the highest surface temperature is registered on asphalt in the area located on the top left angle of the Figure 96 and is equal to 67.52 °C (340.67 K), while the lowest surface temperature is registered on the vegetation area behind the *Building B* and is equal 23.91 °C (297.06 K).

The average surface temperature in the entire district is equal to 41.88 °C (315.03 K).

The results demonstrated that the *All Green* scenario present lower surface temperature than the current scenario: the difference of average surface temperature onto two scenarios, calculated during the day that the solar radiation is highest, is equal to 4.28 °C. Therefore the results demonstrated that the benefit of vegetation is high and permit a considerable decrement of the average surface temperature of the entire district.

The last analysis was considered the court in front of *Building A* and *Building B* in order to calculate the average surface temperature: it is equal to 47.8 °C (320.95 K) in the current scenario (asphalt soil), while equal to 37.88 °C (311.03 K) in the *All Green* scenario (grass soil): the difference is equal about 10 °C.

It is better to underline that, as has been written above, weren't considered the thermal conductivity of different technical solutions and finishing materials of soil and the results could be under estimated.

### **8.3.2. Distribution of mean radiant temperatures**

The distribution of mean radiant temperatures at the ground level (height equal to 2 m) in both scenarios has been extracted and analysed always at 3:00 p.m., when the values were resulted higher and

the global solar radiation has the highest value. The mean radiant temperature is the average effect of radiation from surrounding surfaces. At the center of the room this temperature can be taken as being equal to the mean surface temperature.

Also these data contribute for calculating the operative temperatures of the most interesting parts of the district.

Below are presented the mean radiant temperatures' maps in two analysed scenarios (Figure 97 and Figure 98).

The results of the entire district with actual design of *Building A* and *Building B* in the current scenario, show that the highest mean radiant temperature is registered on asphalt in the area located on the top left angle of the Figure 97 and is equal to 83.42 °C (356.57 K), while the lowest surface temperature is registered on the vegetation area behind the *Building B* and is equal 30.18 °C (303.33 K).

The average surface temperature in the entire district is equal to 57.33 °C (330.48 K).

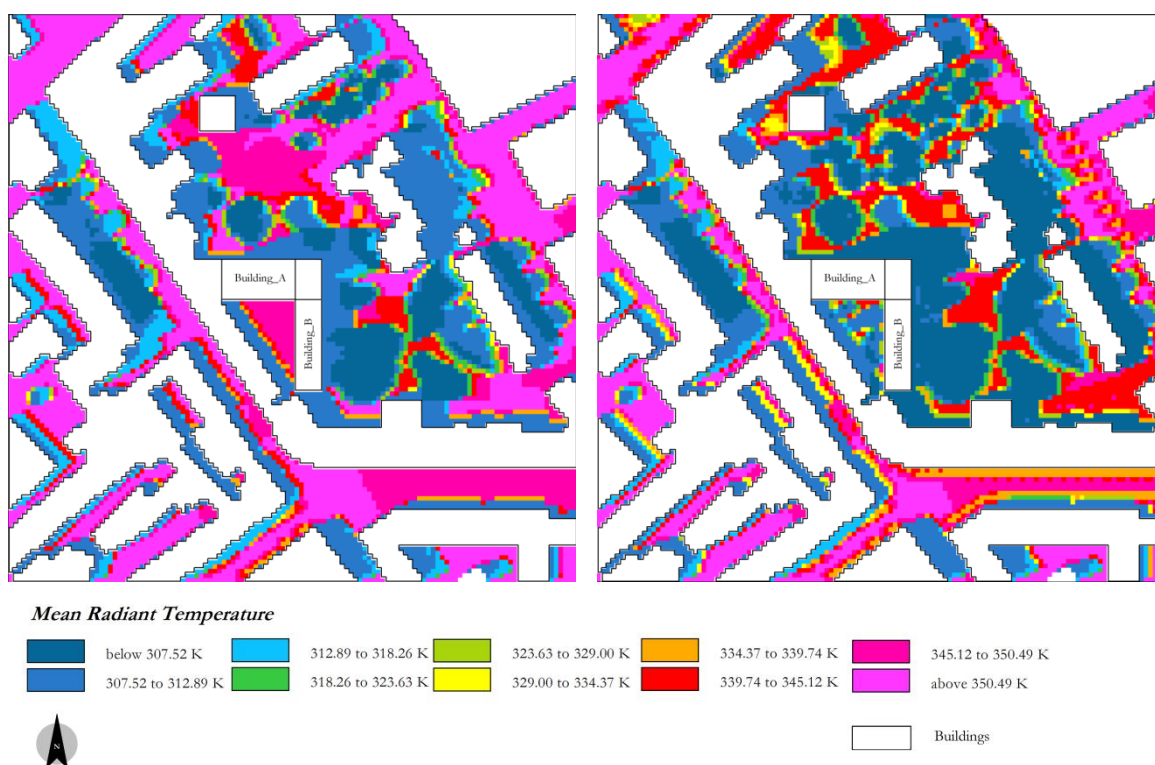


Figure 97. *Current scenario*: horizontal section at ground level, mean radiant temperatures at 3:00 p.m. on the 16th of June.

Figure 98. *All\_Green scenario*: horizontal section at ground level, mean radiant temperatures at 3:00 p.m. on the 16th of June

The results of the entire district with actual design of *Building A* and *Building B* in the *All Green* scenario, show that the highest mean radiant temperature is registered on asphalt in the area located on

the top left angle of the Figure 98 and is equal to 82.73 °C (355.88 K), while the lowest surface temperature is registered on the vegetation area behind the *Building B* and is equal 29.01 °C (302.16 K).

The average surface temperature in the entire district is equal to 52.67 °C (325.73 K).

The results demonstrated that the *All Green* scenario present lower surface temperature than the current scenario: the difference of average surface temperature onto two scenarios, calculated during the day that the solar radiation is highest, is equal to 4.66 °C. Therefore the results demonstrated that the benefit of vegetation is high and permit a considerable decrement of the average surface temperature of the entire district.

The last analysis was considered the court in front of *Building A* and *Building B* in order to calculate the average surface temperature: it is equal to 61.16 °C (334.31 K) in the current scenario (asphalt soil), while equal to 41.06 °C (314.21 K) in the *All Green* scenario (grass soil): the difference is equal about 20 °C.

The knowledge of the values of mean radiant temperature is fundamental for the operative temperatures' calculation. This latter physical magnitude is an index of the people comfort that live in this area and in particular for the new inhabitant that will live in the *Building A* and *Building B*.

After the presentation of the potential temperatures in the district, treated below, will be calculated the average operative temperature of the district and onto the court in front of designed buildings.

### **8.3.3. Distribution of potential temperatures**

Other important data regarding many microclimate aspects are possible to extract from *ENVI-met* analysis. For these types of analyses among other data, the air temperature and wind speed at the ground level in order to analyse the microclimate conditions have been analysed. The data of potential temperatures and wind speed have been analysed.

The calculation of air temperature started from the POTs onto the two scenarios. The potential temperature is defined as the temperature that an unsaturated parcel of dry air would have if brought adiabatically and reversibly from its initial state to a standard pressure,  $P_0$ , typically 100 kPa. Its mathematical expression is:

$$\theta = T \frac{P_0}{P}^k \quad \text{eq. 40}$$

Where:

- $\theta$  is the potential temperature [K];

- $T$  is air temperature at pressure  $P$ [K];
- $P$  is initial pressure;
- $k$  is the Poisson constant equal to 0.286 for dry air.

The potential temperature is more important than the real temperature of the air, from the dynamic point of view. This is because it doesn't affect by vertical displacements associated with the flux in turbulent area or around obstacles. A parcel of air that moves over a small mountain expands and cools during the ascent phase, while heats and compresses it during the descent phase and its potential temperature doesn't change if any external factors involve in the process, as evaporation and condensation.

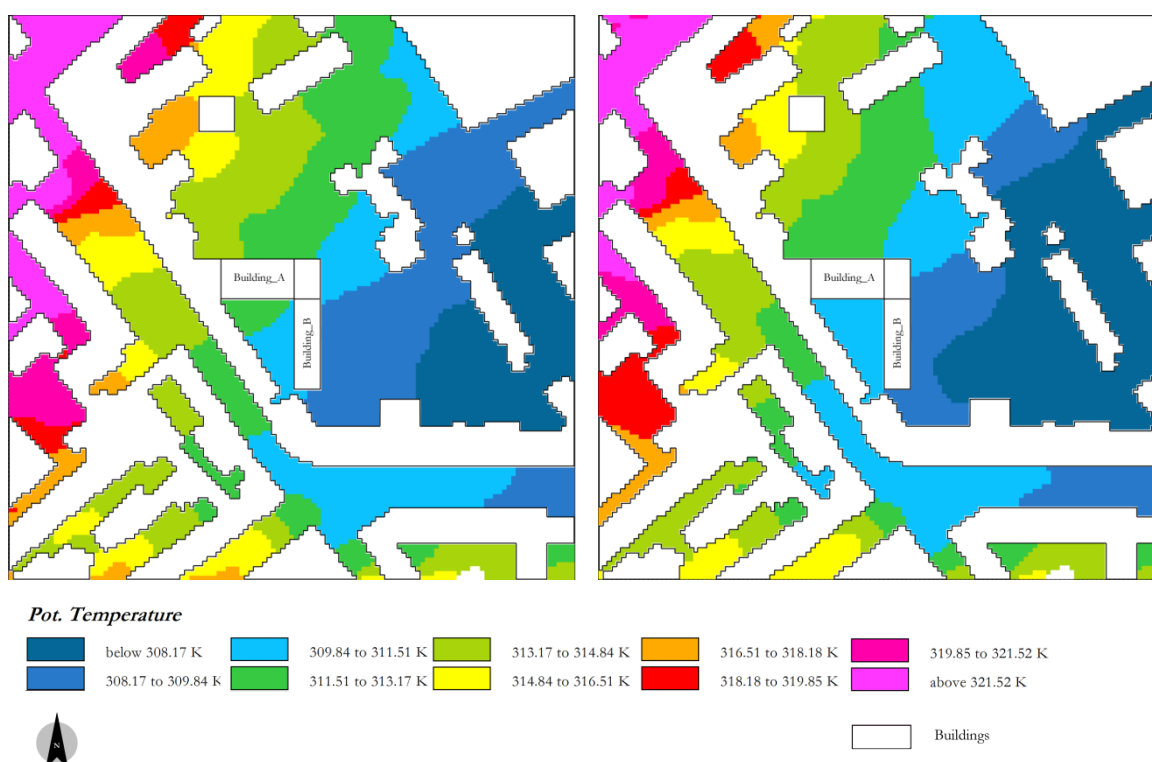


Figure 99. *Current* scenario: horizontal section at ground level, potential temperatures at 3:00 p.m. on the 16th of June.

Figure 100. *All\_Green* scenario: horizontal section at ground level, potential temperatures at 3:00 p.m. on the 16th of June

The potential temperature is a physical magnitude especially used in the meteorological field in order to estimate the potential convective instability.

From the analyses, values of potential temperature from a specific area of the district have been extracted: in particular the values of the court in front of the *Building A* and *Building B* and the POT's average value of entire district.

Figure 99 and Figure 100 show that the distribution of potential temperatures is influenced by the vegetation. The values in legend are expressed in Kelvin because Leonardo doesn't permit to change the unit. In fact from the POT's map is visible the mitigation of urban heat island's effect: the warmer zones in the *All Green* scenario moved far from the central of the district and reduce their POT respect to the current scenario. For example in the court in front of *Building A* and *Building B* the average POT is equal to 38.28 °C (311.43 K) in the current scenario (asphalt soil), while equal to 37.32 °C (310.47 K) in the *All Green* scenario (grass soil): the difference is equal about 1 °C. In the current scenario the highest value in the court is equal to 39.28 °C (312.43 K), while the lowest is equal to 37.74 °C (310.89 K). In the *All Green* scenario the highest value in the court is equal to 38.47 °C (311.62 K), while the lowest is equal to 36.9 °C (310.05 K).

Furthermore the presence of the green system contributes to reduce the average POT of the entire district: that is equal about to 39.7 °C (312.85 K) in the current scenario, while is equal to 38.91 °C (312.06 K) in the *All Green* scenario: the difference is equal about 0.8 °C.

The difference from the hottest area and the lowest is about  $\Delta T = 17.6$  °C in the current scenario and  $\Delta T = 16.7$  °C in the *All Green* scenario. The highest temperature is equal to 51.6 °C (324.75 K) in the current scenario and equal to 50.04 (323.19 K) in the *All Green* scenario, the lowest one is equal to 34.02 °C (307.17 K) in the current scenario and equal to 33.34 °C (306.49 K) in the *All Green* scenario.

These results, reported in the Table 54, confirmed which has been written above: the presence of vegetation mitigates the effect of urban heat island and contributes to move the warmer area far from the "green central" of the district.

The results in term of air temperature using the eq. 40 are summarised in the following table:

Table 54. Values of entire district's air temperatures in the current scenario and *All Green* scenario

Data calculated	Current scenario [°C]	All Green scenario [°C]	$\Delta T$ [°C]
Average air temperature	40.87	40.08	0.79
Highest temperature	52.82	51.25	1.57
Lowest temperature	35.17	34.5	0.67

It's better to underline that the results have been calculated setting the model with the worse conditions, and certainly the values of average POT should be lower if it will be possible to simulate the district distinguishing the value of walls and roofs albedo when *ENVI-met* will permit this setting. However the decrement, equal about to 0.79 °C, will be always the same, because the benefit is given only by the presence of the vegetation, maintaining the same other setting parameters.

The highest air temperature is registered in the area located on the top left angle of the district and is equal to 52.82 °C in the current scenario, while the lowest air temperature is registered on the vegetation area behind the *Building B* and is equal 34.5 °C in the *All Green* scenario.

The difference from highest temperatures in the two scenarios is equal to 1.57 °C, while the difference from lowest temperatures in the two scenarios is equal to 0.67 °C.

Regarding the air temperatures in the court in front of the *Building A* and *Building B*, were reported the results in the Table 55.

The results demonstrated that the decrement of the average temperatures in two scenarios is equal about to 1°C.

The highest air temperature is registered in the court is equal to 40.45 °C in the current scenario, while the lowest air temperature is equal to 38.06 °C in the *All Green* scenario.

The difference from highest temperatures in the two scenarios is equal to 0.81 °C, while the difference from lowest temperatures in the two scenarios is equal to 0.85 °C.

Table 55.Values of air temperatures in the court in front of *Building A* and *Building B* in the current scenario and *All Green* scenario.

Data calculated	Current scenario	All_Green scenario	ΔT [°C]
Average air temperature [°C]	39.45	38.49	0.96
Highest Temperature [°C]	40.45	39.64	0.81
Lowest Temperature [°C]	38.91	38.06	0.85

### 8.3.4. Calculation of operative temperatures

The operative temperature is an index of people comfort, which live in the analysed district. The operative temperature ( $t_0$ ) is defined as a uniform temperature of a radiantly black enclosure in which an occupant would exchange the same amount of heat by radiation plus convection as in the actual non uniform environment.

In design, operative temperature is defined from the combination from the mean radiant and ambient air temperatures, weighted by their respective heat transfer coefficients.

$$t_0 = \frac{h_c t_a + h_r t_{mr}}{h_c + h_r} \quad \text{eq. 41}$$

Where:

- $t_a$  is the air temperature [°C];
- $t_{mr}$  is the mean radiant temperature [°C];

- $h_c$  is the convective heat transfer coefficient [ $\text{Wm}^{-2}\text{K}^{-1}$ ];
- $h_r$  is the linear radiative heat transfer coefficient [ $\text{Wm}^{-2}\text{K}^{-1}$ ].

$$h_r = \varepsilon \cdot h_{r0} \quad \text{eq. 42}$$

$$h_{r0} = 4 \cdot \sigma \cdot T_m^3 \quad \text{eq. 43}$$

Where:

- $\varepsilon$  is the emissivity of the surface (0.9 asphalt) (0.82 soil dry)[ad];
- $h_{r0}$  is the radiative coefficient of the black block's surface [ $\text{Wm}^{-2}\text{K}^{-1}$ ];
- $\sigma$  is the Stefan-Boltzmann's constant ( $5.67 \cdot 10^{-8}$ ) [ $\text{Wm}^{-2}\text{K}^{-1}$ ];
- $T_m$  is the average surface temperature of the area [K].

For the external surfaces:

$$h_c = 4 + 4v \quad \text{eq. 44}$$

Where:

- $v$  is the wind speed [ $\text{ms}^{-1}$ ].

The values were extracted from the *ENVI-met* atmosphere's data: average wind speed in the entire district in the current scenario is equal to about 0.7 m/s, while in the *All Green* scenario is equal to about 0.0 m/s, as predictable. In the court in front of the *Building A* and *Building B* the values of wind speed is equal to about 0.65 m/s in the current scenario, while equal to about 0.0 m/s.

From the previous results, with the mean radiant and air temperatures of the district, were calculated the operative temperature summarized in the Table 56.

Table 56. Values of entire district's average operative temperatures in the current scenario and *All Green* scenario

Data calculated	Current scenario	All_Green scenario	$\Delta T$ [ $^{\circ}\text{C}$ ]
$t_{mr}$ [ $^{\circ}\text{C}$ ]	57.33	52.67	4.66
$t_a$ [ $^{\circ}\text{C}$ ]	40.87	40.08	0.79
$t_0$ [ $^{\circ}\text{C}$ ]	49.00	46.27	2.73

Table 57 reported the operative temperatures' values of the court in front of *Building A* and *Building B*.

Table 57. Values of average operative temperatures in the court in front of *Building A* and *Building B* in the current scenario and *All Green* scenario.

Data calculated	Current scenario [°C]	All_Green scenario [°C]	$\Delta T$ [°C]
$t_{mr}$ [°C]	61.16	41.06	20.01
$t_a$ [°C]	39.45	38.49	0.96
$t_0$ [°C]	53.07	39.98	13.09

Where:

- $t_{mr}$  is the mean radiant temperature (average value) [°C];
- $t_a$  is the air temperature (average value) [°C];
- $t_0$  is the operative temperature (average value) [°C].

The results show that the difference between the operative temperatures in two scenarios is equal to 2.73 °, considering the entire district, while whether considering only the court in front of *Building A* and *Building B* the difference arrives until 13.09 °C. This latter result is very significance because gives an important guideline for the design: in fact the presence of the vegetation in the court produces a high benefit in term of thermal comfort.

### 8.3.5. Distribution of leaf temperatures

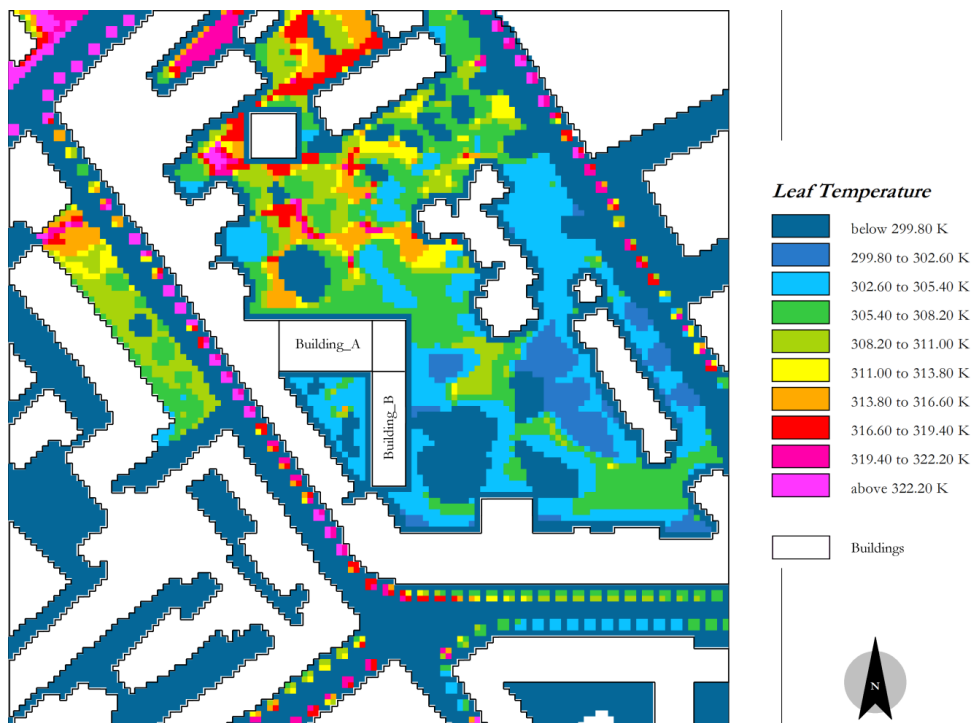


Figure 101. *All Green* scenario: horizontal section at ground level, leaf temperatures at 3:00 p.m. on the 16th of June

In this section of the study are calculated the distribution of leaf temperatures or surface temperature of leaf in the court in front of *Building A* and *Building B*, using Leonardo 3.75 version and Extract *ENVI-met* Data, in order to calculated the influence of evapotranspiration of the vegetation.

The evapotranspiration is the sum of evaporation and plant transpiration from the Earth's land surface to atmosphere. The knowledge of the leaf temperature is very important in order to calculate the heat exchange from the vegetation and the atmosphere and furthermore because the wind is influenced by leaf temperature.

The comparison was done in the *All Green* scenario, on the 16<sup>th</sup> of June at 3:00 p.m, considering the surface temperatures calculated previously and the leaf temperatures extracted.

The Figure 101 shows the map of leaf temperatures' distribution in the entire analysed district in the *All Green* scenario.

Table 58. Comparison from the average surface and leaf temperature in the court in front of *Building A* and *Building B* in the *All Green* scenario.

Average surface temperature [°C]	Average leaf temperature [°C]	$\Delta T$ [°C]
37.88	28.6	9.28

The result underlines that the influence of evapotranspiration in the court is equal to 9.28 °C.

### 8.3.6. Distribution of wind speed in the urban canyons

Regarding the wind data were analysed the wind speed in the urban canyons in order to estimate how the wind speed could change thanks to the vegetation effect. The data were extracted at the ground level (height equal to 2 m) always from the two scenarios previously presented: current and *All Green* scenario.

It is better to remind the data input set for running the simulations: wind speed at 10 m height equal to 2.5 m/s, west/south-west wind direction, roughness length 0.8.

Below are presented the maps of the wind speed vectors in both scenarios. It has decided to analyse two areas underlined in the maps: the court in front of the *Building A* and the *Building B* and one urban canyon on the bottom right in the map.



Figure 102. Current scenario: horizontal section at ground level, wind speed vectors at 3:00 p.m. on the 16th of June

In the Figure 102 are underlined the area that were analysed in detail in order to study the effect of the vegetation on the wind speed.

As just presented before in the calculation of operative temperatures, the wind velocity, in the court in front of the *Building A* and *Building B*, is equal to about 0.0 m/s. This data underlines that the morphology

of the district and the actual design of the new buildings creating a close space don't permit the wind to have any benefit on the thermal comfort and on the temperature of the façades.

The same situation is present in the *All Green* scenario, as it is possible to see in the wind speed vectors presented below.

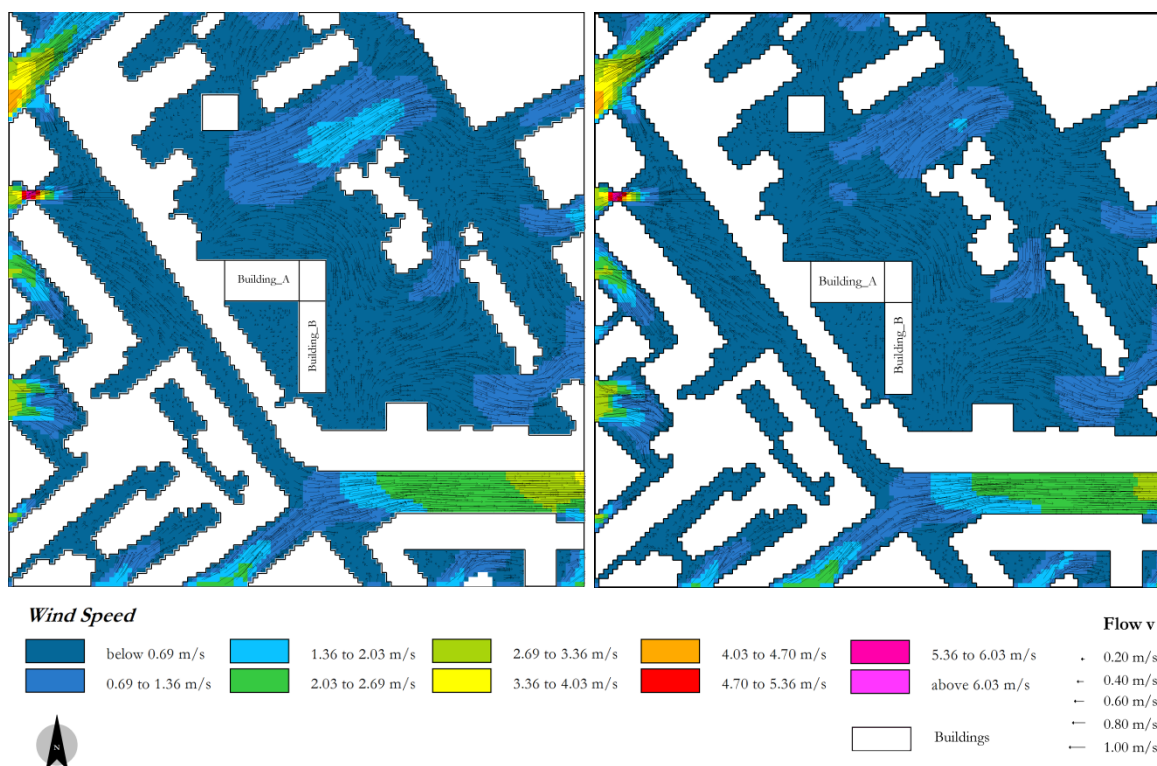


Figure 103. *Current* scenario – Wind speed and wind vector map analysis at level 2.0 m on the 16<sup>th</sup> of June at 3:00 p.m.

Figure 104. *All Green* scenario - Wind speed and wind vector map analysis at level 2.0 m on the 16<sup>th</sup> of June at 3:00 p.m

Regarding the wind speed in the urban canyon were analysed the wind data extract from the microclimate simulation done in *ENVI-met*.

The analysis wants to investigate whether the lined-trees road has lower values of wind speed than the road without trees

The values extracted demonstrated that the average wind speed in the current scenario along the area indicated in red on the map, is equal to 2.5 m/s (height equal to 2 m) , while in the *All Green* scenario, characterized by the lined-trees road with trees of 15 m and light crown is equal to 2,25 m/s. Therefore the reduction of wind speed is equal to 10% thanks to the presence of trees along the street.

Another type of analysis was conducted on the current and the optimized scenario in order to analyse the wind speed between of the *Building A* and *Building B* at different levels.

In fact while in the current scenario the two designed buildings are perpendicular each other along the height, in the solar optimized scenario, the solar optimization has created a space between the *Building A* and *Building B*. This analysis is important for studying the wind speed created by the solar optimization and its direction respect to the façade and have some data for depth analysis to combine the wind actions with the temperatures on the façade.

The analysis was conducted extracting the maps of wind speed from Leonardo 3.75 version: the values of wind speed and wind vectors are reported of the legend. It would have been possible to extract the values using Extract *ENVI-met* Data. However the different configuration of the analysed areas and the continuous changing of buildings orientation in the solar optimised scenario, suggested using Leonardo tool for elaborating the data.

Below are presented the comparison maps of the wind speed for current and solar optimised scenario at different levels on the 16th of June at 3:00 p.m. The maps were extracted until to *Building B*'s height.

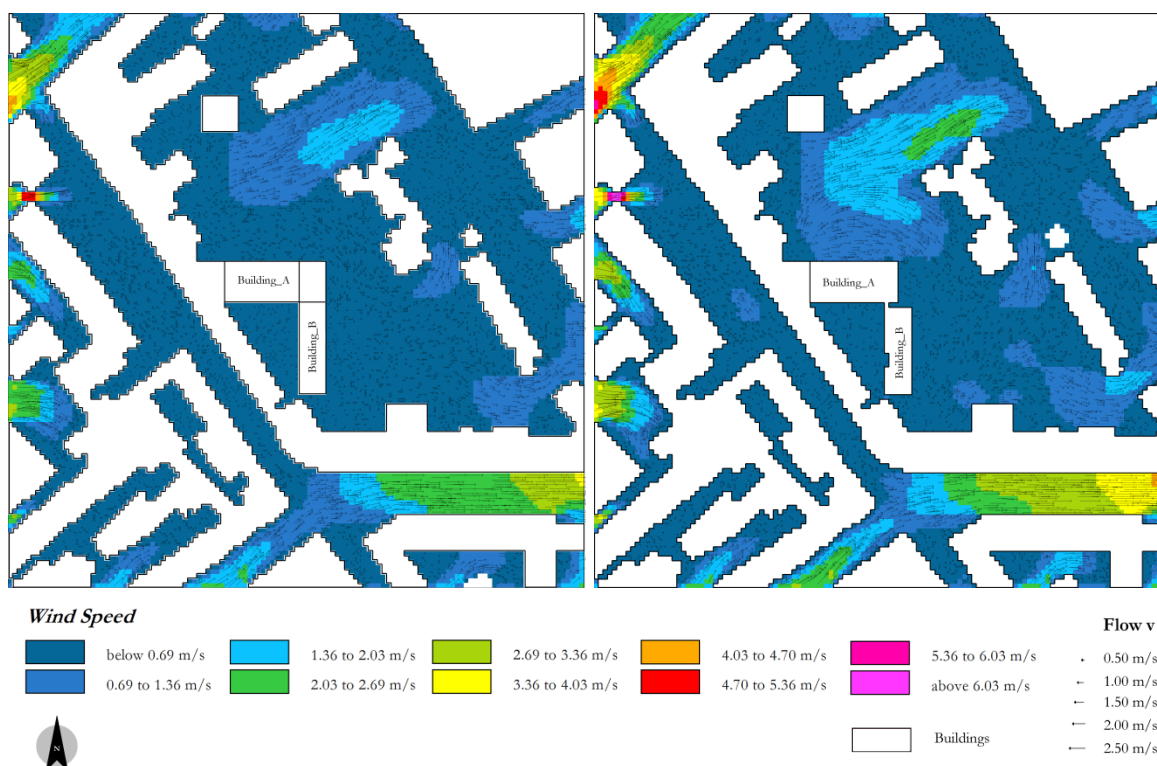


Figure 105. *Current* scenario – Wind speed and wind vector map analysis at level 0.0 m on the 16<sup>th</sup> of June at 3:00 p.m.

Figure 106. *Solar Optimized* scenario - Wind speed and wind vector map analysis at level 0.0 m on the 16<sup>th</sup> of June at 3:00 p.m

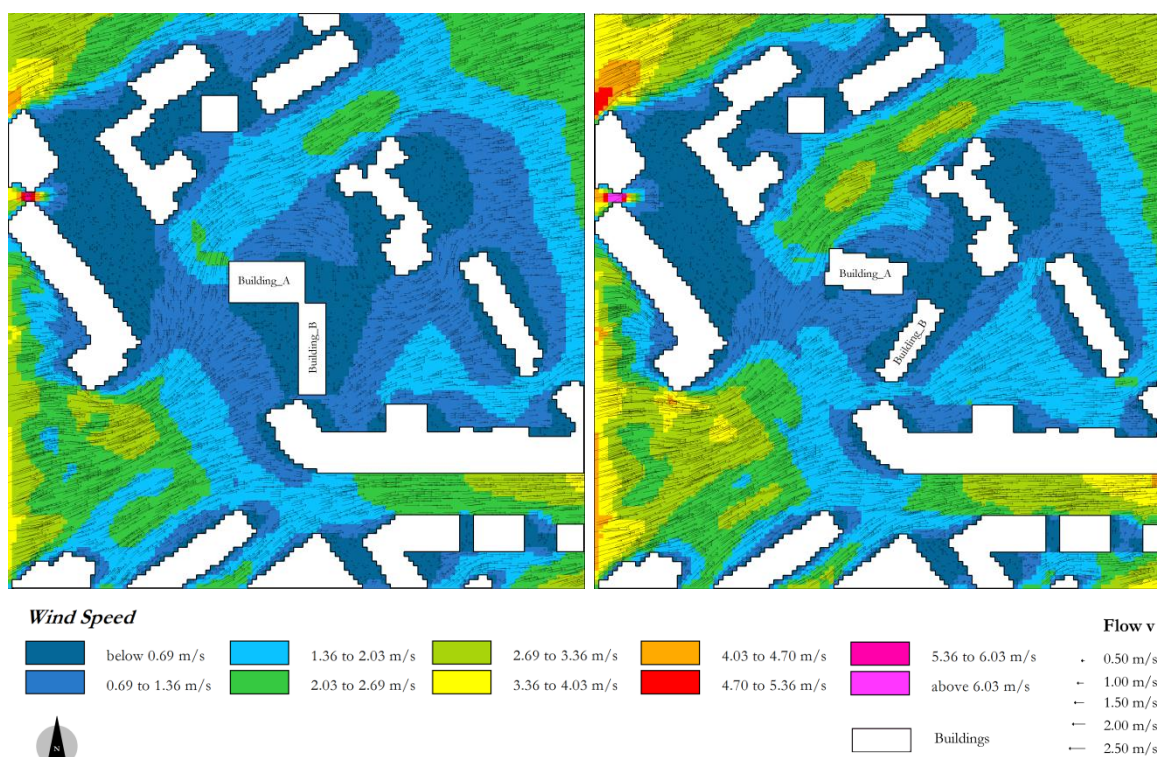


Figure 107. *Current* scenario – Wind speed and wind vector map analysis at level 10.5 m on the 16<sup>th</sup> of June at 3:00 p.m.

Figure 108. *Solar Optimized* scenario - Wind speed and wind vector map analysis at level 10.5 m on the 16<sup>th</sup> of June at 3:00 p.m

The first two analysis presented above were done at the ground level at height of 0.0 m and at the height equal to 10 m.

Firstly is better to remind that the modeling of *Building A* and *Building B* in the solar optimized scenario was elaborated following as much as possible the volume elaborated in *Grasshopper* after the solar optimisation. As has already explained in chapter 5, the modeling has some limits and the results are only qualitative because the shape of the buildings was approximated: in fact *ENVI-met* doesn't allow a complex shape's modeling. Furthermore for testing an entire urban context and tall buildings in particular is usually necessary to conduct set of simulations in wind tunnel where is perfectly created the turbulence of the wind specific for every surrounding.

From the wind speed's maps is possible to visualize the all results of the analysed district: the range of the speed is included from values under to 0.69 m/s to values above to 6.03 m/s.

At the ground level the average speed is equal to 0.67 m/s in the current scenario, while is equal to 0.82 m/s in the solar optimized scenario.

In current scenario the highest values is equal to 5.30 m/s, while the lowest is equal to 0.00 m/s.

In solar optimized scenario the highest values is equal to 6.39 m/s, while the lowest is equal to 0.00 m/s.

The wind speed in the interest area of analysis, the court in front of *Building A* and *Building B*, at the ground level has a value under 0.69 m/s in both scenarios.

At the level of 10.50 m the average speed is equal to 1.05 m/s in the current scenario, while is equal to 1.29 m/s in the solar optimized scenario.

In current scenario the highest values is equal to 5.56 m/s, while the lowest is equal to 0.00 m/s.

In solar optimized scenario the highest values is equal to 6.75 m/s, while the lowest is equal to 0.01 m/s.

Above the court and close to the façades the value of wind speed remains under 0.69 m/s in the current scenario, while in the solar optimized scenario the values increases and it is include from 0.69 m/s to 1.36 m/s. The increment of the wind speed is given by the orientation of the buildings and the presence of the space between *Building A* and *Building B*. In fact in that point, the constriction of section, creates the Venturi effect that increases the speed velocity. Furthermore the configuration of the buildings similar to funnel accentuates this affect channelling the wind. This could explain also the increment of the wind on the façades: however for studying this aspect depth analysis are necessary.

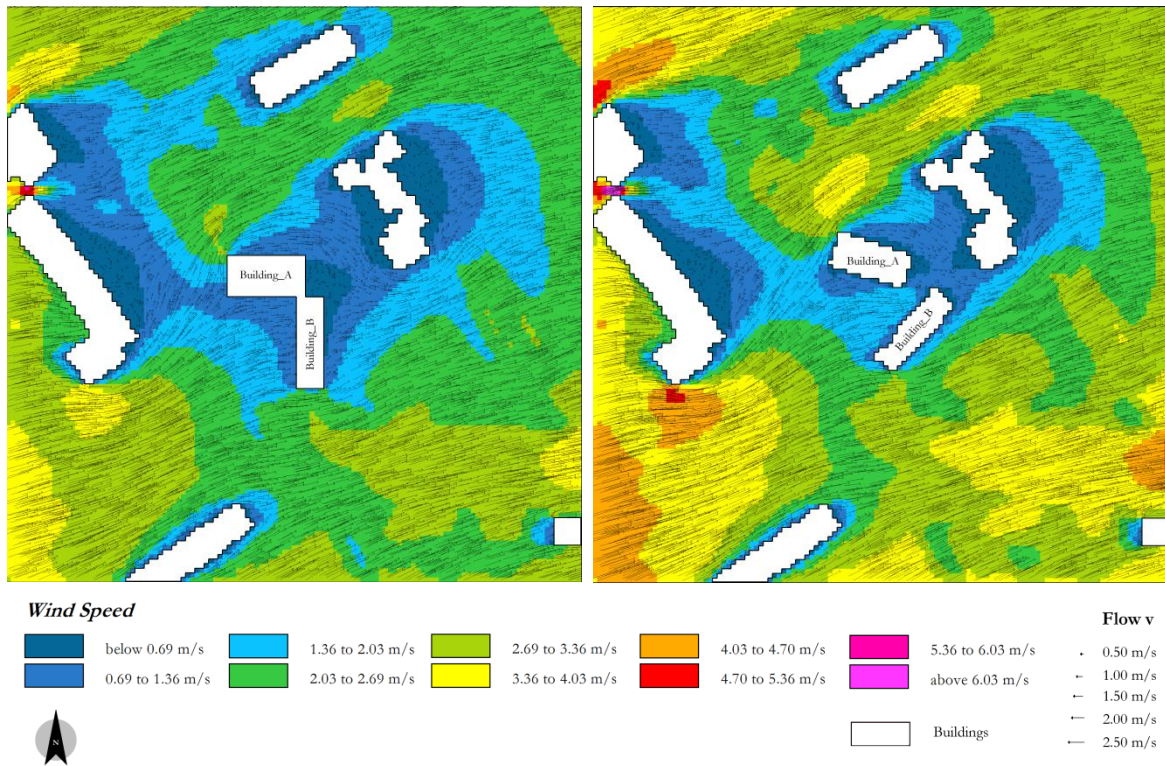


Figure 109. *Current* scenario – Wind speed and wind vector map analysis at level 17.5 m on the 16<sup>th</sup> of June at 3:00 p.m.

Figure 110. *Solar Optimized* scenario - Wind speed and wind vector map analysis at level 17.5 m on the 16<sup>th</sup> of June at 3:00 p.m

At the level of 10.50 m the average speed is equal to 1.78 m/s in the current scenario, while is equal to 2.17 m/s in the solar optimized design.

In current scenario the highest values is equal to 5.36 m/s, while the lowest is equal to 0.06 m/s.

In solar optimized scenario the highest values is equal to 6.49 m/s, while the lowest is equal to 0.04 m/s.

At this level, the value of wind speed above the court and close to the façades is in the range from 0.69 m/s to 1.39 m/s in the current scenario, while in the solar optimized scenario the values increases more and it is include from 1.36 m/s to 2.03 m/s.

Depth and local analysis would be necessary for studying the wind speed at the urban and building scale, but this research wants give only a qualitative analysis of this aspect.

### **8.3.7. Profile of the wind speed on the façade**

In this section of the study are presented the wind speeds on the façade and the wind profile on them.

As known the wind has a considerable influence on the façade's distribution temperatures [132] as well as on the building structure.

Firstly were presented the results of the simple models: were selected the representative case studies in order to study the influence that vegetation has on the wind speed distribution on the façades. Were chosen the case study 1 - A with the building to analyse located in the middle of the district without any vegetation and the three case studies with the analysed building located in the middle of a park composed by trees of 10 metres of height (3 - P), 15 metres of height (5 - P), 20 metres of height (7 - P) and trees placed in regular configuration in the park (11 - P).

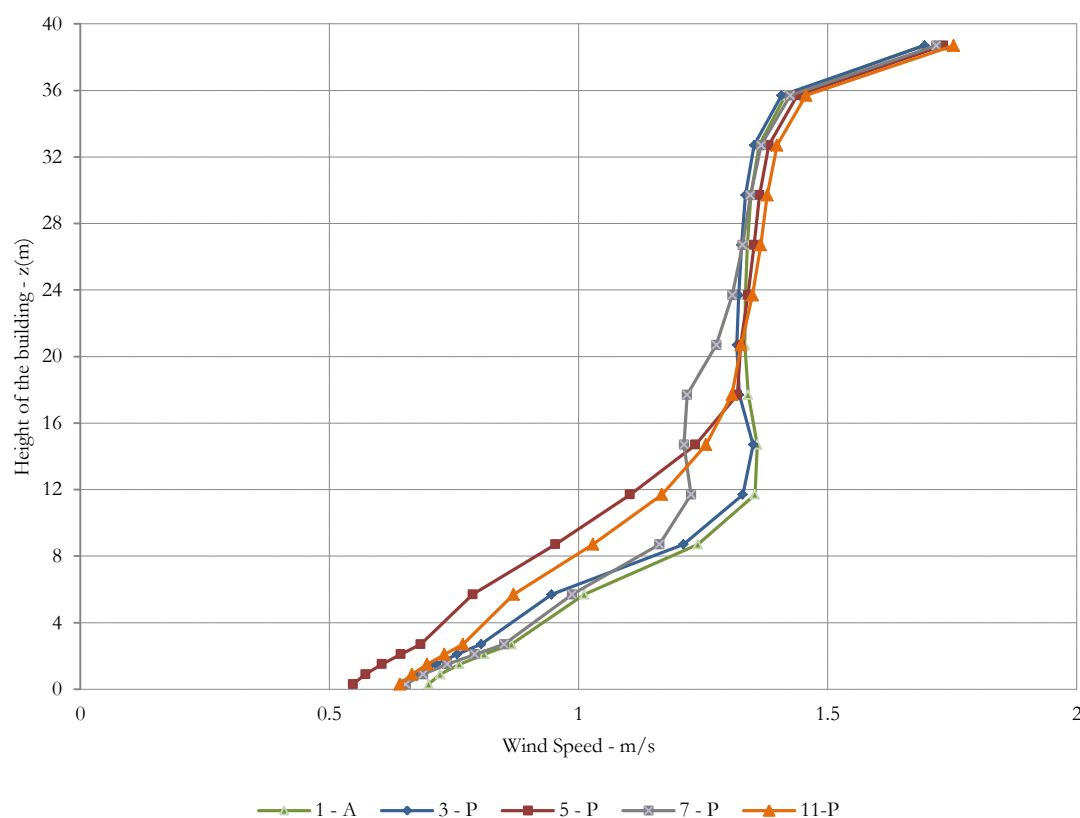
As was done for the temperature on the façades, the all values of the wind on the south façade have been extracted and then calculated the average temperature for every height for drawing the wind profile.

The results show that the wind speed's distributions of the all studies are characterized by a typical profile observable on the Graph 22: the wind speed is low at the ground level and increases with along the height.

From the Graph 22 is clearly that the influence of vegetation decreases the wind speed from the ground level to the level of height of the trees. In fact after the height of the trees (above 20 m), all distribution of wind speeds are more similar each other as well as the values and their profiles follow the same profile of reference case study (1 - A). Furthermore is interesting to notice that inside the crown of tall trees (15m) located in the court in front of the *Building A's* façade, the trees reduce wind speed inside the leaf layer but between the plants the wind is canalised and the reduction effect is considerably less and for the high heights the values of wind are also higher in the green scenario than in the current one. However depth analyses are necessary for studying this aspect.

Another aspect is important to underlines: the influence of the vegetation on the wind speed depends also by the density of the tree's crown: the case studies 5 - P and 11 - P that have trees of 15 m of height have higher decrement of the wind speed until 15 m of height, while the case study 7 - P, characterized by the presence of tree of 20 m of height has higher influence than case studies 5 - P and 11 - P only after the 15 m of height.

Graph 22. Wind profiles of the simple case studies 1 - A, 3 - P, 5 - P, 7 - P and 11 - P considering the average of wind speeds on the south façades



The results confirmed the situations described above: all case studies presented guarantee a decrement of the wind speed respect to the reference case studies. In particular the case study that has the highest percentage of decrement is 7 - P: the wind speed distribution is 10% less than the reference case study.

The vegetation of the case study 3 - P reduces the wind speeds' distribution of 3.6%, the case study 5 - P of a percentage equal to 3% and finally the case study 11 - P until 5%.

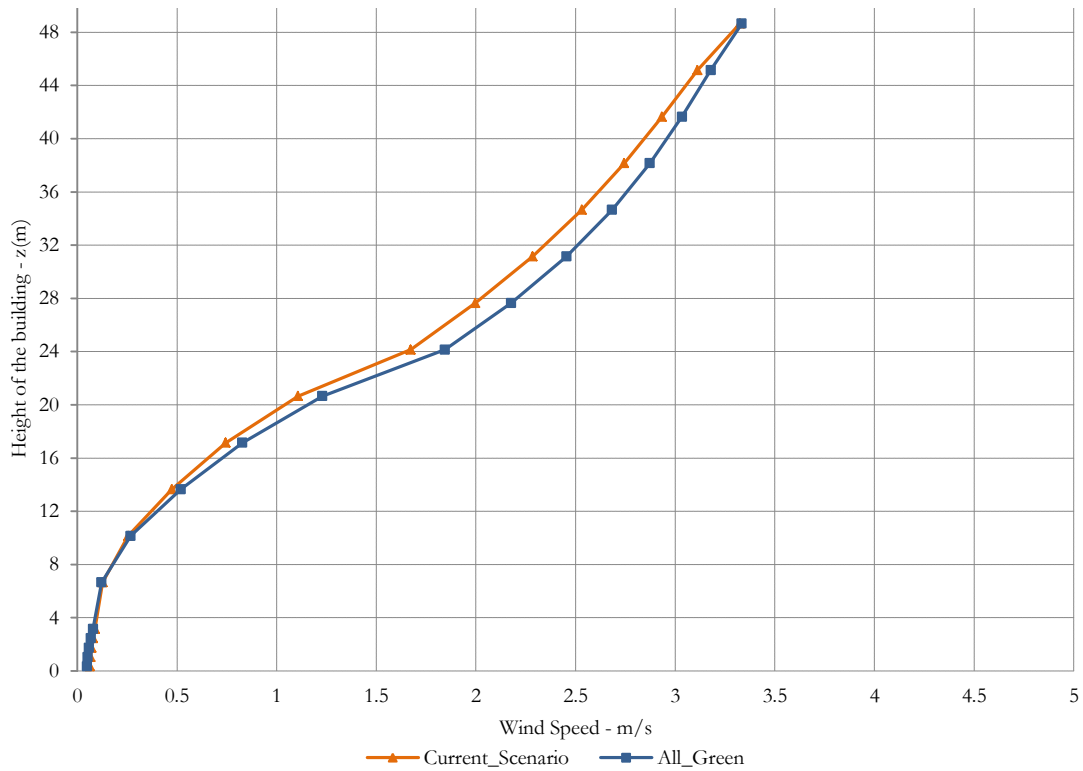
The lowest value of wind speed is about to 0.15 m/s, while the highest value is about to 2.6 m/s both registered in the case study 11 - P.

Regarding the real case study were done the same simulations in order to analyse the wind speeds distribution on the tallest building of the district: *Building A*.

Were compared the wind speeds distribution on the façade in both scenarios: current and *All Green*.

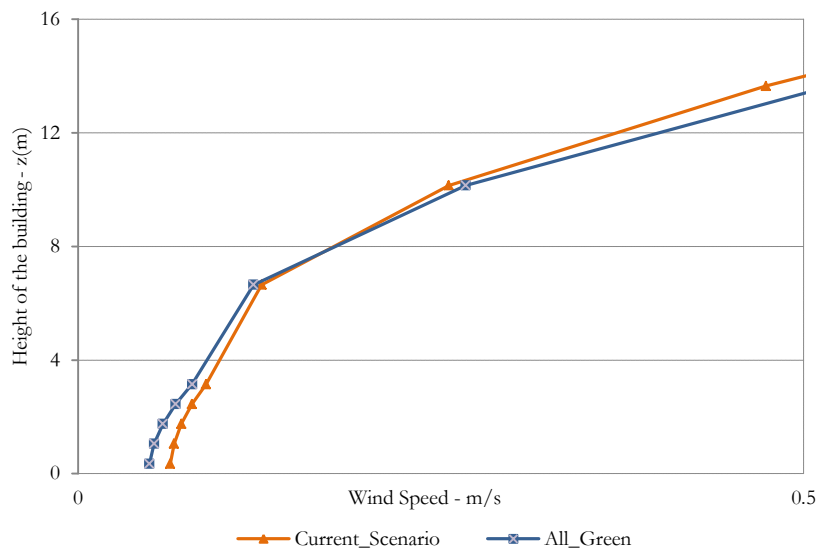
In the Graph 23 are presented the wind profiles on the south façade of the *Building A*.

Graph 23. Wind profiles considering the average of wind speeds on the *Building A*'s south façade in the Current and *All Green* scenario.



The results show that the results are very similar between two scenarios: the average value of wind speed on the façade in the current scenario is higher of 5% than in the *All Green* scenario.

Graph 24. Enlargement of wind profiles considering the average of wind speeds on the *Building A*'s south façade.



This result, as the wind profiles in the Graph 23 confirmed, could be caused from the vegetation configuration: in fact, as visible on the enlargement in Graph 24, the trees reduce wind speed at the ground level, but between the plants the wind could be canalised and the reduction effect is considerably less and for the high heights the values of wind are also higher in the green scenario than in the current one. However the reduction of the wind speed at the ground level arrives until 20% less in the *All Green* scenario than the current one.

It is better to underline again that specific depth analyses, or set of simulations in the wind tunnel are necessary for giving a complete and satisfying comprehension of the wind speed distribution in the urban district and on the façade.

#### **8.4. Conclusion and outcomes**

Results demonstrated the reduction of temperatures and wind speeds due to the introduction of vegetation, with the greatest reductions in the all green scenario.

The results are more similar that the example found in literature and this demonstrated that the simulation gave a good and indications for support the design and planning project until the early design phases.

For analysing deep in detail the wind speed and its effect between the two building and the study if the temperature on the façade decreasing thanks to the effect off the building configuration could be used another specific tool, for example *Austodesk Vasari*, but now only a beta trail version is available and more developments the program has need in order to became a validated tool for scientific analysis.

## **9. Conclusion Section 2**

In the section 2 of this research, it has been shown that there is an important potential of lowering urban temperatures when the urban environment is covered with green system.

It has been pointed out that the global urban temperature can benefit from green system, especially with the presence of trees, that contributes to have a high decrement of surface's temperatures as well.

Temperature decrease due to vegetation is primarily affected by the vegetation itself (amount and geometry).

For the low air velocities inside the canyon, the wind direction does not have any significant effect on temperature decreases due to vegetation.

Regarding the urban geometry, the wider a canyon is, the weaker the effect green systems have on temperature decrease.

For the climate examined, green roofs have a good effect inside the canyon, but they have a greater effect at roof level and, consequently, at the urban scale, as the results demonstrated.

### **9.1. The Climate interaction in a new design approach**

On one hand, the study is focused on the maximization of the solar exposure of the building's volume in order to produce as much energy as possible exploiting the building façades. On the other hand, it is evaluated the minimization of the building's impact on the surrounding in terms of overshadowing, solar mutual reflections, urban heat island effect and air flux interactions.

Some important international architect firms are starting to design achieving the first goal (maximization of solar potential), because today the energetic-environmental success or unsuccess of one project depends on its relation with urban environment. In this scenario the Malaysian architect, Ken Yeang stands out, thank to his environmental studies related to bioclimatic and ecological design.

He, as some of the international firms pioneers, is focused on the passive low-energy design of buildings, as his 'bioclimatic skyscrapers'. This new generation of buildings dialogue with the climate peculiarities of the environment which it is located in. The passive low energy techniques are the key for realizing a new innovative and energetically efficient building making attention on climate and boundary conditions relative to the nearby buildings, green spaces, finishing materials etc. Thus the building becomes interactive with the environment and consumes low energy, guaranteeing high levels of performance and comfort.

The climate conditions suggest a more intelligent and conscious design that start from the use of natural energy and the exploitation of renewable sources. For example, the exposure of the building is fundamental for exploiting the sun radiation on its building envelope and to guarantee an adequate illumination of inner ambient, the design of the façades must be related with the use of the wind in order to create a natural ventilation to maintain the ambient health, the external finishing with eco-friendly materials has to be chosen with an appropriate color and property of reflectance in order to control the effect of solar reflection on the neighborhood buildings. Furthermore the architectural formal research in addition to these energy strategies contribute to give benefits in terms of building's structure and thermal comfort for pedestrian at ground level. At the same time some urban strategies as the regulation on the materials' use and the presence of green system in urban areas permit to mitigate the building's surface temperature and the effect of urban heat island.

On the other hand the great projects, that exploit the solar energy, have often the limit to consider only the projected building: the analyses are conducted only on the new building in order to maximize its energy efficiency, without evaluate the impact that it creates on the built environment around it, in terms of overshadowing, solar reflections and on microclimate effects.

For this reason the guidelines treated for a correct design approach comprehend also the analyses done for evaluating the new building and its effect on the urban context, in order to guarantee the solar access and microclimate comfort for the neighborhood.

For the approach proposed in this dissertation, should be done the analyses at the urban scale. It will be better if the urban planners that define the urban regulations, make attention not also on the landscape or urban parameters, but also on the solar access and thermal comfort, without it should be impossible to align at the energy directives for the existing buildings that are more and more restrained in terms of energy consumptions.

In a urban context where the available soil is going to be reduced more and more and where the growing in height is the only way to develop the buildings, in order to respect the energy directives that oblige to use renewable sources, is easy to understand the importance of having the correct design approach. It has also to be considered that, for the dynamic urban transformation, oblige the designers to conduct iterative study on the project buildings and on the neighborhood ones.

Therefore the second section of the research gave the first answers related to the initial questions written at the beginning of the research and the section as well.

1. *Which are the adequate surface temperatures that permit a good efficiency the solar systems?*

The solar systems have usually a range of temperature where they are working well and its efficiency is totally used for producing energy exploiting the solar radiation incident on them.

Many studies demonstrated that the solar systems potential in terms of energy production depend on the thermal environment conditions. In fact there are many examples of technical solutions that tested the solar systems efficiency respect to external temperatures effect in order to study how is possible to limit the collapse of their performance created by overheating. Among other the use of insulation or the natural ventilation behind the solar systems can contribute to maintain a range of temperatures adequate in order to guarantee their efficiency.

2. *How is possible to decrease the surface temperatures on the façades?*

The answer to this question is liked to the previous one given that the conservation of adequate operative surface temperatures for solar systems is possible to achieve with technical solutions that have been described above, but also an intelligent urban planning in which a good green system strategy can decrease the global district temperature as has been demonstrated by the analysis that have been presented in the second session.

3. *How the vegetation can give a benefit in term of air temperature in a district?*

The results of the second part of the research demonstrated that the presence of vegetation and green roofs lead to the mitigation of temperatures inside the canyon. If applied to only one unit block, green roofs and green system can create a small area of mitigated temperatures to the urban heat island effect, as has been shown in this microclimatic study. If applied to the whole city scale, they could mitigate raised urban temperatures, and, especially for hot climates, bring temperatures down to more “human-friendly” levels and achieve energy saving for cooling buildings.

4. *How is the wind speed on the façades and in the urban canyons?*

5. *How the vegetation can affect the wind speed?*

As the temperatures of the facades the wind speed depends on the urban morphology and on the presence of green system especially considering the ground level. As has just been written above, temperature decrease due to vegetation is primarily affected by the vegetation itself, more than the canyon

orientation in hot periods. In general, the larger amounts of solar radiation a surface receives, the larger its temperature decreases are when it is covered with vegetation and the presence of green system contributes decrease the global temperature of the district.

## **9.2. Future developments and outcomes**

The study demonstrated that is possible to calculate the benefits of vegetation's effects in urban environment through the analyses of urban heat island, surface's temperatures and operative temperatures.

However the study has needed more important future developments in order to calculate deep in detail and with more specific tools or methods of calculation the effect of solar radiation and the presence of vegetation in terms of decrement of global urban temperature and on the façades:

- Analyse the impact of solar radiation on the façade composed by solar systems in order to calculate the temperature effect locally and considering some various technical solutions with insulation or natural ventilation installed behind the façade;
- Improve and test many others tools or methods for calculation in order to have an analyses more in detail using different softwares specific for each aspects to analyse;
- Analyse the effects that the solar optimized design building could create inside the building in terms of indoor thermal comfort.

## References

- [1] H. Girardet, *Creating sustainable cities*, Schumacher Briefing 2. Green Books, 1999.
- [2] «United Nations. *World Urbanization Prospects: The 2007 Revision*,» 2007.
- [3] M. Montavon, «*Optimisation of Urban Form by the Evaluation of the Solar Potential*,» École Polytechnique Fédérale de Lausanne, Losanne, 2010.
- [4] «European Renewable Energy Council (2010).» *RE-thinking 2050-a 100% renewable energy vision for the European Union*, [Online]. Available: <http://www.erec.org/>. [Consultato il giorno 2011].
- [5] IEA - SHC Task 41: *Solar Energy and Architecture*, December 2008. [Online]. Available: [www.iea-shc.org/publications/downloads/task41-Annex.pdf](http://www.iea-shc.org/publications/downloads/task41-Annex.pdf). [Consultato il giorno 2009].
- [6] A. Potvin and C. Demers, "Passive environmental control strategies for a cold climate: the Eugene-H-Kruger Building at Laval University," in *Conference Proceedings of the American Solar Energy Society (ASES), SOLAR 2007*, Cleveland, Ohio, 7-12 July, 2007.
- [7] N. Larsson, "Le Processus de conception intégrée. Ottawa,," 2004. [Online]. Available: [http://www.envirobat-med.net/IMG/pdf/PCI\\_20sommaire\\_20PDF.pdf](http://www.envirobat-med.net/IMG/pdf/PCI_20sommaire_20PDF.pdf).
- [8] H. Livingston, «BIM and Sustainable Design, Part 2. Design software companies use different approaches to reach the same goal,» 2007. [Online]. Available: <http://www.cadalyst.com/cad/building-design/bim-and-sustainable-design-part-2-3618>.
- [9] M. Horvat and W. Maria, "T.41.B.3 Solar design of buildings for architects: Review of solar design tools - Subtask B: Methods and Tools for Solar Design," *Solar Heating & Cooling Programme - International Energy Agency*, 2012.
- [10] R. Compagnon and D. Raydan, "Irradiance and illuminance distributions in urban areas," in *In Proceedings of PLEA 2000*, Cambridge UK, July 2000.
- [11] M. Montavon, J. Scartezzini and R. Compagnon, "Comparison of the solar energy utilisation potential of different urban environments," in *In PLEA2004*, Eindhoven, The Netherlands, 2004.
- [12] D. Robinson, "Urban Morphology and indicators of radiation availability," *International Journal of Solar Energy*, vol. 80, no. 12, p. 1643–1648, 2006.
- [13] J. Mardaljevic and M. Rylatt, "An image-based analysis of solar radiation for urban settings," in *In PLEA 2000*, Cambridge, UK, 2000.
- [14] D. Robinson and A. Stone, "Irradiation modelling made simple: the cumulative sky approach and its applications," in *In Plea2004*, Eindhoven, The Netherlands, 2004.
- [15] J. Kämpf, «*On the Modelling and Optimisation of Urban Energy Fluxes*,» École Polytechnique Fédérale de Lausanne, Lausanne, 2009.
- [16] G. Larson e R. Shakespeare, *Rendering with Radiance: the art and science of lighting visualization*,

San Francisco: Morgan Kaufmann, 1998..

- [17] G. Larson, «RADIANCE File Formats,» 1992. [Online]. Available: <http://radsite.lbl.gov/radiance/refer/filefmts.pdf>.
- [18] «DIVA (Design Iterate Evaluate adapt),» Harvard University, National Research Council Canada and the Fraunhofer Institute for Solar Energy Systems, [Online]. Available: <http://www.daysim.com/>.
- [19] J. Scartezzini, M. Montavon and R. Compagnon, "Computer evaluation of the solar energy potential in an urban environment," in *EuroSun*, Bologna, 2002.
- [20] M. Boukhabla and D. Alkama, "Impact of vegetation on thermal conditions outside, Thermal modeling of urban microclimate, Case study: the street of the republic, Biskra,," *Energy Procedia*, vol. 18, p. 73 – 84, 2012.
- [21] W. Gao, H. Sugiyama e T. Ojima, «Field study of effect of street and its trees on thermal environment of sidewalks,» *Journal of Architecture and Planning Environment Engineering*, vol. 469, pp. 53-64, 1995.
- [22] M. Nikolopoulou and K. Steemers, "Thermal comfort and psychological adaptation as a guide for designing urban spaces," *Energy and Buildings*, vol. 35, no. 1, 2003.
- [23] M. Hegger, M. Fuchs, T. Stark and M. Zeumer, *Energy Manual. Sustainable architecture*, Basel: Birkhäuser – Edition Detail, 2008.
- [24] S. Izquierdo, C. Montanes, C. Dopazo e N. Fueyo, «Roof-top solar Energy potential under performance-based building energy codes: the case of Spain,» *Solar Energy*, vol. 85, pp. 208 - 213, 2010.
- [25] R. Compagnon, «Solar and daylight availability in the urban fabric,» *Energy and Buildings*, vol. 36, pp. 321 - 328, 2004.
- [26] K. Voss and E. Musall, “Net zero energy buildings. International projects of carbon neutrality in buildings,” Institut für Internationale Architektur-Dokumentation, Munich, 2011.
- [27] *Cities: People, Society, Architecture*, Venice: Catalogue of the 10th International Architecture Exhibition, Marsilio, 2006.
- [28] M. Tadi, G. Lobaccaro and S. Vahabzadeh Manesh, “Sustainable urban morphology for a greener city: An integrated approach for the energy-efficiency of neighbourhoods,” in *GreenAge Symposium, Mimar Sinan Fine Arts University*, Faculty of Architecture, Istanbul - Turkey, 2012.
- [29] L. Saylan, O. Sen, H. Toros e A. Arisoy, «Solar energy potential for heating and cooling systems in big cities of Turkey,» *Energy Conversion and Management*, vol. 43, p. 1829 – 1837, 2002.
- [30] H. Lehmann and S. Peter, “Assessment of roof & façade potentials for solar use in Europe,” Institute for sustainable solutions and innovations (ISUSI), Aachen, 2003.
- [31] K. Peippo, P. Lund e E. Vartiainen, «Multivariate optimization of design trade-offs for solar low

- energy buildings,» *Energy and Buildings*, vol. 29, pp. 189-205, 1999.
- [32] D. Li and T. Lam, "An analysis of building energy performances and benefits using solar façades," *Power and Energy*, vol. Vol. 222 Part A, no. Proc. IMechE, 2008.
- [33] A. K. Soteris, «Use of TRNSYS for modelling and simulation of a hybrid PV-thermal solar system for Cyprus.» *Renewable Energy*, vol. 23, pp. 247-260, 2001.
- [34] J. Hofierka e J. Kanuk, «Assessment of photovoltaic potential in urban areas using open-source solar radiation tools,» *Renewable Energy*, , vol. 34, pp. 2206 - 2214, 2009.
- [35] V. Cheng, K. Steemers, M. Montavon e R. Compagnon, «Urban form, density and solar potential,» in *PLEA2006 - The 23rd Conference on Passive and Low Energy Architecture*, Geneva, 2006.
- [36] T. Kuhn, S. Herkel, H.-M. Henning e F. Frontini, «New multifunctional façade components for the building skin,» in *Proceedings of Energy Forum*, Brixen, 2010.
- [37] I. Sartori e a. et, «Criteria for Definition of Net Zero Energy Buildings,» in *Proceedings of Eurosun 2010*, Graz, 2010.
- [38] *Autodesk. 2011. Autodesk Ecotect Analysis 2011.*
- [39] *MATLAB version R2011b. Natick, Massachusetts: The MathWorks Inc., 2011.*
- [40] *Daysim version 3.1b, Harvard University, National Research Council Canada, Fraunhofer Institute for Solar Energy Systems, 2010..*
- [41] I. Reda e A. Andreas, «Solar position algorithm for solar radiation application,» National Renewable Energy Laboratory (NREL) Technical report NREL/TP-560-34302, Colorado, 2003.
- [42] «South East Queensland Regional Plan 2009-2031,» The State of Queensland (Queensland Department of Infrastructure and Planning) ISBN 978-0-9805449-1-6..
- [43] M. Dubois e M. Horvat, «State of the art of digital tools used by architects for solar design,» Task 41 - Solar Energy and Architecture - Subtask B - Methods and Tools for Solar Design, 2010.
- [44] C. Reinhart, «Tutorial on the Use of DAYSIM Simulations for Sustainable Design,» Institute for Research in Construction, National Research Council Canada, Ottawa (Ont.), 2006.
- [45] C. Reinhart, «Tutorial on the Use of Daysim Simulations for Sustainable Design,» Harvard University, Cambridge, MA, 2010.
- [46] «EnergyPlus Energy Simulation Software,» U.S. Department of Energy - Energy Efficiency & Renewable Energy, [Online]. Available: <http://www.eere.energy.gov/buildings/energyplus/weatherdata.html>..
- [47] D. Bourgeois, C. Reinhart and G. Ward, "Standard daylight coefficient model for dynamic daylighting simulations," *Building Research & Information*, vol. 36, no. 1, pp. 68-82, 2008.
- [48] C. Reinhart e S. Herkel, «The Simulation of Annual Daylight Illuminance Distributions- A state of the art comparison of six RADIANCE-based methods,» *Energy & Buildings*, vol. 32, n. 2, pp. 167-

187, 2000.

- [49] C. Reinhart e M. Andersen, «Development and validation of a Radiance model for a translucent panel,» *Energy and Buildings*, vol. 38, pp. 890 - 904, 2006.
- [50] P. Tregenza, «Subdivision of the sky hemisphere for luminance measurements,» *Lighting Research & Technology*, vol. 19, pp. 13-14, 1987.
- [51] C. Reinhart e O. Walkenhorst, «Dynamic Radiance - based daylight simulations for a fullscale test office with outer venetian blinds,» *Energy and Buildings*, vol. 33, n. 7, p. 683 – 697., 2001.
- [52] J. Mardaljevic, «Verification of program accuracy for illuminance modelling: assumptions, methodology and an examination of conflicting findings,» *Lighting Research & Technology*, vol. 36, n. 3, pp. 218-238, 2004.
- [53] R. Perez, R. Seals e J. Michalsky, «All-weather model for sky luminance distribution - preliminary configuration and validation,» *Solar Energy*, vol. 50, n. 3, pp. 235 - 245, 1993.
- [54] J. Mardaljevic, «Daylight simulations: validation, sky models and daylight coefficients,» Ph.D., De Monfort University, 2000.
- [55] J. Mardaljevic, «Simulation of annual daylighting profiles for internal,» *Lighting Research & Technology*, vol. 32, n. 2, pp. 111 - 118, 2000.
- [56] D. Ibarra e C. Reinhart, «Solar availability: a comparison study of six irradiation distribution methods,» in *Proceedings of Building Simulation 2011: 12th Conference of International Building Performance Simulation Association.*, Sydney, 2011.
- [57] C. Reinhart e M. Andersen, «Development and validation of a Radiance model for a translucent panel,» *Energy and Buildings*, vol. 38, n. 7, pp. 890 - 904, 2006.
- [58] «SunEarthTools.com - Tools for consumers and designers of solar,» [Online]. Available: [http://www.sunearthtools.com/dp/tools/pos\\_sun.php](http://www.sunearthtools.com/dp/tools/pos_sun.php).
- [59] G. Lobaccaro, G. Masera and T. Poli, “Solar Districts: Design Strategies to Exploit the Solar Potential of Urban Areas,” in *Proceedings of the XXXVIII LAHS World Congress*, Istanbul, 2012.
- [60] G. Lobaccaro, F. Frontini, G. Masera and T. Poli, “SolarPW: a new solar design tool to exploit solar potential in existing urban areas,” *Energy Procedia*, vol. 30, pp. 1173-1183, 2012.
- [61] M. Santamouris, *Energy and climate in the urban built environment*, London: James & James, 2001.
- [62] B. Lab, «Radiance,» [Online]. Available: <http://radsite.lbl.gov/radiance/>.
- [63] “Lawrence Berkeley National Laboratory,” U.S. Department of Energy National Laboratory Operated by the University of California, [Online]. Available: <http://www.lbl.gov/>.
- [64] G. Lobaccaro, F. Fiorito, G. Masera, Poli and T., “District Geometry Simulation: A Study for the Optimization of Solar Façades in Urban Canopy Layers,” *Energy Procedia*, vol. 30, pp. 1163-1172, 2012.

- [65] S. Carpenter, Learning from experiences with advanced houses of the world, Sittard, The Netherlands: Centre for the Analysis and Dissemination of Demonstrated Energy Technologies, 1995.
- [66] K. Gopinathan, «Solar radiation on variously oriented sloping surface,» *Solar Energy*, vol. 47, p. 173–179, 1991.
- [67] D. Rutten, «Grasshopper - Galapagos,» [Online]. Available: <http://www.grasshopper3d.com/group/galapagos>.
- [68] D. Rutten, «Galapagos - Evolutionary Principle applied to Problem Solving,» [Online]. Available: <http://www.grasshopper3d.com/profiles/blogs/evolutionary-principles>.
- [69] V. Vannini, B. Turkienicz and A. Krenzinger, “Geometric optimization of building façades for BIPV,» in *Proceedings of the Energy Forum 2012*, Bressanone, Italy, 2011.
- [70] P. Bentley, Evolutionary Design by Computers, San Francisco: Morgan Kaufmann, 1999.
- [71] «Grasshopper - genartive modeling rhino,» [Online]. Available: <http://www.grasshopper3d.com/>.
- [72] D. Rutten, «Grasshopper - Tutorials,» [Online]. Available: <http://www.grasshopper3d.com/page/tutorials-1>.
- [73] Uto, «food4Rhino,» [Online]. Available: <http://www.food4rhino.com/project/geco>.
- [74] G. Piacentino, «Giulio Piacentino - Weaverbird - Topological Mesh Editor,» [Online]. Available: <http://www.giuliopiacentino.com/weaverbird/>.
- [75] L. Kera, J. Alstan, N. Jeff and R. Christoph, “Quick Start Guide for the DIVA for Rhino toolbar,» Harvard University - Graduate School of Design, Cambridge, MA 02138, USA, 2010.
- [76] «Radiance,» [Online]. Available: <http://radsite.lbl.gov/radiance/>.
- [77] «Evalglare,» [Online]. Available: [www.ise.fhg.de/radiance](http://www.ise.fhg.de/radiance).
- [78] R. Darren, «GenCumulativeSky,» EPFL, [Online]. Available: <http://leso.epfl.ch/>.
- [79] C. Reinhart, «Daysim - Advanced Daylight Simulation Software,» [Online]. Available: <http://daysim.ning.com/>.
- [80] «DIVA for Rhino - Tutorials and Guide,» [Online]. Available: <http://www.diva-for-rhino.com/usersforum.html>.
- [81] G. Lobaccaro, F. Fiorito, G. Masera and D. Prasad, “Urban solar district: a case study of geometric optimization of solar façades for a residential building in Milan,» in *Solar 2012 Conference*, Melbourne, 2012.
- [82] M. Eigensatz, M. Kilian, A. Schiftner, N. Mitra, H. Pottmann e M. Pauly, «Paneling architectural freeform surfaces,» *ACM Transactions on Graphics*, vol. 29, n. 4, 2010.
- [83] H. Pottmann, A. Schiftner, P. Bo, H. Schmiehofer, W. Wang, N. Baldassini e J. Wallner, «Freeform surfaces from single curved panels,» *ACM Transactions on Graphics (TOG)*, vol. 27, n. 3,

- 2008.
- [84] R. Issa e R. McNeel, *PanelingTools Manual*, Robert McNeel & Associates., 2010.
- [85] Robert McNeel & Associates, [Online]. Available: <http://wiki.mcneel.com/labs/panelingtools>.
- [86] A. Payne e R. Issa, *Grasshopper premier*, 2009.
- [87] W. Sung, «Grasshopper learning material,» in *Syracuse architecture*, 2010.
- [88] M. Munari Probst, C. Roecker and Al., “T.41.A.2: Solar Energy systems in Architecture - Integration Criteria and Guidelines,” International Energy Agency, 2012.
- [89] T. Oke, «Urban climates and global environmental change,» in *Applied Climatology*, R. Thompson e A. Perry, A cura di, Routledge, 1997, p. 273–287.
- [90] M. & T. Bruse, «ENVI-met 3.1: A Microscale Urban Climate Model,» 1997-2000.
- [91] D. Alkam and M. Boukhabl, “Impact of Vegetation on Thermal Conditions Outside, Thermal Modeling of Urban Microclimate, Case Study: The Street of the Republic, Biskra,” *Energy Procedia*, vol. 18, p. 73–84, 2012.
- [92] M. Bruse, «Simulating microscale climate interactions in complex terrain with a high-resolution numerical model: A case study for the Sydney CBD Area,» in *Proceedings International Conference on Urban Climatology & International Congress of Biometeorology*, Sydney, Australia, 1999.
- [93] R. Emmanuel, H. Rosenlund e E. Johansson, «Urban shading — A design option for the tropics? A study in Colombo, Sri Lanka,» *International Journal of Climatology*, vol. 27, p. 1995–2004, 2007.
- [94] P. Kastner-Klein, R. Berkowicz and R. Britter, *The influence of street architecture on flow and dispersion in street canyons.*, Meteorological Atmospheric Physics, 2004.
- [95] R. Paolini, «Urban Envelope: Thermal Influence of Built Environment Surfaces on Urban Microclimate,» PhD Thesis, Politecnico di Milano, Milano, 2010.
- [96] M. Aida, «Urban albedo as a function of the urban structure — A model experiment (part I),» *Boundary-Layer Meteorology*, vol. 23, pp. 405-413, 1982.
- [97] M. Aida and K. Gotoh, “Urban albedo as a function of the urban structure — A two-dimensional numerical simulation (part II),” *Boundary-Layer Meteorology*, vol. 23, pp. 415-424, 1982.
- [98] «Solar Tool 2011,» Autodesk Ecotect Analysis 2011, 2011.
- [99] A. Marsh, «Autodesk Ecotect Analysis».
- [100] R. Stull, *Meteorology for Scientists and Engineers*, 2nd Edition, Belmont, CA, USA: Cengage Learning, 2000.
- [101] C. Ahrens, *Meteorology Today: An Introduction to Weather, Climate, and the Environment*, 9th Edition, Belmont, CA, USA: Cengage Learning, 2009.
- [102] T. Oke, *Boundary Layer Climates*, 2nd Edition, London: Methuen, 1988.

- [103] F. Chapin, P. Matson e H. Mooney, *Principles of Terrestrial Ecosystem Ecology*, New York, NY, USA: Springer-Verlag, 2002.
- [104] T. Oke, «Methods in urban climatology,» *In Applied Climatology*, vol. 14, pp. 19-29., 1984.
- [105] S. Solomon, D. Qin, M. Manning, Z. Chen, M. Marquis, K. Averyt, M. Tignor e H. (. Miller, *Climate Change 2007: The Physical Science Basis. Contribution of Working Group I to the Fourth Assessment Report of the Intergovernmental Panel on Climate Change*, Cambridge, United Kingdom and New York, NY, USA: Cambridge University Press, 2007.
- [106] C. Collier, «The impact of urban areas on weather,» *Quarterly Journal of the Royal Meteorological Society*, vol. 132, n. 614, p. 1–25, 2006.
- [107] M. Jin e J. Shepherd, «Inclusion of Urban Landscape in a Climate Model: How Can Satellite Data Help?,» *Bulletin of the American Meteorological Society*, vol. 86, n. 5, pp. 681-689, 2005.
- [108] M. Jin, R. Dickinson e D.-L. Zhang, «The Footprint of Urban Areas on Global Climate as Characterized by MODIS,» *Journal of Climate*, vol. 18, n. 10, pp. 1551-1565, 2005.
- [109] A. Schneider, M. Friedl e C. Woodcock, «Mapping Urban Areas by Fusing Multiple Sources of Coarse Resolution Remotely Sensed Data,» *Photogrammetric Engineering & Remote Sensing*, vol. 69, n. 12, pp. 1377-1386, 2003.
- [110] K. Trusilova, M. Jung e G. Churkina, «On Climate Impacts of a Potential Expansion of Urban Land in Europe,» *Journal of Applied Meteorology and Climatology*, vol. 48, n. 9, pp. 1971-1980, 2009.
- [111] E. Kalnay e M. Cai, «Impact of urbanization and land-use change on climate,» *Nature*, vol. 423, pp. 528-531, 2003.
- [112] T. Oke, «The urban energy balance,» *Progress in Physical Geography*, vol. 12, n. 4, pp. 471-508, 1988.
- [113] C. Frey, G. Rigo e E. Parlow, «Urban radiation balance of two coastal cities in a hot and dry environment,» *International Journal of Remote Sensing*, vol. 28, n. 12, p. 2695–2712, 2007.
- [114] B. Offerle, C. Grimmond e T. Oke, «Parameterization of Net All-Wave Radiation for Urban Areas,» *Journal of Applied Meteorology*, vol. 42, n. 8, pp. 1157-1173, 2003.
- [115] C. Wu e A. Murray, «Estimating impervious surface distribution by spectral mixture analysis,» *Remote Sensing of Environment*, vol. 84, n. 4, p. 493–505, 2003.
- [116] H. Taha, H. Akbari, A. Rosenfeld e J. Huang, «Residential Cooling Loads and the Urban Heat Island—The Effects of Albedo,» *Building and Environment*, vol. 23, n. 4, p. 271–283, 1988.
- [117] M. Bruse e H. Fleer, «Simulating surface – Plant–air interactions inside urban environments with a three dimensional numerical model,» *Environmental Modelling & Software*, vol. 13, n. 3–4, p. 373–384, 1998.
- [118] M. Bruse, «ENVI-met 3.1,» [Online]. Available: <http://www.envi-met.com/>.
- [119] M. Bruse, «ENVI-met 3.0: Updated model overview,» Bochum, Germany, 2004.

- [120] M. Bruse e H. Fleer, «Simulating surface–plant–air interactions inside urban environments with a three dimensional numerical model,» *Environmental Modelling and Software*, vol. 13, p. 373–84, 1998.
- [121] J. Liu, T. Black, J. Chen and M. Novak, “E-epsilon modelling of turbulent air flow downwind of a model forest edge,» *Boundary-Layer Meteorology*, vol. 77, no. 1, p. 21–44, 1996.
- [122] T. Yamada, «A numerical model study of turbulent airflow in and above a forest canopy,» *Journal of the Meteorological Society of Japan*, vol. 60, pp. 439-454, 1982.
- [123] B. Launder and B. Spalding, “The numerical computation of turbulent flows,» *Computer Methods in Applied Mechanics and Engineering*, vol. 3, no. 2, p. 269–289, 1974.
- [124] J. Wilson, «A second-order closure model for flow through vegetation,» *Boundary-Layer Meteorology*, vol. 42, n. 4, pp. 371-392, 1988.
- [125] M. Tjernström, «Some tests with a surface energy balance scheme, including a bulk parameterisation for vegetation, in a mesoscale model,» *Boundary-Layer Meteorology*, vol. 48, n. 1-2, pp. 33-68, 1989.
- [126] R. Clapp e G. Hornberger, «Empirical equations for some soil hydraulic properties,» *Water Resources Research*, vol. 14, n. 4, p. 601–604, 1978.
- [127] H. Barden, «Simulationsmodell für den Wasser-, Energie- und Stoffhaushalt in Pflanzenbeständen,» *Berichte des Instituts für Meteorologie und Klimatologie der Technischen Universität Hannover*, vol. 23, pp. 149-160, 1982.
- [128] V. Schilling, «A parameterization for modelling the meteorological effects of tall forests — A case study of a large clearing,» *Boundary-Layer Meteorology*, vol. 55, n. 3, pp. 283-304, 1991.
- [129] J. Deardorff, «Efficient prediction of ground surface temperature and moisture, with inclusion of a layer of vegetation,» *Journal of Geophysical Research*, vol. 83, n. C4, pp. 1889-1904, 1978.
- [130] T. Asaeda and V. Ca, “The subsurface transport of heat and moisture and its effect on the environment: A numerical model,» *Boundary-Layer Meteorology*, Vols. 1-2, no. 65, pp. 159-179, 1993.
- [131] A. Patrinos e A. Kistler, «A numerical study of the Chicago lake breeze,» *Boundary-Layer Meteorology*, vol. 12, n. 1, pp. 93-123, 1977.
- [132] A. Carfan, E. Galvani e J. Nery, «Study of thermal comfort in the City of São Paulo using ENVI-met model,» *Investigaciones Geográficas, Boletín del Instituto de Geografía, UNAM*, vol. 78, pp. 34-47, 2012.
- [133] F. Ali-Toudert and H. Mayer, “Numerical study on the effects of aspect ratio and orientation of an urban street canyon on outdoor thermal comfort in hot and dry climate,» *Building and Environment*, vol. 41, no. 2, p. 94–108, 2006.
- [134] P. Fanger, *Thermal comfort: Analysis and applications in environmental engineering*, New York: McGraw-Hill, 1970.
- [135] D. Kunrn, S. Bretz e H. Akbari, «The potential for reducing urban air temperature and energy consumption through vegetative cooling,» in *Proceeding of the 1994 Summer Study on Energy Effects in Building*, Pacific Grove, CA, USA, 1994.

- [136] “DGR 8/8745 - Regione Lombardia,” 22th December 2008. [Online]. Available: [http://www.provincia.milano.it/export/sites/default/ambiente/doc/n\\_energia\\_2008\\_dgr8745.pdf](http://www.provincia.milano.it/export/sites/default/ambiente/doc/n_energia_2008_dgr8745.pdf).
- [137] «Windfinder,» WindFinder.com GmbH & Co. KG, [Online]. Available: <http://www.windfinder.com/>.
- [138] Y. Chen e N. Wong, «Thermal benefits of city parks,» *Energy and Buildings*, vol. 38, n. 2, pp. 105-120, 2006.
- [139] M. Bruse e C. J. Skinner, «Rooftop Greening and local climate: A case study in Melbourne,» in *Proceedings International Conference on Urban Climatology & International Congress of Biometeorology*, Sydney, 8-12. Nov, Australia, 1999.
- [140] W. N. H. Chen Yu, «Thermal benefits of city parks,» *Energy and Buildings*, vol. 38, p. 105–120, 2006.
- [141] P. J. Eleftheria Alexandri, «Temperature decreases in an urban canyon due to green walls and green roofs in diverse climates,» *Building and Environment*, vol. 43, p. 480–493, 2008.
- [142] A. Dimoudi e M. Nikolopoulou, «Vegetation in the urban environment: microclimatic analysis and benefits,» *Energy and Buildings*, vol. 35, n. 1, pp. 69-76, 2003.
- [143] A. Eleftheri e J. Phil, «Temperature decreases in an urban canyon due to green walls and green roofs in diverse climates,» *Building and Environment*, vol. 43, p. 480–493, 2008.
- [144] C. Koppe, K. S., G. Jendritzky e B. Menne, «Health and global environmental change; heat-waves: risks and responses, series no. 2, energy, environment and sustainable development,» in *World Health Organization*, Copenhagen, 2004.
- [145] K. White e al, Technical summary, climate change 2001: impacts, adaptation and vulnerability., Cambridge: Cambridge University, 2001, p. 19–73.
- [146] A. Dimoudi e M. Nikolopoulou, «Vegetation in the urban environment: microclimatic analysis and benefits,» PRECis project, the European Commission, Directorate General XII, Joule III, contract JOR3-CT97-0192., Pikermion, 2000.
- [147] R. Giridharam, S. Ganasan e S. Lau, «Daytime urban heat island in high-rise and high-density residential developments in Hong Kong,» *Energy and Buildings*, vol. 36, p. 525–34, 2004.
- [148] M. Bruse e C. J. Skinner, «Rooftop Greening and local climate: A case study in Melbourne,» in *Proceedings International Conference on Urban Climatology & International Congress of Biometeorology*, Sydney , 8 -12 Nov, Australia, 1999.
- [149] Y. Chen e N. Wong, «Thermal benefits of city parks,» *Energy and Buildings*, vol. 38, p. 105–120, 2006.
- [150] T. Oke, «The energetic basis of the urban heat island,» *Quarterly Journal of the Royal Meteorological Society*, vol. 108, p. 1–24, 1982.
- [151] I. Sandholt, K. Rasmussen e J. Andersen, «A simple interpretation of the surface temperature/vegetation index space for assessment of surface moisture status,» *Remote Sensing of Environment*, vol. 79, p. 213–224, 2002.

- [152] R. Larson e W. Carnahan, «The influence of surface characteristics on urban radiant temperatures,» *Geocarto International*, vol. 12, p. 5–16, 1997.
- [153] H. Akbari, D. Kurn, T. Taha, S. Bretz e J. Hanford, «Peak power and cooling energy savings of shade trees,» *Energy and Buildings*, vol. 25(2), pp. 139-148, 1997.
- [154] J. Finnigan, «Improving the physical urban environment with trees,» in *Proceedings of the 2nd National Urban Tree Seminar on Urban Trees: the challenge for Australian cities and towns*, 1994.
- [155] B. Givoni, «Urban design in different climates,» World Meteorological Organization, 1989.
- [156] H. Akbari, A. Rosenfeld e T. Taha, «Summer heat islands, urban trees, and white surfaces,» in *ASHRAE Proceedings. Also Lawrence Berkeley National Laboratory Report LBL-28308, Berkeley CA, Atlanta, GA*, 1990.
- [157] S. Goward, «Thermal behavior of urban landscapes and the urban heat island,» *Phys. Geog.*, vol. 2(1), pp. 19-33, 1981.
- [158] M. Spiller, «Roof gardens and green facades for the improvement of urban environments,» Thesis B. L. Arch, University of NSW, 1993.
- [159] R. Emmanuel, H. Rosenlund e E. Johansson, «Urban-shading the design option for the tropics? A study in Colombo, Sri Lanka,» *International Journal of Climatology*, vol. 27, n. 14, pp. 1995-2004, 2007.
- [160] M. Fahmy e S. Sharples, «On the development of an urban passive thermal comfort system in Cairo, Egypt,» *Building and Environment*, vol. 44, n. 9, pp. 1907-1916, 2009.
- [161] C. Bueno e L. Bartholomeu, «Influence of vegetation on thermal comfort in urban and built environment,» Thesis (Ph. D.), Faculdade de Engenharia Civil, Universidade Estadual de Campinas, 2003.
- [162] A. J. T. Guerra e S. B. Cunha, «Environmental impacts in urban Brazil,» Bertrand Brazil, Rio de Janeiro., 2009.
- [163] M. A. S. Gomes e M. C. C. T. Amorim, «Afforestation and thermal comfort in urban space: a case study in public squares of Presidente Prudente (SP),» *Paths of Geography*, vol. 7, n. 10, pp. 94-106, 2003.
- [164] E. Jauregui, «Influence of a large urban park on temperature and convective precipitation in a tropical city,» *Energy and Buildings*, vol. 15–16, p. 457–463, 1990/1991.
- [165] A. Liebard e A. De Herde.

## Annex 1

### Dynamic daylighting simulation and solar position scheme

The DDS sky division scheme divides the hemisphere vertically into 7 superimposed horizontal rows [50], each representing a differential altitude of  $12^\circ$ , with the hemisphere topped at its zenith by a circular segment having a half-cone angle of  $6^\circ$ . Each horizontal row is then divided into rectangular segments based on the Tregenza convention, defined in Table 2, for a total of 144 rectangular and 1 circular segments. The ordering scheme is based on the Daysim convention, shown in Figure 8 (on the right), where the first segment starts at the lowest row along the horizon with a centre azimuth of  $6^\circ$  north of east, with subsequent segments following counter clockwise, moving up a row once a  $360^\circ$  span of the horizon is completed. The 145 DDS indirect solar positions are centred on the 145 sky segments except for the first row above the horizon, taking on an altitude of  $2^\circ$  rather than  $6^\circ$ . The ordering scheme is the same as with diffuse sky segments.

A scaling factor,  $F$ , is introduced to increase the number of dynamic daylighting simulation direct solar positions. Consider the following expressions of the static differential altitude of the original 7 Tregenza rows,  $\alpha$ , the number of solar positions per row,  $N_{\text{positions/row}}$ , and the total number of solar positions in the sky,  $N_{\text{total}}$ , as a function of  $F$ :

$$\alpha = \frac{90^\circ}{2^F \cdot 7 + 1} \quad \text{eq. 45}$$

$$N_{\text{position/rows}} = N_{\text{Tregenza/rows}} \cdot 2^F \quad \text{eq. 46}$$

$$N_{\text{total}} = 4^F 144 + 1 \quad \text{eq. 47}$$

If  $F$  is set to 0, then  $\alpha$  becomes  $12^\circ$ ,  $N_{\text{positions/row}}$ <sup>1</sup> becomes 30 and  $N_{\text{total}}$  becomes 145, i.e. the original Tregenza variables. Values of  $F$  greater than 0 trigger a decrease in differential altitude, a corresponding increase in the number of rows, and an increase in the number of positions per row<sup>1</sup>:

- For  $F = 1$ ,  $\alpha = 6^\circ$ ,  $N_{\text{total}} = 577$ , and  $N_{\text{positions/row}}$ <sup>1</sup> = 60;
- For  $F = 2$ ,  $\alpha = \sim 3.2^\circ$ ,  $N_{\text{total}} = 2305$ , and  $N_{\text{positions/row}}$ <sup>1</sup> = 120;
- For  $F = 3$ ,  $\alpha = \sim 1.6^\circ$ ,  $N_{\text{total}} = 9217$ , and  $N_{\text{positions/row}}$ <sup>1</sup> = 240.

---

<sup>1</sup> By default, dynamic daylighting simulation assumes a scaling factor,  $F$ , of 2. In all cases, solar positions are evenly-distributed across the hemisphere, while maintaining a single zenith position.

## Annex 2

### Main difference between Rhinoceros and Grasshopper

The example regards usual work process to make an apple in *Rhinoceros* work environment.

The first step is drawing a profile curve and a rotation axis. Then, type in 'Revolve' then pick the profile and rotation curves with starting and ending angles. In this case, it supplies 0 as the starting angle and 360 as the ending angle to get a whole apple.

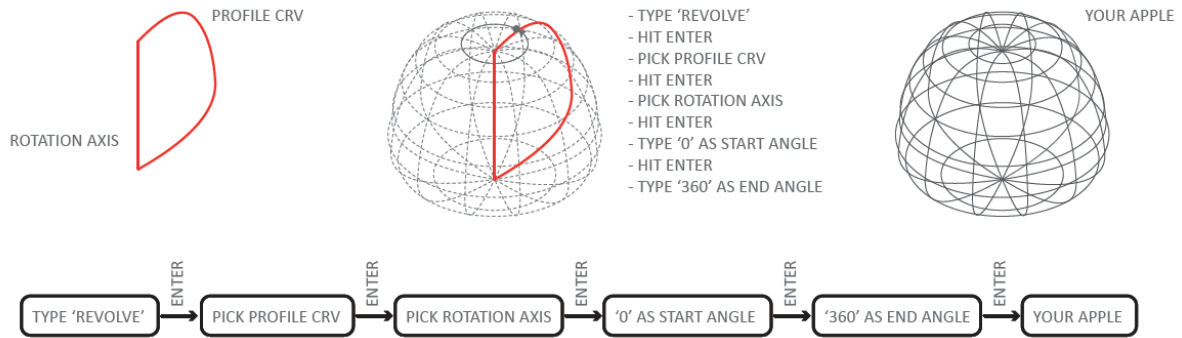
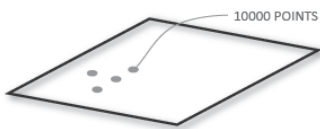


Figure 111. Steps of the process for making the an apple in *Rhinoceros* work environment

Now, your boss wants to have a table on which 5,000 apples, 2,500 three quarter apples, 1,250 two quarter apples, and 1,250 one quarter apples are distributed randomly. First you should make a table which has 10,000 reference points on it. Then make 4 different types of apple, copy and move one by one to the reference points. Don't forget to count apples so as to make your boss happy.

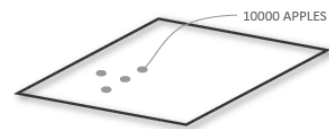
#### BUILD A TABLE WITH 10000 POINTS ON IT



#### BUILD APPLES



#### ARRAY THEM ON THE TABLE



Your boss is not happy with this. He wants to change the mixing ratio of apples. You have two choices; do it again, or find another job.

#### DO IT AGAIN, OR KILL YOUR BOSS AND GET A NEW JOB



In *Grasshopper*, you don't work on the real geometries. Rather, you work on the logic behind the geometries. Once the apple making logic has been set up, you can change parameters such as starting and ending angles. Also you can change the shape of apples by supplying different profile curves as well as rotation axis. Or you can make multiple apples out of just one definition by supplying multiple angle values and/or profile/rotation curves to the definition.

